PURDUE RESEARCH FOUNDATION
Project No. 3728

OCTOBER 16, 1964

A STUDY OF INCOMPRESSIBLE TURBULENT BOUNDED JETS

by

J. F. Foss

J. B. Jones

prepared for BR 310

HARRY DIAMOND LABORATORIES
Army Materiel Command
Washington, D. C. 20438

Contract DA-83(D) AMXDO-CSA 40 (A)

Blank Page

Purdue Research Foundation

Lafayette, Indiana

Project No. 3728

A STUDY OF INCOMPRESSIBLE, BOUNDED TURBULENT JETS

by

J. F. FOSS

J. B. JONES

a report prepared for

ARMY MATERIEL COMMAND

HARRY DIAMOND LABORATORIES

Washington, D.C. 20438

November 1964

Contract DA-83(D) AMXDO-CSA 40(A)

ACKNOWLEDGMENTS

The author is indebted to, and wishes to express his appreciation to:

The Harry Diamond Laboratories for the financial support of both the project and the writer's final year in graduate school,

Dr. J. B. Jones for his interest, availability, and encouragement during his last year at Purdue and especially for his undiminished assistance when his official connection with Purdue was terminated in order to accept the position as Mechanical Engineering Department Head at the Virginia Polytechnic Institute,

Dr. R. W. Fox for accepting, as an overload, the guidance of the present study for the final four months,

Mr. J. Hall for his superb craftsmanship in the construction of the intricate parts of the traverse devices used and for the design suggestions which markedly increased their ability to carry out the desired operations.

As in the case of many graduate students, the writer's wife has provided immeasurable assistance in terms of mental support for the duration of the program. The additional support of many hours of typing and data plotting (in addition to the duties of a mother) has meant that many rush deadlines have been met and that this amount of time was freed for productive efforts.

TABLE OF CONTENTS

Page

LIST OF TABLES

LIST OF ILLUSTRATIONS

APPENDIX A

APPENDIX B

APPENDIX D

ABSTRACT

Foss, John F., Ph. D., Purdue University, January 1965. A Study of Incompressible Bounded Turbulent Jets. Major Professor: Dr. J.B. Jones

The intent of this investigation was twofold.

A portion of the study was directed to the establishment and investigation of the three-dimensional effects of a single bounded jet flow between parallel plates. From velocity traverses taken between the bounding plates, the existence of an important three-dimensional effect was observed. A physical flow model was postulated, the vortex stretching hypothesis, to explain this observation. A series of experiments were conducted to examine predictions made on the basis of the model; the agreement between the observed and predicted mean flow characteristics and distributions provides substantial support for the vortex stretching hypothesis. A capsule description of the vortex stretching hypothesis follows.

Vortex filaments will be generated in the velocity gradient

of the bell-shaped jet velocity profile. The vortex filaments, which will end on the bounding plates, are always formed from the same fluid particles until they are dissipated by viscous action. Because of the no-slip condition at the wall, the filament is both stretched and reoriented as the central portion is swept downstream. This reorientation induces an inflow to the jet near the midplane between the bounding plates and an outflow near the bounding plates. The stretching increases the vorticity and thus intensifies the effect.

The second portion of the experimental program was an investigation of the jet interaction problem which is the governing factor in all proportional fluid jet amplifier devices and is an important factor in the operation of bistable amplifier elements. Because few data were available in the literature concerning detailed flow phenomena, the investigation of the intersecting jet problem was also an exploratory one. Four studies were conducted with the intent of establishing "information bench marks" from which further information could be inferred. The tests were:

i) A jet deflection study. The measured quantities were: the deflection angle, the apparent pivot point and the static pressures assisting in the deflection for momentum

flux ratios of 0.05, 0.10, 0.15 and 0.20 and for three geometries.

ii) A detailed mean flow survey in which the velocity profiles, flow angles, static pressure distributions, and mass, momentum, and energy flux ratios were determined for seven planes between the bounding plates at three longitudinal locations.

iii) and iv) Two series of tests to establish the effect of the nozzle geometry and the effect of the momentum flux ratios were conducted.

From the data of study (i) it was determined that the geometry used caused a significant increase in the deflection angle with respect to the momentum flux action alone. Also, the analytical model which was proposed provides a satisfactory prediction method for the geometry with the highest gain.

From ii), iii) and iv) it was determined that the intersection of the jets leads to an increase in the vortex-stretching effects and that the nozzle geometry and the momentum flux ratio have significant effects on the resultant jet.

INTRODUCTION

Since 1960 considerable effort has been expended on purely pneumatic elements for control and logic systems. The proportional fluid jet amplifier, which has been successfully used in certain control systems, is such an element. Figure 1 shows a schematic diagram of a typical proportional amplifier, and by use of terms defined in the figure, a qualitative description of the operation of the device can be given as follows.

For a zero difference in the control jet flows, the power jet flow is evenly divided by the splitter and the flows from the two output ports are equal. If the control jet flows are unequal, the imbalance will deflect the power jet such that the flows from the output ports are no longer equal. The difference in mass flux, momentum flux, energy flux, or pressure of the two outlet streams is related to the difference in the same quantities at the control jet input stations. From a comparison of the flow conditions at the inlet and outlet, the gain of the amplifier is defined. For example, the mass flux gain — G — is commonly defined as

$$G = \frac{(-1)\left[\dot{m}_{left} - \dot{m}_{right}\right]_{output}}{\left[\dot{m}_{left} - \dot{m}_{right}\right]_{control\ jets}}$$

where $\dot{m}$ is the mass rate of flow.

Comparing the purely pneumatic device with the electronic amplifier shows that the power jet flow is analogous to the plate current and the control jet serves the same function as the grid circuit. If

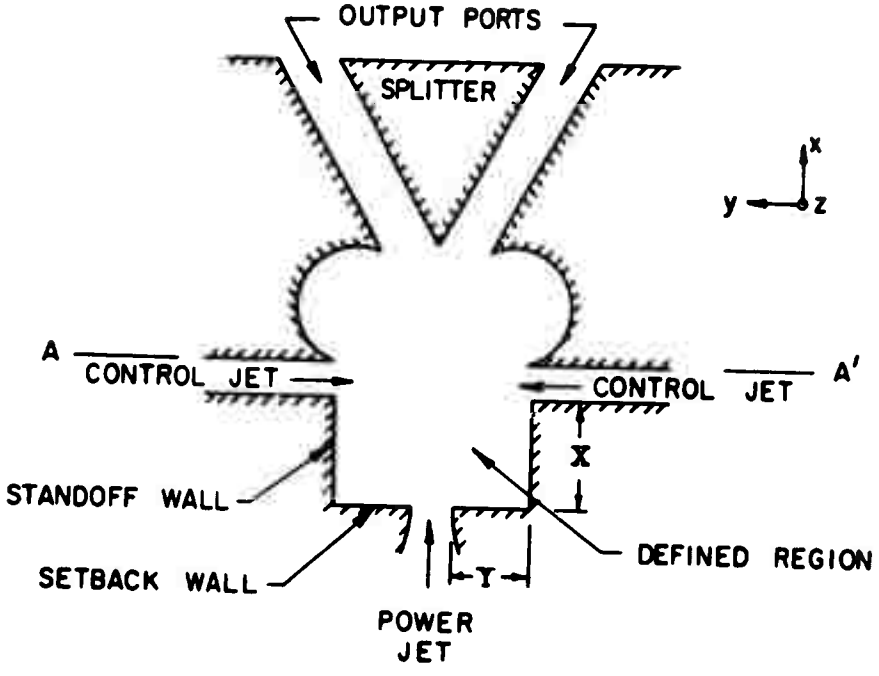

NOTE: DEPTH OF UNIT ≈ 6 - 8 NOZZLE WIDTHS

FIG. 1 A TYPICAL FLUID JET AMPLIFIER DESIGN

simplifying assumptions are made for the form of the velocity profiles (both entering and leaving the mixing region) and if the static pressure distribution is similarly dealt with by assumption, it is possible to predict quantitatively the performance of the proportional fluid jet amplifier.* Much of the effort to analyze this particular device has been directed toward this approach.

From a designer's viewpoint, this method of predicting the performance would be greatly improved if the mean velocity distribution leaving the interaction region were known. In addition, if other details of the flow leaving the interaction region (e.g., static pressures and turbulence velocities) were known, this information could provide valuable insight into the actual interaction phenomena. Finally, if detailed measurements were taken in the interaction region itself, then the character of the momentum interchange and the role of the static pressure might become known. This would greatly facilitate the design of such elements.

Figure 1 shows one of the many possible geometries which can be employed for the proportional fluid jet amplifier; however, other configurations may also be employed for this device. The interaction of two jets is the governing phenomenon which is common to all proportional amplifiers and is an important factor for the bi-stable elements (oscillators, and switches); therefore, any insight into this interaction phenomenon can lead to a better understanding of the operation of all such devices.

---

* This method would employ the conventional control volume approach (see e.g. Reference 1, Shames)

The intent of the present work is to provide information that will be important to the understanding of the jet interaction problem from both a fundamental and a design viewpoint. In order to separate the characteristics of the flow which result from the interaction of the two jets from those characteristics induced by the downstream geometry, the experimental configuration was that of Figure 1 with the section above the line A – A' completely open. An aspect ratio of 6 was used.

A characteristic of all three-dimensional * turbulent shear flows is that the system of equations describing the flow is incomplete. That is, for the four basic equations of continuity and momentum, there are ten unknowns, viz. three mean velocity components, the static pressure, and six independent components of the Reynolds stress tensor, $-\rho \overline{u_i u_j}$. Thus to render the system of equations mathematically tractable, one must make certain simplifying assumptions. A plausible assumption for this geometry would be that the flow has a two-dimensional character over a significant region between the bounding plates. If the two-dimensional assumption is applicable in this region, then the phenomenological theories (e.g., Prandtl's mixing length theory) may be useful in gaining an analytical solution for the mean velocity. An early portion of the experimental program was designed to check this assumption of two-dimensionality

---

* Since typical aspect ratios (height to width ratio of the power jet nozzle) for the fluid jet amplifiers are from 6 to 8, the flow is three-dimensional.

by means of velocity traverses between the plates, viz. u(z) for a fixed x value and various y values (see Figure 1 for coordinates). These data were taken for the single bounded jet case in the absence of side jets.

The remaining experimental investigation was directed to the following:

i) mean velocity and static pressure profiles of the jet which emerge from the interaction region (resultant jet),

ii) deflection angles of the resultant jet as a function of (a) the ratio of the control and power jet momentum fluxes and (b) the nozzle geometry.

iii) the effects on the character of the resultant jet which are caused by different nozzle geometries and different momentum flux ratios.

NOMENCLATURE

a	nozzle exit width
app	apparent pivot point of resultant jet
B	barometric pressure in inches of mercury
b	momentum flux thickness, $\frac{1}{2} \int_{-\infty}^{\infty} (u/u_c)^2 \, dy$
cj	control jet
C_p	pressure coefficient, $\frac{P - P_{ATM}}{\frac{1}{2} \rho u_c^2}$ (except as noted)
e	energy flux thickness, $\int_{-\infty}^{\infty} (q/q_c)(u/u_c) \, dy$
E	energy flux, $e \, q_c \, u_c$
h_T	total pressure head
h_s	static pressure head
k	ratio of geometric lengths Y/X
k'	ratio of geometric lengths, Y'/X'
K	proportionality factor for velocity computation, $15.89 \sqrt{(T/B)}$
l	mixing length
m	mass flux width $\int_{-\infty}^{\infty} u/u_c \, dy$
M	mass flux, $\rho \, m \, u_c$
mfr	momentum flux ratio, $a_2 u_{2_0}^2 / a_1 u_{1_0}^2$
N_R	Reynolds number

P	static pressure
pj	power jet
q	dynamic head, $(h_T - h_s)$; except for section VII-A where q = momentum flux per unit depth
R	radius of curvature of jet
t	dial reading for the x - y - Θ traverse device
u	x - component of mean velocity vector
u_*	ζ component of mean velocity vector
v	y - component of mean velocity vector
V	magnitude of mean velocity
w	z - component of mean velocity vector
x	longitudinal distance (see figure)
x_o	apparent origin of the jet
X	length of standoff wall (see figure)
X'	X + a/2
y	transverse distance (see figure)
Y	length of setback wall (see figure)
Y'	Y + a/2
$\Delta y_{\mathbb{Q}}$	transverse displacement of the centerline for the resultant jet
y*	$y - \Delta y_{\mathbb{Q}}$

z vertical distance; x - y - z form a right hand orthoganol co-ordinate system (see figure)

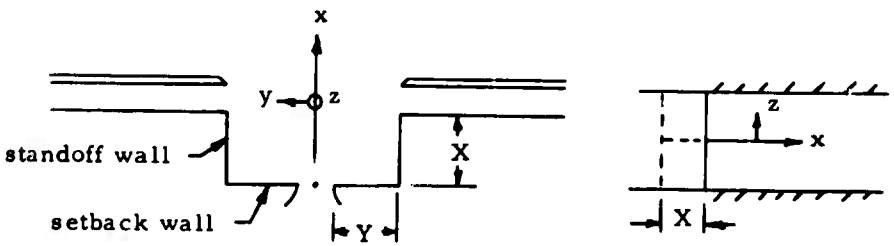

Greek Symbols

α deflection angle of the resultant jet (see Figure 29)

β angle used in analytical study (see Figure 29)

γ angle used in analytical study (see Figure 29)

δ length ratio x_{app} / X'

ϵ eddy viscosity

ζ longitudinal co-ordinate measured along the axis of the resultant jet (origin at the power jet nozzle exit)

η non-dimensional co-ordinate, y/b or y^* / b

η_* ξ / b_*

ρ density of fluid (room air)

σ	standard deviation
τ	shear stress
Θ	flow angle, arc tan (v/u)
Θ^*	flow angle with respect to resultant jet, $\Theta - \Theta_c$
ξ	transverse co-ordinate measured with respect to the resultant jet (ζ, ξ, z form an orthoganol right hand co-ordinate system.)

Subscripts

app	quantity at the apparent pivot point
c	quantity at the maximum velocity point of the profile
L	left pocket of the defined region (for the present study this is the near pocket)
m	quantity at the maximum velocity point of the profile and for z/a = 0
0	quantity at the power jet nozzle exit (except for x_o)
R	right pocket of the defined region (for the present study this is the far pocket)
1	power jet nozzle flow
2	control jet nozzle flow
*	quantity referred to the ζ, ξ, z co-ordinate system

Superscripts

$( )'$	turbulent fluctuation of ( )
$\overline{( )}$	time average of ( )
$( )^{>}$	vector quantity of ( )

SURVEY OF THE LITERATURE

Introduction

Although purely pneumatic devices are a recent development, a sizeable literature dealing with them is already available. Commercial applications account for most of the interest, and this product orientation is primarily responsible for the literature emphasis on the gross performance or system characteristics of the devices. References 2 and 3 are representative of the majority of the current literature. Although these papers provide valuable information for the systems designer, they provide little insight into the details of the interaction phenomena.

Significant simplifications in the analytical model for the intersecting jets problem can be effected if the two-dimensional approximation is valid for the central region of the flow field. Since previous investigations (17 - 21) of jet interaction between parallel plates have made use of the two-dimensional jet studies, a review of the two-dimensional jet flow literature is given below.

The Two-Dimensional Jet

In 1926, Tollmien (4) applied the then recently developed Prandtl mixing length theory to the two-dimensional jet flow problem. To achieve an analytical solution for the mean velocity distribution he introduced the following assumptions:

i) The mixing length is constant in any plane normal to the mean flow.

ii) The static pressure gradient in the direction of flow is negligible.

iii) Viscous shear is negligible in comparison with the Reynolds (or turbulent) stress.

iv) The instantaneous velocity fluctuation in the direction of flow is very small in comparison with the mean velocity component.

v) The flow is in a self-preserving state.

With the above assumptions and the defining equation for mixing length, the system of equations (continuity and momentum) is determinate.

Starting with the continuity and momentum equations and using $u(x, \eta)$, where η is the similarity variable, $y/g(x)$, Tollmien was able to form the solution for the velocity, $u(x, \eta)$. $g(x)$ is a characteristic parameter which describes the jet as a function of x (the velocity on the jet axis -- $u_c(x)$ -- is such a parameter).

The solution, which is not readily presented analytically, appears in tabular form in Reference 4.

From an analysis of the transverse equation of motion, Tollmien predicted that the static pressures in the jet would be greater than atmospheric. He also applied the conservation of momentum criterion to show that $u_c(x)$ is proportional to $x^{-\frac{1}{2}}$ downstream of the potential flow core.

Two other phenomenological theories were applied to the two-dimensional jet problem. Görtler (5) postulated a constant eddy viscosity, ϵ, across the mixing layer and after making assumptions as those of Tollmien, ii), iv), and v), he obtained the following expression for the mean velocity:

$$\frac{u}{u_c} = \operatorname{sech}^2 \frac{\eta}{2} A$$

where $\eta = y/x$ and $A = (\epsilon / x)_C$.

Reichardt (6) started with the fact that the Gaussian error curve provides an accurate representation of the experimentally determined non-dimensional velocity profile. The one-dimensional diffusion equation yields a solution of this form and this led Reichardt to make the following analysis. Starting with the x-direction momentum equation (neglecting viscous effects and the x-direction static pressure gradient),

$$\frac{\partial}{\partial x} (u^2) + \frac{\partial}{\partial y} (uv) = 0$$

he made the substitution

$$uv = -\lambda(x) \quad \partial(u^2) / \partial y$$

and thus obtained the one-dimensional diffusion equation

$$\frac{\partial u^2}{\partial x} = \lambda(x) \frac{\partial^2 u^2}{\partial y^2} \quad .$$

Note in the above equations that u is the instantaneous turbulent velocity and that $\lambda(x)$ is independent of y. The assumption implied by the substitution is that the transport of the x-momentum by the velocity transverse to the mean flow is proportional to the gradient of the x-direction momentum flux in the transverse direction. This assumption serves as the basis of the Reichardt Inductive Theory. The non-dimensional velocity profile for the Reichardt theory is:

$$u/u_C = \exp(-\pi / 8) \eta^2 \quad *$$

---

* The constant $(-\pi/8)$ was experimentally determined by Miller and Comings (9).

where: $\eta = y/b(x)$ and $b(x) = \int_{-\infty}^{\infty} (u/u_c)^2 \, dy$.

The above phenomenological theories have all been shown to be lacking in complete physical rigor. Hinze (7) provides an excellent summary of the phenomenological theories and their shortcomings (see pages 277-293).

In 1934, Forthman (8) conducted an experimental program motivated by the analysis of Tollmien. The accuracy of the results of this investigation are uncertain inasmuch as the static pressure probe used by Forthman gave a reading which was greater than atmospheric. It is interesting to note that Forthman's first probe (an L-head, closed end type) gave negative gage static pressure readings in the jet. Because Tollmien's analysis had incorrectly predicted positive gage pressures, a new probe which did give positive pressures, was built and used.

Miller and Comings (9) have experimentally verified the relation proposed by Townsend (10), viz., $P(y) + \rho \overline{v}^2 = P_{(atmospheric)}$. This formula is based on an order of magnitude analysis of the transverse equation of motion. The relation and its verification show that the static pressures in the jet are less than atmospheric.

The work of Miller and Comings also shows that the experimental data for the mean velocity profile are well matched by the Gaussian error curve and that the prediction of Tollmien for the center line velocity decay is accurate to within three percent. The velocity profile of Gortler is also presented by Miller and Comings along with their experimental data. For the central portion of the jet ($u/u_c \geq 0.3$) the agreement is quite good; however, for the outer portion the percentage error of the

analytical prediction is quite high. For example, at $(u/u_c) = 0.1$ the percentage error, defined as

$$[u_{actual} - u''_{Gortler}] / u_{actual} \times 100,$$

is approximately 32 percent. This percentage error increases strongly for decreasing u/u_c values.

Measured values of $\overline{u'^2}$ and calculated values of $\overline{v^2}$ and $-\rho\ \overline{u'v'}$ are presented by Miller and Comings. The computed values were obtained from an analysis of the equations of motion.

Van der Hegge Zijnen (11) made measurements in a plane jet of air. The nozzle system used was a rectangular slit in the closed end of a circular pipe. Both a circular arc and a straight - 45 degree bevel were used as nozzle shapes. The results of this investigation indicate that the Gaussian error curve provides the best prediction of the experimental data; however, the constant in the exponential was found to be a function of the aspect ratio, its value being -75 for an aspect ratio of 20 and -70.7 for an aspect ratio of 25. This difference, and the difference in apparent origins of the jet (0.6a and 1.7a for aspect ratios of 20 and 25) are believed to result from the nozzle and plenum chamber design.

The velocity measurements were made with a total head tube which was corrected for turbulence intensity effects on the total pressure readings. The probe readings were not corrected for angular deflections; the static pressure was not measured and the computed value of $u(y)$ was not corrected for the angle of the mean velocity. Consequently, the figures of (11) which are labeled as u/u_c could be more accurately labeled as:

$\left[\frac{h_T(y)}{h_{T_c}}\right]^{1/2}$ corrected for $\overline{u'^2}$.

An analytical contribution of (11) is that of calculating the eddy viscosity as a function of y for an assumed Gaussian distribution without recourse to turbulent stress measurements.

Albertson, et al. (12) have also investigated the two-dimensional jet. Their data, in agreement with the results of (9) and (11), indicate that the Gaussian error curve provides a satisfactory fit to the experimental mean velocity profile. However, it should be noted that the profiles of Albertson, et al. show a much larger scatter in the data than the profiles of either (9) or (11). The authors have shown that the velocity profiles in the mixing zone adjacent to the potential core region (i.e. the zone where $u_c = u_0$) may be well approximated as a single curve by the relation

$$\log_{10} \frac{u}{u_0} = -18.4 \left[0.096 + \frac{y - a/2}{x}\right]^2$$

for the majority of the jet profile (i.e. $u/u_0 \geq 0.1$). The lateral component of velocity was computed from the measured magnitude and direction of the mean velocity vector. Neglecting $\frac{\partial p}{\partial x}$ and all components of the Reynolds stress tensor except $-\rho \overline{uv}$, they were able to compute the $\tau(y)$ distribution. From this and the known velocity profile they computed the mixing length and eddy viscosity as functions of y.

Three important characteristics of the two-dimensional jet are presented by Albertson et al.. Plots of the following ratios:

$\frac{M}{M_0}$ = (mass rate of flow at x = x) / (mass rate of flow at x = 0),

$\frac{2bq_c}{aq_0}$ = (momentum flux at x = x) / (momentum flux at x = 0)

$\frac{E}{E_0}$ = (kinetic energy flux at x = x) / (kinetic energy flux at x = 0)

show that downstream from the potential core, M/M_0 increases exponentially with distance (viz., $(M/M_0) = (x/a)^{0.469}$), $2bq_c/aq_0$ remains constant, and E/E_0 decreases exponentially with distance (viz., $E/E_0 = (x/a)^{-0.470}$). The second important characteristic is the angular deflection of the flow from the axis y = 0. The velocity vector was found to have a maximum outward angle of 10 degrees (away from the x-axis) in the neighborhood of y/x = 0.15; angles approaching 90 degrees inward were found for the extremities of the jet. A third characteristic of the two-dimensional jet is the length of the potential core, i.e. the region where $u_c = u_0$. Albertson et al. indicate that this potential core closes at approximately five nozzle widths; Miller and Comings' data indicate that this length is about six nozzle widths and the data of v. d. H. Zijnen indicates that the core closes at 4 to 4.5 nozzle widths. Although these differences may appear insignificant, the prediction of the downstream value of u_c is strongly dependent on the x location of the core termination. Since the physical flow property u_c is not exactly constant in this core region, as indicated by the data in (9), (11), and (12), it is difficult to establish an exact value for the length of the region. The measurements of Albertson, et al.

covered a Reynolds number range of 1,600 to 13,000. Miller and Comings' data are for a Reynolds number of 19,000 and v. d. H. Zijnen's data are for a Reynolds number of 13,300.

In a separate study using the same flow system as in (11) v. d. H. Zijnen has also made turbulence measurements in a plane jet of air (13). Measurements of $\overline{u^2}$, $\overline{v^2}$, $\overline{uv}$ as a function of y and $\overline{u^2}$, $\overline{v^2}$, as a function of x for y = 0 are presented. The transverse measurements were made for six x/a values from 17.5 to 35. The $\overline{u^2}$, $\overline{uv}$ measurements indicate reasonably similar distributions, whereas $\overline{v^2}$ shows a large scatter. This may be a direct result of the nozzle geometry. In (13), v. d. H. Zijnen shows that turbulence measurements, made with the hot wire and with the diffusion technique are in agreement when the $(\overline{u^2})^{1/2}$ data are non-dimensionalized using $[u + (\overline{u^2})^{1/2}]$ instead of the mean velocity u.

Heskestad (14) has made mean flow and turbulence measurements in a two-dimensional jet. The geometric configuration of the flow system is different from that of any of the previous investigators. A channel, which was 60 inches by 1 inch in cross-section and 60 inches long, was placed between the plenum chamber and the nozzle. The nozzle, with an outlet cross-section of 60 inches by $\frac{1}{2}$ inch, had straight walls making an angle of 45 degrees with the larger walls of the approach channel. No reason was given for the long approach channel upstream of the nozzle.

The major contribution of this paper is turbulence measurements for very large x/a values. The rms fluctuations, $\overline{uv}$, a turbulence energy balance, the triple moment, intermittency and the value $(\partial [\overline{u^2}]^{1/2} / \partial t)^2$ were measured. A brief comparison between the turbulence data available from (9), (13), and (14) is presented in the following table.

Table 1

Turbulence data from the literature

Investigator	$\overline{u^2}$ max/ u_c^2	$\overline{v^2}$ max/ u_c^2	$\overline{uv}$ max/ u_c^2
Reference (9)	0.068	0.055	0.025
(13)	0.032	0.023	0.018
(14)	0.070	0.035	0.017

Note: The values are all approximate.

A more complete comparison for $\overline{u^2}$ is given in the section "Single Bounded Jet Study."

The important differences among the data sources are: (i) the values from (9) and (13) were taken at 40 and 35 nozzle widths whereas (14) is for 101 nozzle widths, (ii) the $\overline{v^2}/u^2_c$ and $\overline{uv}/u^2_c$ values from (9) were caluculated from the two-dimensional equations of motion and the continuity equation whereas the data of (13) and (14) are taken from direct measurements.

Angular deflections of the mean flow and the mean velocity profiles as a function of x/a were also investigated by Heskestad. If the mean velocity distributions are compared with those of previous investigators the effect of the unique upstream geometry may be inferred. Most significantly, the mean velocity profiles do not indicate a self-preserving form before x/a = 65, whereas

Reference 9 shows that self-preservation is obtained by $x/a = 10$. Heskestad compares his self-preserving mean velocity profile with only that of Görtler; the data from (14) are in good agreement with Görtler's curve up to a $(y/x-x_o)$ value of 0.17 (a u/u_c value of 0.2); for larger $(y/x-x_o)$ values the analytical curve is significantly higher than the experimental points. From this agreement it appears that for the fully developed region there is little memory effect of the upstream geometry. This is certainly to be expected because of the high entrainment rates of a jet flow and the physical distance from the nozzle.

Positive values of the angle of the mean flow with respect to the x-axis show a maximum of about 3 degrees at $x/a = 100$. When the angular distribution is compared with that calculated from the continuity equation, the agreement is quite good. Albertson, et al. (12) also made flow angle measurements and compared them with computed values from the continuity equation. The measurements from (12) show a maximum angle of about 10 degrees; consequently this angular distribution differs from the measurements of (14) as well as the computed values of (12) and (14). It is presumed that the experimental technique of (12) is in error. A dual total probe arrangement with a splitter plate separating the tubes was used; in order to obtain a null reading of this probe in a large mean velocity gradient, the probe would have to be shifted to a larger-than-true angle. This could readily account for the presumed experimental error of about 7 degrees in (12).

Liepmann and Laufer (15) have made an extensive experimental study of the half jet which is formed by extending

one of the nozzle walls past the nozzle exit (parallel to the mean flow velocity at the exit) and by terminating the other wall in the usual manner for a two-dimensional jet. An aspect ratio of eight (60 x 7.5 inches) was employed for a nozzle exit. The downstream section was unbounded, normal to the 60 inch dimension, and all measurements were taken within an x/a range of 0 to 4.92 nozzle widths. They treated the flow as two-dimensional for the region bounded by the plane of maximum velocity and the atmosphere.

Liepmann and Laufer measured velocity profiles and presented them with the analytical predictions of Tollmien, Görtler, and Reichardt. For the presentation of the mean velocity data, Liepmann and Laufer chose the non-dimensional variable $\eta = \sigma y/x$ where σ is a free parameter which is chosen to provide the best fit between the data and the analytical curve under consideration. This free parameter was used to force the analytical profiles to fit the experimental ones at the location where $u/u_c = 0.5$. The physical location of $u/u_c = 0.5$ also served as the $y = 0$ point for the co-ordinate selection. In order to match the experimental data, the solution of Tollmien requires that σ be equal to 12.0; the solution of Görtler requires that σ be 11.0, and the error curve of Reichardt requires σ to be 13.5. Liepmann and Laufer conclude that the Görtler solution provides the closest approximation of their experimental data. The mean velocity profiles of Liepmann and Laufer are not considered valid for the two-dimensional jet case for the following reasons:

i) Their geometry is not truly two-dimensional.

ii) The co-ordinate selection is arbitrary.

iii) References (9), (11), and (12) indicate that the profile is best approximated by the error integral curve.

Liepmann and Laufer's measurements of the turbulent fluctuation velocity $(\overline{v^2})^{1/2}$, the correlation $\overline{uv}$, the microscale, and the turbulence energy terms are believed to be unique for this type of two-dimensional free turbulent mixing. From measurements of the mean velocity profiles and the Reynolds stress, $-\rho\,\overline{u'v'}$ they were able to calculate the values of the mixing length and eddy viscosity across the mixing layer. Even though the geometry is not exactly the same, these measurements and computed quantities are of interest in connection with the two-dimensional jet problem.

A comparison of the ϵ and l curves between Albertson, et al., and Liepmann and Laufer reveals gross dissimilarities in the shapes of both sets of curves. These differences arise from the different geometries or from the fact that the latter curves (15) are from a direct calculation, whereas the former curves (12) were obtained from a graphical integration of experimental data. Although references (15) and (12) do not agree on the distributions for ϵ and l, the two sets of curves indicate that ϵ deviates less from a constant value than does l.

The relation between the half jet and the two-dimensional jet is not well understood. All the measurements of Liepmann and Laufer were taken within a length $(4.92 = x/a)$ that would not allow for the closing of the potential core in a two-dimensional jet. Although the self-preserving velocity profiles are somewhat similar to those of the two-dimensional jet, it is difficult to compare the non self-preserving turbulence data because of the

dissimilar downstream establishment rates. Another factor, with an influence that is hard to estimate, is the effect of the high production of turbulence energy near the extended plate on the turbulence and mean flow properties of the region which was analytically treated as a two-dimensional jet.

The nozzle used by Liepmann and Laufer was (apparently) a beam deflection nozzle. This type of nozzle design provides for a smooth acceleration of the fluid through the nozzle (see Appendix A.). A circular nozzle curvature was used by Miller and Comings (9) and by Albertson, et al. (12); this is known to produce a non-uniform velocity profile at the location of the abrupt change in the radius of curvature. The ratio of radius of curvature to nozzle width was greater than 6:1 for (9), whereas for (12) this ratio was approximately 1. The scatter in the experimental data (12) for the mean velocity distribution as opposed to the smooth profiles of (9) may be a result of this difference in the nozzle construction. One of the nozzle designs used in (11) and that employed in (14) seriously violate this requirement for a smooth acceleration by using a straight - wall nozzle design.

Olson and Miller (16) present a rather clever analytical development leading to an expression which allows for the prediction of the length of the potential core region, the center line velocity decay, and the axial variation of the y coordinate at the u/u_c value of 0.5. The latter can be used as a measure of the jet spreading. As presented, the analysis is for compressible flow and involves the assumption of constant eddy viscosity and a Gaussian mean velocity distribution. These two assumptions would be incompatible for incompressible flow.

In summary:

i) The mean velocity profile for the two-dimensional jet can be accurately approximated by the Gaussian error curve (9), (11), and (12); the Görtler solution provides a satisfactory approximation to this profile (9), (11), and (14).

ii) Characteristics for the two-dimensional jet, such as mass, momentum, and energy fluxes (12), center line velocity decay (4), (9), and (12), velocity vector angles (11) and (14), and the static pressure distribution (9) and (10) are known.

iii) Turbulence data near the nozzle exit (9) and (11) and a more complete turbulence survey for large x/a (14) are available. However, certain important discrepencies in the various results exist as indicated by the previous discussion.

iv) Details of the turbulence structure as well as the eddy viscosity, mixing length, and mean velocity distributions are known for the half jet (15).

Intersecting Jets

Several references in the general area of fluid jet amplification are of direct interest to the present study. A general description of these is given below. Specific items to be referenced from each will be treated in later sections wherein results of the present study are discussed.

Manion and Goto (17) have analytically and experimentally investigated the jet deflection problem for a "defined region." The study was initiated as a result of indications from another source that the presence of the "setback" and "standoff" walls induced a greater deflection angle than that predicted from momentum flux considerations alone. From the input data of the power and control jet momentum fluxes, the pressure in the far side pocket, and geometric constants of the defined region, the analysis of Manion and Goto provides a prediction of the angular deflection of the resultant jet. A key step in the analysis is the prediction of the near side pocket pressure by assuming an inelastic collision between the power and control jets and an absence of any shear-induced entrainment effects of the control jet by the power jet. The experimental program was conducted on an air flow system of small physical dimensions ($a = 0.032"$, aspect ratio = 8). The flow regime was compressible; power jet plenum pressures were 5, 10, and 20 psig for the tests reported. The deflection angle α was determined by a null reading from a dual total pressure probe. The agreement between the analysis and the measured values of $\tan \alpha$ is satisfactory if the correct value of the arbitrary far side pocket pressure is used.

An analytical investigation of the jet interaction problem in a defined region was also conducted by Goto (18). Two simultaneous control jet flows are considered and as in (17) a prediction equation for the angle α was the main objective of the study. The computation equation for tangent α involves the geometric constants, input momentum fluxes, and the pressure in one of the pockets. This pressure is, in turn, given

as an independent function of the input momentum fluxes, the geometric constants, and the deflection angle α. Consequently a trial and error solution is implied.

Reilly and Kallevig (19) and Reilly and Moynihan (20) have presented some of the work on the more common type of fluid jet amplifier (i.e. $X = 0$ and $Y \geq 0$) which has been carried on at the Military Products Research Department of Honeywell Incorporated. These presentations deal with the gain of the amplifier, a prediction of the gain by different flow models and corresponding experimental investigations. Of particular interest to the present study are the velocity profiles taken in the $z = 0$ plane of a bounded, incompressible, three - jet flow system (aspect ratio = 6). The profiles, shown in (19), indicate that the resultant profile rapidly approaches a symmetric (but not self preserving) shape (about the x axis). They also indicate that a smooth, two-dimensional like, velocity profile is not attained by 10 nozzle widths.

Olson (22) has taken jet deflection data for a power and control jet geometry similar to that of the "defined region" with the exception that the "standoff" and "setback" walls are absent. An interesting result of this investigation is that the apparent impingement point (apparent pivot point) has been displaced downstream of the geometric intersection point. This displacement appears to be correlated with the momentum flux ratio (mfr), having a value of 8a for an mfr of 0.016 and decreasing in an exponential fashion to a value of 0.4a at an mfr of 0.1. Olson attributes this displaced effective origin to the elapsed time between the physical impingement and the effective momentum interchange. The velocity profiles,

which are apparently taken from total pressure data only, show good symmetry and smoothness by eight nozzle widths downstream. These profiles, as well as those from (19), indicate that if a serious velocity discontinuity is present at the intersection point, it is rapidly smoothed by turbulent mixing. The data from (22) was taken for a power jet exit Mach number of 0.66.

The majority of the paper by Pepperone, et al. (21) is not of direct interest to the present study; however several items from the second section, "Jet Streams," are of importance. With reference to an unpublished investigation of velocity profiles in the $z = 0$ plane of a bounded (aspect ratio = 8) jet flow, they note that the momentum flux indicated by these profiles is not constant but falls off in the downstream direction as a result of the shear effects on the jet by the bounding plates. They further note that this would make the jet appear to emanate from a point farther upstream than for the regular two-dimensional jet type flow. Although no indication is given as to how it was defined, they state that the apparent origin is four nozzle widths upstream of the physical nozzle exit. These data were apparently collected with a total pressure probe only and for the compressible flow case of a power jet plenum pressure of 10 psig.

OBJECTIVES

General Objectives

The intent of the present study was to establish certain important features of jet flows between parallel plates, a complex flow phenomenon. A complete and fully detailed investigation which considered all the parameters would require an inordinate amount of time. Therefore, specific topics were chosen and tests (ii) to (v) were conducted to establish "information bench marks" from which a much wider information area could be surmised. The five specific subject areas considered include

i) the single bounded jet;

ii) the deflection angle (α) of the resultant jet as a function of nozzle geometry and the momentum flux ratio;

iii) the mean flow characteristics of the resultant jet as a function of the three co-ordinates (x, y, z) including flow angles, mean velocity and static pressure distribution, and mass, energy, and momentum flux ratios;

iv) the effect of nozzle geometry on the resultant jet;

v) the effect of the mfr on the resultant jet.

Although the tests will be discussed separately their common intent is to obtain information that will allow the results

for a specific set of conditions to be extrapolated to other geometric and flow conditions.

To obtain a complete solution of the jet interaction problem for the geometry chosen would require that the turbulent velocity $V(x, y, z, t)$ be known as a function of the variables X, Y, and the momentum flux ratio (mfr). Since the problem is inherently one of a three-dimensional turbulent flow, a complete analytical formulation involves ten unknowns and four equations, rendering a complete analytical solution impossible. The mode of attack on the problem is then governed by what information is desired; this information is, of necessity, short of the complete solution. The five specific investigations and their function in the overall scheme of the present study are discussed below.

Objectives of Several Experiments

Although a desirable (and necessary) analytical simplification can be effected by the assumption of two-dimensional flow, the flow regime of the majority of fluid jet amplifiers will be three-dimensional. This is true because of the aspect ratios of 6 to 8 which are commonly used. The relative importance of the three-dimensional effects is dependent on the characteristic being investigated and the downstream distance for any given geometry. The objectives of the first series of tests was to establish information concerning the three-dimensional character of a single bounded jet.

The operation of a proportional amplifier is strongly dependent on the physical displacement of the resultant jet following the interaction. If the resultant jet follows a linear path from the

interaction, then the deflection angle α and the apparent pivot point are sufficient to specify the physical position of the resultant jet. As noted in (17) and (18), the near and far side pocket pressures will have a significant effect on the deflection of the jet. A series of tests was conducted to determine the angle α and the apparent pivot point as a function of the geometric variables, X and Y, and the flow variable, the mfr. Standoff wall static pressures were also recorded for the near and far pockets.

If the angle α and the apparent pivot point are known for known input momentum fluxes, static pressure distributions, and the geometry, the momentum flux of the resultant jet can be deduced by a control volume analysis without knowledge of the profile shape. However, the mass or energy flux values of the resultant jet cannot be so determined inasmuch as they are dependent upon the shape of the velocity profile of the resultant jet. For this reason, and because they would perhaps provide information on the interaction process, a rather complete series of velocity profiles were taken at x/a values of 5, 15, and 30; $z/a = 0, \pm 1, \pm 2$, and $\pm 2\frac{1}{2}$; and for $X = Y = 2a$ with an mfr value of 0.1. There are two obvious restrictions on the generality of the results from this detailed velocity profile survey; these are the single value of the geometric conditions and the single value of the mfr.

The fourth specific test conducted was to determine the effect of nozzle geometry on a single bounded jet and to provide information that could be used to extrapolate the results of the detailed velocity traverses to other geometric

conditions. The purpose of the fifth test, which was similar in intent to the fourth, was to provide information on the relationship between the profile characteristics and the value of the mfr.

EQUIPMENT, MEASURING DEVICES, AND INSTRUMENTATION

Preliminary Flow Study

An early decision, in the overall planning for this study, was to conduct a preliminary experimental program to determine the magnitude of the three-dimensional effects present in a single jet flow between parallel plates. A general description of the experimental flow system for this preliminary study is given below with special emphasis on the construction characteristics which had an apparent effect on the data.

The output of a small centrifugal blower was passed through a diffuser to a plenum chamber; the chamber, which measured 3 x 12 inches in cross-section, contained a honeycomb straightener and screens. A nozzle section, of the beam deflection design, * measuring 3 x 0.5 inches at the exit, was placed downstream of the plenum chamber. The nozzle blocks were cut from a solid piece of wood and then sanded smooth. The flow at the exit of the nozzle was bounded by parallel plates normal to the 3 inch dimension. With this configuration, the flow region was open to the atmosphere on three sides. Although the plexiglass faced upper plate was one continuous piece from the plenum chamber forward, the sheet metal

---

* Appendix A provides an explanation of why this design was chosen.

covered lower plate was, for construction purposes, continuous only from the nozzle exit.

The construction of the traverse device, which provided three translational degrees of freedom, allowed the total and static probes to survey the upper two-thirds of the 3-inch space between the plates for any x, y location.

The velocity profiles, u(z), showed a high degree of asymmetry with respect to the y and z axes. These results indicated that either the flow for this geometry was naturally asymmetric or that the flow was highly sensitive to irregularities in the surface geometry. In order to separate these two possible causes, certain components of the final flow system were assembeled to allow for a study of the single bounded jet.

Single Bounded Jet Study

Flow System

Figure 2 is a schematic drawing of the flow system used for the single jet study. The flow bleed ports at the exit of the diffuser serve three purposes. They provide

i) flow rate control through the nozzle,

ii) stabilization of the diffuser flow,

iii) attainment of stable operating conditions for the centrifugal blower by allowing a high enough flow rate through the blower.

The grid at the inlet of the plenum chamber increased the mixing of the diffuser efflux flow with the fluid in the plenum. This mixing was necessitated by the cross-sectional area difference between the plenum and diffuser exit. The contraction, from the plenum to the egg crate straightener, and the nozzle

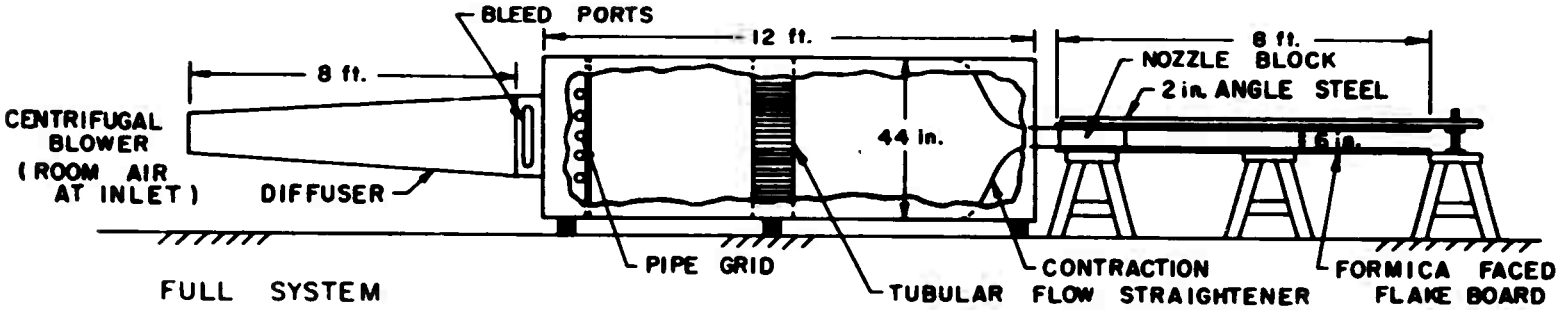

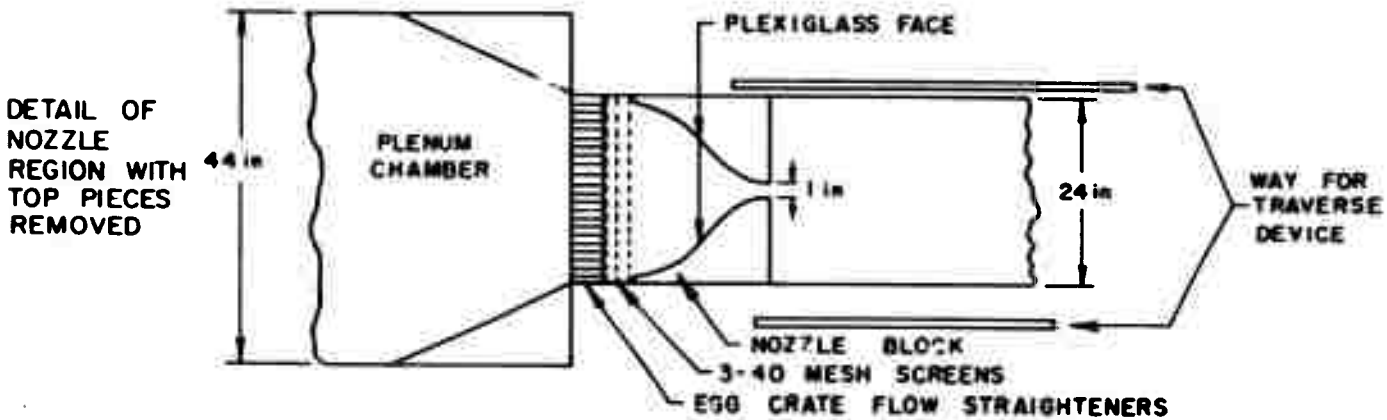

FIG. 2 FLOW SYSTEM - SINGLE BOUNDED JET

shape both followed the beam deflection curve. The honeycomb was 3 inches deep with $\frac{3}{4}$ -inch square openings. Three 40-mesh screens, spaced $1\frac{1}{2}$ -inches apart, were placed downstream of the egg crate straightener.

The nozzle blocks were constructed from eight pieces of $\frac{3}{4}$ -inch plywood which were cut simultaneously to follow the beam deflection curve. After sanding for smoothness, four of the pieces were used with four spacing pieces ($\frac{3}{4}$ -inch) to form each nozzle block. A plexiglass sheet, 0.015 inch thickness, was then fitted and cemented to the plywood.

Since both nozzle blocks came from the same original cutting, the nozzle was symmetric in its final form. The contraction ratio of the nozzle itself was 24; the contraction ratio from the plenum chamber to the nozzle ex was 294. After the flow system was assembled, it was discovered that the vertical faces of the nozzle blocks at the exit were not parallel; this resulted in a 3 per cent variation in the nozzle width. The plates which formed the bounding surfaces for the jet were 5/8" flakeboard with a 1/16" Formica facing. Three 2-inch angle pieces of 0.25 inch thickness supported the upper plate. For the region in the neighborhood of the jet, the plate separation was equal to six inches $\pm$ $1\frac{1}{2}$ per cent.

Measuring Probes, Instrumentation, and Traverse Device

Number 22 hypodermic needles (0.025 inch O. D., 0.0135 inch I. D.), ground to provide a 30 degree conical tip (included angle), were used as total head tubes. This conical tip provided a constant value of the impact pressure over a rather large range of yaw; it also guaranteed that the displacement effect on the total head reading would be negligible

even for the high velocity gradients encountered in boundary layer and jet flows. The response of this probe with respect to yaw is given in Appendix B. Static pressures were measured with a closed end, twelve-hole, cylindrical probe. This probe, proposed by Fage (23) in 1936, has a known yaw and turbulence intensity correction.* A special probe was constructed to provide an accurate location of the maximum velocity position in the flow field. This probe, which employs two total head tubes with a fixed spacing of 3/16 inches, is shown in Figure 3. The probe was mounted with the total and static probes on the variable z traverse device (discussed below). A micromanometer was used to measure the total and static pressures; the instrument has a minimum reading of 0.001 inch of water.

The longitudinal velocity fluctuation, $\overline{u'^2}$, was measured with a Flow Corporation constant current hot-wire anemometer using a tungsten wire of 0.00015 inch diameter and 0.040 inch unplated length. The signal from the amplifier output was observed on a Hewlett - Packard oscilloscope, Model 120A, and quantitative measurements were taken from the Model 12A1 random signal voltmeter. High frequency noise was elminated at the amplifier output by a 7kc low pass filter.

---

* The factor 0.25 given by Fage for the correction coefficient K, where K = (probe reading true-static pressure) $/\rho[\overline{v'^2} + \overline{w'^2}]$ has been recalculated by the writer for the known turbulence structure of the flow between parallel plates. The value for K, used in the present work, was 0.147. The yaw correction given by Fage was for a rather limited velocity range (30-40 fps). A new formulation for yaw corrections was deduced by the writer and is presented in Appendix B.

In order to survey the entire flow field between the bounding plates, a traverse device with three translational degrees of freedom was designed and constructed (x - y - z device). This device is shown in Figure 3 with the total head, static head, and maximum velocity detector probes mounted for a data traverse run. The vertical motion is accomplished by a gear train. A pair of bevel gears change the operator-applied rotation in the x - z plane into a rotation of two spur gears in the x - y plane. A threaded rod, which is fastened to the second spur gear, drives the triangular drill rods. Thus, the vertical position of the probe tip can be directly related to the angular position of the external drive handle. Accurate probe positioning was possible since a vertical motion of 0.05 inches corresponds to an angular rotation of 361 least count divisions on the graduated dial used for the exterior measurement of rotation. The initial z position of each probe was set an exact distance from the plate by the following method.

i) Leads from an ohmmeter were attached to a steel scale (24 - inch) and to the base of the probe (total or static).

ii) The vertical traverse carriage was then moved toward the plate until the probe tip made firm electrical contact with the steel scale which was held on the plate.

iii) Since the steel scale was of known thickness, the vertical position of the probe tip was accurately fixed by advancing the vertical carriage away from the plate and noting where electrical contact was first broken. This latter technique eliminated gear train backlash error.

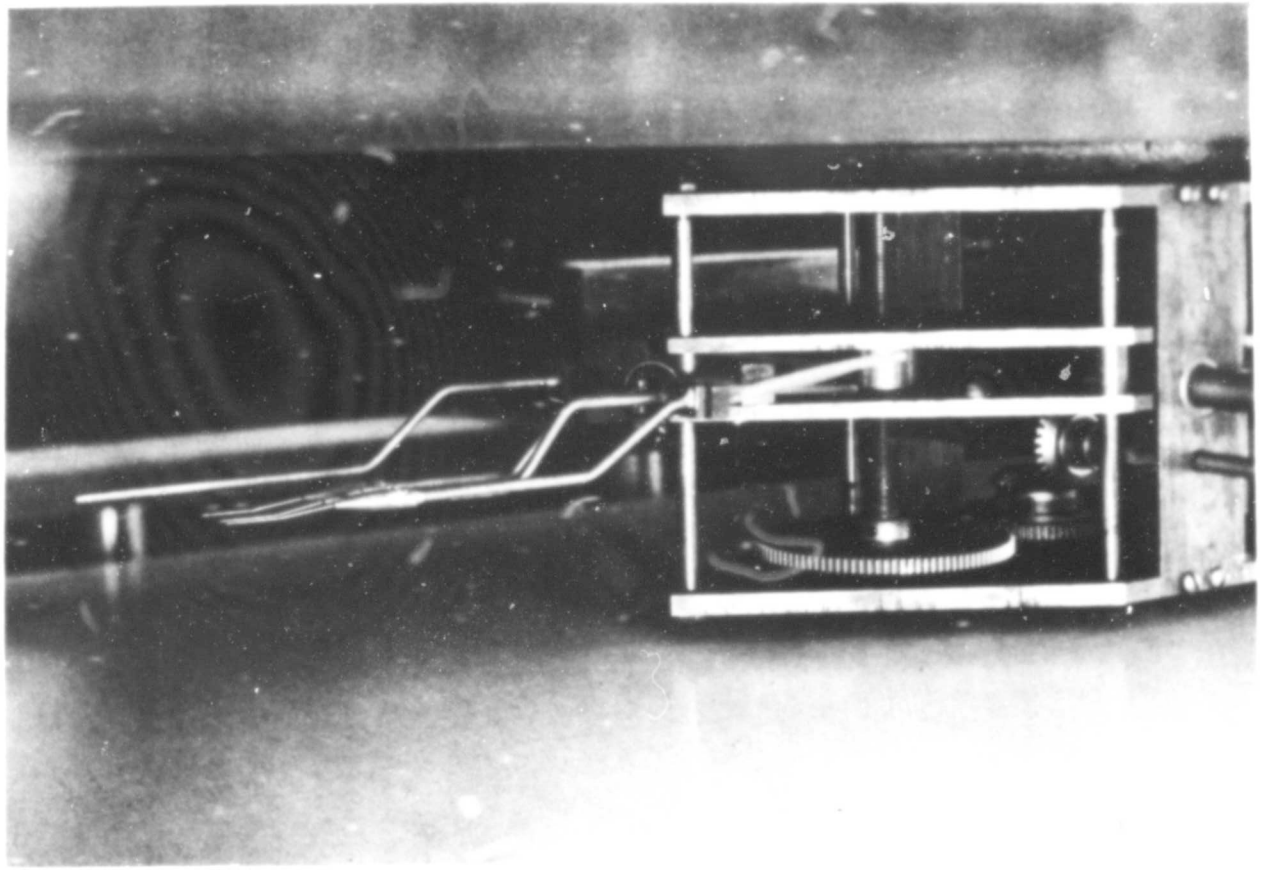

Figure 3 Total, static, and dual probes mounted on the x - y - z traverse device

Intersecting Jets

Flow System

The left control jet nozzle and the right side dummy nozzle shown in Figure 4 were the only additions which were required to change the single jet to the intersecting jet flow system. Both nozzles were constructed with seven static pressure taps (0.04 - inch diameter) set on 0.125 inch centers and located in the $z = 0$ plane of the standoff wall face. The control jet nozzle widths were fixed at 1 inch. Values of $X = 2$ with $Y = 1, 2, 3$ were employed for the present study (X and Y are shown in Figure 1). A thin plexiglas sheet was again used for the nozzle surface. The air supply for the control jet flow was obtained from a separate blower and plenum system.

Measuring Probes, Instrumentation and Traverse Device

The total head, static head, and maximum velocity detector probes used for the single jet study were also used for the intersecting jets. Because of its insensitivity to yaw and its limited upstream disturbance effect, a plate static probe was used in the pockets formed by the nozzle geometry of the interaction region.

An important aspect of the intersecting jets problem is the magnitude of the deflection of the mean flow leaving the interaction region. In addition, to gain accurate data surveys, the local velocity vector must also be known. These two requirements were met with a direction-finding probe.

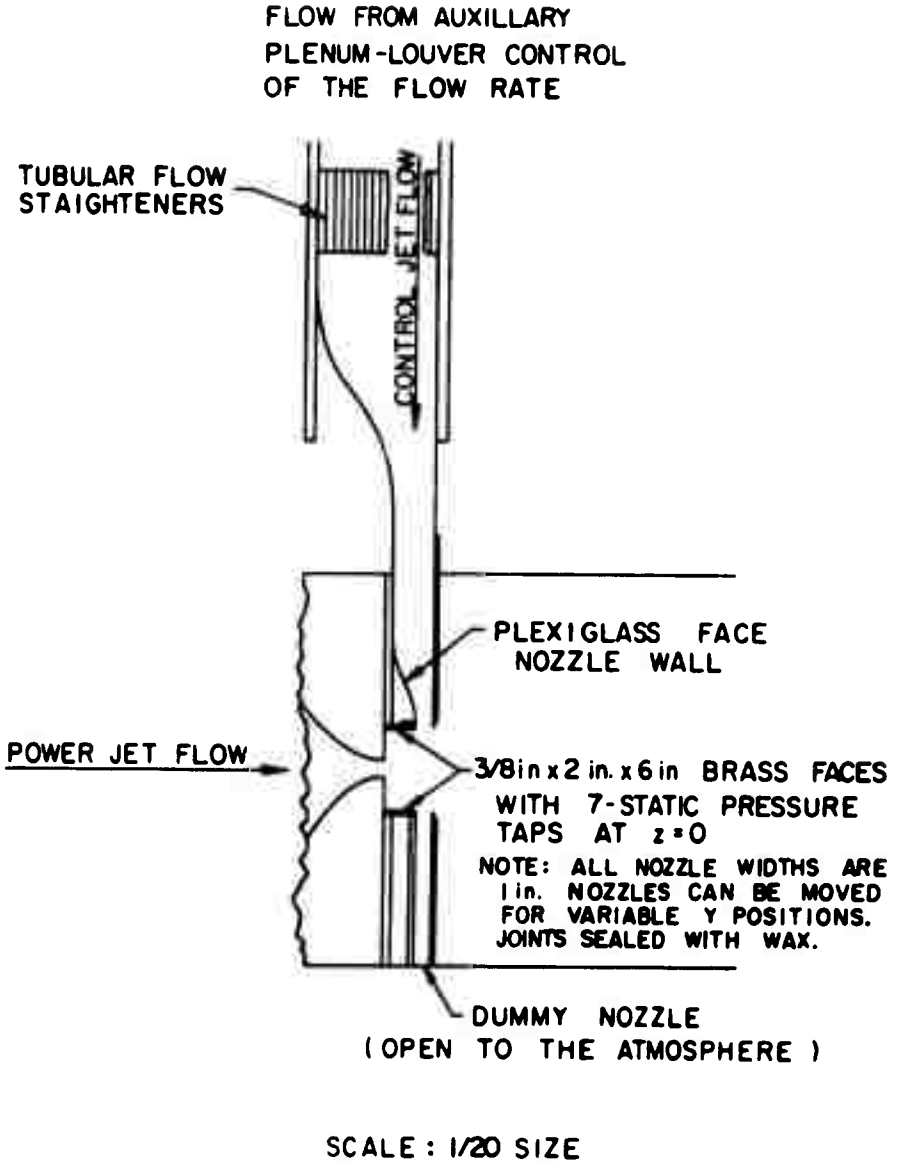

FIG. 4 MODIFIED FLOW SYSTEM FOR THE INTERSECTING JET FLOW STUDY

A three tube probe (trident) shown on the x-y-Θ traverse device in Figure 5, was used as the direction finder. A null-reading between the upper and lower tubes, which were ground to opposing 45 degree angles, gave the mean flow direction. The center tube has a circular opening and responded to the total pressure. The sensitivity of this device was dependent upon the magnitude of the dynamic pressure and varied from $\pm$ 0.05 to approximately $\pm$ 0.4 degrees throughout the entire flow field of interest. This probe was also used with a second positioning technique. For a fixed geometric orientation, a differential readings was used to indicate the angular deflection of the flow for a known value of the dynamic head. Appendix B describes the calibration technique and the calibration formula that was deduced for the fixed position method.

Since the flow leaving the interaction region was not directed along the x-axis, a third geometric variable, Θ(Θ = arc tan v/ u), was required to specify the flow properties. Since various deflection angles would be encountered in this study, a traverse device was designed and constructed that would provide two translational and one rotational degrees of freedom (x-y-Θ device). The traverse device is shown in Figure 5 with the trident probe in the operating position. An important characteristic of this device is that the three variables x, y, and Θ are independent since the rotating element of the traverse device is a circular arc with the probe measuring station fixed at its center. (The variables x, y, Θ are not independent if the axis of rotation is at the base of the probe.) As in the

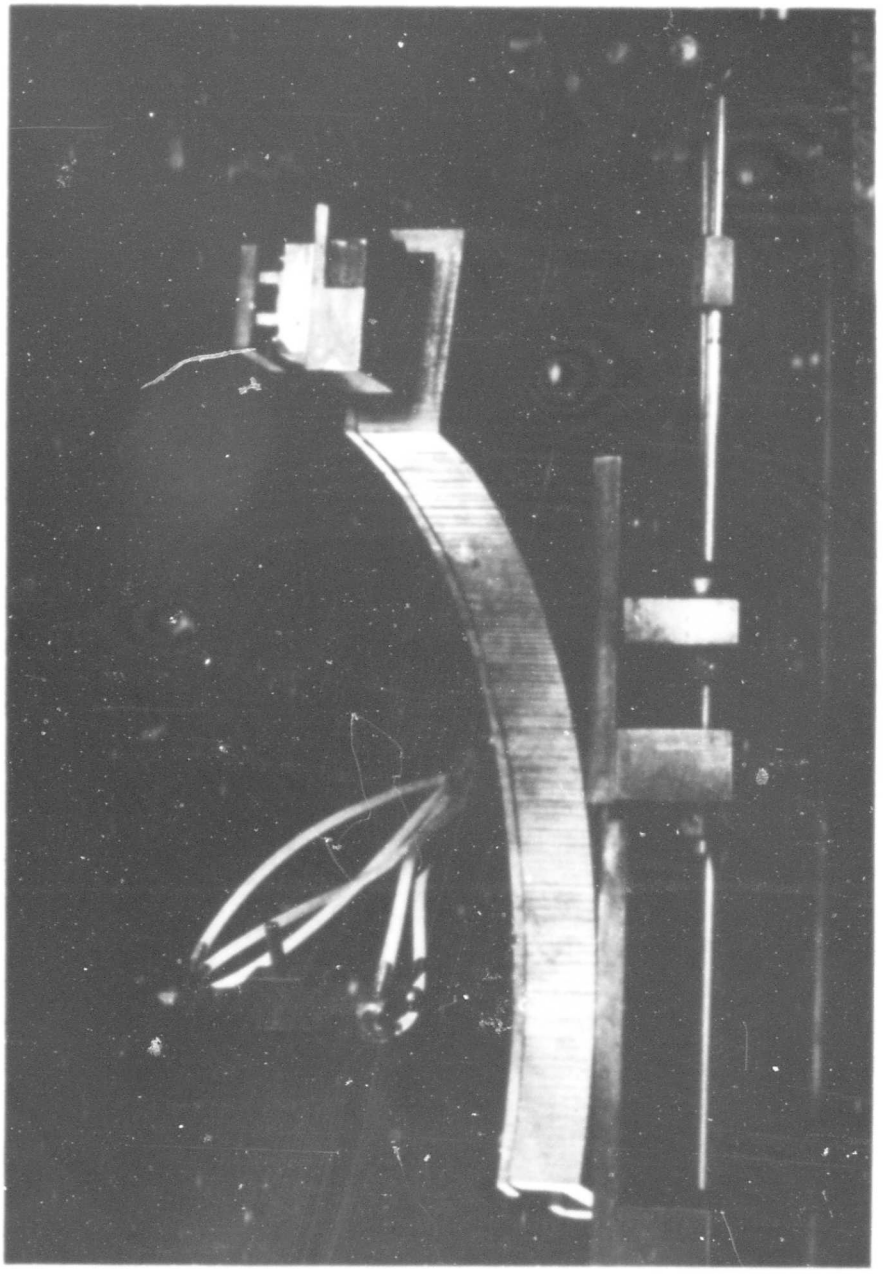

Figure 5 Trident probe mounted on x - y- θ traverse device

operation of the x, y, z traverse device, an exterior rotation by the operator in the x - z plane is converted to an x - y rotation of two spur gears, the second of which is mounted on the arc holding the probe. The exterior rotation is measured and converted into a measurement of the angular position (Θ) of the probe.

Both the traverse devices were checked for possible upstream disturbance effects. Neither device caused a detectable upstream effect on the total pressure as proved by the negative results for the following test:

i) For the carriage in various positions in the flow field, an obstruction was placed at the base of the probe (a 2 inch x 2 inch steel block was used).

ii) The reading of a static pressure probe, mounted on the probe holding device in the normal manner, was recorded with and without the obstruction in place.

iii) The procedure of (ii) was repeated using the total head probe.

The static pressure was unaffected by the x - y - z carriage; however, the x - y - Θ device seriously disturbed the static pressure readings. Consequently, all static pressure measurements were made with the x - y - z carriage and yaw corrections were applied to the static pressure readings so obtained. The correction technique is discussed in detail in a later section.

SINGLE BOUNDED JET STUDY

Results

If the mean velocity distribution for a jet flow is given in a non-dimensional form, two further variables must be specified in order to fix the actual magnitude of the velocity at a given point in the flow field. These two variables, the center line velocity and a quantity which can be used as a measure of the jet width (e.g. b), are referred to as the principal characteristics of the jet. The apparent origin, the length of the potential core region, and mass flux and energy flux widths are additional jet characteristics.

Figure 6* shows the values of the momentum flux thickness, b, for $z/a = 0$ from the present study as compared with b for a two-dimensional jet (Reference 9). Table 3** indicates the values of m, b, and e at $z/a = 0$ and +2 from the present study. Mass, momentum and energy flux ratios, viz., (M/M_0), $2bq_c/aq_0$, and (E/E_0), are presented in Figure 7 along with data from (12) for a two-dimensional jet. Figure 8 presents values of u_m/u_0 from References 9 and 12 and the values from the present study. Also shown on the plot is the value of u_m/u_0 which would be obtained if the velocity measurement (of the present study) were taken from a total pressure probe only. Values of u_c/u_0 for $z/a = 0$ and ± 2 are presented in Table 2.

---

* All figures presenting single bounded jet study results may be found at the end of this section, see page 70 ff.

** The tables are presented in the section "Discussion of Results" page 47 ff.

The reduction of the total and static pressure data for the computation of m, b and e as well as the computations for u(y), v(y), $C_p(y)$ and V(y) are discussed in section VIII A. This discussion is presented in the later section to provide simultaneous discussion of similar measurement and data reduction techniques.

Velocity profiles that span the full 6" between the parallel plates are presented in Figure 9. These $u(z/a)/u_m$ profiles were taken at x/a = 15 and y/a values of 0, $\pm\frac{1}{2}$, ± 1, $\pm 1\frac{1}{2}$, ± 2, and $\pm 2\frac{1}{2}$. The data used in the computation of these profiles were not corrected for turbulence intensity or yaw effects on the total and static probes. The magnitude of these errors is estimated to be such that the computed velocities are approximately 5 per cent too high at $y/a = \pm 2\frac{1}{2}$; the yaw induced errors will decrease to zero at y/a = 0.

Static pressure data, obtained from the traverses for u(z), are presented as a series of isobaric contours in Figure 10. These data are presented as $h_s(y, z)$; the intent is to emphasize the magnitude of the negative static pressures present in the jet core. To permit a ready calculation of a non-dimensional pressure distribution the value of $\frac{1}{2}\rho u_m^2$ (in the same units as h_s) is listed on the figure. A total of 420 data points were used to determine the contours.

Velocity traverses were made at x/a = 5, 10, 15, and 30 for z/a = 0 and x/a = 5, 15, and 30 for $z/a = \pm 2$. The $u(\eta)/u_m$ data points from the z/a = 0 traverses are shown in Figure 11; for reference the analytical curve due to Reichardt (Gaussian error curve) is shown on the same figure. The inclusion of the error curve also provides for the comparison with other two-dimensional jet data. In order to provide a comparison

between $z/a = 0$ and $+2$ which is not clouded by non-dimensionalization on b, Figures 12 to 14 indicate the values of $u(y/a)/u_m$ for $z/a = 0$ and $+2$ at x/a values of 5, 15, and 30.

Distributions of Θ and C_p are presented in the same manner as the lateral velocity profiles. The $\Theta(y)$ distributions are presented in Figures 15 to 18. For visual symmetry, the values of $+\Theta$ are plotted for $+y$ and $-\Theta$ for $-y$. The $C_p(\eta)$ distributions for $x/a = 5$, 10, 15, 20 and $z/a = 0$ are compared with those of the two-dimensional jet (9) in Figures 19 to 22. $C_p(y)$ distributions for $z/a = 0$ and $+2$ are shown in Figures 23 to 25.

A complete tabular listing of the processed data from the y traverses, as obtained from the computer program, is presented in Appendix E.

Figure 26 shows $\bar{u}^2/u_m^2$ data from the three published sources and from the present study for $x/a = 15$ and $z/a = 0$. The data from Heskestad (14) were taken at an x/a value of 47; this was the closest data station to $x/a = 15$ presented in (14). Data from (9) are presented for $x/a = 10$ and 20 (to bracket 15); the data from (13) were taken at $x/a = 17.5$. Figure 27 presents a comparison of $\bar{u}^2/u_c^2$ for $x/a = 15$ and $z/a = 0$ and $+2$.

In order to check the accuracy of the hot-wire equipment, a single point check was made prior to the above noted measurements by measuring $\bar{u}^2$ on the center line of a long smooth pipe (fully-developed flow); agreement to within 2 per cent of published data (23) was found.

Discussion of Results

In the execution of the experimental program, the initial effort was directed to the establishment of detailed velocity traverses as a function of z, at $x/a = 15$, for eleven values of y/a. These profiles, shown in Figure 9, were to provide indications of the flow symmetry and the degree to which the flow appeared to possess a two-dimensional character. The profiles showed a definite bulge near the bounding plates; the maximum point of the bulge moved toward the wall and became more pronounced for increasing values of y. The difference between $u_{z=0}$ and u_{max} became quite large; for example, at $y/a = 2\frac{1}{2}$, $u_{max}/u_{z=0} = 2.50$.

Vortex Stretching Hypothesis

To explain this unexpected phenomenon, a hypothesis based on the action of stretched vortex filaments in the jet was formulated. This hypothesis and further tests which support it are considered to be one of the major contributions of the present study.

A vortex filament, which is generated from the u(y) velocity gradient and extends between the bounding plates, is convected with the mean flow in such a manner that the central portion is swept downstream, whereas the portion attached to the wall is stationary. It is hypothesized that the resultant stretching and re-orientation are responsible for the u(z) velocity profiles, departures from two-dimensional jet characteristics, and other significant effects.

The hypothesis is based on the following physical reasoning. With reference to Figure 28, assume that a vortex filament, which extends from plate to plate, is generated at the location A at time t. Since the vortex filament is, by definition, formed from a given collection of particles, the vortex tube will be convected downstream by the mean flow. The particles adjacent to the bounding plates will remain stationary because of the no slip condition at the wall; the particles in the neighborhood of $z = 0$ will not be constrained and will therefore be swept downstream with the mean flow. Figure 28 also shows the assumed position of the vortex filament at time $t + \Delta t$. The convection does two things; it stretches the filament and reorients the vorticity vector. At time t this vector has a strong component only in the z-direction; at time $t + \Delta t$ the vector will have a weak y component and a strong x and z component near the plates. In an inviscid fluid, the product of the vorticity and the cross-sectional area of a vortex filament is constant. Therefore, if the filament is stretched, the cross-sectional area is decreased and the angular rotation of the fluid particles will be increased. For a viscous flow the effect described above is changed only in degree; the qualitative nature of the phenomenon is unchanged.

The assumed reorientation of the vortex filament performs two functions. The filament is stretched, increasing the vorticity, and a non-random pattern is established which produces an inflow near the $z = 0$ plane and an outflow near the bounding plates.

Two further confirmations (following the u(z) profiles) of the above hypothesis are available from the literature. During

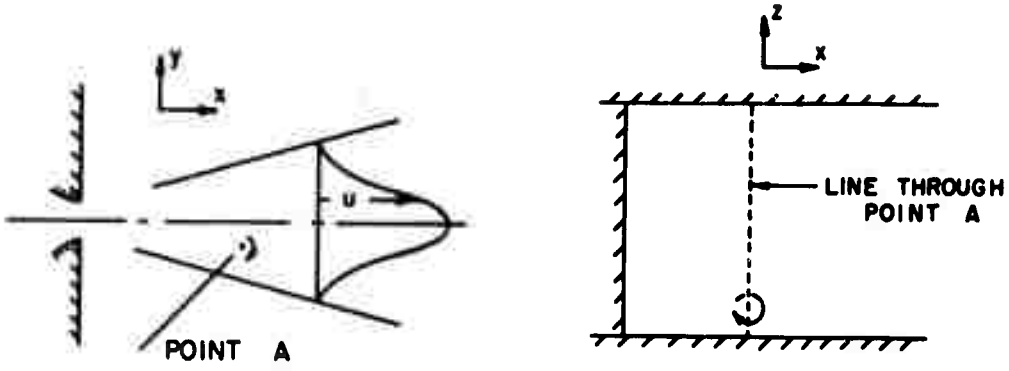

(a.) VORTEX GENERATION AT TIME t

(b.) VORTEX FILAMENT AFTER TIME Δt

FIG. 28 ASSUMED VORTEX PRODUCTION AND STRETCHING

preliminary studies, v. d. H. Zijnen (11) attached two bounding plates at the nozzle exit (geometrically the same as the present study except that an aspect ratio of 20 was used). Measurements of the total pressure at y = 0 and x/a = 40 as a function of z show a definite velocity increase away from the z = 0 plane. The maximum velocity is approximately 12 per cent higher than u_m. Similarly, Curtet (25) has reported data which is an aside to his principal investigation. The geometry of (25) is a rectangular jet exhausting into a rectangular channel. The system of (25) differed from the present study in that there were walls at $\pm y = 5a$ (for the test of interest) and a secondary flow could be introduced parallel to the primary flow at x = 0. Also, the aspect ratio of the nozzle was 10. Curtet made measurements of the velocity in the y = 0 plane at x/a = 200. The results of these measurements show a maximum velocity at z/a = 4 (upper and lower plates at z/a = 5) which is approximately 12 per cent higher than u_m (at the same x/a location). Although the geometry is somewhat different from the present study (viz., the presence of the side walls), the vortex stretching hypothesis may also be used to explain the observations of Curtet.

Although the farthest downstream check was at x/a = 25, data from the present study indicate the same trend as (11) and (25). From Table 2

Table 2

u_c/u_0 As a Function of x/a

z/a	x/a = 5	10	15	25
+ 2	0.995	0.870	0.716	0.552
0	0.988	0.840	0.705	0.531
- 2	0.997	0.843	0.686	0.535

u_c / u_0 at $z/a = +2$ is approximately 4 per cent greater than u_m / u_0 for an $x/a = 25$. For $z/a = -2$ u_c / u_0 is only slightly greater than u_m / u_0 at $x/a = 25$; however, the ratio $u_{z/a=-2} / u_m$ at $x/a = 25$ does show a marked increase with respect to $x/a = 15$. A conclusive statement about the effect is prohibited by the unsymmetric behavior of the u_c / u_0 values with respect to z (probably caused by the 3 per cent deviation in the nozzle width over the height of the nozzle), and the variations of u_c / u_0 with respect to u_m / u_0 as a function of x. These variations may be indicative of a significant flow phenomenon; however, the data presented are not sufficient to establish what this might be.

These three observations, that the velocity is higher away from the $z = 0$ plane, indicate an important aspect of the vortex stretching hypothesis, viz., that the phenomenon is convective. Since there will be a retardation of the flow adjacent to the wall, and since this will manifest itself as a boundary layer-like profile (near the wall) the fluid near the plates will be decelerated. If this effect were to continue (in the absence of other effects) a profile would develop with a maximum velocity at $z = 0$. In order to overcome this effect and establish a higher velocity near the plates, a convective action must occur. This convective action is allowed for in the hypothesis by the inflow at $z = 0$ and the outflow near the plates with the resulting flow from the $z = 0$ plane toward the bounding plates in the neighborhood of $y = 0$.

A natural consequence of the vortex stretching hypothesis would be the existence of larger Θ values as well

as larger mass, momentum, and energy flux thicknesses at $z/a = +2$ as compared with $z/a = 0$ for a given x. Also, a ratio formed in this comparison should have a larger value for larger x/a stations, e.g.

$$\left(\frac{b\,|\,z/a = +2}{b\,|\,z/a = 0}\right)_{x = 30} > \left(\frac{b\,|\,z/a = +2}{b\,|\,z/a = 0}\right)_{x/a = 15}.$$

Figures 15, 17, and 18 show the $\Theta(y/(x-x_o))$ values for $z/a = 0$ and +2, for the x/a values of 5, 15, and 30. Figure 16 shows $\Theta(y/(x-x_o))$ for $z/a = 0$ and $x/a = 10$. The measured Θ values for a two-dimensional jet (14) are also shown on the figures.* The predicted differences in the distribution

---

* The similarity variable, $y/(x-x_o)$, was used because the data of (14) are presented with Θ as a function of $y/(x-x_o)$. The intent of using the non-dimenionalizing factor $x-x_o$ makes a jet of finite width appear to emanate from a nozzle of infinitesimal width. However, there are two commonly used ways to define x_o; they are: (i) the location where the straight line drawn through the u_c/u_o points (for large x/a) crosses the value 1.0 on Figure 8, or (ii) the location where the measure-of-the-jet-width is equal to zero when extrapolated upstream of the core's closing point (e.g. $x_o = -1.572a$) for (9) as indicated on Figure 6. From Heskestad's data the two definitions give the same x_o of 6a; however, it should be noted that the velocity distribution was not measured closer to the nozzle than $x/a = 47$, so that the value of x_o was obtained by a very long estrapolation of the linear curve passed through the data points. Neither of the two distributions follows a linear relationship for the bounded jet nor do they lead to the same x_o (the latter item is in agreement with the results of (9)). For the present study x_o was taken as -3a; it was arrived at by extrapolating the line, which was faired through the four points of the present study, to the x-axis. It is felt that the intent of using the variable $x-x_o$ is better served if the infinitesimal jet width criterion is satisfied, as opposed to the maximum x location where $u_c = u_o$. Finally, the problem of choosing the variable x_o offers a good reason for using a more well defined non-dimensionalizing variable such as b.

are not present for x/a = 5 and 15; however, the Θ distribution for x/a = 30 clearly shows the effect of the vortex stretching. The $u(z/a)/u_m$ profiles at x/a = 15, Figure 9, indicate that the velocity bumps appear closer to the plate than z/a = 2. Therefore, the similar Θ distributions at x/a = 5 and 15 for z/a = 0 and +2 do not provide a rejection of the hypothesis; they merely indicate that the major part of the outflow from the y = 0 plane occurs for z/a greater than +2 at these x/a = locations.

The values of the three flux thicknesses shown in Table 3 also support the hypothesis.

Table 3

Values of m, b, and e for the Single Bounded Jet

		x/a			
	z/a	5	10	15	30
m	0	1.48	2.20	2.92	5.39
m_*	+2	1.50	--	3.05	6.76
b	0	0.534	0.786	1.06	2.02
b	+2	0.564	--	1.10	2.51
e	0	0.869	1.26	1.73	3.33
e	+2	0.951	--	1.80	4.12

The comparison of the ratio's defined above, indicate that the predictions based on a vortex stretching model are correct with the exception of the b and e ratio comparisons between x/a = 5 and 15. As noted above, the u(z) profiles for x/a = 15 indicate velocity bumps for $|z/a|$ greater than 2 indicating that the convection effects of the vortex stretching are not yet felt at z/a = +2. Consequently, the lack of agreement between prediction and observation is not taken as a rejection of the hypothesis.

Another comparison which also supports the hypothesis is shown in Figures 12 to 14, viz. the $u(y/a)/u_c$ velocity profiles for $z/a = 0$ and $+2$. As in the two cases above, only slight differences appear for $x/a = 5$ and 15; however, the profiles at $x/a = 30$ clearly indicate the effect of the outflow from the $y = 0$ plane at $z = +2$ as well as the convection of momentum from $z/a = 0$ to $z/a = 2$.

The static pressure contours, shown in Figure 10 were not expected a priori. From an examination of the figure it appears that the cross section may be broken into three regions; they are:

i) the central portion, approximately bounded by the planes $z = \pm 2$, where the $\frac{\partial P}{\partial y}$ component is the dominant part of the pressure gradient,

ii) a region where the isobars are parallel to the bounding plates and $\frac{\partial P}{\partial z}$ is not only the dominant term of the pressure gradient but has a rather large value,

iii) a transition region between i) and ii).

Athough the following argument is not amenable to quantitative proof at present, it is advanced as an explanation of the observed phenomenon and is based on the vortex stretching hypothesis.

The static pressure distribution in region (i) is of the same general shape as that for a two-dimensional jet (for large x/a). (This comparison is discussed in a later section.) The distribution in the second region (ii) cannot be attributed to either a jet or a boundary layer type of flow. However, if the convected flow due to the vortex stretching is considered as being directed toward the plate with sufficient velocity, the

large (and positive) $\partial P/\partial z$ pressure gradient is simply the decelerating agent for the convected flow. If more complete data were available, the $\partial P/\partial z$ term could be employed as a part of an analysis to evaluate the strength of the convective flow.

Static pressure distributions, presented as $C_p(y)$, for $z/a = 0$ and 2 at $x/a = 5$, 15, and 30 are shown in Figures 23 to 25. The important feature of Figures 24 and 25 is the high velocity portion at $z/a = +2$ wherein the pressure is constant for a width of (approximately) ± 1 inch and ± 2 inches. As noted in the discussion of the static pressure contours for the $x/a = 15$ location, the higher pressure near the wall is probably the decelerating agent for the convected flow from the $z = 0$ plane.

Turbulence Measurements

Measurements of $\overline{u^2}$ were made in the $z/a = 0$ and +2 planes with the intent of providing data for comparison with the two-dimensional jet and possible support data for the proposed vortex stretching hypothesis. Figure 26 presents the $\overline{u^2}$ data which is available for the two-dimensional jet; data from the present study for $z/a = 0$ is presented on the same figure. It is obvious from the figure that there is no general agreement for the two-dimensional jet case. There are several possible explanations for the differences among the results of (9), (15), and (14). It is unlikely that the Reynolds number differences will account for the different magnitudes and curve shapes since all tests were conducted in the subsonic range and the Reynolds numbers are within the same order of magnitude. It would not seem likely that the aspect ratio

differences would be significant; the only discrepancy may lie in the work of (13) wherein the ratio of 25 may be too low to obtain a two-dimensional flow. The instruments used are noted for reference puposes. The symbols I and T on the figure denote the type of instrument used (I = constant denotes a constant current device, T = constant denotes a constant temperature device). The linearity of the constant current instrument may be in question for high relative intensities; near the outer portion of the jet the local intensity approaches values of 50 to 60 per cent ($\bar{u}^2 / u^2$). The two most likely factors that might cause the observed differences are the nozzle geometry used and the turbulence intensity at $x/a = 0$. The $\bar{u}_0^2 / u_0^2$ factor was not reported for (13) or (14); however the $\bar{u}_0^2 / u_0^2$ for (14) will probably be of the same order as the value for fully developed flow between parallel plates. Of the three nozzles used, the one from (9) would appear to be the form most commonly used for applications.

With the lack of a known reference curve for a two-dimensional jet, it is difficult to make a meaningful comparison with the two-dimensional case; however, certain differences are pertinent. With reference to the curves from (9) and (14), it appears that there is less turbulence energy in the central portion of the bounded jet than in the two-dimensional jet. Since the velocity gradient, u(y), is similar to that for the two-dimensional jet (in fact, it is slightly steeper), one would expect at least as much turbulence energy for the central portion of the bounded jet. If this is indeed the case, three other effects could cause the lower $\bar{u}^2 / u_m^2$ curves for $0 \leq |y/x| \leq 0.06$. If a convective action were present, the lower $\bar{u}^2 / u_m^2$ in

this region could be the result of a convection from the $z = 0$ plane to the $\pm$ z planes. Alternatively, if a non-random flow pattern existed with its major flow components in the y and/or z directions, the energy apparently missing from the $\bar{u}^2$ term could be present in the $\bar{v}^2$ and/or $\bar{w}^2$ terms. Therefore, if the total turbulence energies for the two cases were equivalent, this would explain the lower values of $\bar{u}^2 / u_c^2$. These two effects are natural results of the vortex stretching hypothesis. The third possibility is an increase in the dissipation of the turbulence energy. An energy balance in (14) indicates that the dissipation term is fairly large in the neighborhood of $y = 0$. Therefore, if some action increased the dissipation, this would also explain the lower $\bar{u}^2 / u_c^2$. A higher dissipation would result from a larger fraction of the energy in the small eddies; however, there is no reason to attribute this effect to the vortex stretching action. The generation of small eddies by the plates* is not a reasonable explanation unless there is a strong transport effect that would carry them from the relatively thin boundary layer up to the $z/a = 0$ plane. The convection due to the vortex stretching will not do this; this convective action will primarily transport large eddies from the outer portion of the jet.

With regard to Figure 27 which compares the

---

*Although there is no way to compare directly free shear and boundary layer type flows, the boundary layer flows will, in general, have more energy in their small eddies; this is due to the existence of the very high velocity gradients near the wall and the small length scale of the boundary layer thickness.

$\bar{u}^2 / u_c^2$ values of $z/a = 0$ and $+2$, three regions are apparent:

i) region (i), for $0 \leq y/x < 0.07$

ii) region (ii), for $0.07 \leq y/x < 0.14$

iii) region (iii), for $y/x \geq 0.14$.

The significance of (i) is that the $\bar{u}^2$ for $z/a = +2$ is higher than for $z/a = 0$. Since the u(y) gradient for $z/a = +2$ is less steep than that of $z/a = 0$, the (apparently) greater turbulence energy for $z/a = +2$ requires explanation. A convection effect from $z/a = 0$ to $\pm z/a$ values for the neighborhood of $y = 0$ is predicted by the hypothesis; therefore, the turbulence energy may be convected toward the boundary plates and this would explain the greater $\bar{u}^2$ at $z/a = +2$. However, the apparent energy is still much less than that for (9) and (14). The energy generated in the wall shear layer and diffused outward may account for all or part of the difference and this explanation would be independent of the hypothesis. Without further measurements these two effects cannot be accurately separated. There is however no production of turbulence from the $-\rho\overline{uw}$ stresses, since $\partial u/\partial z = 0$ as seen in Figure 9.

Region (ii) is undoubtedly a direct result of the steeper velocity gradient at $z/a = 0$ leading to a higher production of turbulence energy.

Region (iii) is interesting but nebulous. The jet is physically wider, and this alone may account for the difference in $\bar{u}^2 / u_c^2$. Also, production of turbulence energy will result from the term $\overline{uw}\ \partial u/\partial z$. The much higher intermittency factor for $z/a = +2$ means that the relative intensity of turbulence in the turbulent fluid at $z/a = +2$ is much lower than

for $z/a = +2$. This result is incompatible with the vortex stretching hypothesis as stated because the convective action of the secondary flow should introduce high turbulence intensity fluid for large $|z|$ (from the central region) and low turbulence intensity fluid for small $|z|$ (which has been entrained from the atmosphere). However, there are three possible explanations for this.

i) If the secondary flow occurs entirely within the jet as bounded by the viscous super layer * proposed by Corrsin and Kistler, then the secondary flow will not bring in ambient fluid, but will convect fluid from the region near the plates to the region of $z/a = 0$. Since some of this fluid will have come from the shear layer near the plate it will have a relatively high turbulence intensity.

If this explanation describes the actual flow conditions, then the explanation of a higher dissipation for small $|z|$ and small $|y|$ (as compared with large $|z|$ and small $|y|$) would be supported. The original discussion of this point is on page 57.

ii) Diffusion in the $\pm y$ directions of the relatively high intensity turbulence from the middle section of the jet at $z/a = 0$ may be strong enough to overcome the convective action of the vortex stretching.

---

* The viscous super layer, in the model of (26), is a very thin region (wherein viscous forces predominate) which is the actual and instananeous boundary of the jet. It is the contention of (26) that the entrainment of ambient fluid occurs in the interaction between this layer and the ambient fluid; that is, vorticity is transmitted only through this interaction.

iii) The constant current device used is also unreliable for large turbulence intensities ($(\overline{d}^2)^{1/2} / u = 30$ per cent) and the intermittency factor was determined simply from a visual inspection of the oscilloscope. Both factors make the accuracy of the data somewhat questionable. It should be noted that whereas the actual difference in $\overline{d}^2 / u^2_c$ values for the two z values is no greater than for region (i), the value at $z/a = +2$ is 50 per cent higher than that for $z/a = 0$ in region (iii). Although it is also true of the turbulence data in general, no concrete statements may be made about (iii) without more information; however, for a reasonable understanding of the jet flow between bounding plates, these and other phenomena should be investigated further.

Comparison with the Two-Dimensional Jet

It should be borne in mind throughout this discussion that the existence of the vortex stretching action prohibits the flow from assuming a truly two-dimensional character. However, certain properties may exhibit behavior which are sufficiently two-dimensional in nature to assist in the understanding of jet flow between parallel plates as well as to provide certain bases for prediction and design efforts.

From the literature survey, the Gaussian error curve provides an accurate representation of the non-dimensional velocity profile. From Figure 11 it can be seen that the non-dimensional profiles of the present study agree quite well with those of the two-dimensional jet. However, this is only part of a meaningful comparison. Two parameters are employed to non-dimensionalize the profiles, u_m and b. Consequently, if a comparison of the actual velocities were of interest, it would also be necessary to compare the u_m / u_0 and b(x) distributions. From Figures 6 and 8 it may be seen that b is less and u_m is greater for the bounded jet at a given x in the region downstream of the core's closing. Considering these two effects, it is only fortuitous that they combine to yield a non-dimensional distribution which agrees so well with the Gaussian curve of (9). These two effects, higher u_m and lower b, are compatible with the vortex stretching hypothesis. Because of the inflow at z = 0 the jet should be narrower (lower b), and from continuity considerations the central region velocity should be higher, (higher u_m). Another observation with regard to Figure 8 is that u_m approaches the two-dimensional value for large x/a. It is assumed that this is

natural result of the vortex stretching convective effects. The vortex stretching convective action is discussed in detail in the previous section on the vortex stretching hypothesis.

Another example of the importance of comparing more than the non-dimensional profiles is available from the literature. Olson and Miller (16) state that their velocity profiles follow a Gaussian distribution. This might lead one to presume that the jet flow between bounding plates (aspect ratio 12), and at a Mach number at the power jet exit of 0.66, was equivalent to the incompressible two-dimensional jet flow. However, Figure 8 shows the values of u_m / u_0 for two two-dimensional jet flows and the values from Olson and Miller (16); the much higher values from (16) indicate that the jet is spreading less rapidly (since the non- dimensional profiles are both Gaussian distributions). A measure of the rate of spread may be taken from the angle that a line connecting the $u_m / 2$ velocity points makes with the x axis. This angle for Olson's data was 4.3 degrees; it was 5.5 degrees for the data of Miller and Comings.

The mean velocity profiles provide an example of a comparison based on the distribution of a given quantity. Other comparisons of this type are presented later. The u_m and b comparisons are examples of two comparisons based on the characteristics of the jet.

A third comparison between the characteristics of the two flow cases is offered by Figure 7 which shows the mass, momentum, and energy flux ratios. (Actually, physically meaningful values of the mass, momentum and energy fluxes for the bounded jet at a given x/a location should be determined as an average of measurements at several z/a locations. However, the intent

here is to compare the center plane flow with the two-dimensional case; consequently, the single traverse evaluation for the ratios is a suitable one to use.) The higher ratios for the bounded jet up to $x/a = 15$ indicate that a greater entrainment is occurring up to this x location. The ratio values at $x/a = 30$ are less than would be expected on the basis of the values up to $x/a = 15$. The lower values at $x/a = 30$ may be explained by the convective effects of the vortex stretching hypothesis. Lower ratio values for $z/a = 0$ would occur if a convective action swept the high velocity fluid from the central region of the jet. As observed in the earlier section, the convective action appears to be much stronger for $x/a = 15$ to 30 than for $x/a = 0$ to 15. This is also compatible with the hypothesis in that it appears to be a developing effect. Also, in view of the definitions of the three ratios, the energy flux ratio should be the most sensitive to this loss in high velocity fluid and the mass flux ratio should be the least sensitive. From the figure, it is seen that this is indeed the case.

Two other items are noteworthy. The first of these involves a comparison between the three flux ratios for the bounded jet as compared with the two-dimensional jet. Specifically, the difference between the E/E_0 values is greater than the difference between the $2bq_m/aq_0$ values or the M/M_0 values. The reason for this is two-fold; (i) E was calculated in (12) by integrating the term u^3; in the present study, it was evaluated by integrating (q) (u) (Note: $q = \frac{1}{2} \rho V^2 \neq \frac{1}{2} \rho u^2$) and (ii) the higher u_m/u_0 as shown in Figure 8 leads to greater E values since the integral is dependent on the third power of the velocity.

The second item is the existence of momentum flux ratio values which are greater than 1.0. This can be partly explained by the static pressure distribution across the jet. Consider a control volume with surfaces that are the nozzle exit, a downstream plane of constant x, two side planes which are placed such that the entrainment flow enters the control volume at a Θ of $\pm$ 90 degrees, and two planes of constant z placed at $z = +\Delta z$ and $z = -\Delta z$ (where Δz is small with respect to the $|z|$ of the bounding plates). The x-direction momentum equation can then be written as:

$$\int_{-\Delta z}^{+\Delta z} \int_{-\frac{W}{2}}^{\frac{W}{2}} \rho u^2 \, dy \, dz - 4aq_0 \Delta z - \underset{\text{at } z = -\Delta z}{\int_{-\frac{W}{2}}^{\frac{W}{2}} \int_0^x \rho uw \, dx dy} + \underset{\text{at } z = +\Delta z}{\int_{-\frac{W}{2}}^{\frac{W}{2}} \int_0^x \rho uw \, dx dy}$$

$$= \int_{-\Delta z}^{\Delta z} \int_{-\frac{W}{2}}^{\frac{W}{2}} P_{x=0} \, dy \, dz - \int_{-\Delta z}^{\Delta z} \int_{-\frac{W}{2}}^{\frac{W}{2}} P_{x=x} \, dy \, dz + \underset{\text{at } z = +\Delta z}{\int_{-\frac{W}{2}}^{\frac{W}{2}} \int_0^x (-\rho \overline{dw}) \, dx \, dy} - \underset{\text{at } z = -\Delta z}{\int_{-\frac{W}{2}}^{\frac{W}{2}} \int_0^x (-\rho \overline{dw}) \, dx \, dy}$$

where W is the width of the control volume and the viscous shear is assumed to be negligibly small. It is reasonable to assume that $P_{x=0}$ is approximately equal to atmospheric pressure; consequently, if $P_{x=x}$ is considered to be a gage pressure the first left hand side term is zero.

The effect due to the x-momentum which is carried in by the (three dimensional) velocity component w is probably a significant factor; however, there is no data from which this term may be evaluated.

The shear stress terms (on the right side) are of unknown importance. It is reasonable to assume that the correlation term $(\overline{u'w'})$ is small because of the flat u(z) velocity profile, see Figure 9; however, the area over which this shear stress acts is quite large, viz., xW.

Although four of the eight terms of the equation cannot be numerically specified, the equation can be manipulated to yield the effect of the static pressure.

Dividing by $4aq_0 \Delta z$ and rewriting the equation yields

$$\frac{2bq_m}{aq_0} - 1$$

for the first two terms on the left side of the equation. (Note that the first integral on the left is equivalent to $8bq_m \Delta z$.) This quantity can be formed from the sum of three similar terms that result from the two independent sets of terms on the right side and the last two terms on the left side, viz., the pressure, the shear stress and the negative of the other momentum flux terms. For example the pressure effect may be solved for as

$$\left[\frac{2bq_m}{aq_0} - 1\right]_{\substack{\text{pressure} \\ \text{effect only}}} = -\int_{-\frac{W}{2}}^{\frac{W}{2}} \frac{P_{x=x}}{2aq_0}\, dy \,.$$

In order to obtain a quantitative evaluation for the magnitude of the pressure effect, the above integral was evaluated at $x/a = 15$ using the C_p data of Figure 24 and the value was found to be $-0.015\, aq_0$.

The value of $2bq_m / aq_0$ that was computed from the experimental data was 1.07; consequently, the static pressure effect accounts for approximately one-fourth of the difference between $2bq_m / aq_0$ and 1.0. This implies that either one or both of the terms resulting from the other two effects are quite important. It is also possible that the static pressure assumption is in error, viz., $P_{x=0} = 0$, however, it is not expected that this is the case.

In addition to the velocity profiles, three other distribution comparisons may be employed; they are $\overline{u^2} / u_m^2$, Θ, and C_p. The distribution of $\overline{u^2} / u_m^2$ from the present study has been compared with the distributions of three two-dimensional jets in the preceding section (VI - B - 1). Figures 15 and 18 present the $\Theta(y/[x-x_o])$ distribution from the present study as compared with the data of Heskestad. The choice of x_o for the present study is discussed in the previous section. Although the data from (14) is taken at an $x/a = 100$, the comparison with the present study is still valid since the Θ solution is similar (for the two-dimensional jet). The striking difference between the distributions for the two-dimensional and the bounded jet is the magnitude of Θ for small y values. This may indicate that the vortex stretching action is not the sole difference between the two flows since the Θ differences cannot be explained by the hypothesis.

The C_p distributions as a function of η are shown in Figures 19 to 22 along with the data from (9). The C_p profiles for x/a = 5 and 10 are quite different from those of the two-dimensional jet. The distribution at x/a = 5 resembles the shape of the distributions for the developing flow region of (9). This may indicate that the bounded jet develops much more slowly even though the non-dimensional velocity profile at x/a = 5 appears to possess a similarity solution, (see Figure 11). The C_p distribution at x/a = 10 for the bounded jet appears to follow a fairly smooth transition in shape from x/a = 5 to x/a = 15 but it does not correspond to the two-dimensional distribution. The shape of the curve and the magnitudes of the values for the bounded jet are again quite different from the two-dimensional jet at x/a = 15. The magnitude of the difference is increased but the curve shape is becoming more like the two-dimensional case for x/a = 30. If the absolute values of the static pressures were compared, the magnitude differences would be greater for x/a = 15 and 30 because, with reference to Figure 8, u_m/u_0 is greater for the bounded jet at the same x/a location. Two factors are of importance in the over-all comparison between the bounded and the two-dimensional jet: (i) the lower pressures and (ii) the wider regions about y = 0 of these lower pressures. In a previous section, it was stated that the lower $\overline{u}^2/u_c^2$ values of the bounded jet for the neighborhood of y = 0 might be a result of more turbulence energy being present in the $\overline{v}^2$ and $\overline{w}^2$ components. If it is assumed that the relationship for the two-dimensional jet (proposed by Townsend (10) and verified by Miller and

Comings (9)) viz.,

$$P + \rho \overline{v}^2 = P_{atm},$$

provides at least an approximate description for the flow at $z/a = 0$ for the bounded jet, then the large differences in the static pressure magnitudes would result from a relatively higher $\overline{v}^2$. This would support the earlier contention that more turbulence energy is contained in the $\overline{v}^2$ component.

Conclusions From the Study of the Single Bounded Jet

An incompressible turbulent jet issuing from a nozzle of rectangular cross-section with an aspect ratio of 6 and bounded by parallel plates normal to the longer sides of the nozzle is highly three-dimensional and has the following characteristics (where the jet axis is in the x-direction and the bounding plates are planes of constant z):

i) Complete velocity profiles 15 nozzle widths downstream from the nozzle exit show that in planes of constant y removed from $y = 0$ the maximum velocity occurs near the bounding plates and not midway between them. For example, the ratio of the maximum velocity to the centerplane velocity was approximately 2.5 at a y distance of 2.5 nozzle widths.

ii) The non-dimensional velocity profiles in xy planes of the bounded jet agree with those of the two-dimensional jet of Reference 9.

iii) The centerline velocity is higher and the momentum flux width is lower (downstream of the potential flow core) than for a two-dimensional jet.

iv) In the high velocity region of the jet in an xy plane, the flow angle of the mean velocity (directed away from the $y = 0$ plane) is larger for the bounded jet than for the two-dimensional jet.

v) For sufficiently large downstream distances, the flux ratios (mass, momentum and energy with respect to the nozzle exit) in xy planes near the bounding plates are greater than those in the midplane between the bounding plates.

vi) For all x/a locations, the static pressure distribution (as a function of y) shows a marked change from that of the two-dimensional jet. Near the bounding plates, $\partial P/\partial y = 0$ in the high velocity region of the jet.

vii) The distribution of $\overline{u}^2$ across a bounded jet is unlike that across a two-dimensional jet (even though there is lack of agreement in the literature for the two-dimensional distribution of $\overline{u}^2$.

The vortex stretching hypothesis which was formulated to explain the above item i) has been verified by or found to be compatible with items ii) to vii).

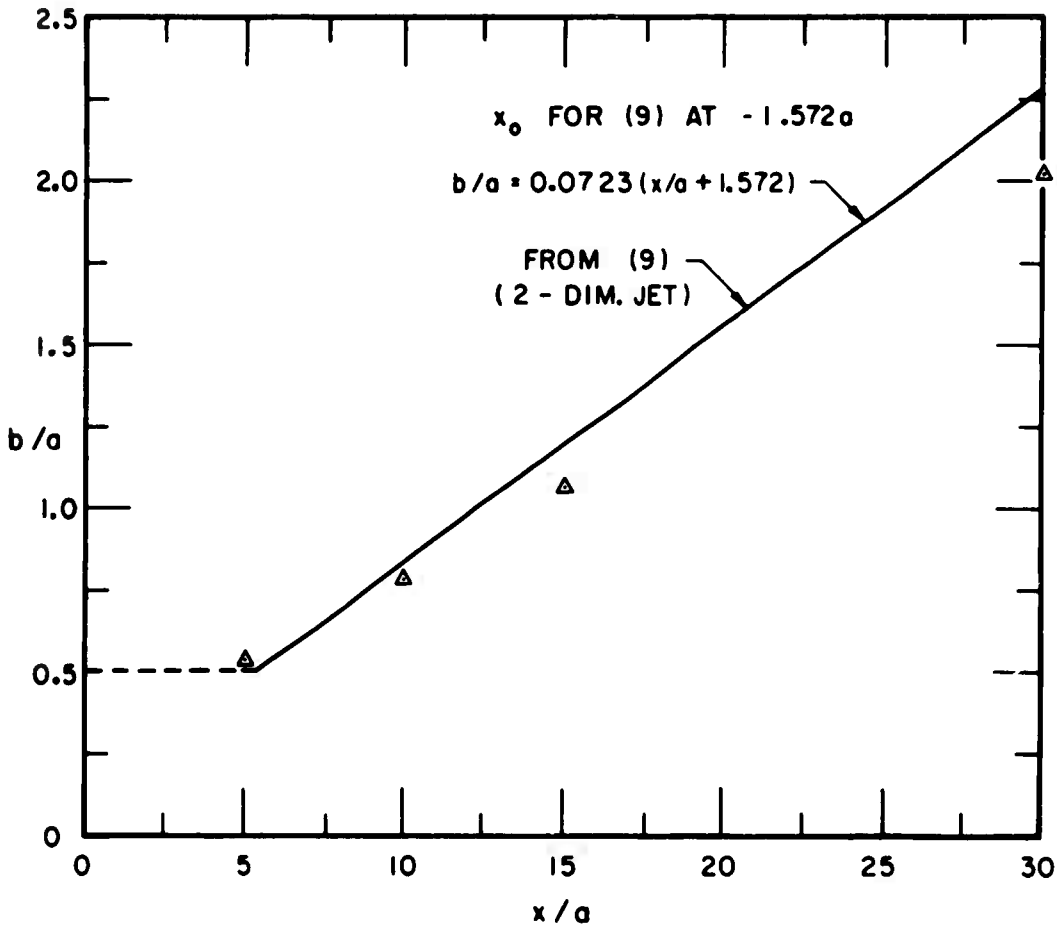

FIG. 6 b/a VERSUS x/a

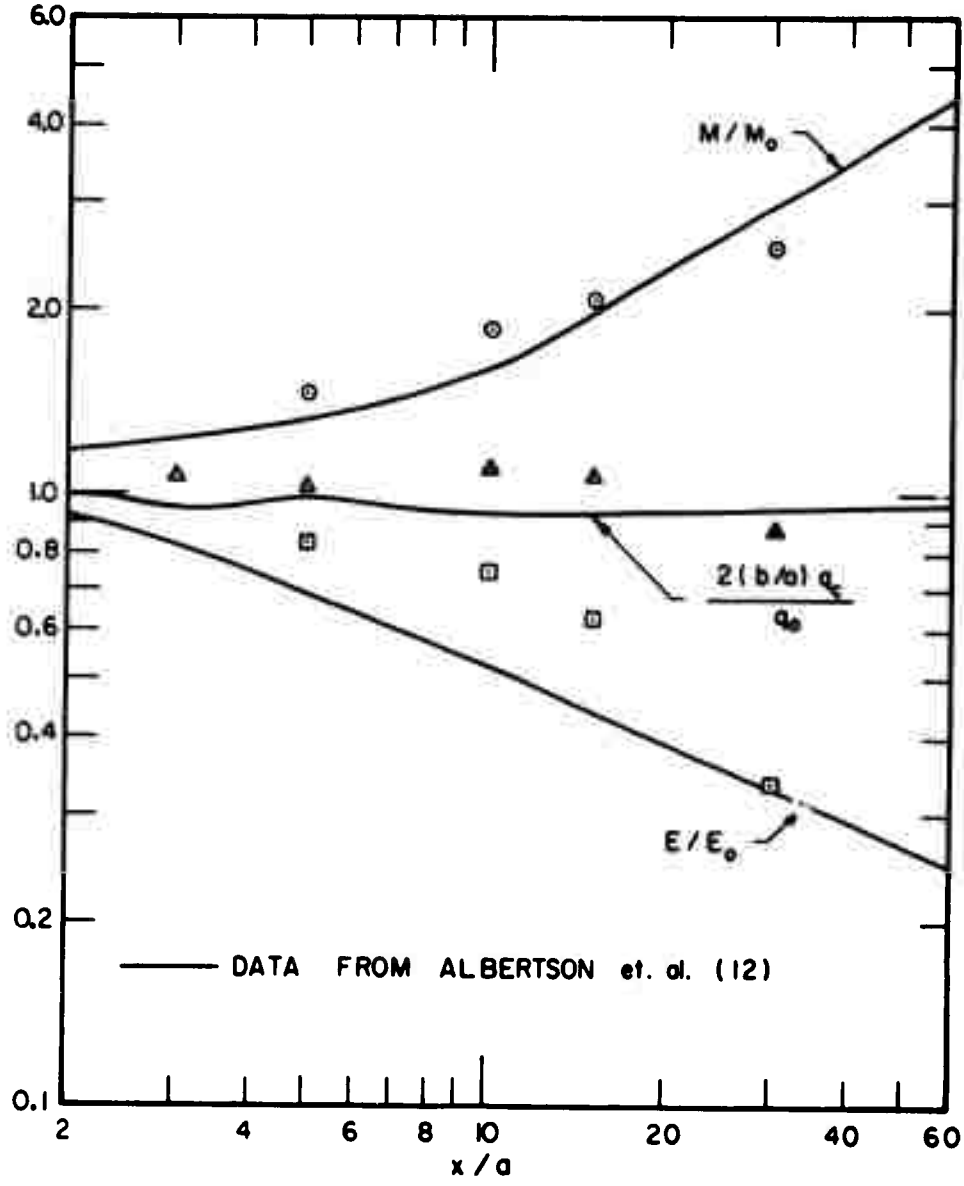

FIG. 7 MASS, MOMENTUM, AND ENERGY FLUX RATES FOR THE BOUNDED AND THE TWO DIMENSIONAL JET

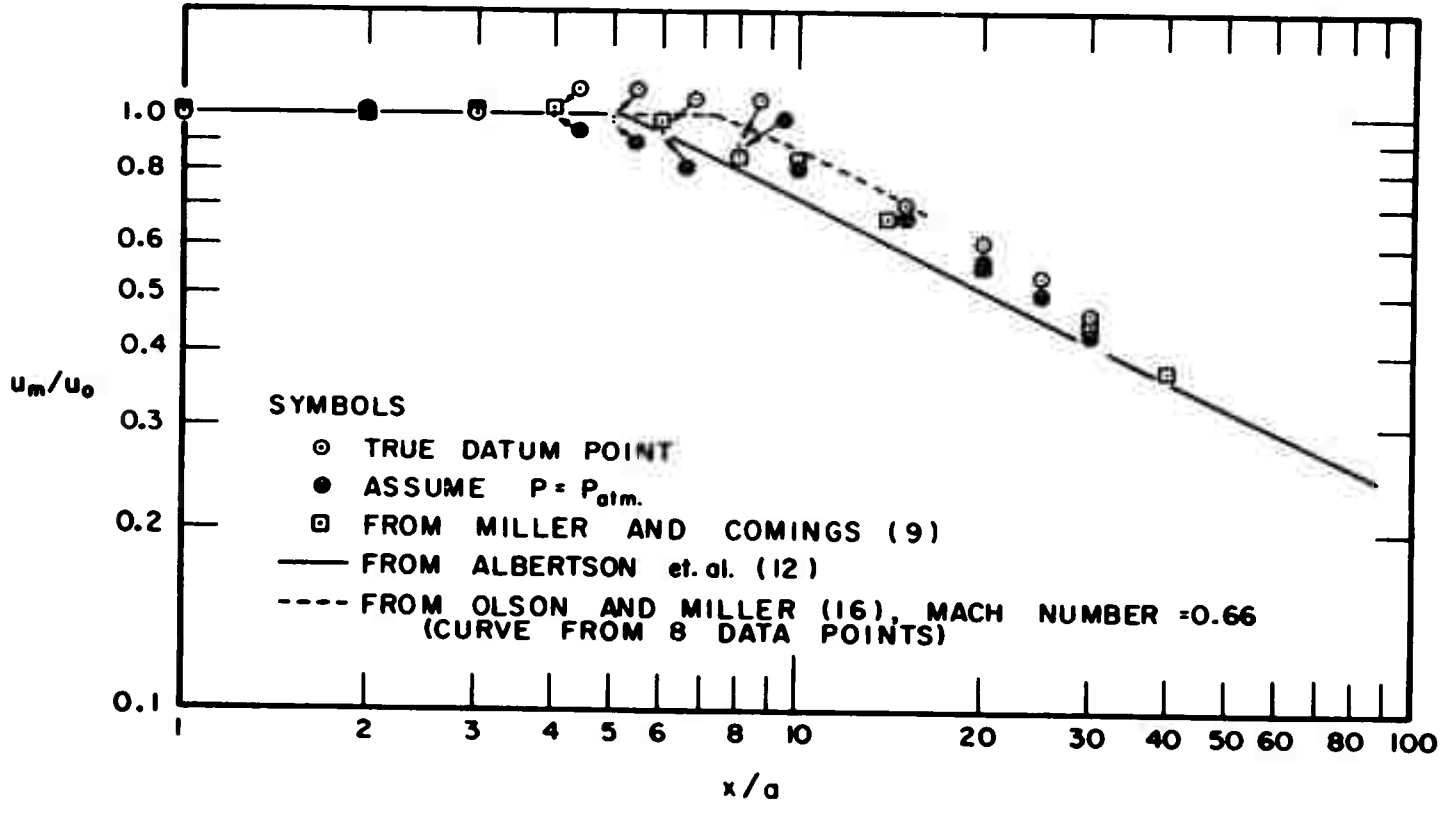

FIG. 8 u_m/u_o FROM (9), (12), (16), AND THE PRESENT STUDY

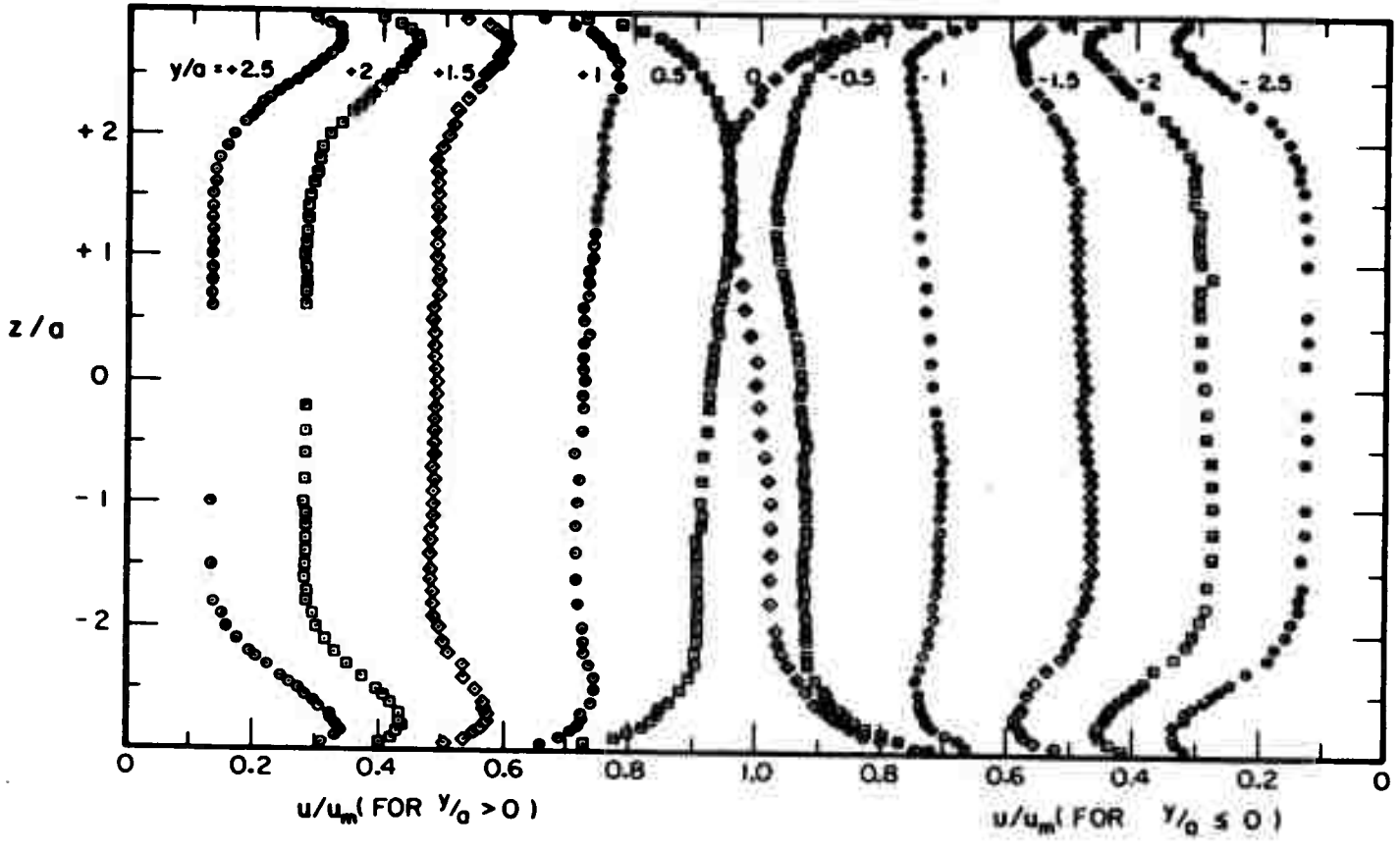

FIG. 9 $u(z/a)/u_m$ AT $x/a = 15$

NOTE: I) NUMERICAL VALUES ARE NEGATIVE INCHES OF WATER GAGE PRESSURE $\times 10^3$, e.g. $80 = -(P - P_{atm}) \times 10^3$ in. water

II) CONTOURS ARE BASED ON 420 DATA POINTS

III) $1/2\ \rho\ u_m^2 = 1104 \times 10^{-3}$ in. water

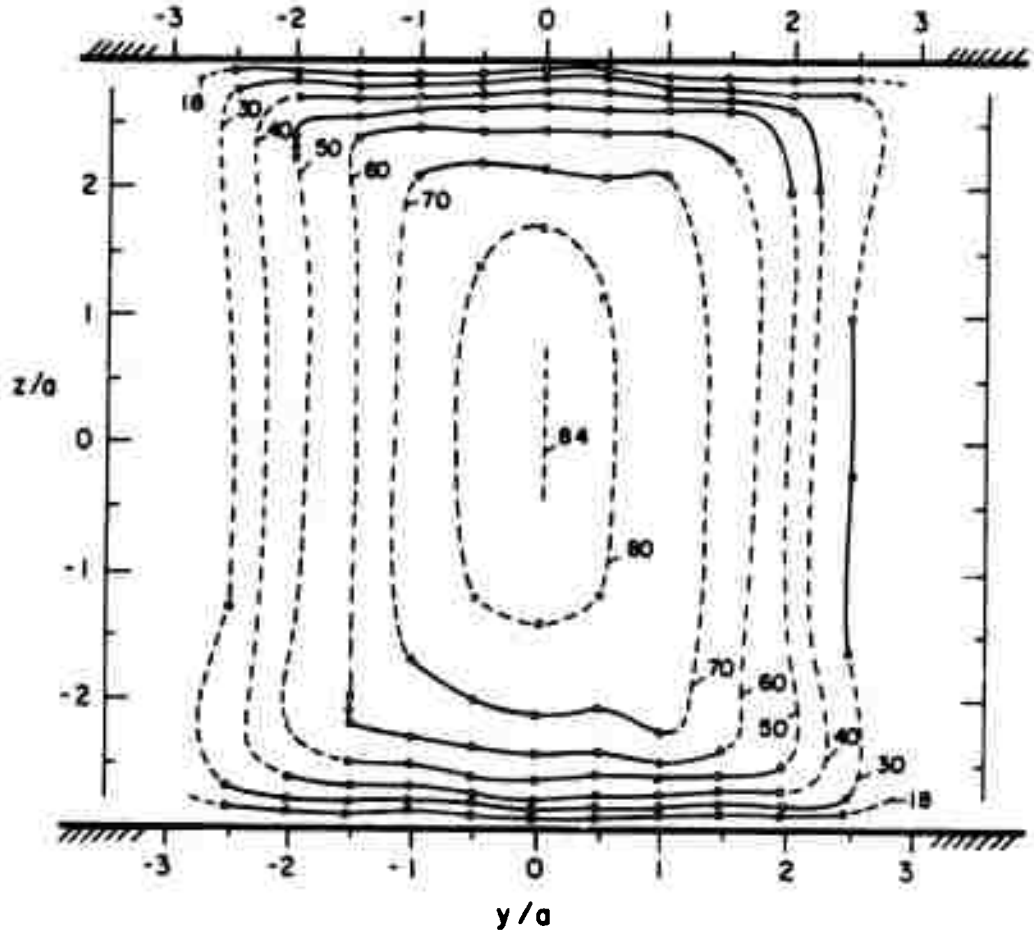

FIG. 10 STATIC PRESSURE CONTOURS , x/a = 15

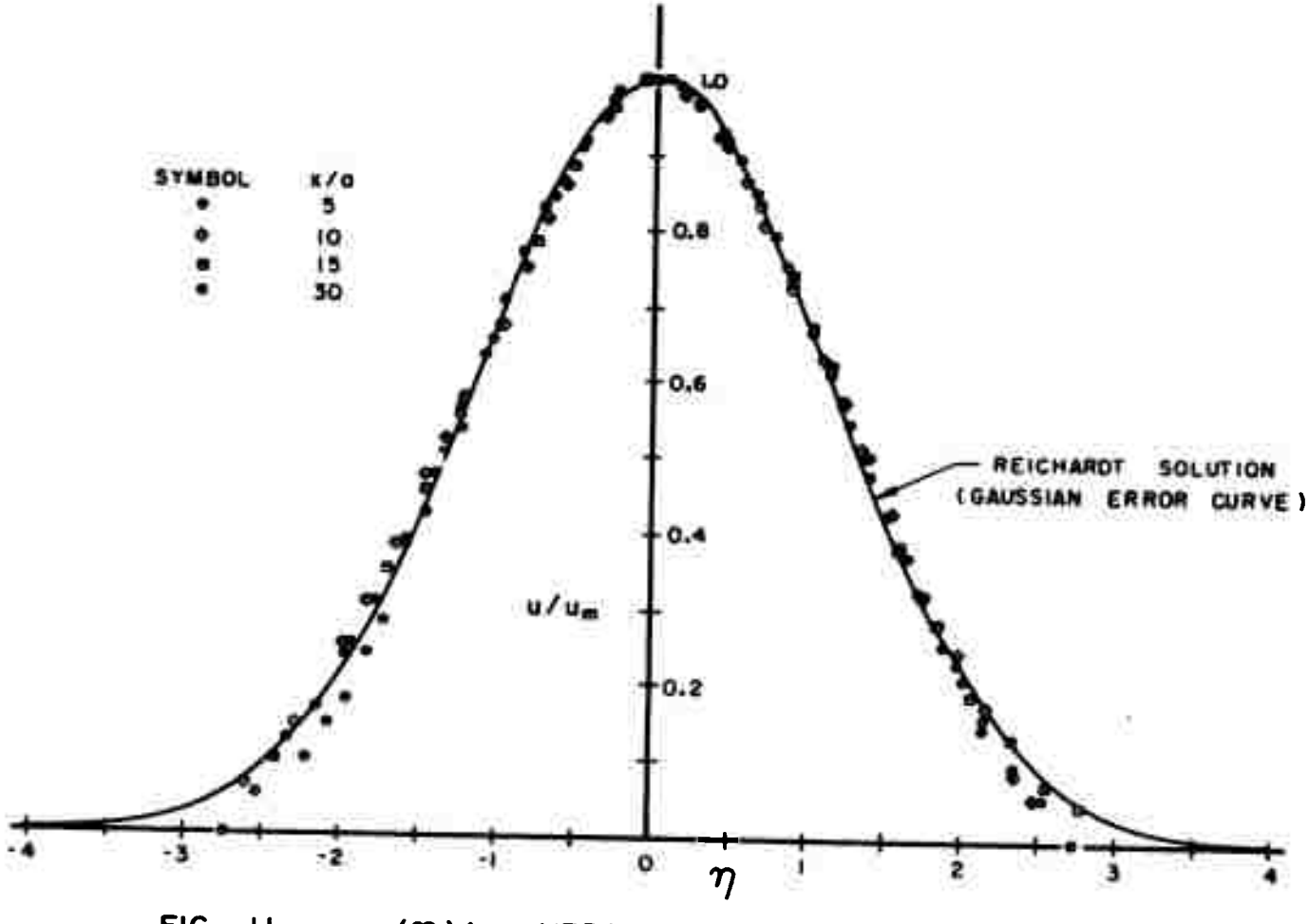

FIG. 11 $u(\eta)/u_m$ VERSUS η WITH THE REICHARDT SOLUTION

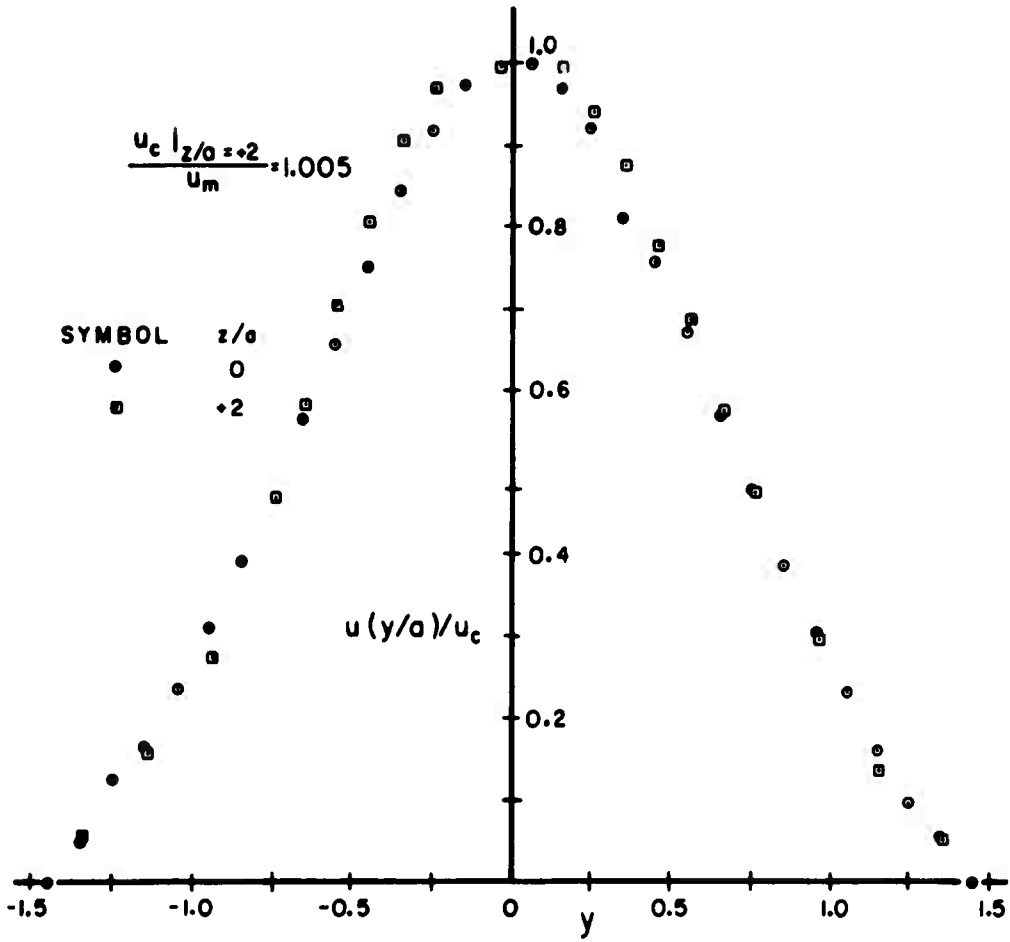

FIG. 12 $u(y/a)/u_c$ VERSUS y FOR $x/a=5$, $z/a=0, +2$

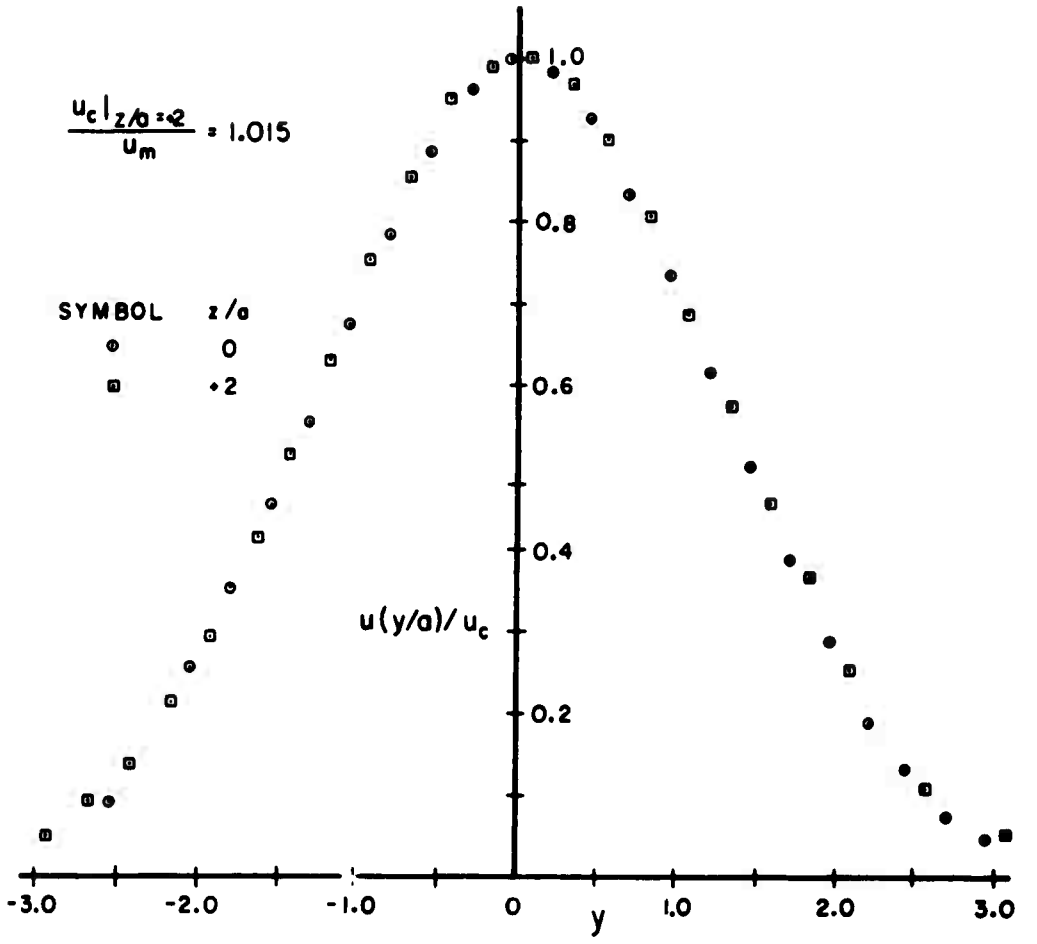

FIG. 13 $u(y/a)/u_c$ VERSUS y FOR $x/a = 15$, $z/a = 0, \pm 2$

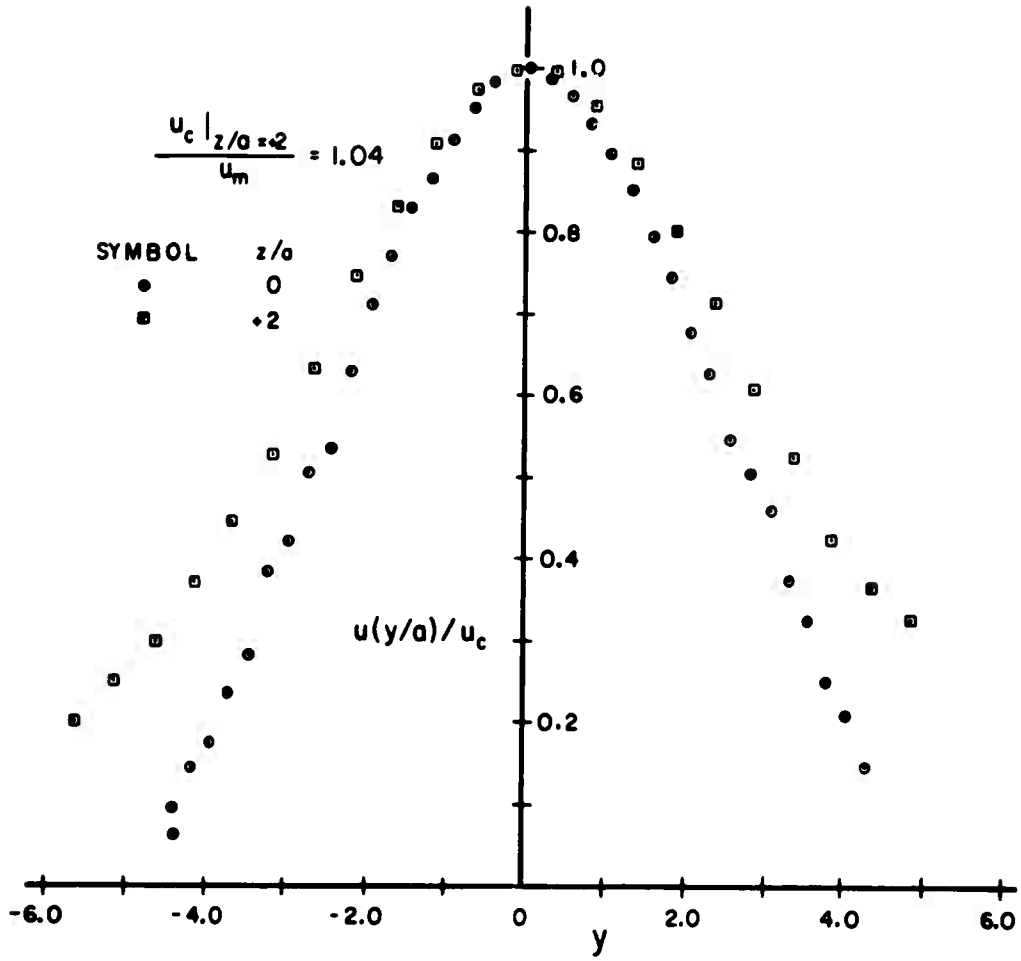

FIG. 14 $u(y/a)/u_c$ VERSUS y FOR $x/a=30$, $z/a=0,+2$

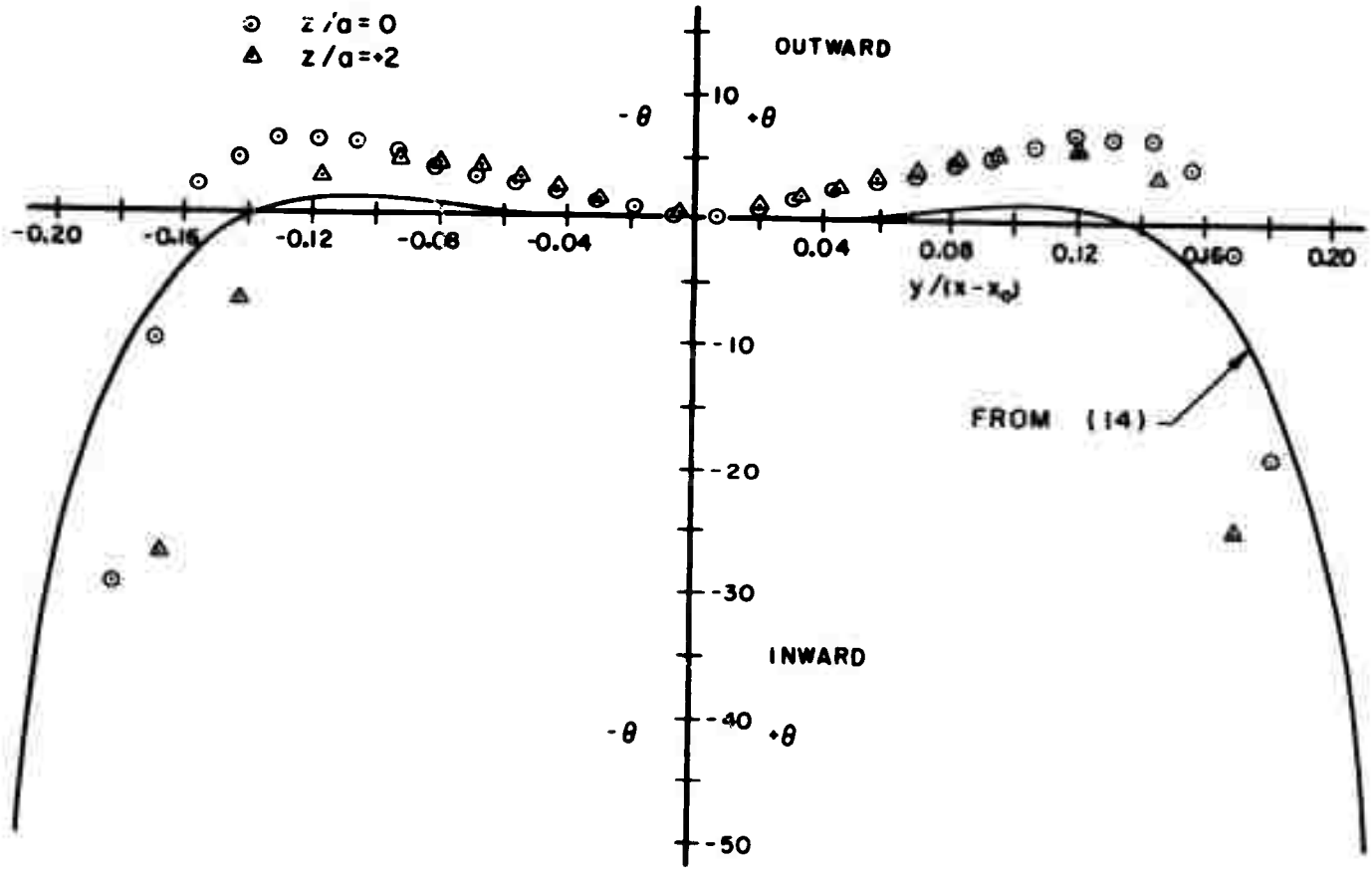

FIG. 15 θ VERSUS $y/(x-x_0)$ FOR $x/a = 5$, $z/a = 0, +2$

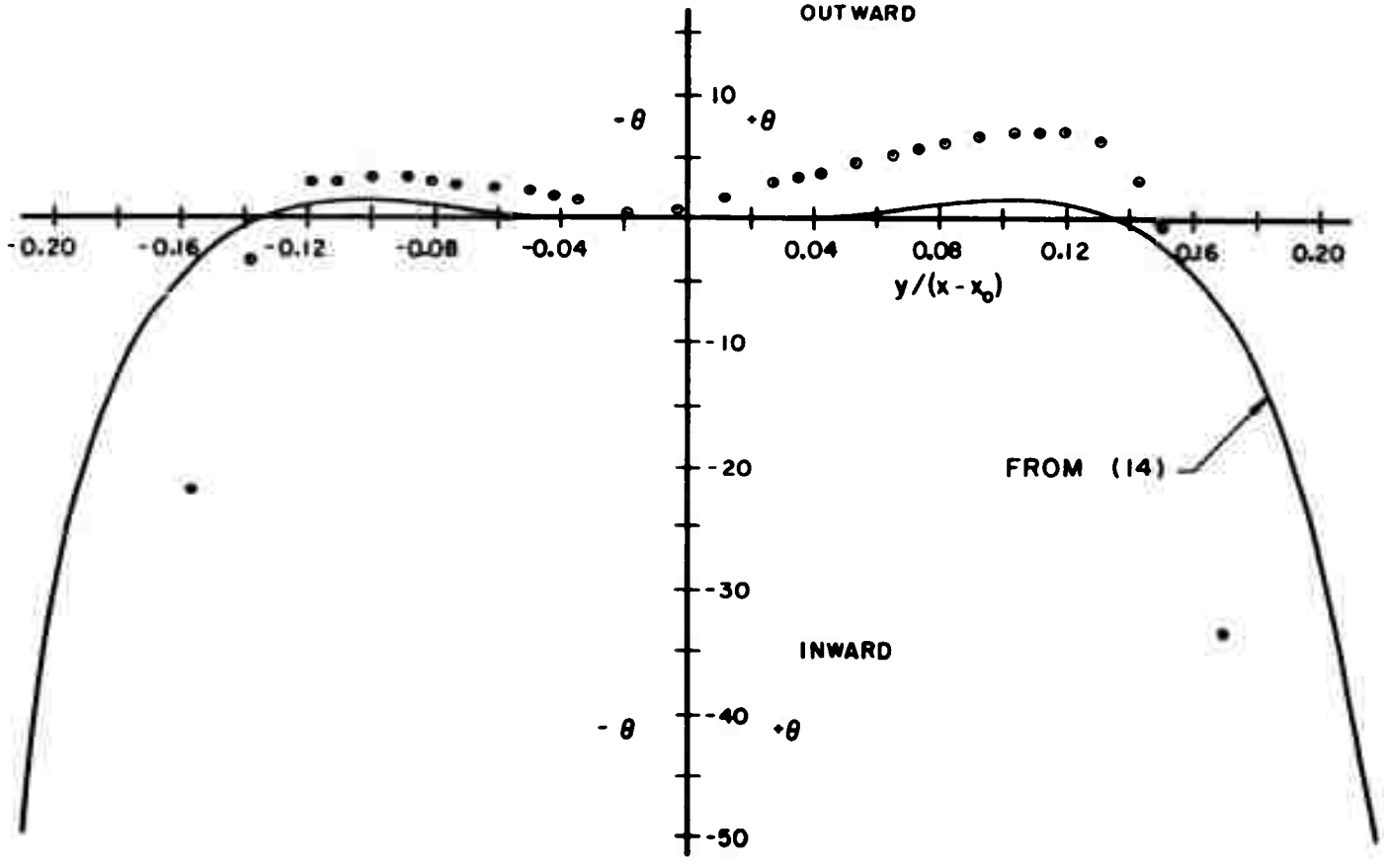

FIG. 16 θ VERSUS $y/(x-x_0)$ FOR $x/a=10$, $z/a=0$

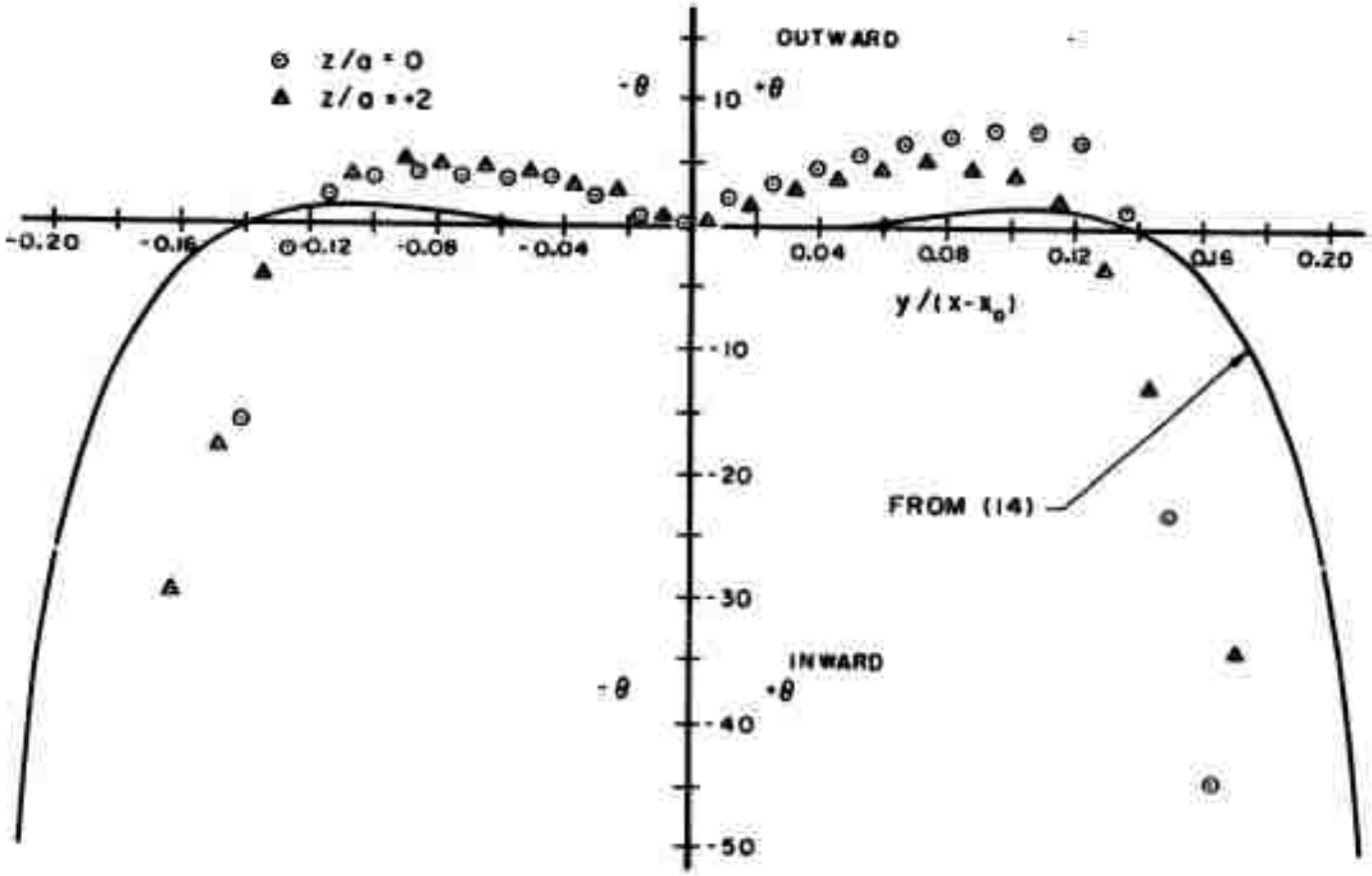

FIG. 17 θ VERSUS $y/(x-x_0)$ FOR $x/a = 15$, $z/a = 0, +2$

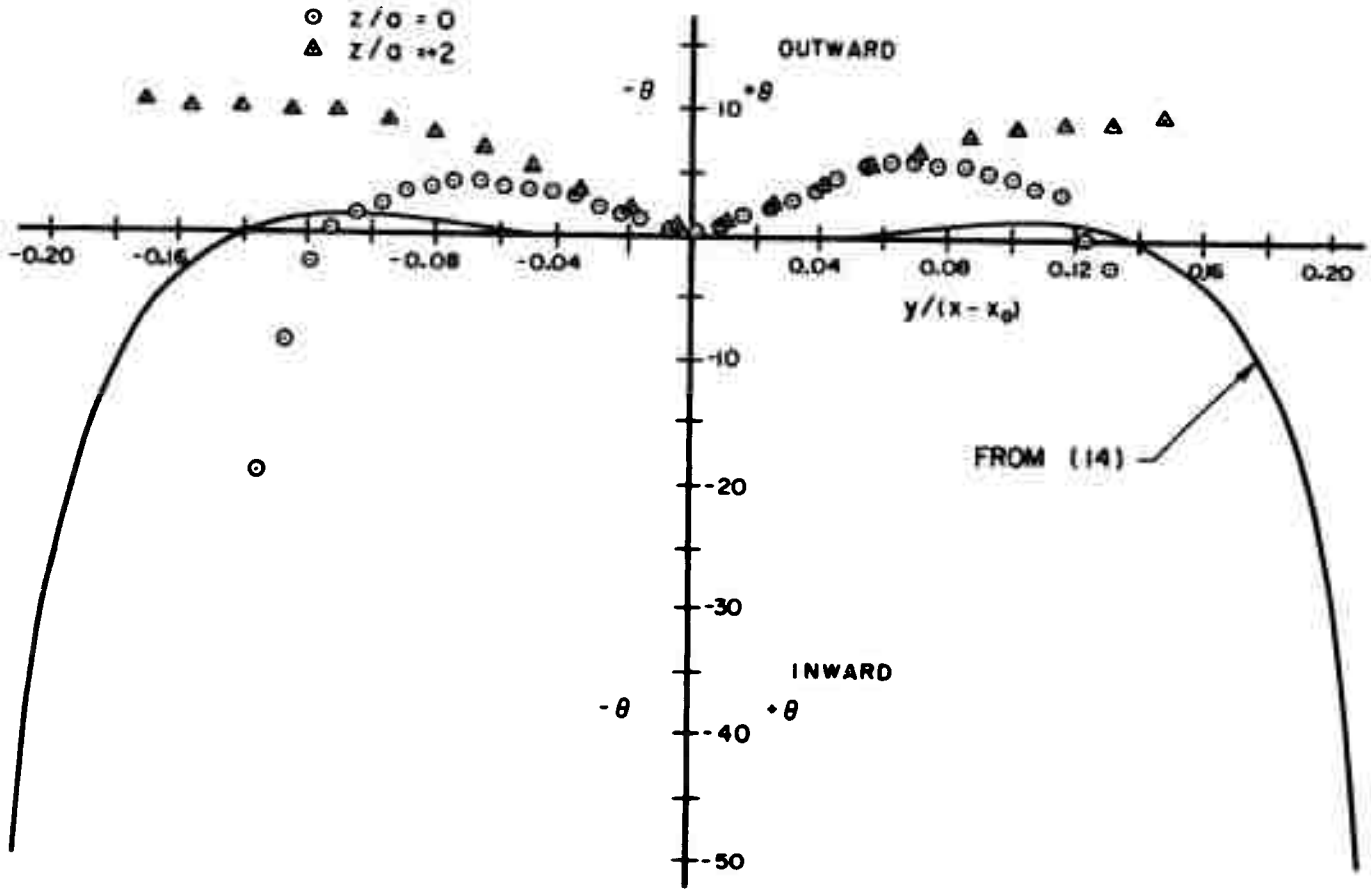

FIG. 18 θ VERSUS $y/(x-x_0)$ FOR $x/a=30$, $z/a=0,+2$

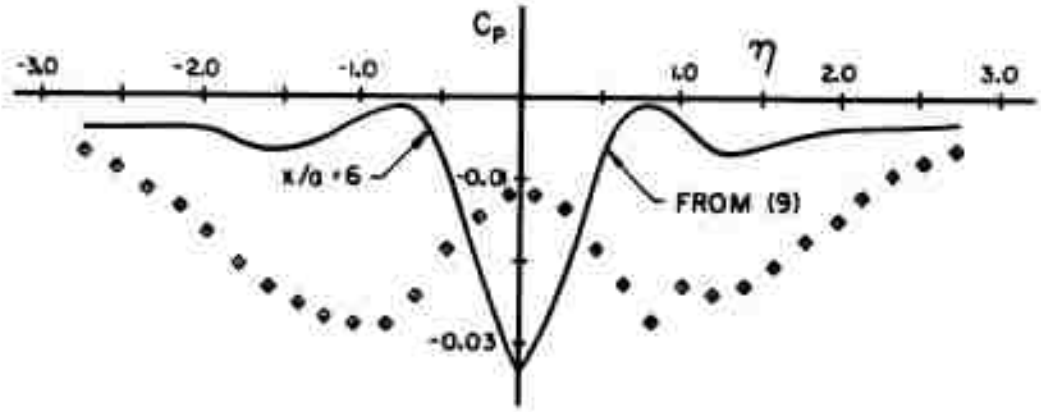

FIG. 19 C_p VERSUS η FOR $x/a = 5$

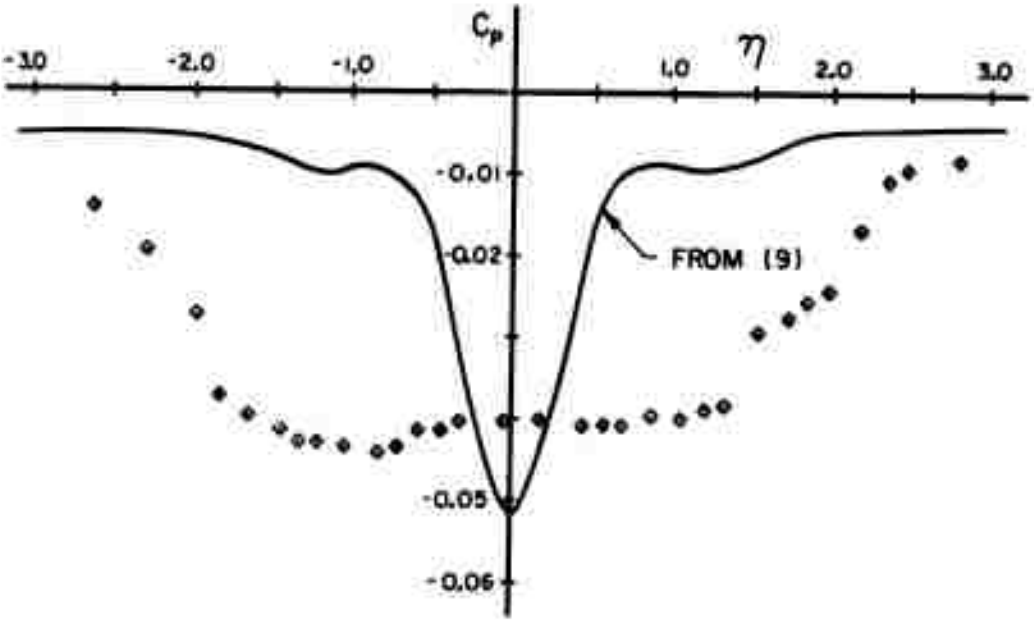

FIG. 20 C_p VERSUS η FOR $x/a = 10, z/a = 0$

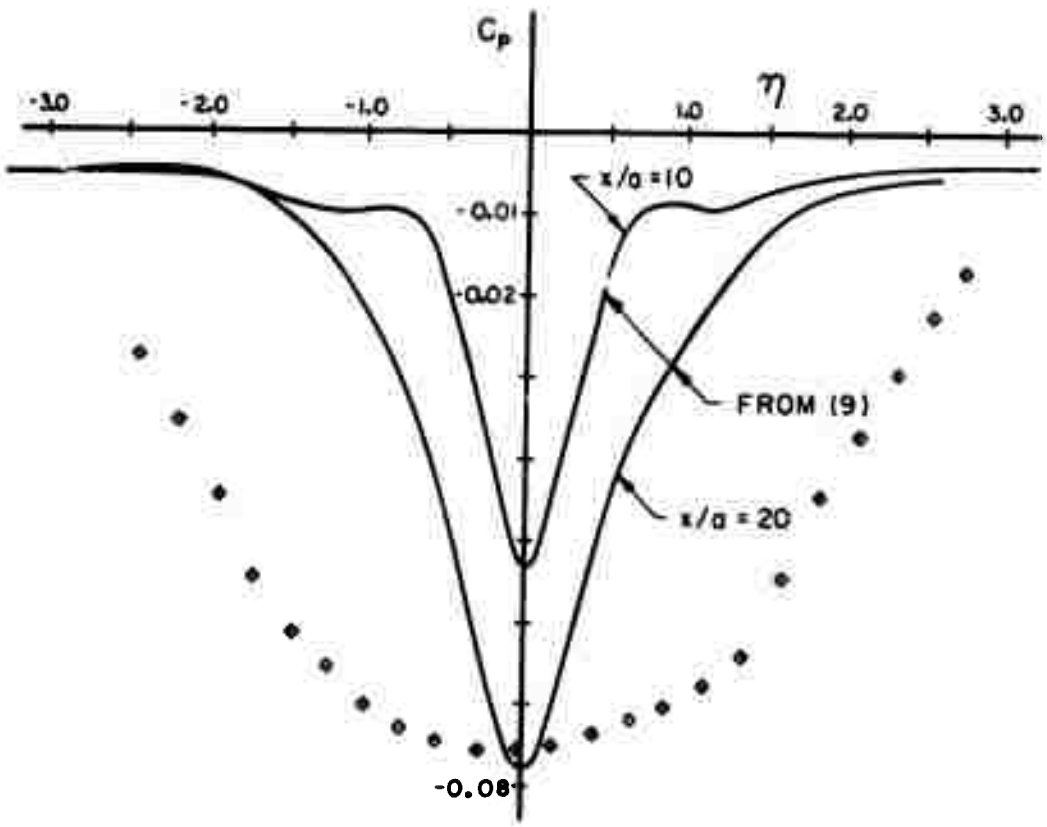

FIG. 21 C_p VERSUS η FOR $x/a=15$, $z/a=0$

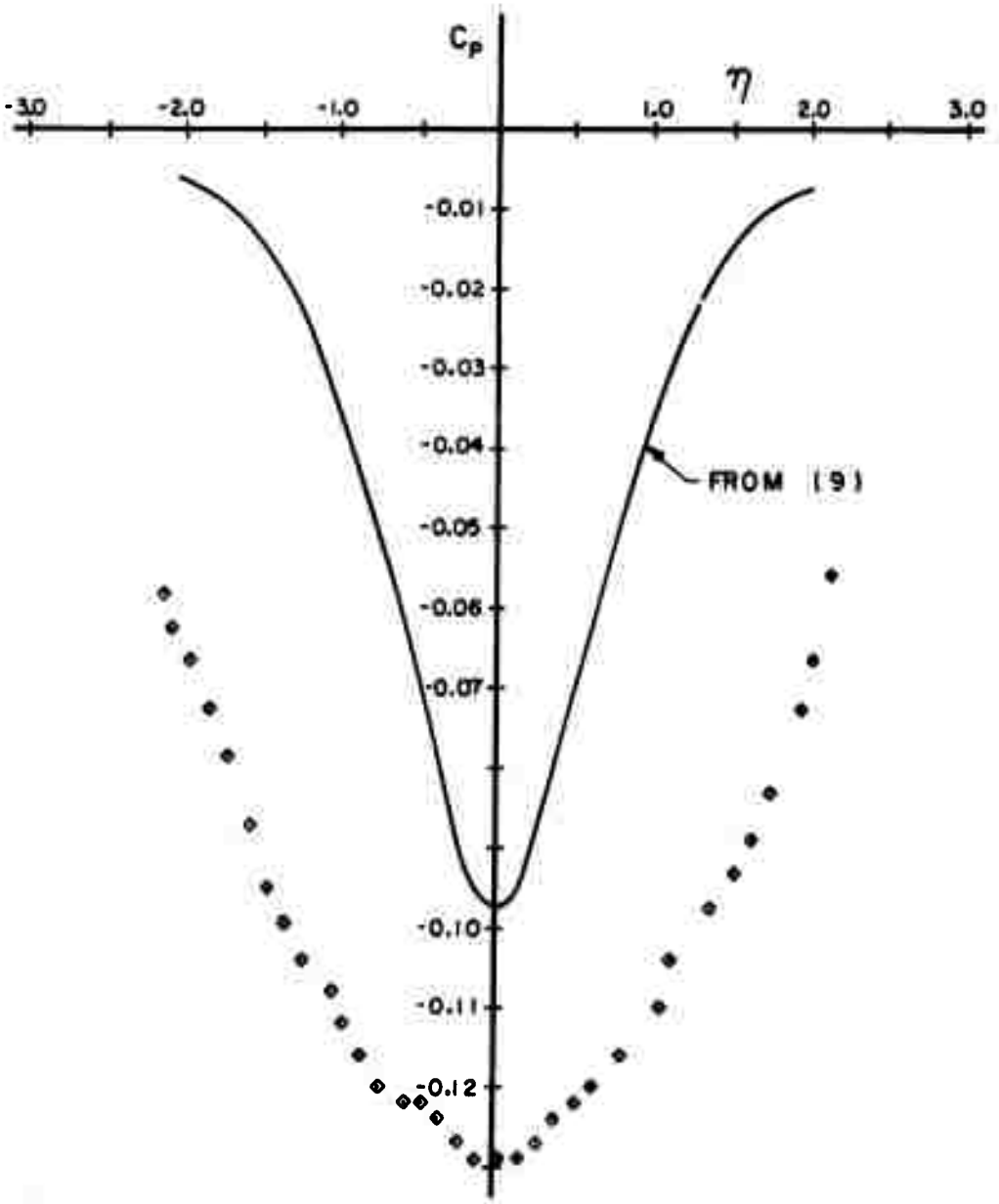

FIG. 22 C_p VERSUS η FOR $x/a = 30$, $z/a = 0$

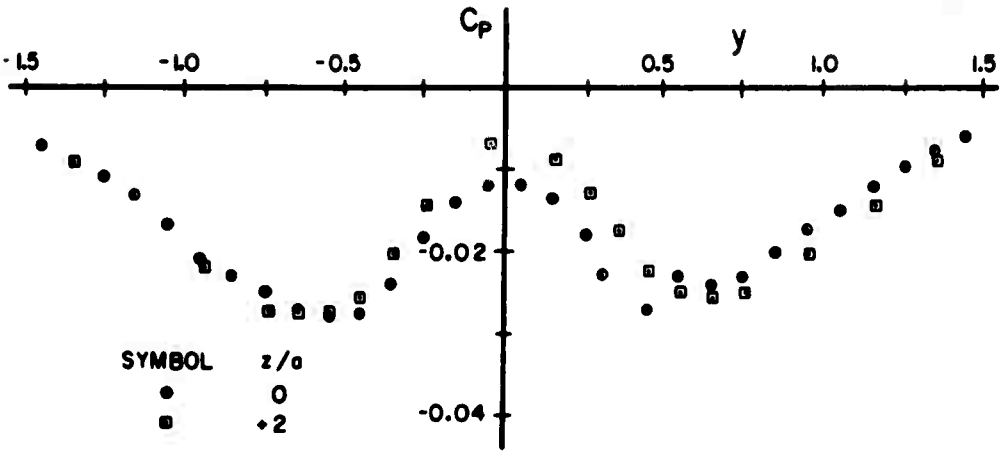

FIG. 23 $C_p(y)$ VERSUS y FOR $x/a = 5, z/a = 0, +2$

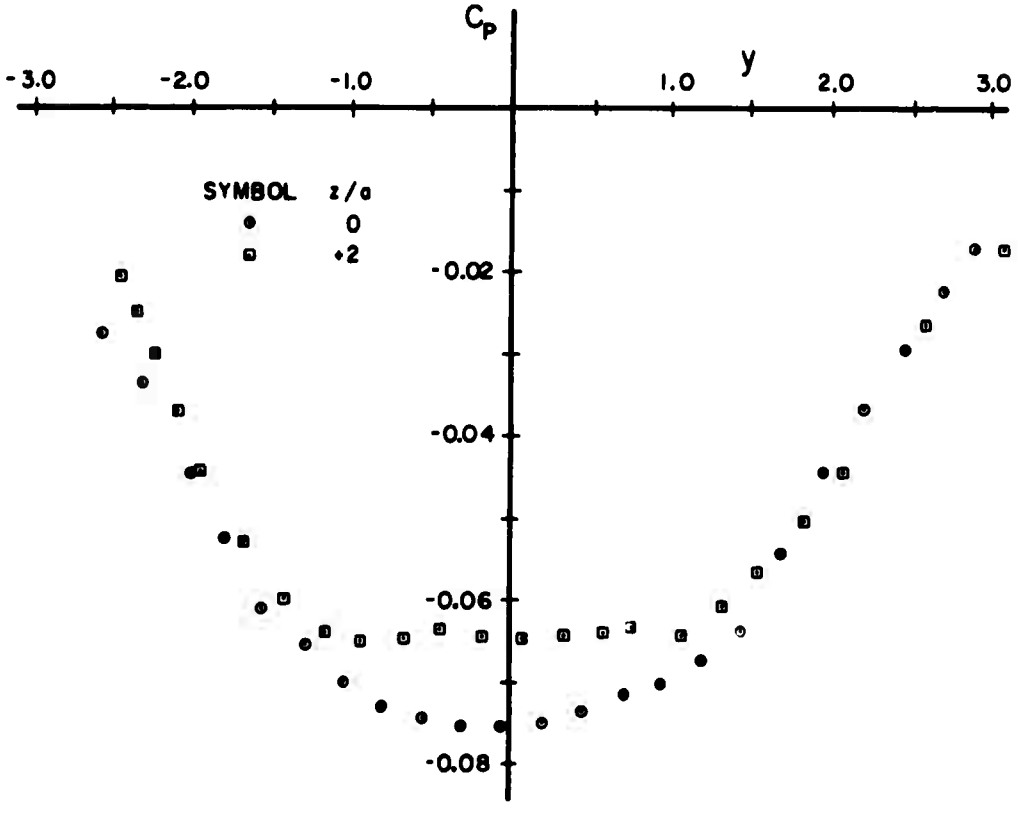

FIG. 24 $C_p(y)$ VERSUS y FOR $x/a = 15, z/a = 0, +2$

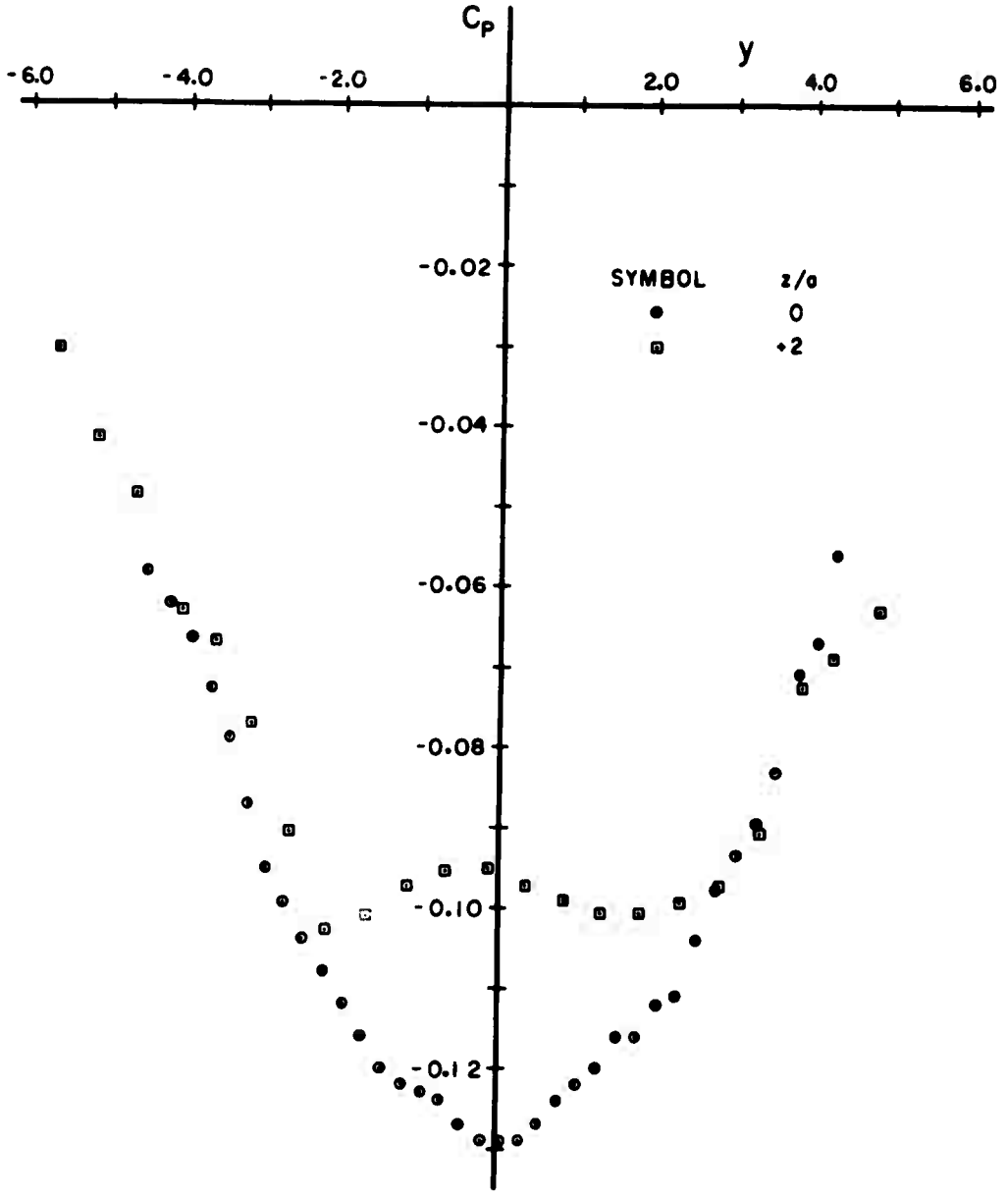

FIG. 25 $C_p(y)$ VERSUS y FOR $x/a = 30$, $z/a = 0, +2$

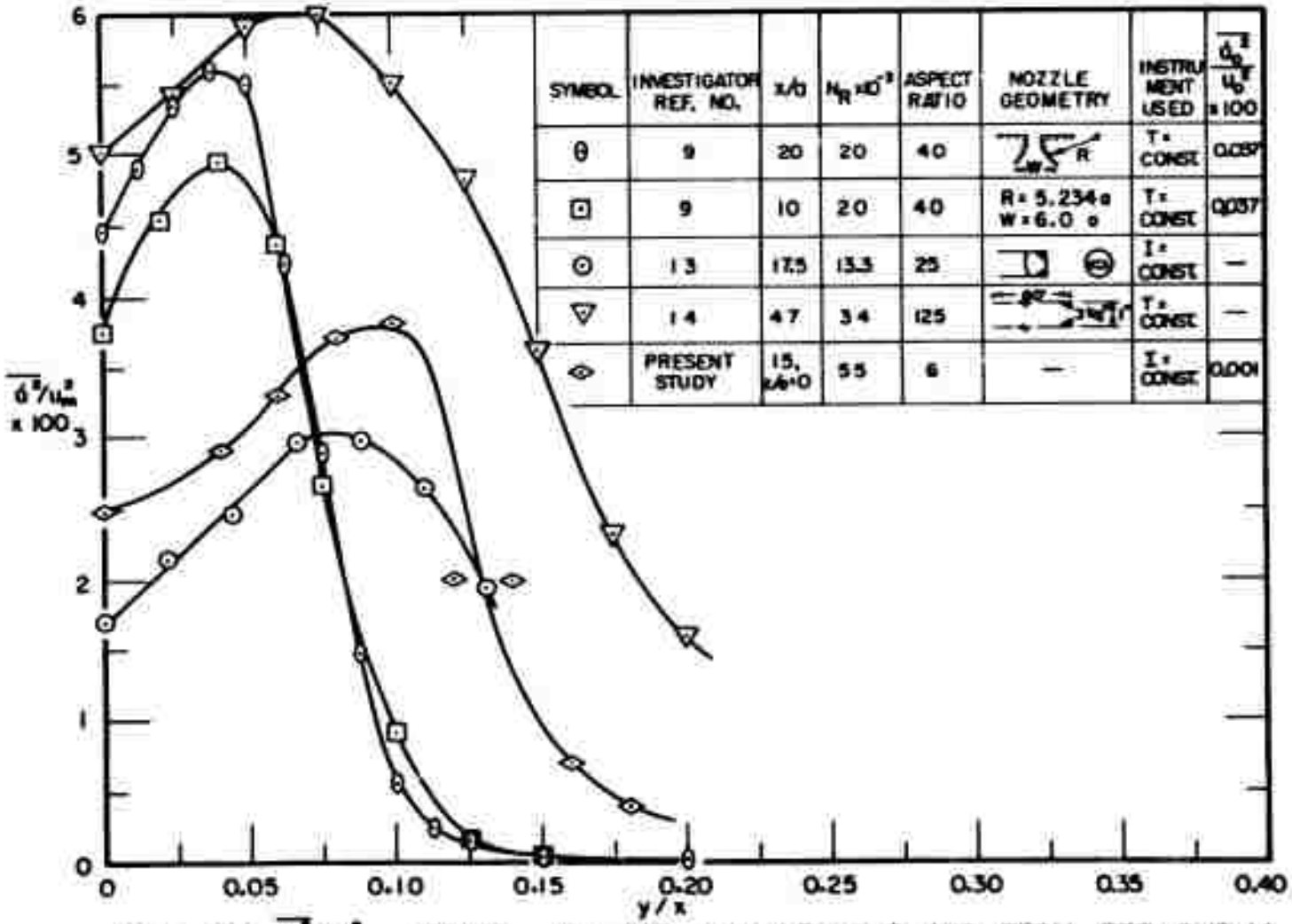

FIG. 26 $\overline{q^2}/u_m^2$ VERSUS y/x FOR x/a = 15, z/a=0 AND FROM REF. 9,13,14

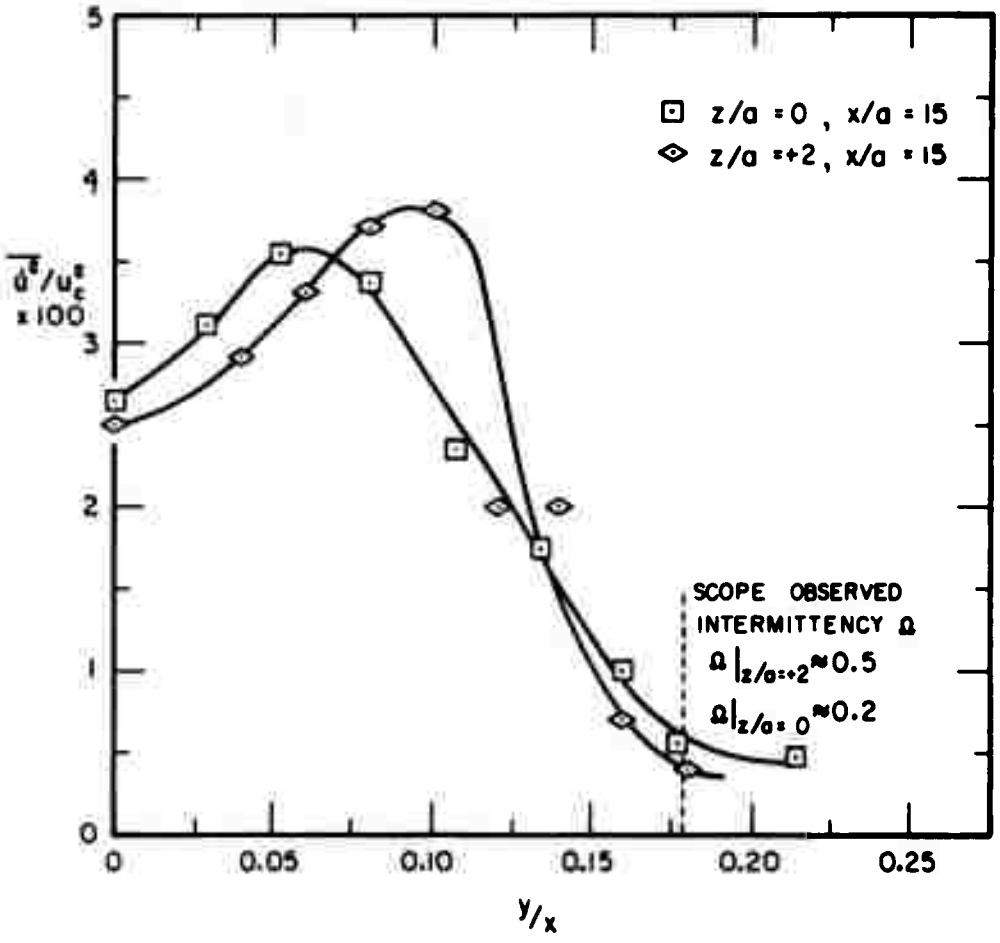

FIG. 27 $\overline{u^2}/u_c^2$ VERSUS y/x FOR $x/a = 15$, $z/a = 0, +2$

JET DEFLECTION STUDY

Analytical Prediction of α and P_R, P_L.

As noted in the literature survey, references 17 and 18 present analyses which predict $\tan\alpha$ from known input and geometric conditions for the "defined region jet interaction problem." A shortcoming of the more involved analysis in 17 is the empirical value of the far side pocket pressure since no reliable relationship (empirical or analytical) between this pressure and the other geometric and flow variables is known. It is also felt that the computation technique for the near side pocket pressure involves rather tenuous assumptions which were unavoidable because of the method of attack on the problem.

In the analysis presented below, the problem of the apparent pivot point is skirted by using an empirical formula (deduced from the present study). By so doing, the formulation for the near side pocket pressure of (17) was avoided and the empirical far side pocket pressure of (17) was replaced by the empirical apparent pivot point formulation.

Figure 29 indicates the geometry considered and defines the terms to be used.

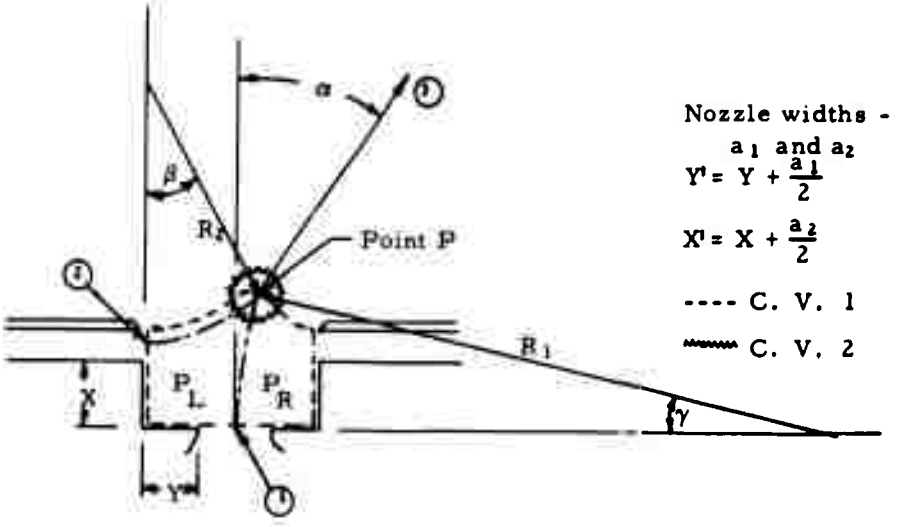

FIGURE 29 Definition of terms used in analysis

For a curved flow the equation of motion normal to a streamline may be written as

$$\frac{dP}{dn} = \rho \frac{V^2}{R} \qquad [1]$$

where: R is the radius of curvature at the location under investigation; n is the co-ordinate normal to the streamline.

The following assumptions are made:

i) the flow is steady and two-dimensional;

ii) there is no jet spreading before point P;

iii) atmospheric pressure acts on the open surfaces of the control volume;

iv) $\frac{dP_L}{dn} = \frac{P_L - P_{atm}}{a_2} = \rho \frac{V_2^2}{R_2}$

$$\frac{dP_R}{dn} = \frac{P_L - P_R}{a_1} = \rho \frac{V_1^2}{R_1}$$

v) some circulatory flow exists in the far side pocket such that the pressure on the walls of the pocket may be different from atmospheric pressure.

Then for P_L and P_R as gage pressures,

$$P_L = \rho \frac{V_2^2 a_2}{R_2} = \frac{q_2}{R_2} \qquad [2]$$

$$P_L - P_R = \rho \frac{V_3^2 a_3}{R_1} = \frac{q_1}{R_1}$$

Solving for P_R gives

$$P_R = \frac{q_2}{R_2} - \frac{q_1}{R_1} \qquad [3]$$

where q is the momentum flux per unit depth.

In the analysis of control volume 1, the following assumptions are made:

i) constant pressures P_L and P_R act on the control volume surfaces defined by the setback and standoff walls plus a/2.

ii) atmospheric pressure acts on the other half of the control jet nozzle and on the open surface of the control volume.

From the general equation, *

$$\Sigma \vec{F}_s + \vec{B}_{c.v.} = \int_{c.s.} \int \vec{V}(\rho \vec{V} \cdot d\vec{A}) + \frac{\partial}{\partial t} \int_{c.v.} \int \rho \vec{V} \, dvol.$$

the component equations may be written as:

y direction

$$[P_L - P_R] \; X = q_3 \sin \alpha - q_2$$

---

* $\vec{F}_s$ represents the surface forces and $\vec{B}_{c.v.}$ represents the body forces acting on the control volume.

c.s. stands for "control surface"

c.v. stands for "control volume"

x direction

$$[P_L + P_R]\ Y' = q_3 \cos\alpha - q_1$$

and solving these one obtains

$$\tan\alpha = \frac{[P_L - P_R]\ X' + q_2}{[P_L + P_R]\ Y' + q_1} \quad . \qquad [4]$$

Static pressure measurements made in the present study show that the assumption of constant pressure on the standoff and setback walls is quite reasonable and that the assumption of atmospheric pressure on the open surface is satisfactory (see Figure 40). However, the assumption of constant values of P_L and P_R to develop equations 2 and 3 is probably in serious error near the point P. To compensate for this, control volume 2 can be analyzed as if the net pressure forces are zero. This assumption then allows for the momentum flux components to be added (vectorially) yielding a second equation for tan α.

The y component of the momentum equation yields

$$q_3 \sin\alpha = q_1 \sin\gamma + q_2 \cos\beta.$$

For the x component we obtain

$$q_3 \cos\alpha = q_1 \cos\gamma + q_2 \sin\beta .$$

Combining these gives

$$\tan\alpha = \frac{q_1 \sin\gamma + q_2 \cos\beta}{q_1 \cos\gamma + q_2 \sin\beta} \qquad [5]$$

Two more equations may be obtained from purely geometric conditions

$$R_1 + Y' = R_1 \cos\gamma + R_2 \sin\beta$$

or

$$1 + Y'/R_1 = \cos\gamma + R_2/R_1 \sin\beta \qquad [6]$$

and

$$R_2 + X' = R_1 \sin \gamma + R_2 \cos \beta$$

or

$$1 + X'/R = (R_1/R_2) \sin \gamma + \cos \beta \qquad [7]$$

At this point, 6 independent equations for 7 variables are available. A relationship for P_L could be introduced which would be patterned after the analysis of (17). However, since this is felt to be a weakness in the analysis of (17), this will not be done. One new variable, the apparent pivot point, will be introduced which will provide an additional geometric equation and which will necessitate the introduction of an empirical relationship. This, of course, sacrifices the purely analytical character of the analysis. The sketch below illustrates the geometry for the equation involving the apparent pivot point.

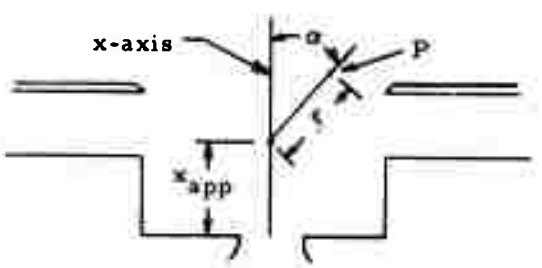

FIGURE 30 Definition of the apparent pivot point

$$\sin \alpha = R_1 (1 - \cos \gamma)$$

$$\cos \alpha + x_{app} = R_1 \sin \gamma$$

$$\tan \alpha = \frac{R_1 (1 - \cos \gamma)}{R_1 \sin \gamma - x_{app}} \qquad [8]$$

The empirical relation

$$\frac{x_{app}}{X'} = 0.25\,k\,\frac{Y}{Y'} + 0.875\,\frac{X}{X'} \qquad [9]$$

where: $k = (Y/X)$

has been deduced from experimental data of the present study.

Thus, there are 8 equations involving the 8 variables (viz., R_1, R_2, P_L, P_R, α, β, γ, x_{app}).

An outline of the reduction of these equations is presented in Appendix C; the 8 equations are reduced to 2 equations as $R'_1 = R_1(\gamma)$ where $R'_1 = R_1/X'$. A computer solution was employed to determine the correct R_1 as a function of γ for a given k and mfr, and the procedure was then repeated for mfr values of 0.05, 0.1, 0.15, 0.2, 0.25 as well as k values of 0.5, 1.0 and 1.5. The results for tan α, C_{P_L}, C_{P_R}, R'_1, and R_2 from these calculations are shown in Table 6. C_{P_L} and C_{P_R} are defined in equations 2a and 3a below; they provide a dimensionless representation of P_L and P_R.

$$C_{P_L} = \frac{X' P_L}{q_1} = \frac{mfr}{R'_2} \qquad [2a]$$

$$C_{P_R} = \frac{X' P_R}{q_1} = \frac{mfr}{R'_2} - \frac{1}{R'_1} \qquad [3a]$$

Method of Testing and Data Evaluation

For each geometry, the following experimental method was employed to determine the value of α as a function of the momentum flux ratio:

i) The mfr value was fixed by setting the dynamic head at the control jet nozzle exit at a given fraction of the power jet dynamic head. Since both nozzle exits were of the same exit area, the dynamic head ratio was equivalent to the mfr. The control jet setting was made with no flow through the power jet nozzle.

ii) The x - y - Θ device was then used to determine the position and flow direction of the maximum velocity of the resultant jet (in the $z = 0$ plane). The maximum velocity location was determined from a null reading of a dual-impact probe ($\frac{1}{4}$" spacing). These data were taken at x/a values of 5, 10, 15, 20, 30.

iii) A new mfr value was then set and the steps (i) to (iii) were repeated until all the mfr values, viz. 0.05, 0.10, 0.15, and 0.20 were investigated.

iv) The control jet flow was then turned off and the undeflected values of y and Θ were recorded.

Plots of $(\Delta y_{\Sigma}/a)$ vs (x/a) were then prepared for each mfr setting. From these the value of tan α and the apparent pivot point could be determined; a sample plot is shown in Figure 31.

The above technique was employed in the $z/a = 0$ plane. However, this does not limit the generality of the results since it was determined that the resultant jet was deflected evenly as a function of z. This observation is in agreement with the results of (17).

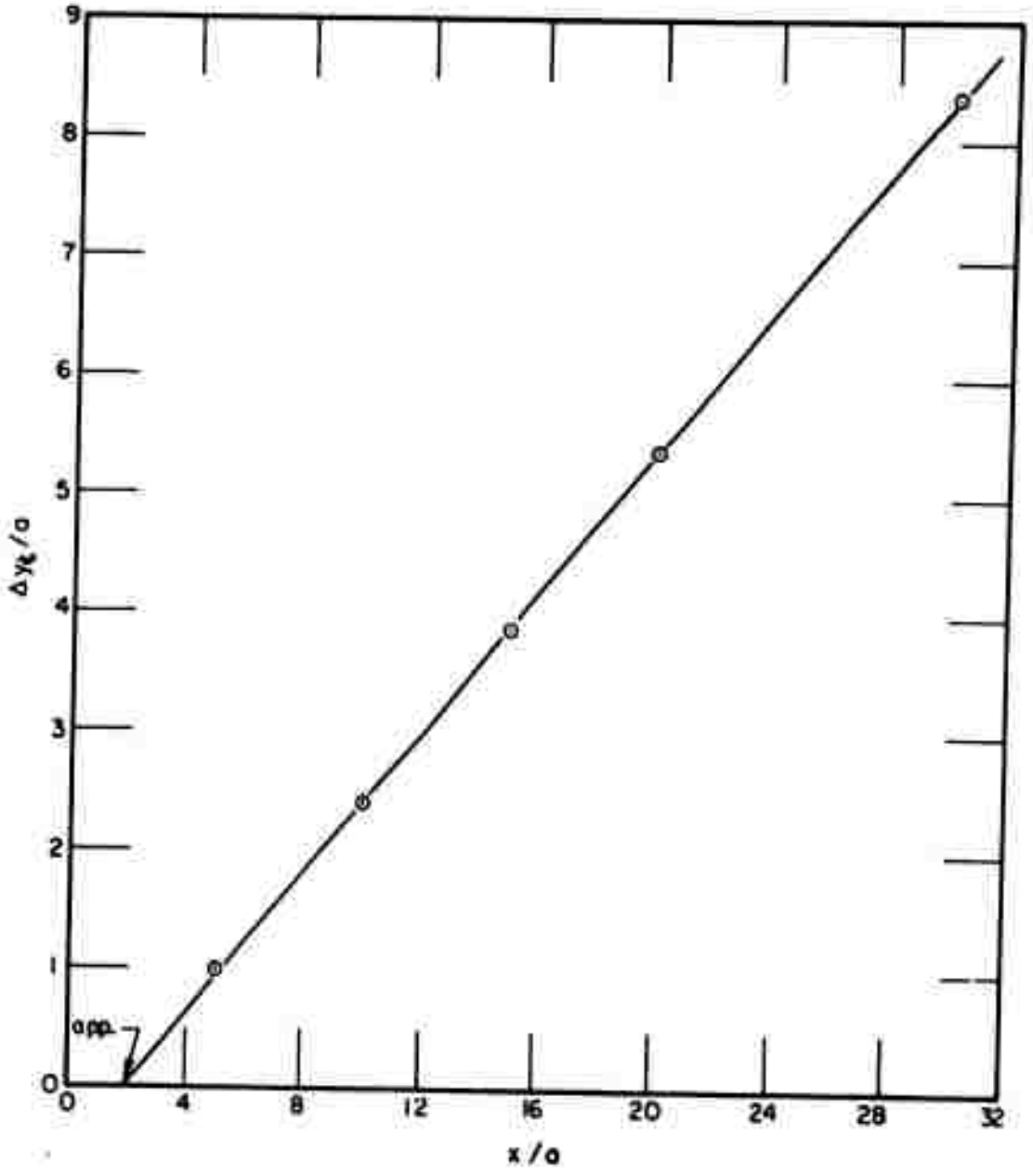

FIG. 31 $\Delta y_\ell / a$ VERSUS x/a FOR $X = 2a$, $Y = 1a$

Results

Values of Cp, x_{app} and tan from the present study are given in Table 4.* Four definitions of Cp are presented in order to ascertain whether any of these would exhibit the same functional character for the different geometries. Experimental values of the tan have been determined by the methods described in the previous section. The agreement between these two independent methods of measuring tan is excellent. Table 5 presents a comparison of the experimental values of Cp_L, Cp_R and tan with those predicted by the analysis of reference (17) and the analysis of section VII-A. A comparison is also presented wherein the value of tan is computed by the control volume equation of (18) using the measured values of Cp_L and Cp_R. Figures 32 to 37** offer a graphical comparison of the tan and the Cp_L values.

Table 6 is included to present the complete results from the computer solution of the analytical prediction equations. As shown in this table, there were two possible solutions for most values of k and the mfr. The "correct" one was chosen as that which gave the lower value of tan . The other solution may represent a physically unstable case.

Manion and Goto determined tan as a function of the mfr for three geometries: X = Y = 1a, X = Y = 3a and X = 1a, Y = 3a; three power jet plenum pressures of 5, 10 and 20 psig were considered for each geometry. Since the geometries differ from those of the present study, a direct comparison is not possible; however, a valid comparison may

---

* The tables that present the results of the jet deflection study can be found in the "Discussion of Results" section.

** The figures that present the results of the jet deflection study can be found at the end of the section, see page 112 ff.

be to compare the results for $X = Y = 2a$ (present study) with those for $X = Y = 1a$ and $3a$ of (17). Figures 38 and 39 show this comparison.

A static pressure survey was made with the plate static probe (from Reference 9) in the interaction region for the condition $X = Y = 2a$, and a mfr = 0.1. The results of this survey, which are shown as $h_s(x, y)$ for $z/a = 0$ in Figure 40, should be considered as a presentation of approximately true values of the static pressure with the error being dependent on the proximity of the probe to the jet. This probe is highly sensitive to pitch and there was no reliable way to align the probe; however, the probe and the wall taps did give the same reading for a probe position $\frac{1}{2}$ - inch from the wall. This indicates that in the regions which are not in the jet flows the probe readings should be rather accurate. The probe was also used to traverse the z direction; no significant changes in the h_s reading were noted with respect to z.

Discussion of Results

Effect of Probe Spacing

With regard to the experimental results of this section it is important to note an arbitrary definition which necessarily was made at the beginning of the tests. Since a dual pitot probe with a fixed spacing of 0.25 inches was used for all x stations, it must be acknowledged that the quantity measured is simply the y location where such a probe gives a null reading. The intent, of course, is to locate the y position of maximum velocity. If the total pressure profile and the static pressure profile were symmetric about the maximum

velocity, the spacing of the dual probe would be immaterial. However, neither of these two conditions is realized; the asymmetries are most pronounced for high mfr and low x/a values. It can be reasonably argued that no single quantity provides a complete description of the jet deflection. For example, the maximum velocity location and the locations which divide each of M, $2bq_c$, and E into two equal parts would yield four unequal values of y for the center line of the resultant jet. Consequently, the use of a dual probe is an arbitrary selection of the location of the resultant jet and this particular selection is a matter of convenience.

Because of the small size of the experimental flow system and physical limitations on the smallness of their probe, Manion and Goto employed a dual probe with a spacing of 2.88a. It would seem that the probe response, for the 2.88a spacing, would be insensitive to positions at low x/a values since the majority of the jet is contained within the probes. The dual probe of the present study (spacing of 0.25a) was rather insensitive to location changes at x/a = 30 because of the flat velocity profile. It would also appear that a probe with a spacing of 2.88a would be more susceptible to a skewed velocity profile if such a profile resulted from the interaction process.

Interpretation of Results from the Present Study

The most significant result to be gained from the present study (see Table 4) is the pronounced effect of the geometry. This can be seen by noting the mfr necessary to obtain the same value of tan α for the three geometries. A mfr of 0.10, 0.15, and 0.20 will yield (approximately) the same

TABLE 4

Results of the Jet Deflection Study

mfr	x_{app}	$C_{P_{L-cj}}$	$C_{P_{L-pj}}$	$C_{P_{R-cj}}$	$C_{P_{R-pj}}$	Tan α From Δy_{ℓ}	Tan α From $\Delta \theta$
X/a = 2	Y/a = 1						
0.05	1.9	+0.54	+0.024	-0.55	-0.028	0.120	0.121
0.10	2.0	+0.54	+0.065	-0.33	-0.034	0.235	0.236
0.15	1.9	+0.60	+0.09	-0.26	-0.038	0.295	0.302
0.20	2.0	+0.59	+0.120	-0.24	-0.047	0.362	0.375
X/a = 2	Y/a = 2						
0.05	2.4	0.24	0.013	-0.29	-0.014	0.081	0.082
0.10	2.2	0.37	0.037	-0.14	-0.014	0.149	-
0.15	2.4	0.41	0.061	-0.095	-0.014	0.23	0.233
0.20	2.2	0.41	0.082	-0.072	-0.014	0.29	0.294
X/a = 2	Y/a = 3						
0.05	2.2	0.170	0.0085	-0.142	-0.007	0.0625	0.061
0.10	2.4	0.254	0.0254	-0.066	-0.0066	0.119	0.118
0.15	2.6	0.287	0.0430	-0.053	-0.0080	0.192	0.186
0.20	2.8	0.294	0.0586	-0.047	-0.0093	0.247	0.233

$C_{P_{(i-k)}} = P_i - P_{ATM} / 1/2 \ \rho V_k^2$ where P_i = Average Wall Pressure

tan α * for the geometries X/a = 2, Y/a = 1, 2, and 3 respectively. As previously noted, the actual jet deflection depends not only on tan α but also on the apparent pivot point. Comparing the approximate x_{app} values for the above three cases, one sees that for smaller Y values, not only is tan α larger, but the apparent pivot point is closer to the power jet nozzle.

In the analysis of the data in Table 4 it should be borne in mind that if the momentum of the control jet were the only deflecting agent, then the value of the mfr and the tan α would be equal. The difference between these two can then be used as a measure of the static pressure effect induced by the defined region geometry. For example, comparing tan α at mfr values of 0.05 and 0.2 for the three geometries, one obtains for the ratio (tan α - mfr) / mfr the following values:

Table 7

Values to Indicate the Effect of the Static Pressure

$$\frac{\tan \alpha - \text{mfr}}{\text{mfr}}$$

		mfr	
X/a	Y/a	0.05	0.20
2	1	1.40	0.80
2	2	0.60	0.45
2	3	0.25	0.24

* For this and subsequent comparisons the value of tan α is taken from the Δy_{ℓ} data except as noted.

Another method by which to gain an appreciation of the magnitude of the pressure effects is to compare $C_{P_{L-pj}} - C_{P_{R-pj}}$ values for the different geometries. The difference is important because it is the net pressure force which contributes to the actual deflection. From the deflection angle results it is apparent that the geometry $X/a = 2$ and $Y/a = 1$ is the most effective in obtaining a maximum deflection for a given mfr. These results indicate that the gain of the proportional amplifier increases with decreasing Y/X values; however, the range over which this generalization is valid has only been investigated for Y/X values greater than or equal to $\frac{1}{2}$ and was made for data which employed a constant X value. Further investigations are necessary to reliably extend the range of the generalization.

With regard to the values of $C_{P_{(i-k)}}$*, it appears that no simple method of non-dimensionalization offers a reliable prediction of the pocket pressures. If a non-dimensionalization technique is to yield a predictable C_p value, it is obvious that the Y length as well as some combination of the power and control jet dynamic head or momentum fluxes must be incorporated in the definition. This was not pursued because of the rather limited experimental data with regard to X, X', Y, and Y'.

From other literature sources (e.g. (1) to (3)) the mfr range covered in the present study appears to encompass the range of current interest for amplifier applications.

Comparison with Published Data

Manion and Goto (17) present the only data which can be utilized for a direct comparison with the results of the

---

* $C_{P_{(i-k)}}$ is defined in Table 4.

present study. As noted in the literature survey, their work was for compressible flow and an aspect ratio of 8. With reference to Figures 38 and 39, it can be seen that the deflection angles of the present study are of the same order as the maximum angles found in (17). Furthermore, the data of (17) are for three power jet plenum pressures and the pattern "a greater plenum pressure yields a greater angle α for the same mfr" is clearly established. Three statements can be made with regard to this observation; it cannot be ascertained which statement or which combination of statements provides the most accurate representation of the physical case without further experimental, or more refined analytical, investigations. However, the statements do have significance for the designer. They are:

i) Assuming that the trend, in (17), of increasing α for an increasing V_{pj}, at a given mfr may be extrapolated to the incompressible regime, then the large angles (α) of the present study are attributable to the strong effect of the aspect ratio. That is, the gain of the proportional amplifier is higher for smaller aspect ratios.

ii) Assuming that the aspect ratio effect between 6 and 8 is of negligible importance, the incompressible regime is seen to yield better amplifier performance than the compressible regime.

iii) The comparison with (17) is predicated on the assumption that the performance of X = Y = 2a should lie between X = Y = la and X = Y = 3a, all the other factors being equal. The physical phenomena involved may not be amenable to such a simple analysis. This would mean that the

designer must be rather careful in extrapolating and interpolating his experience with previous configurations.

An insight into the jet deflection phenomenon can be gained if the results of the present study are compared with those of Olson (22). The apparent pivot point for the majority of the tests in the present study was upstream of the geometric intersection whereas in (22) it lay downstream of this intersection. Olson attributed the observed displacement to a time delay in the momentum exchange process. This explanation is not dependent on the geometry considered and therefore the same time delay should occur in the interaction process of the present study. The effect is not observed in the majority of the runs; however, for Y = 3a the apparent pivot point does move downstream with increasing mfr values. These two observations suggest that the apparent pivot point is strongly related to the relative magnitude of the pocket static pressure. As indicated in Table 7 the static pressure induced deflection (as a percentage of the deflection due to the momentum flux) is 25 per cent for Y = 3a and 80 to 140 per cent for Y = la. Consequently the larger x_{app} values for Y = 3a are in agreement with Olson's results since the momentum interchange is more important for this geometry. However, Olson also notes that the displacement is reduced for increasing mfr values; a trend which is the inverse of the trend observed in the present study. A possible conclusion from this is that the presence of the walls and the greater-than-atmospheric pressure in the near side pocket of the present study induces a change in the momentum exchange

process of the intersecting jets. Another important factor in the comparison is that a power jet exit Mach number of 0.66 was used in (22). However, there is no apparent reason why this would induce the observed trend of the x_{app} with the mfr.

Comparison with the Analytical Prediction

A principal requirement of a successful analytical model is that it provide an accurate representation of the physical phenomenon described. Figures 32 to 37 and Table 5 offer this comparison for the model proposed here and also present the results of the Manion and Goto analysis (17). The latter were obtained from a computer solution of the equations in (17); the nozzle geometry, the mfr, and the right side pocket pressure were the required data inputs for the program*.

The present analysis for tan α gives a rather good approximation for k = 0.5; the agreement is within 10 per cent up to a mfr of 0.2. However, for a k of 1.0 the agreement is only within 25 per cent up to a mfr of 0.20. It is fortuitous that the agreement is best for a k of 0.5 since this geometry offers the best performance of the three tested. The agreements shown for k = 1.0 and 1.5 are, of course, better than no prediction whatever, but would probably not be sufficient for the design of an operational amplifier.

---

* The writer is indebted to the Harry Diamond Laboratories for the computer solutions of the Manion and Goto analysis.

TABLE 5

Comparison of the Analytical and Experimental Results

for the Jet Deflection Study

k	mfr	C_{P_L}			C_{P_R}		tan α			
		Experimental	Analytical	Analytical (17)	Experimental	Analytical	Experimental	Analytical	Analytical (17)	* See Note
0.5	0.05	0.03	0.0829	0.0107	-0.0362	0.0026	0.120	0.130	0.098	0.104
0.5	0.10	0.0813	0.146	0.0220	-0.0425	0.0102	0.235	0.233	0.174	0.195
0.5	0.15	0.113	0.200	0.0339	-0.0475	0.0193	0.295	0.324	0.248	0.272
0.5	0.20	0.150	0.246	0.0464	-0.059	0.028	0.362	0.405	0.325	0.354
1.0	0.05	0.0163	0.044	0.0053	-0.0175	-0.0014	0.081	0.096	0.074	0.078
1.0	0.10	0.0462	0.082	0.0108	-0.0175	-0.0097	0.149	0.183	0.133	0.148
1.0	0.15	0.0765	0.115	0.0165	-0.0175	-0.0088	0.230	0.266	0.191	0.216
1.0	0.20	0.101	0.143	0.0220	-0.0175	-0.0036	0.290	0.35	0.248	0.278
1.5	0.05	0.016	0.030	0.0035	-0.0088	-0.0013	0.0625	0.0818	0.0635	0.066
1.5	0.10	0.0318	0.057	0.007	-0.0083	-0.0020	0.119	0.159	0.118	0.128
1.5	0.15	0.0538	0.080	0.0106	-0.010	-0.0056	0.192	0.238	0.174	0.191
1.5	0.20	0.0734	0.100	0.0140	-0.012	-0.0083	0.247	0.317	0.227	0.250

*Note: The values in this column were computed by the control volume equation of (18) using the measured static pressures.

Tan α and the location of the apparent pivot point will define the location of the resultant jet; consequently, agreement of the tan α values is the most important criterion for the analytic model. However, an appreciation for the accuracy of the analysis may also be gained from the predicted pocket pressures. This comparison is offered in Figures 35 to 37 and Table 5. The C_{p_R} values were not plotted because of the wide discrepancy between the observed and predicted values, a difference that is obvious from the table. It is interesting to note that the C_{p_L} value that shows the largest discrepancy is for k = 0.5, the geometry for which tan α showed the best agreement. The agreement of the experimental values for k = 0.5 and 1.0 with the analysis for k = 1.0 and 1.5 (respectively) is interesting; but, it is not believed to be indicative of any significant phenomenon.

A striking feature that is apparent from the figures is the good agreement between tan α values predicted by the Manion and Goto analysis and measured values for the geometry of k = 1.5 and the poorer agreement for lower k values. The analysis of (17) gave the best P_R prediction for k = 0.5 and poorer agreement for increasing k values. This pattern is the inverse of that between the present analysis and observations.

The analysis, as presented in the earlier section, has several arbitrary steps and assumptions which were necessary to obtain a complete formulation of the problem. The test of the "correctness" of these is, of course, the agreement with experimental results. After one finds the

degree of agreement, he can then either change certain assumptions or modify the analysis; the former is more easily done. Recommendations for modifying the assumptions are given first; the problem of modifying the basic analysis is then considered.

Since the predicted tan α values were too high, the assumption of constant pressure over the length X' could be replaced by a constant pressure over X. Also, the near side pocket pressure could be assumed to act over Y + a instead of Y'. The assumption of constant static pressure up to point P leads to constant values of R_1 and R_2. If these two values are constant the analysis is greatly simplified; however, the necessary assumptions of constant P_L and P_R are not true and lead to too large values of α. In the analysis, only the values of R_1, R_2, γ and β associated with point P are required; consequently, an arbitrary fraction of P_L and P_R (e.g. 0.5) could be employed for the calculations in (2) and (3), e.g.

$$P_L/2 = q_2/R_2 \qquad (2c)$$

$$P_R/2 = q_2/R_2 - q_1/R_1 \qquad (3c)$$

To modify the basic analysis, the method of (17) could be employed to predict the near side pocket pressure and this would eliminate the need for the empirical relation [9]. Since the analyses have inverse success patterns a combination of the two analytical models might provide a more satisfactory set of prediction equations. Furthermore, if more were known about the intersection phenomenon, then the questionable assumptions, in (17), of no entrainment and

no penetration of the control jet could be eliminated, leaving the basic part of the analysis which is quite plausible.

The analysis produced two possible solutions for most combinations of k and the mfr. If there is, in the physical sense, another solution that is possible, it could lead to important implications for the operational amplifier. The tan α values for the second case was much higher than the solution chosen as the correct one. It is assumed that the second solution represents an unstable case. The significance to the operational amplifier would be that it may be possible to bias the amplifier with a low pressure in the far side pocket and have it operate on the second or higher gain solution curve.

TABLE 6

Complete Solution for the Jet Deflection Analysis

Possible Solutions for Equations 2a - 9 for $\delta = 0.2k + 0.7$

k	mfr	γ	R_1'	R_2'	tan α	C_{P_L}	C_{P_R}
0.5	0.05	6.8	12.5	0.602	0.130	0.0829	0.0026
0.5	0.05	34.4	1.97	3.22	1.10	0.0156	-0.492
0.5	0.10	11.7	7.35	0.682	0.233	0.146	0.0102
0.5	0.15	15.6	5.55	0.752	0.324	0.200	0.0193
0.5	0.20	18.9	4.61	0.815	0.405	0.246	0.028
0.5	0.25	21.8	4.01	0.875	0.481	0.286	0.037
1.0	0.05	4.68	22.3	1.13	0.096	0.0442	-0.00138
1.0	0.05	15.9	4.64	2.72	0.441	0.0184	-0.198
1.0	0.10	8.36	12.1	1.22	0.183	0.0819	-0.0097
1.0	0.10	18.8	4.11	2.47	0.579	0.0409	-0.203
1.0	0.15	11.6	8.68	1.31	0.266	0.115	-0.0088
1.0	0.15	21.2	3.76	2.37	0.700	0.0635	-0.202
1.0	0.20	14.6	6.81	1.40	0.35	0.143	-0.0036
1.0	0.20	23.3	3.55	2.32	0.807	0.0844	-0.1987
1.0	0.25	16.9	5.86	1.42	0.421	0.171	-0.0003
1.0	0.25	25.3	3.31	2.31	0.874	0.108	-0.194
1.50	0.05	3.79	29.8	1.67	0.0818	0.0303	-0.0013
1.50	0.05	12.6	6.23	4.04	0.382	0.0124	-0.150
1.50	0.10	6.95	17.1	1.77	0.159	0.0565	-0.020
1.50	0.10	15.0	5.61	3.60	0.535	0.0287	-0.155
1.50	0.15	9.82	11.9	1.88	0.238	0.0797	-0.0056
1.50	0.15	17.1	5.20	3.10	0.603	0.045	-0.149
1.50	0.20	12.4	9.23	1.99	0.317	0.10	-0.0083
1.50	0.20	18.8	4.94	2.96	0.676	0.0682	-0.135
1.50	0.25	14.8	7.66	2.04	0.375	0.124	-0.0125
1.50	0.25	20.2	4.75	2.83	0.709	0.0836	-0.122

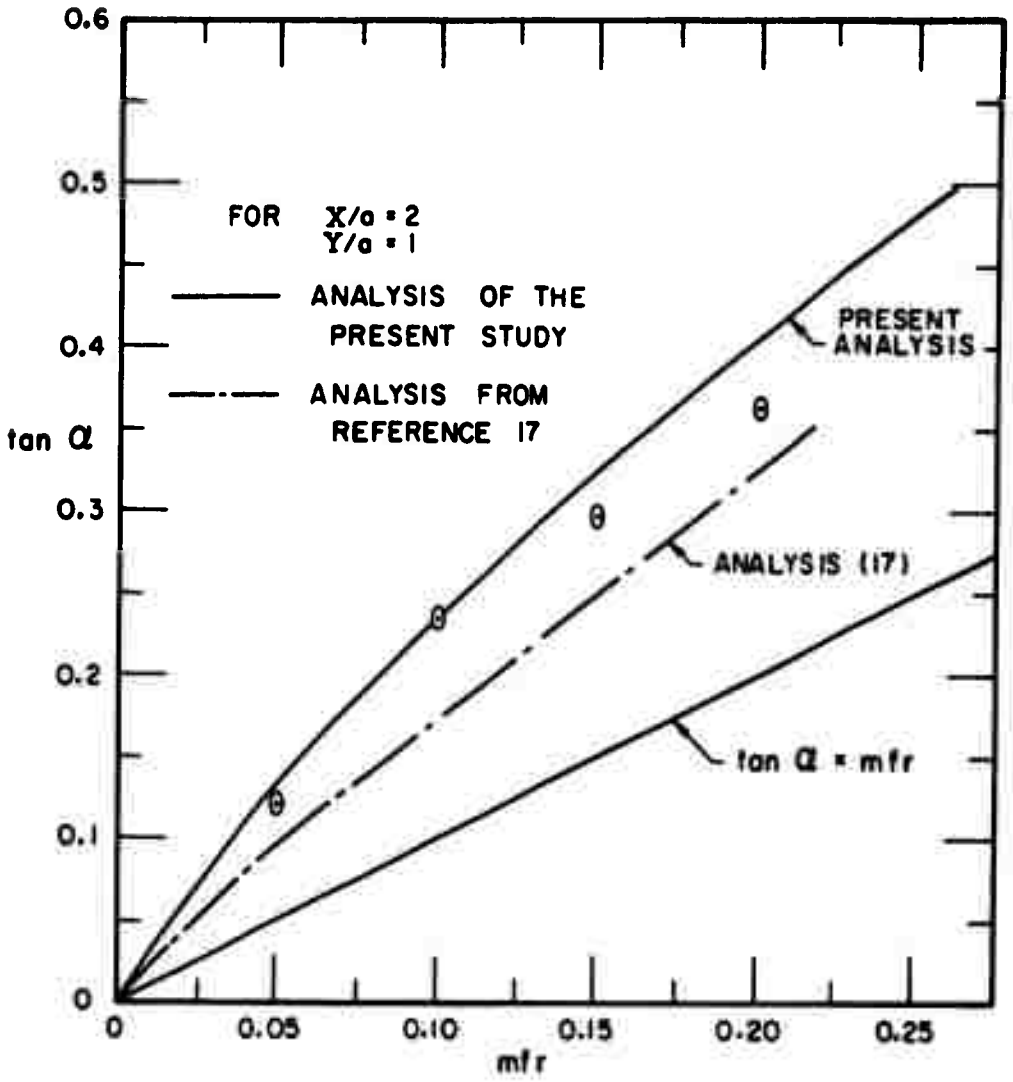

FIG. 32 tan α VERSUS mfr , EXPERIMENTAL AND ANALYTICAL VALUES , k =0.5

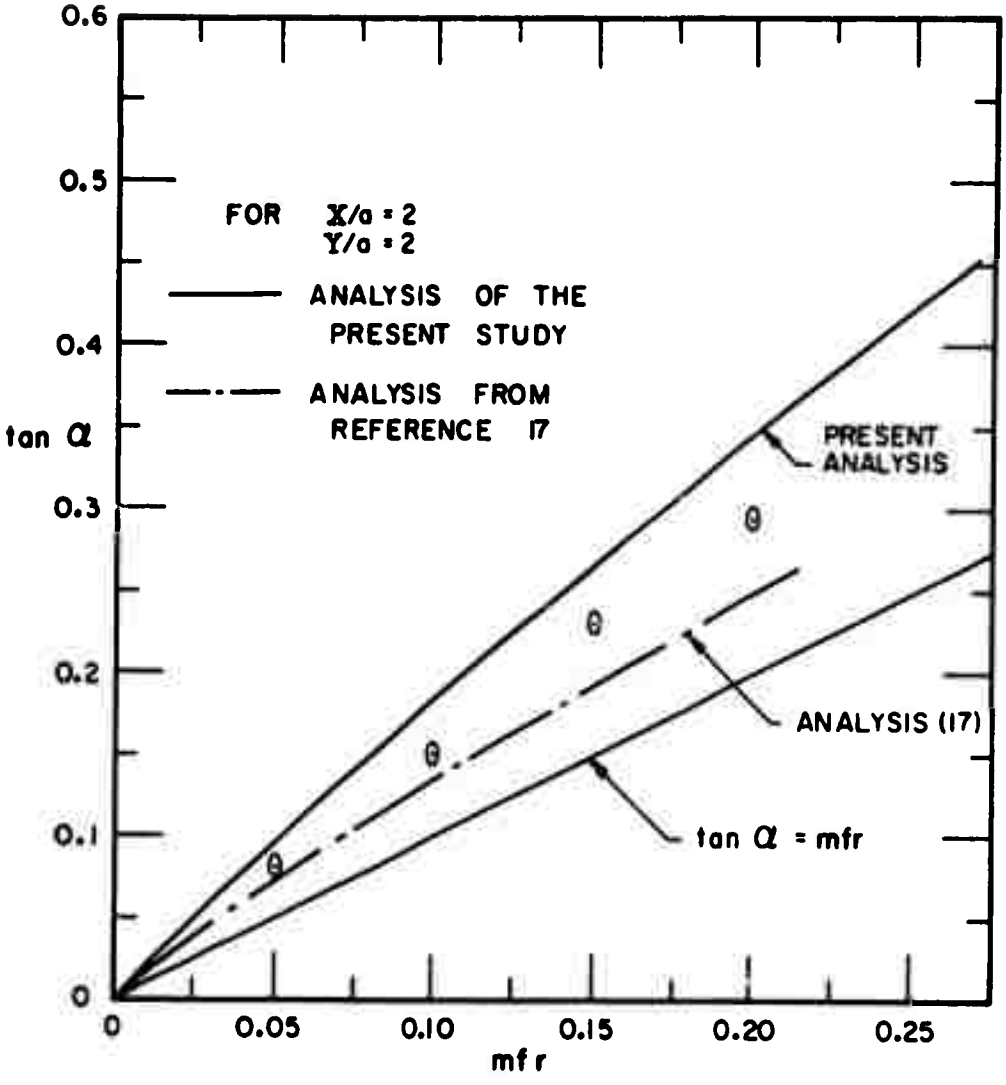

FIG. 33 tan α VERSUS mfr , EXPERIMENTAL AND ANALYTICAL VALUES , k = 1.0

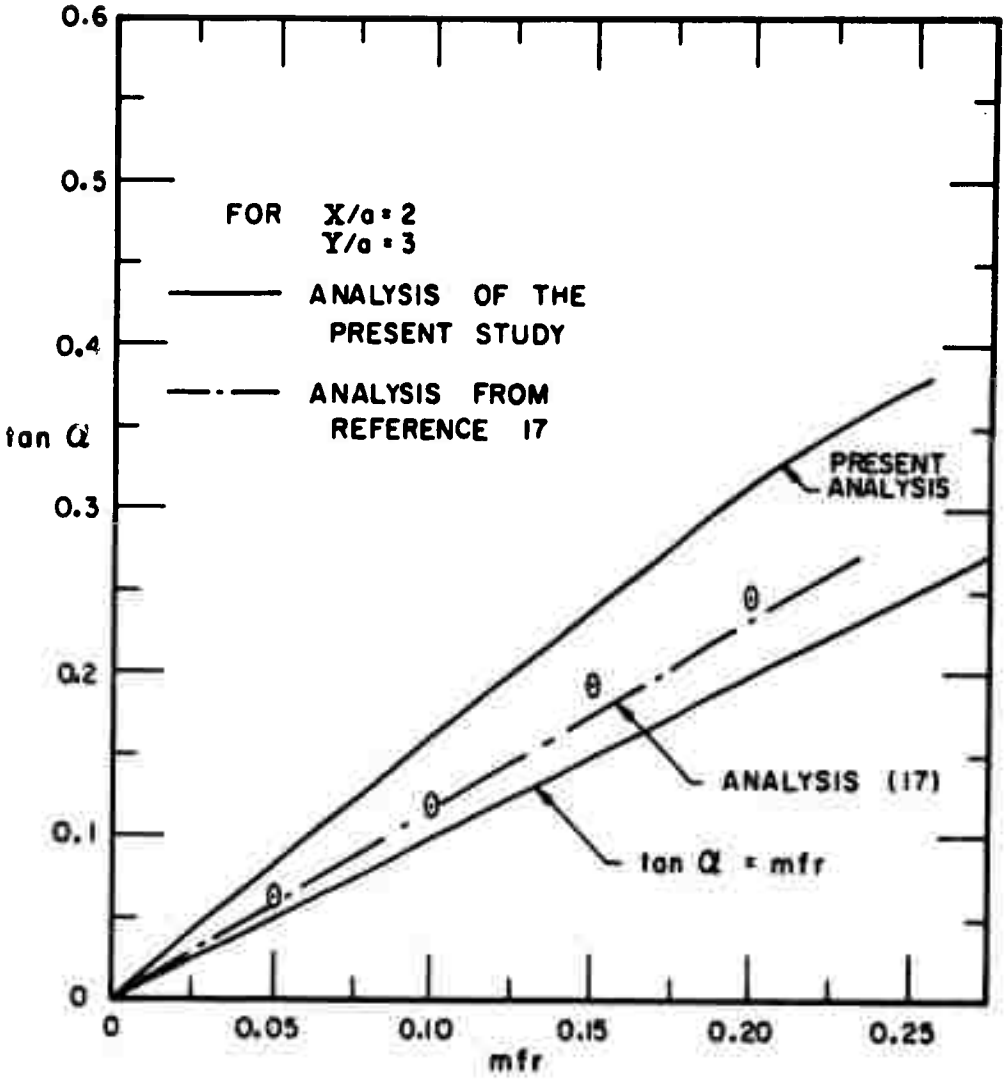

FIG. 34 tan α VERSUS mfr , EXPERIMENTAL AND ANALYTICAL VALUES , k = 1.5

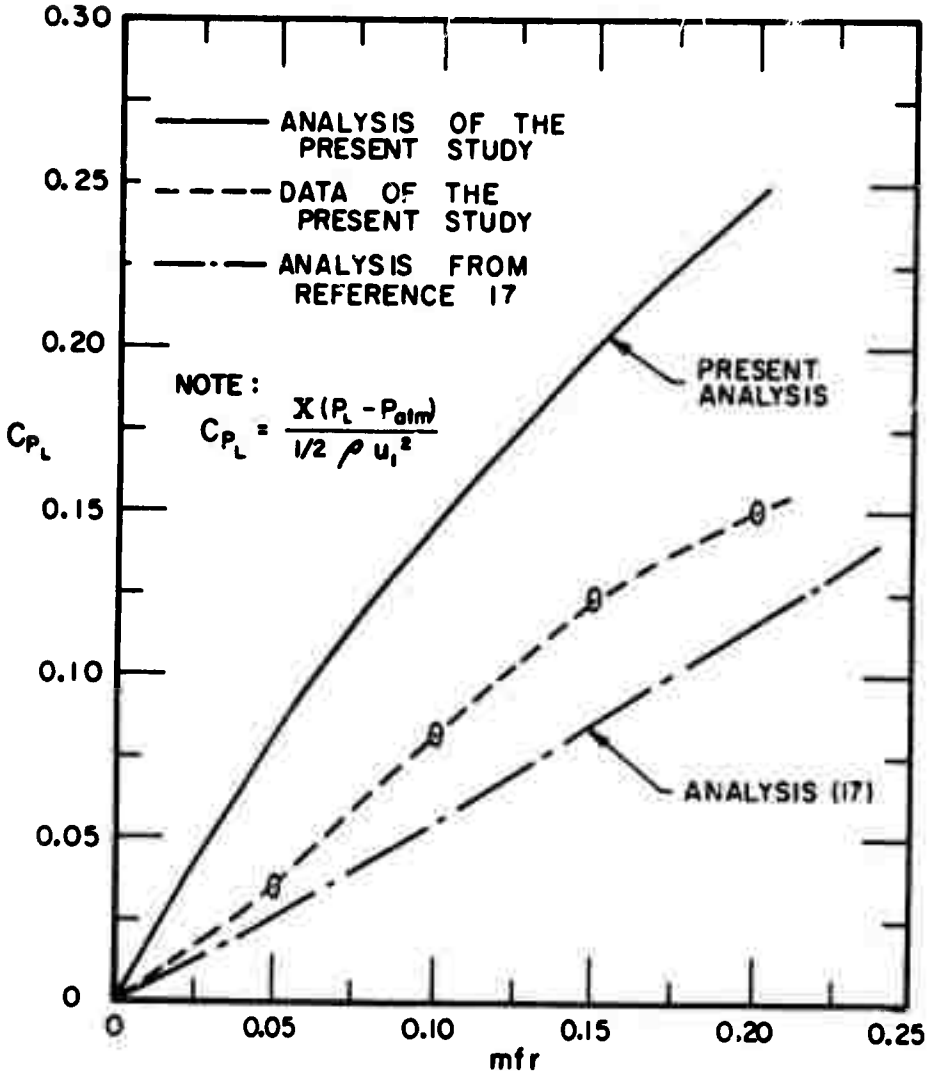

FIG. 35 C_{P_L} VERSUS mfr , EXPERIMENTAL AND ANALYTICAL VALUES , k =0.5

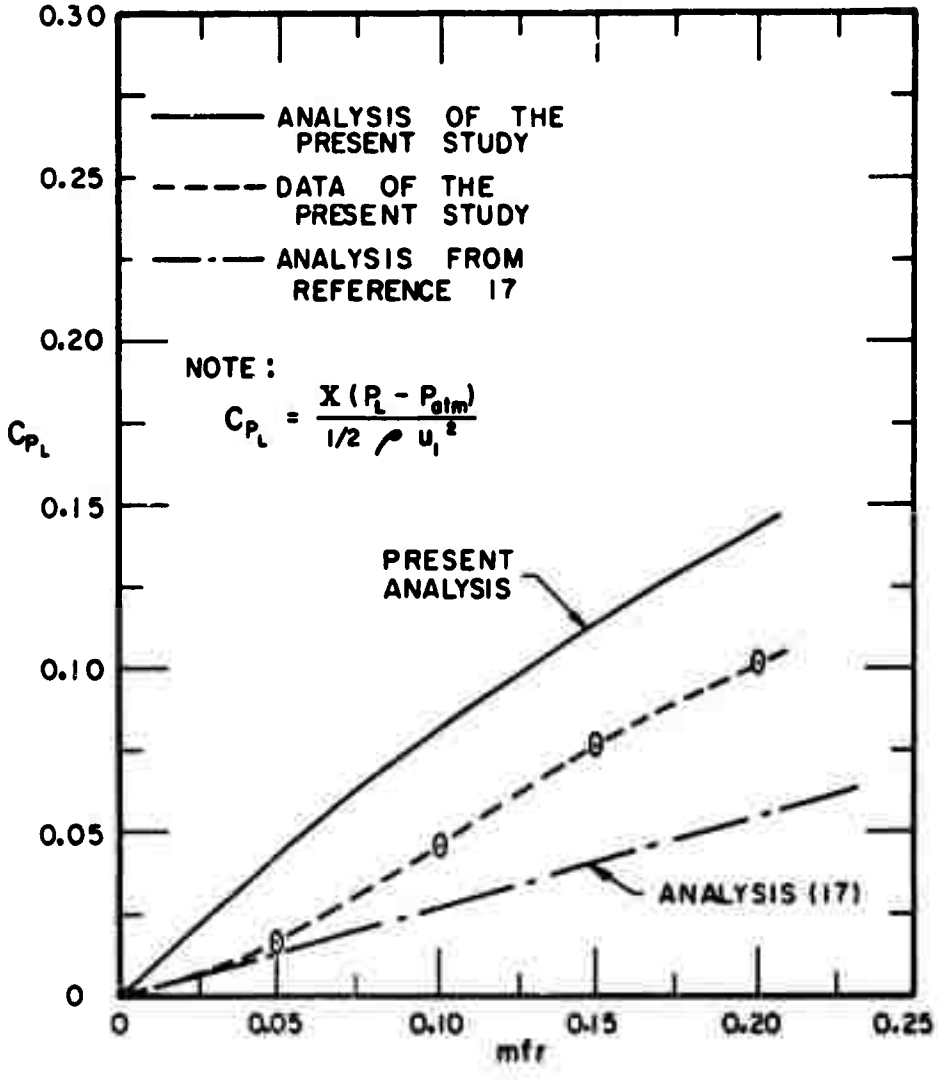

FIG. 36 C_{P_L} VERSUS mfr , EXPERIMENTAL AND ANALYTICAL VALUES , k = 1.0

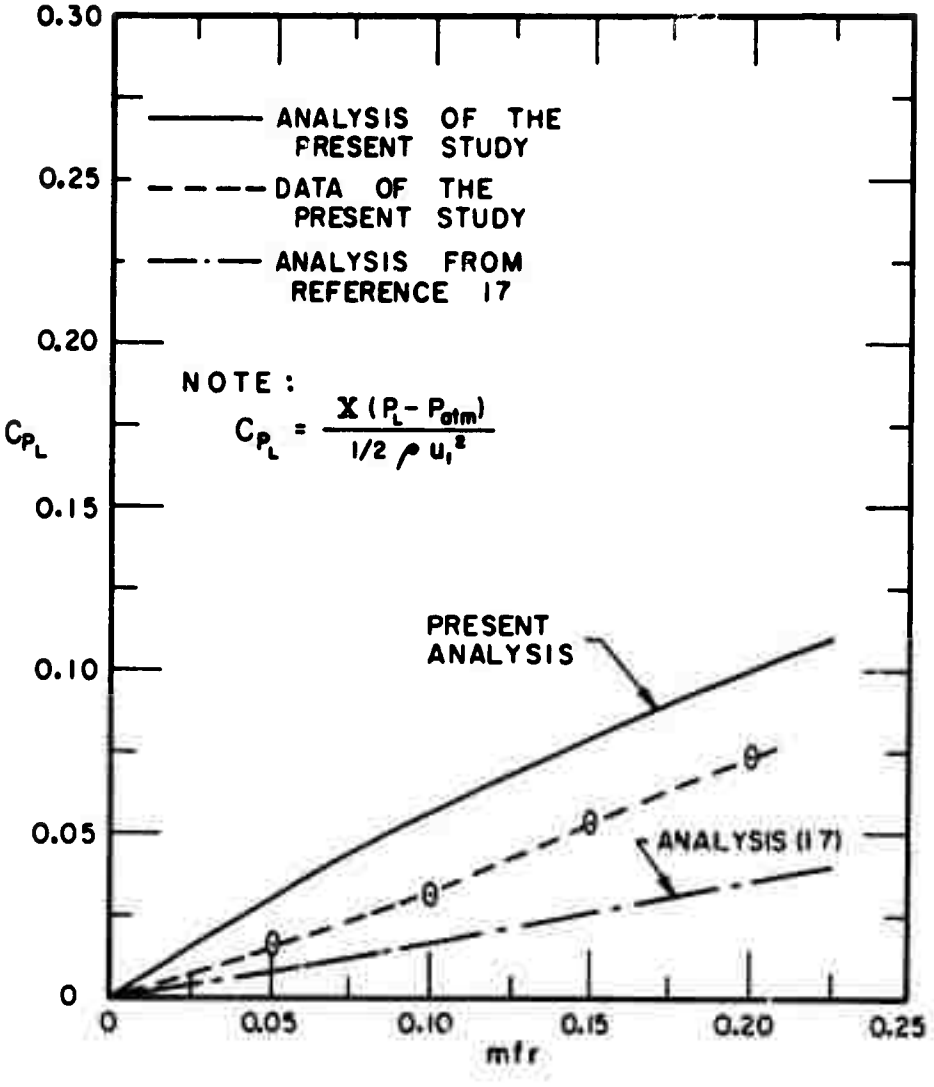

FIG. 37 C_{P_L} VERSUS mfr , EXPERIMENTAL AND ANALYTICAL VALUES , k = 1.5

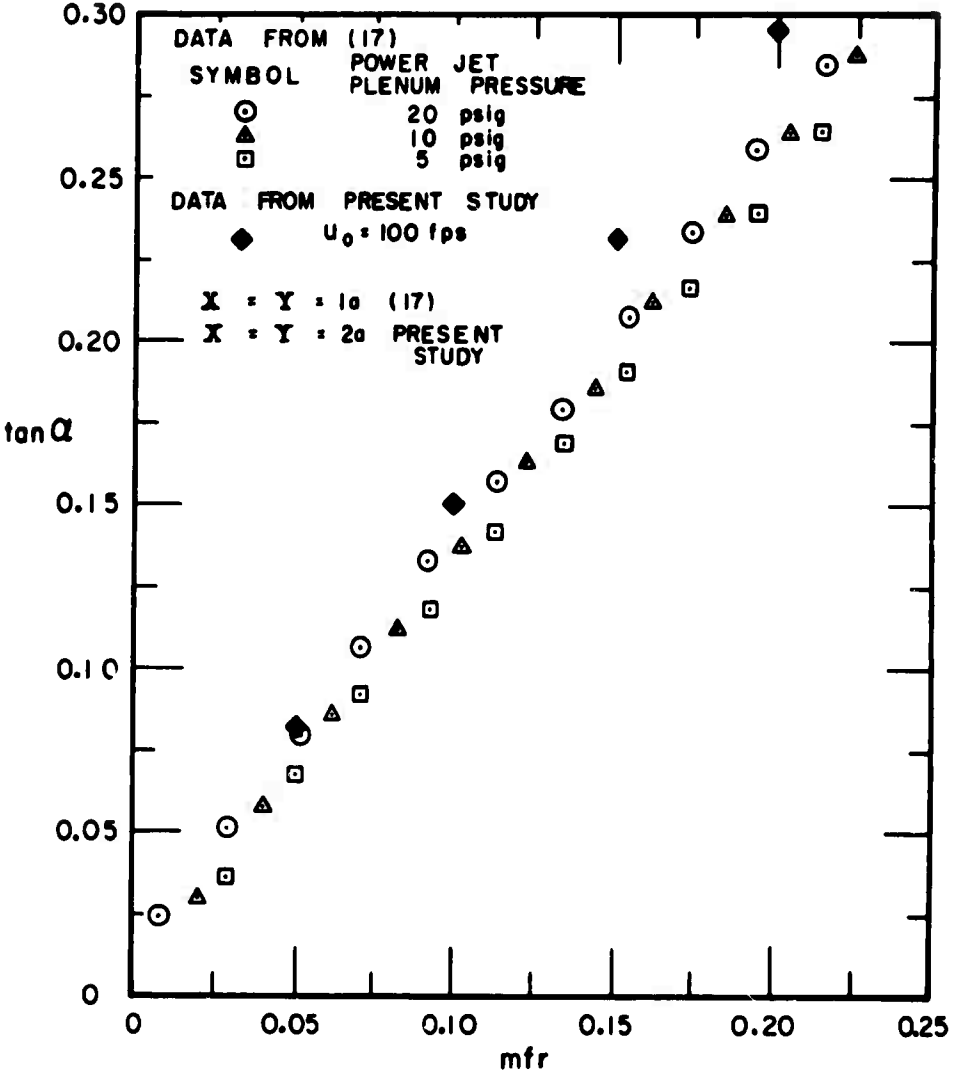

FIG. 38 COMPARISON OF tan α FROM (17) AND THE PRESENT STUDY

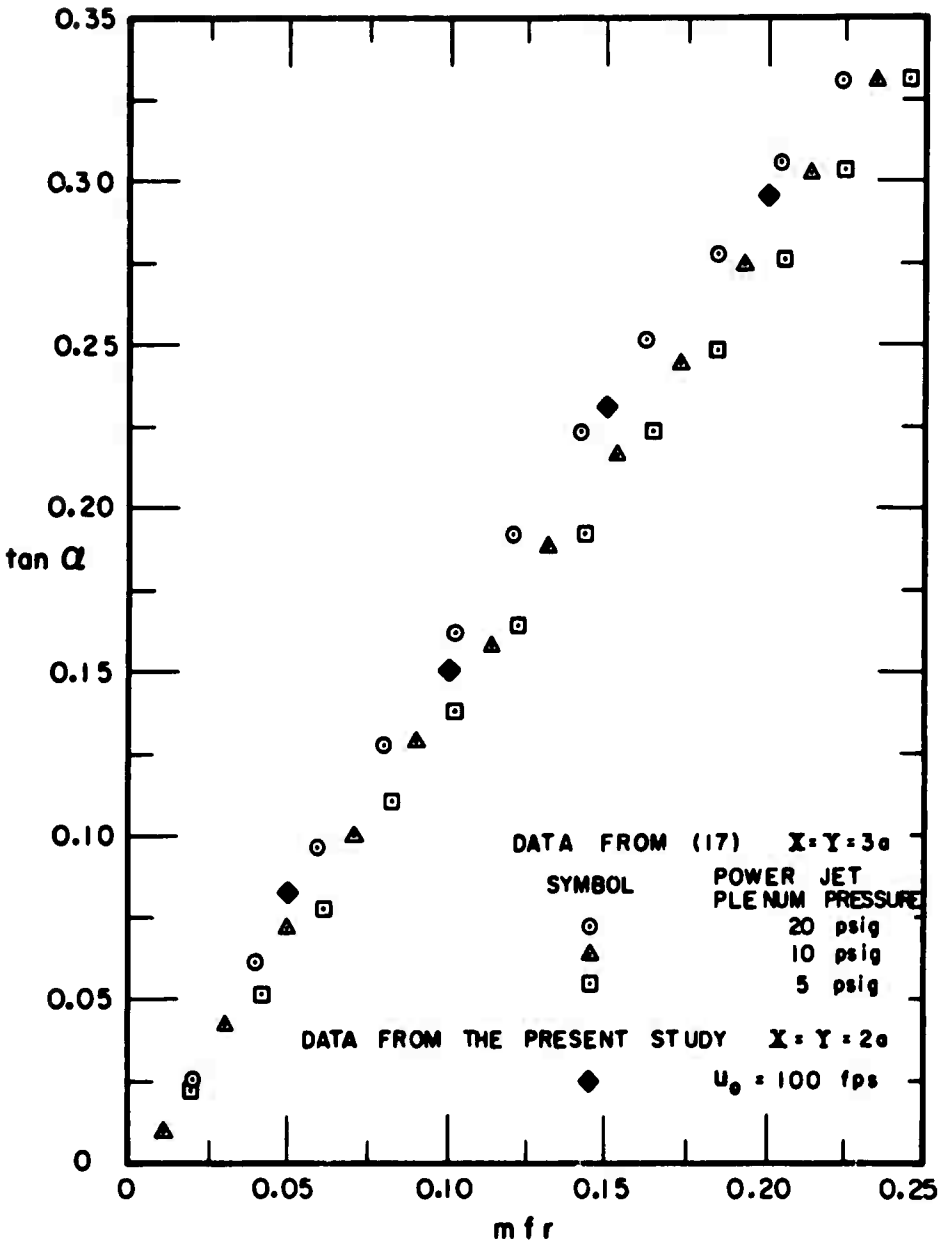

FIG. 39 COMPARISON OF tan α FROM (17) AND THE PRESENT STUDY

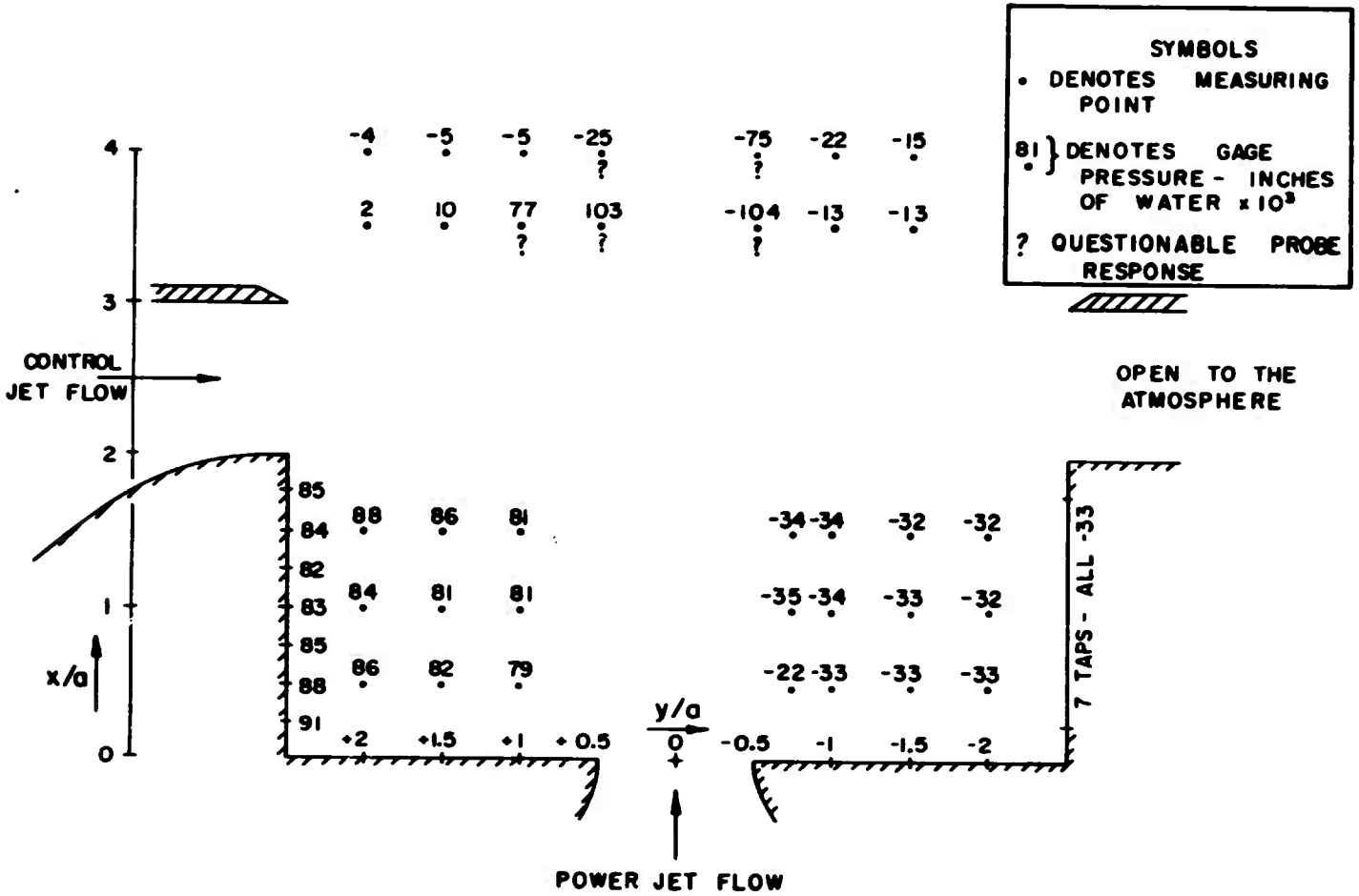

FIG. 40 STATIC PRESSURE DISTRIBUTION FOR mfr = 0.1, X = Y = 2a

DETAILED MEAN FLOW SURVEY - RESULTANT JET

Methods of Measurement and Data Evaluation

Flow Angle Measurements

Two methods of measurement were necessary to obtain complete $u(\overset{*}{y})$ data. The x - y - Θ traverse could only be used for direct measurements at $z/a = 0$ and +2. Consequently another method had to be devised to obtain the flow direction for $z/a = \pm 1, -2$, and $\pm 2\frac{1}{2}$. The trident probe, mounted in the $\Theta = 0$ position, was used for these angular measurements.

After mounting the trident probe on the x - y - z traverse device, a traverse was made to obtain the differential reading from the two 45 degree impact tubes. The total pressure was also recorded for this traverse. This differential reading was denoted as $\Delta h_{T_{45}}$. In a separate series of calibration runs (see Appendix B) the relationship

$$\Theta = \Theta \left(\Delta h_{T_{45}/q} \right)$$

was determined. Consequently, if the values of q and $\Delta h_{T_{45}}$ are known as a function of $\overset{*}{y}$, the $\Theta(\overset{*}{y}/a)$ distribution can be considered to be known. A discussion of the calibration technique and the presumed accuracy of this method as well as the comparison of the $u(\overset{*}{y}/a)/u_c$ and $\Theta(\overset{*}{y})$ distributions from the two methods are presented in Appendix B.

Data Processing

Since two measurement methods were used, the data processing was similarly of two distinct types. These will be discussed separately; they are referred to as method 1 for the data collected by the x - y -Θ device and method 2 for the data collected by the x - y - z device.

Method 1 was the more direct in that the flow angle and the total pressure could be measured directly. The static pressure was measured in a separate traverse. In order to ensure a matching of these separate traverses, h_T was measured in the same traverse as h_S and the $h_T(y^*)$ from the x - y - Θ device was then compared with the $h_T(y^*)$ from the x - y - z device. By this procedure, the matching of the corresponding y values depended upon matching 15 to 20 measurements from each traverse and is considered to be quite reliable in a statistical sense. The data were then considered to be ready for the computer. A discussion of the computations performed will be deferred until the description of method 2 is given.

Two traverses were also required for method 2. The first traverse was made with the tapered total and the forward facing static probes mounted on the x - y - z traverse device; h_T and $\Delta h_{T_{45}}$ were measured on the second using the trident probe in the Θ = 0 position. A matching of the $h_T(y^*)$ profiles similar to that of method 1 ensured a matching of the y^* values. The data for method 2 was then compiled as h_T, h_S, and $\Delta h_{T_{45}}$ as a function of y^*.

The quantities computed from all traverses were:

(a) as a function of y^*

i) Θ, V, u, v, $P/\frac{1}{2}\rho u_c^2$, q

ii) u/u_c, $(u/u_c)^2$, (v/u_c)

iii) u_*/u_{c_*}, $(u_*/u_{c_*})^2$

(b) for each traverse

i) $\int_{-y_{max}}^{y_{max}} (u/u_c)^N \, dy$ and

$\int_{-y_{max}}^{y_{max}} (q/q_c) \quad (u/u_c) \, dy$

ii) $\int_{-\xi_{max}}^{\xi_{max}} (u_*/u_{c_*})^N \quad d\xi$ and

$\int_{-\xi_{max}}^{\xi_{max}} (q/q_c) \quad (u_*/u_{c_*}) \quad d\xi$

for N = 1 and 2

u_* is the mean velocity component parallel to the axis of the resultant jet; u_{c_*} is the maximum value of u_*.

The integrations in part (b) above yield mass, momentum and energy flux thickness with respect to the fixed geometric co-ordinates x, y, z and the streamline co-ordinates ζ, ξ, z.

The computer program written for these computations is presented in Appendix D. Because of the differences in the

experimental techniques, the program has two input paths; however, once the value of Θ is known, the computational procedure for the values of V, u, v, (u/u_c), (v/u_c), $(u/u_c)^2$, and $P/\frac{1}{2}\rho u_c^2$ were quite straightforward.

Since the measurements were made with respect to the geometric variables x, y, z, the velocity components u and v are given with respect to these co-ordinates. However, if one wishes to compare the resultant jet profile with the undeflected jet or with a two-dimensional jet this comparison could also be made with the profile expressed in ζ, ξ, z co-ordinates. (ζ is measured along the axis of the resultant jet with its origin at the power jet nozzle exit, ξ is measured perpendicular to ζ and z, and ζ, ξ, and z form a right hand orthogonal co-ordinate system.) The question is then, "How should the u(x, y) be translated into $u_*(\zeta, \xi)$?" The following technique was adopted for the computation of $u_*(\zeta, \xi)$. First, $u_*(x, y)$ was computed. Then a Taylor series was employed, with only the first two terms being considered, giving

$$u_*(\zeta, \xi) = u_*(x, y^*) + \frac{\partial}{\partial \zeta} u_*(x, y^*) \Delta\zeta$$

Note that $\Delta\zeta = 0$

The term $\frac{\partial}{\partial \zeta} u_*(x, y^*)$ was evaluated by considering the $u_*(x, y^*)$ to behave as a two-dimensional jet (i.e. the mean velocity follows a Gaussian distribution). The center line velocity decay was assumed to be equivalent to the decay relation from the previously obtained single bounded jet data. The momentum flux thickness was available from the calculated value of b in an earlier step of the program. The details of the computational procedure are presented in Appendix D.

Results

The two primary objectives of the detailed flow study are (i) to determine the character of the mean flow in the resultant jet and (ii) to determine the nature of the interaction process by inference from the characteristics of the resultant jet.

The character of the resultant jet can be inferred from several comparisons. Three-dimensional effects are indicated by differences in the velocity profiles, the flux ratios, and the centerline velocity variation (with x) as a function of z. The character of the resultant jet can also be assessed by a comparison of pertinent items with the single bounded jet.

The role of the vortex stretching will be very important in determining the nature of the resultant jet.

Three basic sets of results are presented for this section; they are:

(i) the complete velocity profiles, see Figures 41 to 46,*

(ii) isobaric contours in Figures 47 to 49,

(iii) characteristics of the jet, viz., centerline velocity distribution and mass, momentum, and energy flux ratios, see Figures 50 to 53.

The velocity profiles are presented for seven z/a and three x/a locations and are shown as $u(y^*)/u_c$ and $u_*(\eta_*)/u_{c_*}$. The isobaric contours are formed from given values of the non-dimensional pressure, $(P_{atm} - P) / \frac{1}{2} \rho u^2_m$. These are presented as a function of ξ, z, i.e. in a plane normal to the mean flow. The measurements were made as a function of y and z but the value of $\frac{\partial P}{\partial \xi}$ is sufficiently small to set

---

* The figures that present the results of the detailed mean flow survey may be found at the end of this section, see page 131.

$P(y^*) = P(\xi)$ for all the y^* values encountered. The dashed portions of the contours are extrapolations to regions where no data were taken.

In the presentation of the results for the jet characteristics, the increase in mass flow rate was considered. For example, the term $M_0(1 + (mfr)^{\frac{1}{2}})$ was used instead of M_0 to account for the increased mass flow; $E_0(1 + (mfr)^{\frac{1}{2}})$ was used instead of E_0 to account for the increased energy flux. Since the value of the x-direction momentum flux ratio was used, the term aq_0 describes the initial momentum flux. The profiles at $x/a = 30$ are actually not sufficiently complete to yield a highly accurate measure of the flux ratios because they do not extend to low enough u/u_c values to consider the integration to be from $-\infty$ to $+\infty$. However, this defect is not serious since the outer portions of the profile contribute only a small portion of the total integral. This defect is most serious for the mass flux and least serious for the energy flux ratio.

Discussion of Results

From an examination of the results of this section, the following model is proposed to describe and account for the observed phenomena.

As the control jet flow strikes the power jet, the portion of the control jet adjacent to the near side pocket is directed into the near pocket. As Manion and Goto (17) describe it, this is similar to a jet impinging on a solid wall where half the normal component of flow goes to either side;

note however that the "solid wall" analogy is only used for the near side of the control jet. The remainder of the control jet flow "passes through" the power jet in what can be described as an infiltration process. This action is opposed to the inelastic impact model of intersecting jets. The infiltration process requires a substantial amount of time; consequently, the mean velocity of the power jet carries the mixing process downstream. The vortex stretching convective action in the resultant jet is of a different nature from that in the single bounded jet. This leads to an important difference in the character of the resultant jet as compared with the bounded jet; viz., the resultant jet is relatively wider. Finally, the interaction process is a three-dimensional one even though the downstream length is relatively small in comparison with the width between the plates ($(z_{max} - z_{min}) / x_{app} \approx 3$).

Aspects of the above flow model are discussed below in terms of ther individual and related effects. Data of the present study and other references which are pertinent are employed for the discussion.

As Manion and Goto (17) indicate, the control jet fluid which is directed into the near side pocket after the intersection is responsible for the increased static pressure in this region, see the data in Table 4. Since the fluid in the near pocket is probably composed of the same particles (i.e., a standing vortex) with the exception of entrainment by the power jet, the increased pressure results from a pumping action wherein the control jet entrains part of the near side pocket fluid and redirects it into the pocket. Figure 54 shows the

proposed flow pattern. The decelerating agent is the increased

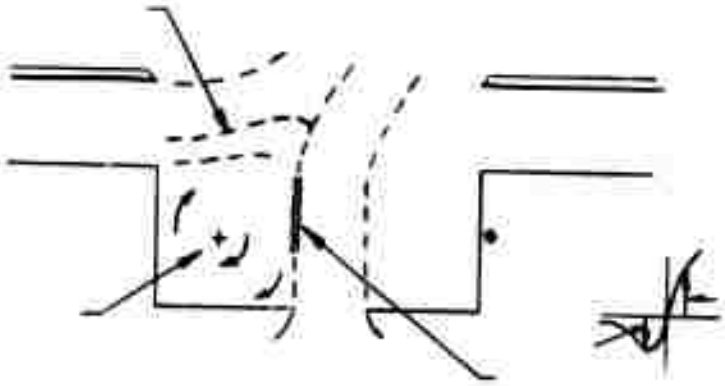

FIGURE 54 Definition of terms used in jet intersection model

pressure. There are wo other direct results from this splitting of the control jet flow; there are (i) a very strong vortex production in the near side of the power jet and (ii) initial profiles of the resultant jet which are skewed to the left ($+ y'$)*. The result of the vortex production, caused by the power jet - returning control jet velocity distribution, will probably have the form of a well defined vortex sheet. The initial profiles which are skewed to the left are shown in Figure 44. The Gaussian error curve is included on each z/a plot for reference; the skewness of the profiles is apparent by comparison with the symmetric reference curve.

The infiltration process by the control jet is seen in the non-dimensional velocity profiles for the resultant jet at x/a = 15 and 30, see Figures 45 and 46. The original skewed

---

* The control jet flow enters the defined region from the left control jet. A distribution is skewed to the left if the third moment is positive (with the co-ordinate system of the present study where +y is to the left).

left profiles are now skewed to the right ($-y^*$) with the effect being more pronounced at $x/a = 30$ than at 15. The rate of infiltration is related to the degree of skewness with respect to the downstream distance since the longitudinal distance is the product of the convection velocity (viz., some fraction of u_{c_*}) and the infiltration time. The presence of two effects makes the net effect difficult to measure quantitatively. The $+y^*$ side of the jet at $x/a = 30$ is closer to the Gaussian curve than at $x/a = 15$. This indicates that the infiltration process has passed through the left side and the jet is returning to the form of a single bounded jet. Whether the infiltration process was completed before $x/a = 15$ cannot be ascertained from the data at hand. As discussed in the "Literature Survey" section, Olson (22)* has observed that the resultant jet appears to leave the interaction region from a point downstream of the intersection. He attributes this to a time delay in the interaction process. This observation and the proposed flow model are compatible.

That the convective effects of the vortex stretching are much stronger for the resultant jet can be seen by an examination of Figure 50. Although the difference in magnitudes of the u_c / u_0 values is slight, there is a pattern wherein u_m is less and u_c at $z/a = +2$ is greater when the resultant jet is compared with the single bounded jet.

This stronger vortex stretching effect may be explained by the flow model and the observed profiles of $u(y^*/a)$. The part of the control jet that turns upstream produces a very

---

* Olson's flow system is geometrically similar to the present study except the standoff and setback walls are removed.

strong vortex sheet on the left side ($+ y^*$), see Figure 54. Also, the right side of the jet has a steeper than usual profile because of the turning of the jet. Both of these effects give the vortex stretching action a stronger-than-normal start.

That the interaction process is inherently three-dimensional is inferred from data at $x/a = 5$, a station which is assumed to be close enough to the intersection zone that the intervening flow will not induce strong three-dimensional effects. The $u(y^*/a)$ profiles show that the velocity profiles differ with respect to z (Figure 41), the velocity being higher for a given y^* as $|\pm z|$ increases. Isobaric contours at $x/a = 5$ also show a strong three-dimensional character. The longitudinal distributions of $2bq_c/aq_0$ and E/E_0 $[1 + (mfr)^{3/2}]$ are also indicative of a three-dimensional phenomenon in the interaction region. While these distributions for the single bounded jet start together and then diverge, the distributions for the resultant jet are divergent between $x/a = 5$ and 30. This is interpreted as a developing three-dimensional effect for the former case and a fully three-dimensional effect for the latter.

Several pertinent observations may be made with regard to the overall data. The entrainment rate of the ambient fluid for the two flow cases is equivalent although the mass flux for the resultant jet is less than expected. The isobaric contours for $x/a = 15$ and 30 indicate that this aspect of the resultant jet flow has not yet attained the single bounded jet distribution.

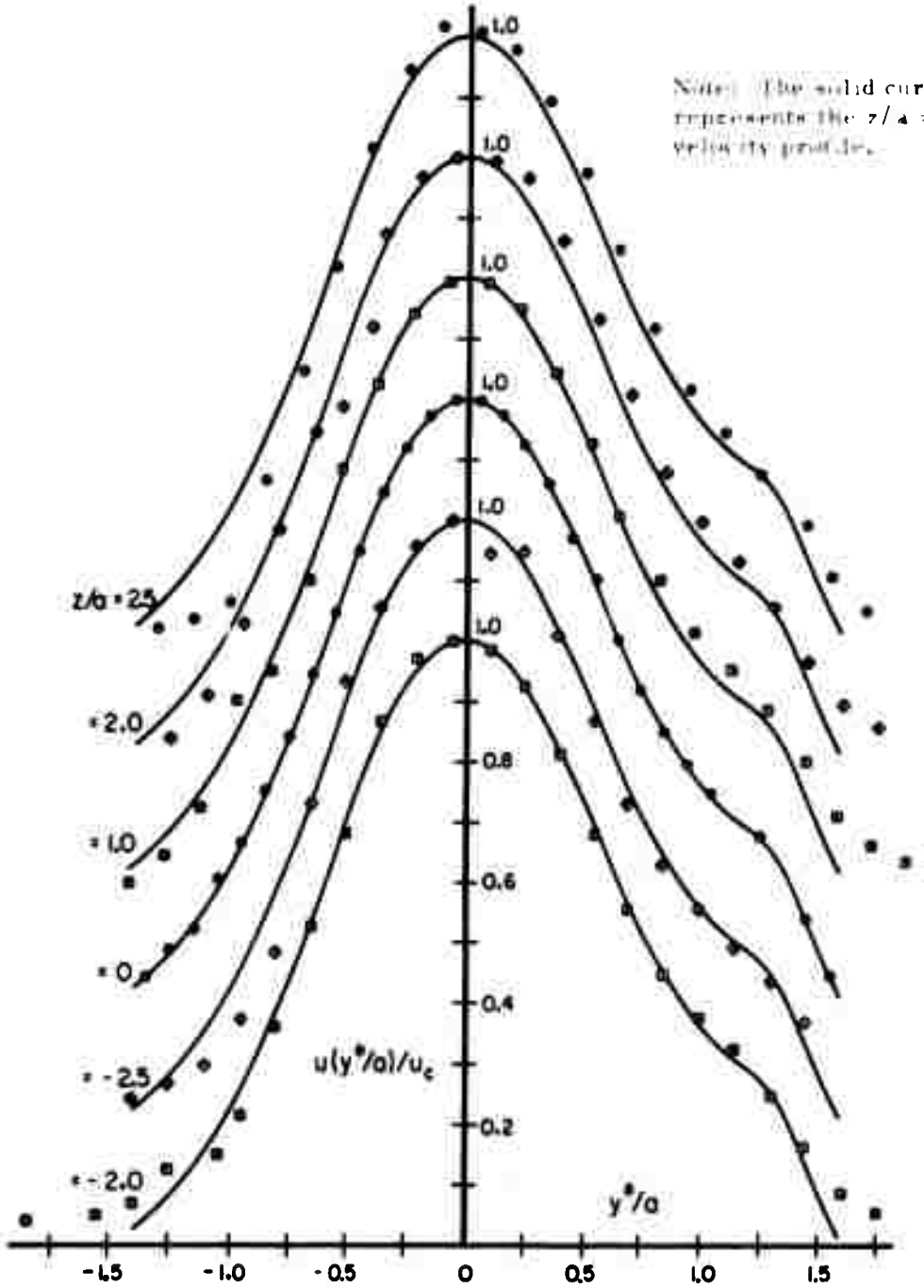

FIG. 41 $u(y^*/a)/u_c$ VERSUS y^*/a FOR $x/a = 5$, mfr=0.1, k= 1.0

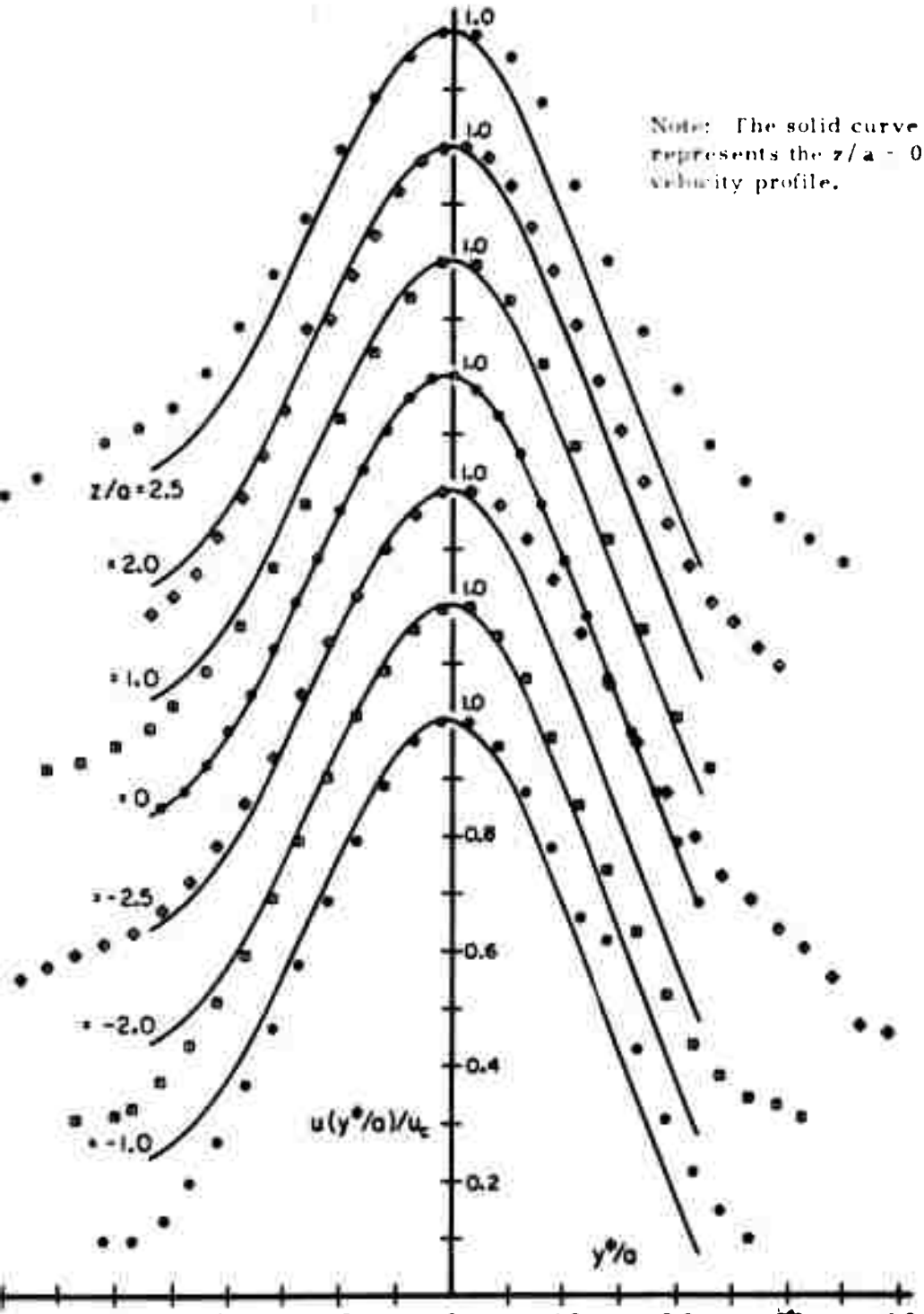

FIG. 42 $u(y^*/a)/u_c$ VERSUS y^*/a FOR $x/a=15$, mfr=0.1 , k = 1.0

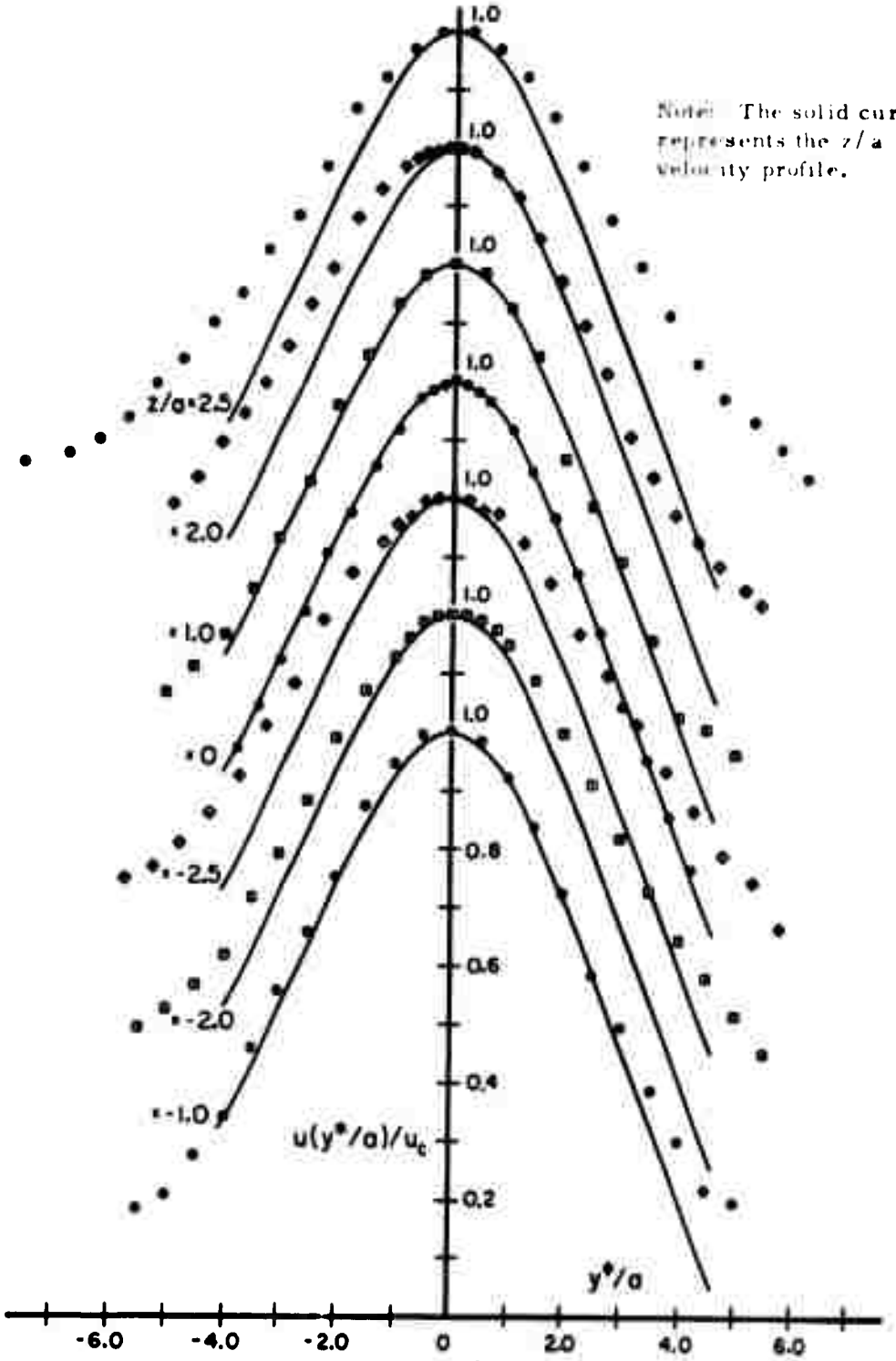

FIG. 43 $u(y^*/a)/u_c$ VERSUS y^*/a FOR $x/a=30$, mfr=0.1, k=1.0

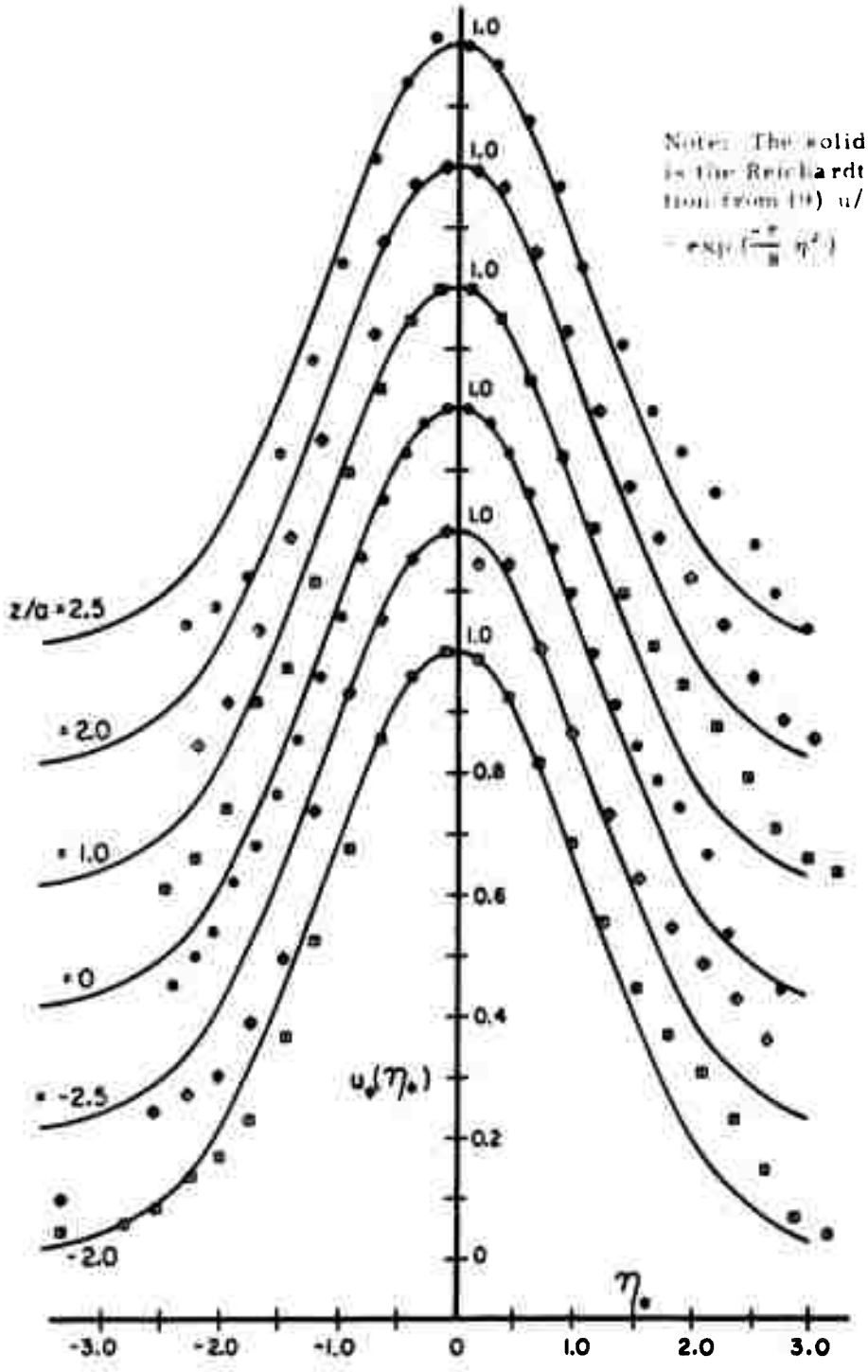

FIG. 44 $u_*(\eta_*)$ VERSUS η_* FOR x/a=5, mfr =0.1, k = 1.0

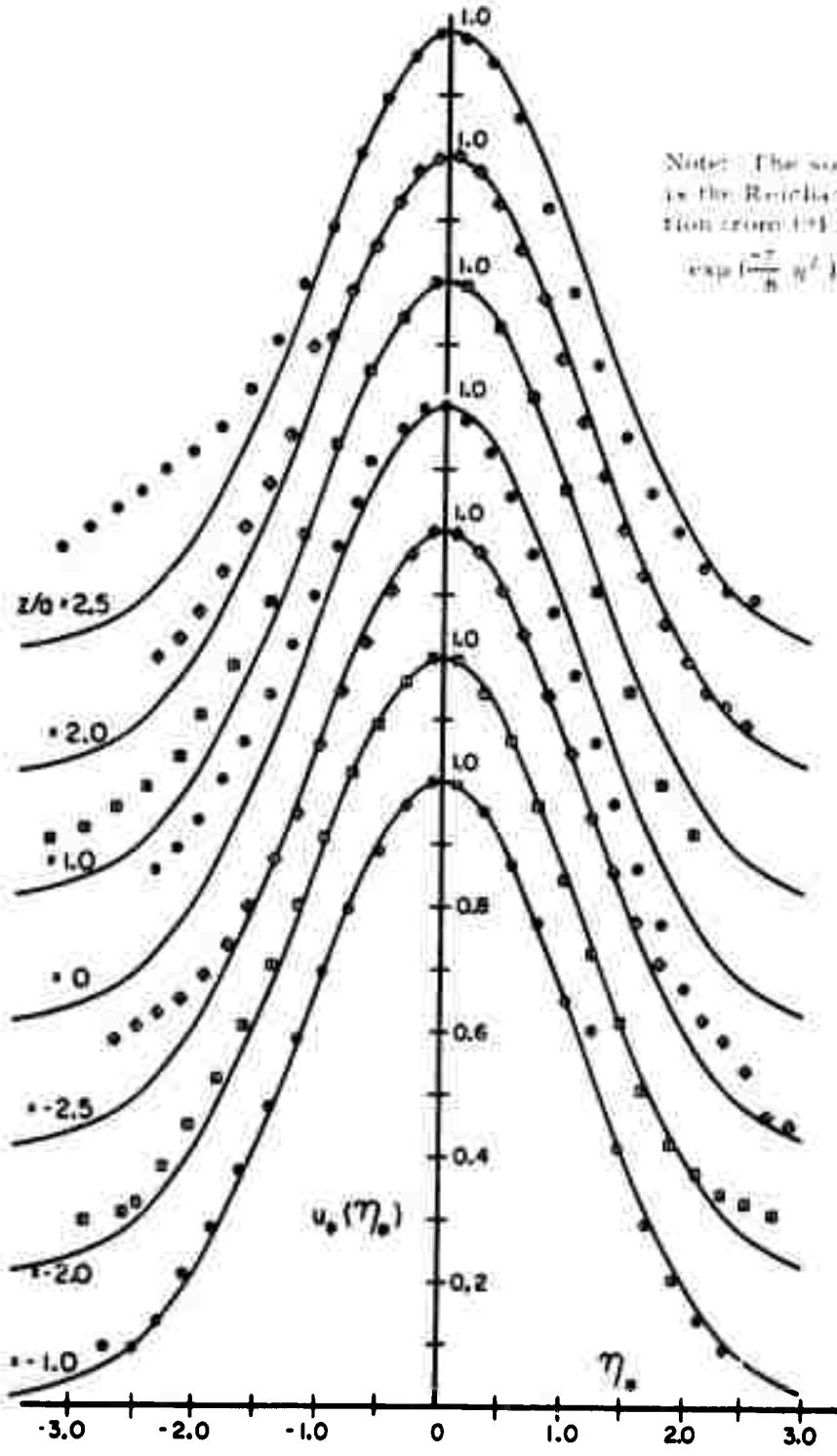

FIG. 45 $u_*(\eta_*)$ VERSUS η_* FOR x/b=15, mfr=0.1, k=1.0

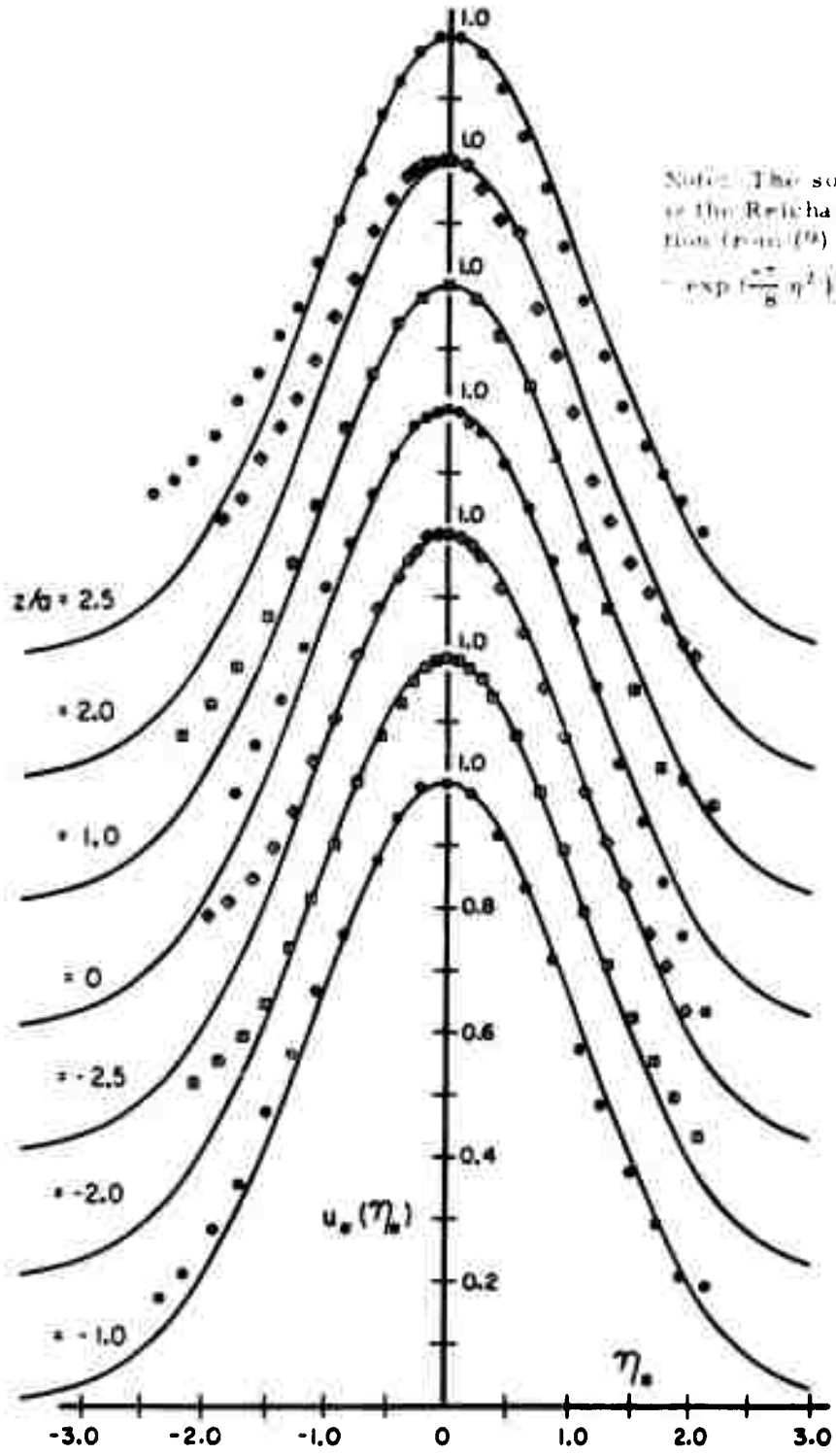

FIG. 46 $u_*(\eta_*)$ VERSUS η_* FOR x/a=30, mfr=0.1, k=1.0

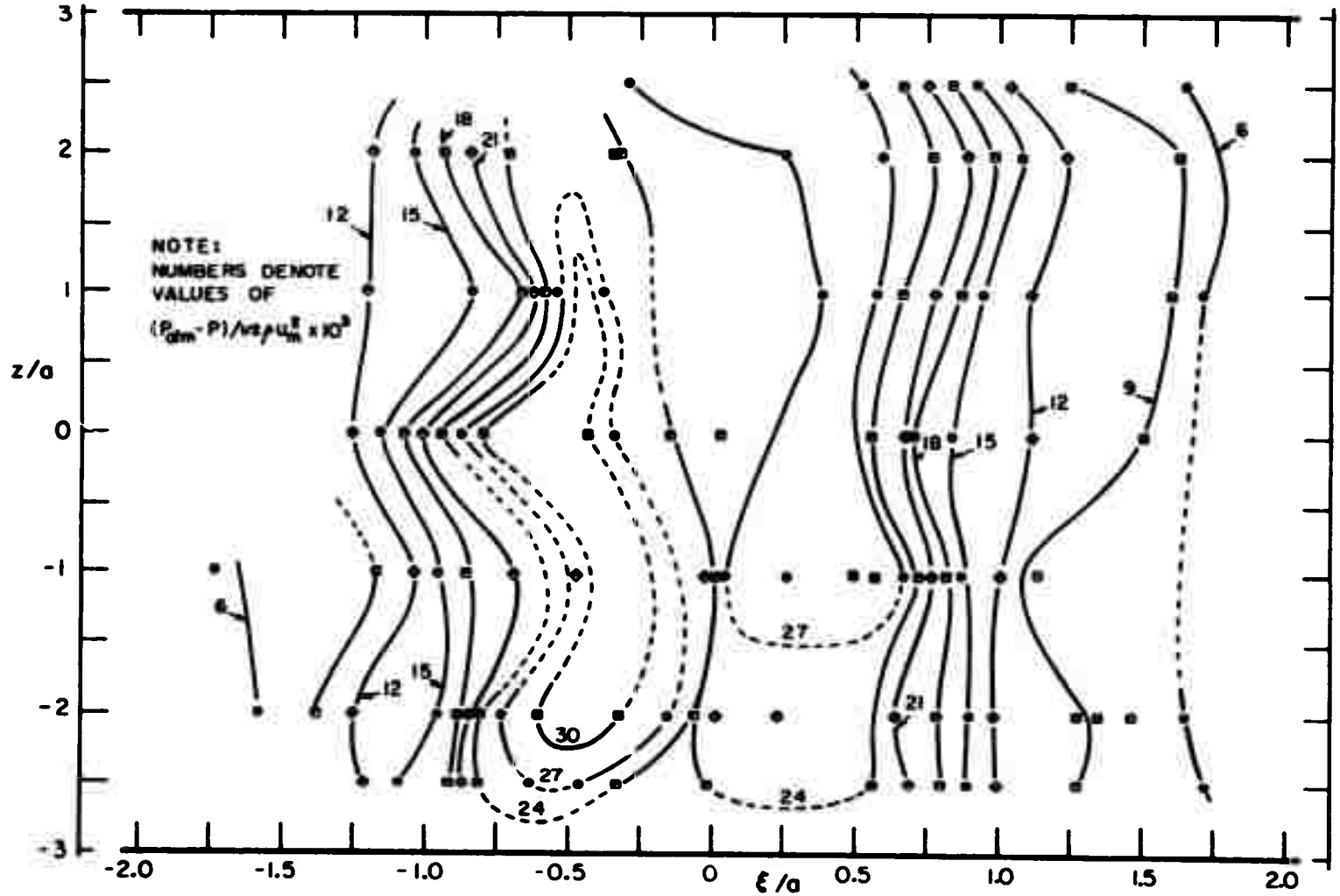

FIG. 47 ISOBARIC CONTOURS FOR $x/a = 5$, $(P - P_{atm})/\frac{1}{2}\rho u_m^2$ VERSUS ξ AND z

mfr = 0.1 , k = 1.0

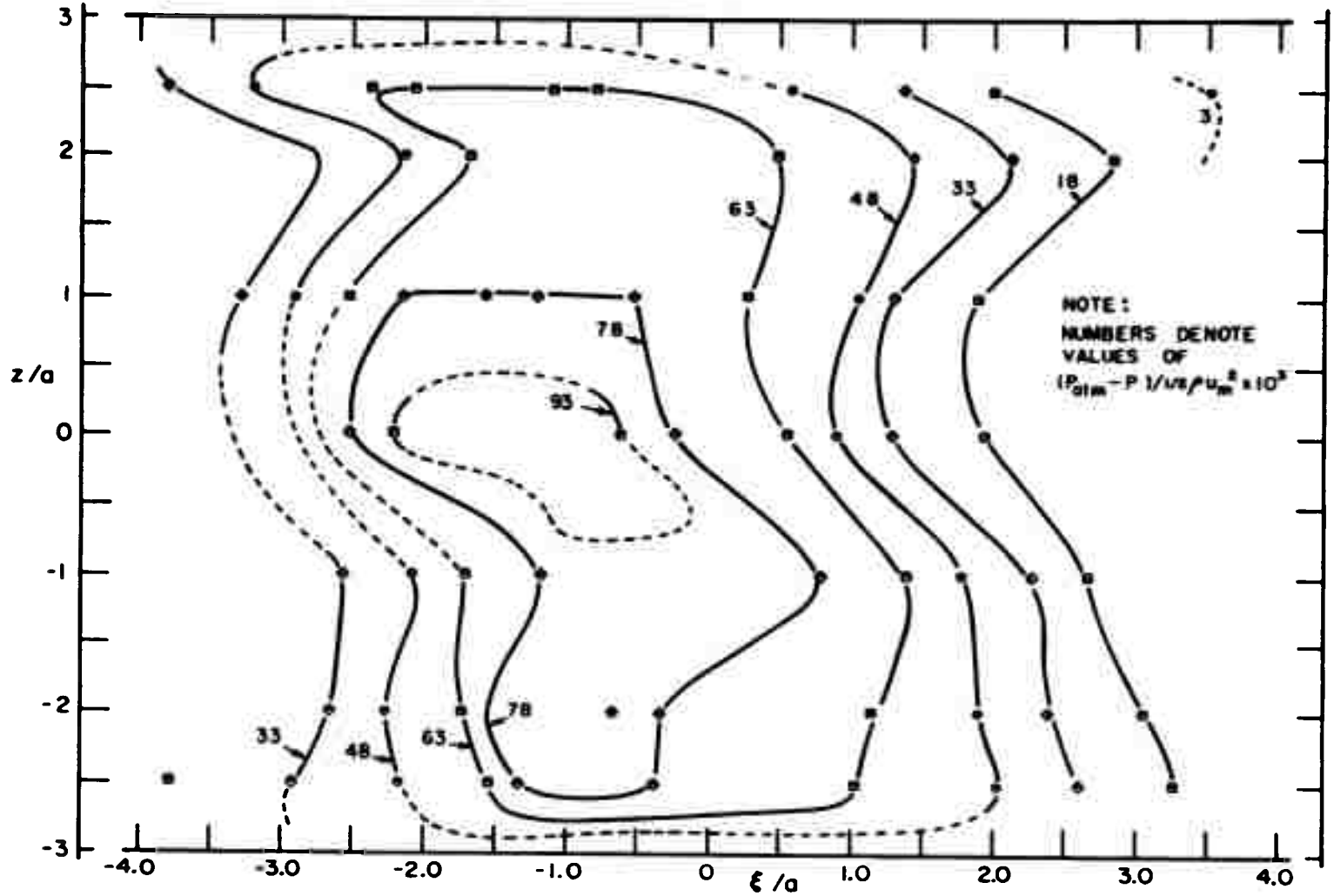

FIG. 48 ISOBARIC CONTOURS FOR $x/a = 15$, $(P - P_{atm})/1/2\rho u_m^2$ VERSUS ε AND z

mfr = 0.1 , k = 1.0

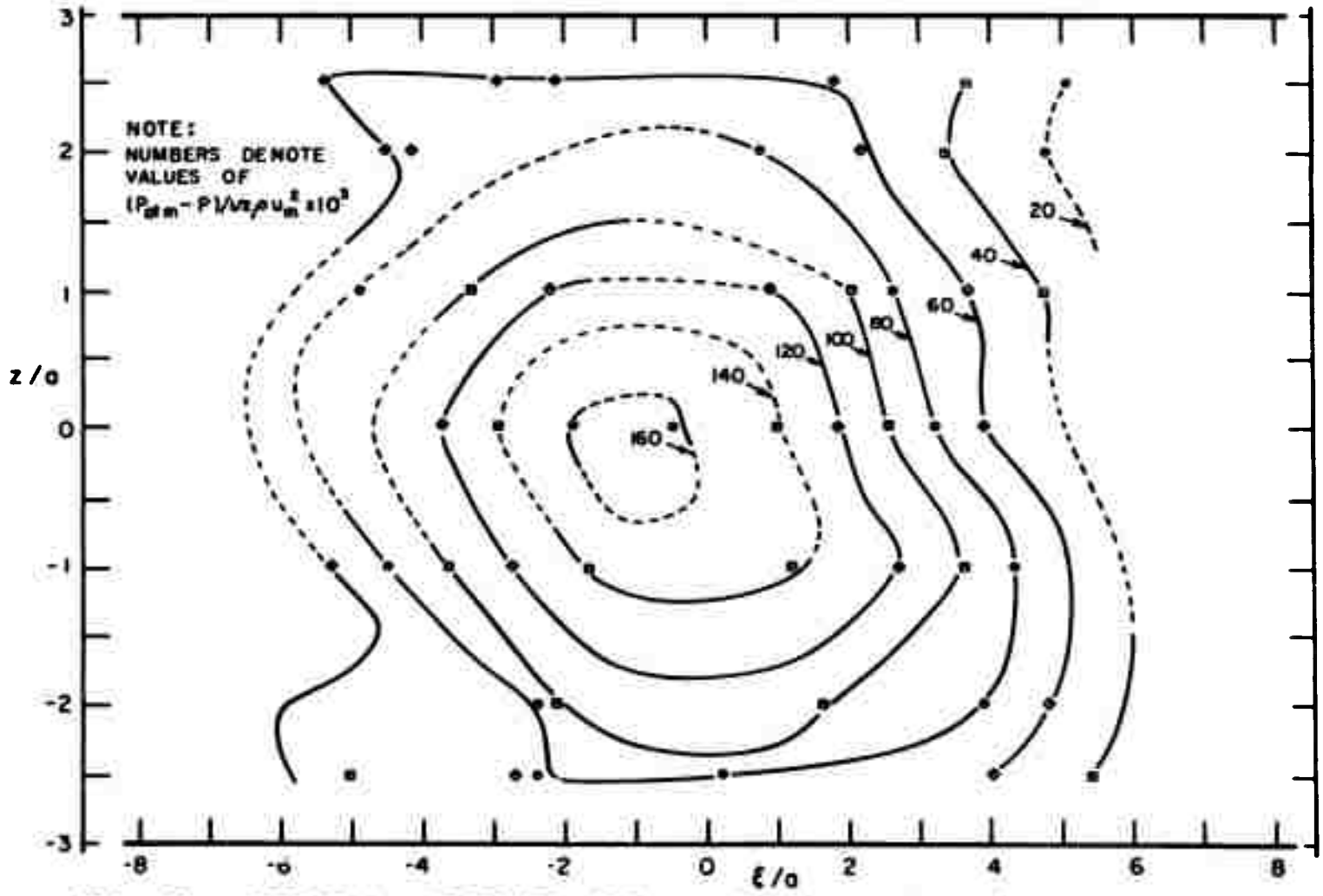

FIG. 49 ISOBARIC CONTOURS FOR $x/a = 30$, $(P - P_{atm})/\frac{1}{2}\rho u_m^2$ VERSUS ℓ AND z
$mfr = 0.1$, $k = 1.0$

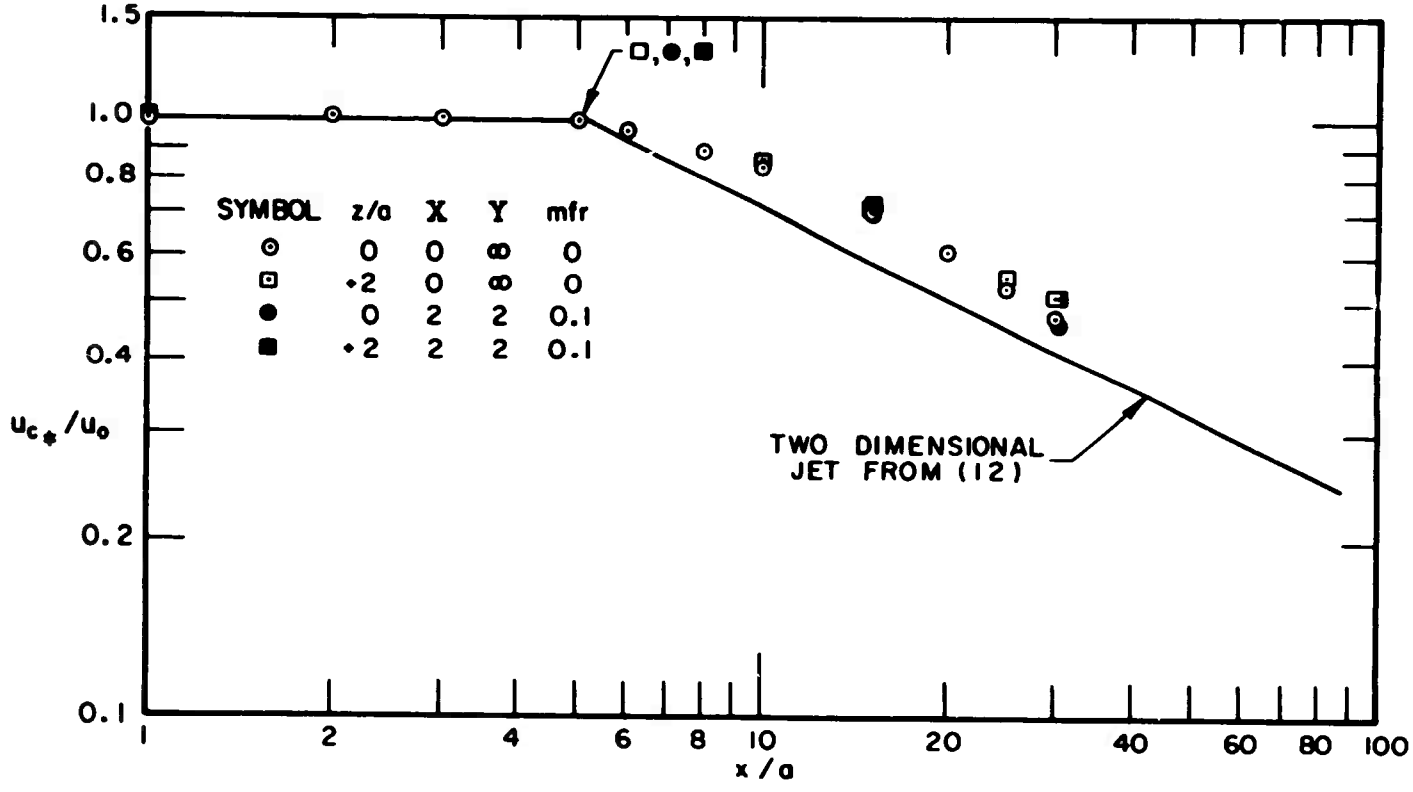

FIG. 50 CENTERLINE VELOCITY DISTRIBUTION FOR THE RESULTANT AND THE SINGLE BOUNDED JET

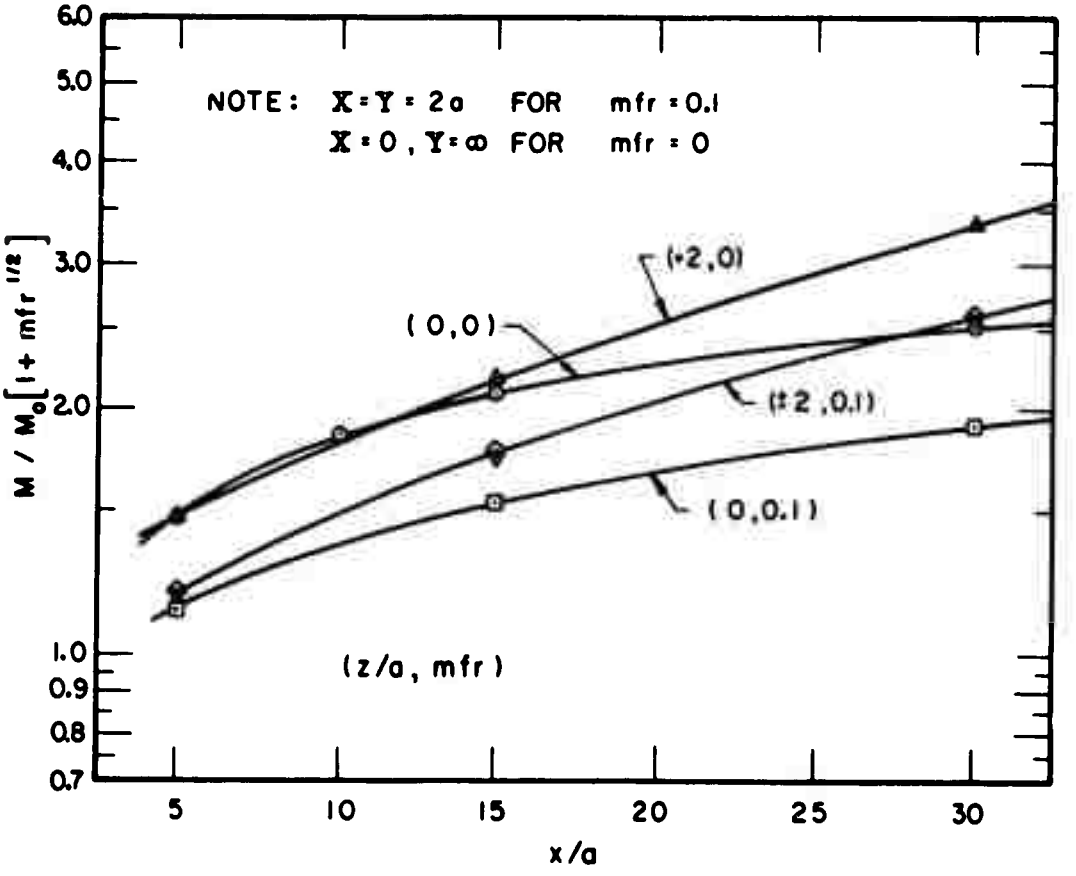

FIG. 51 MASS FLUX RATIOS FOR THE RESULTANT AND THE SINGLE BOUNDED JETS

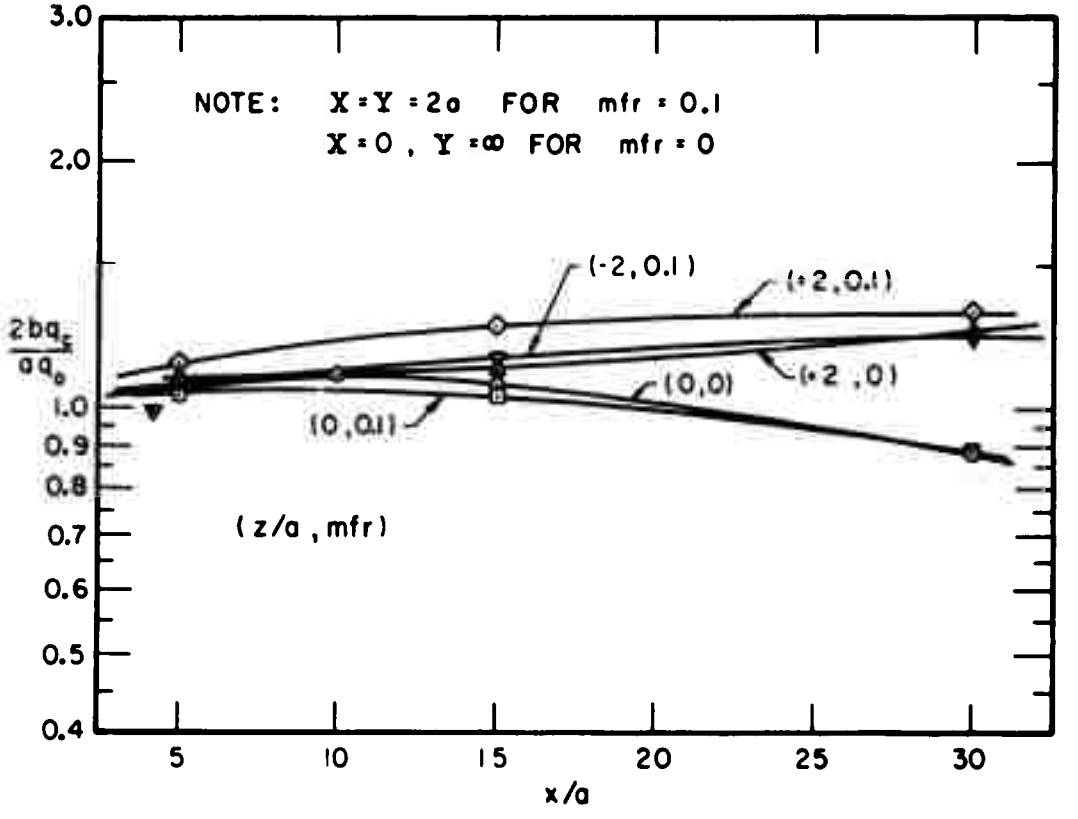

FIG. 52 MOMENTUM FLUX RATIOS FOR THE RESULTANT AND THE SINGLE BOUNDED JETS

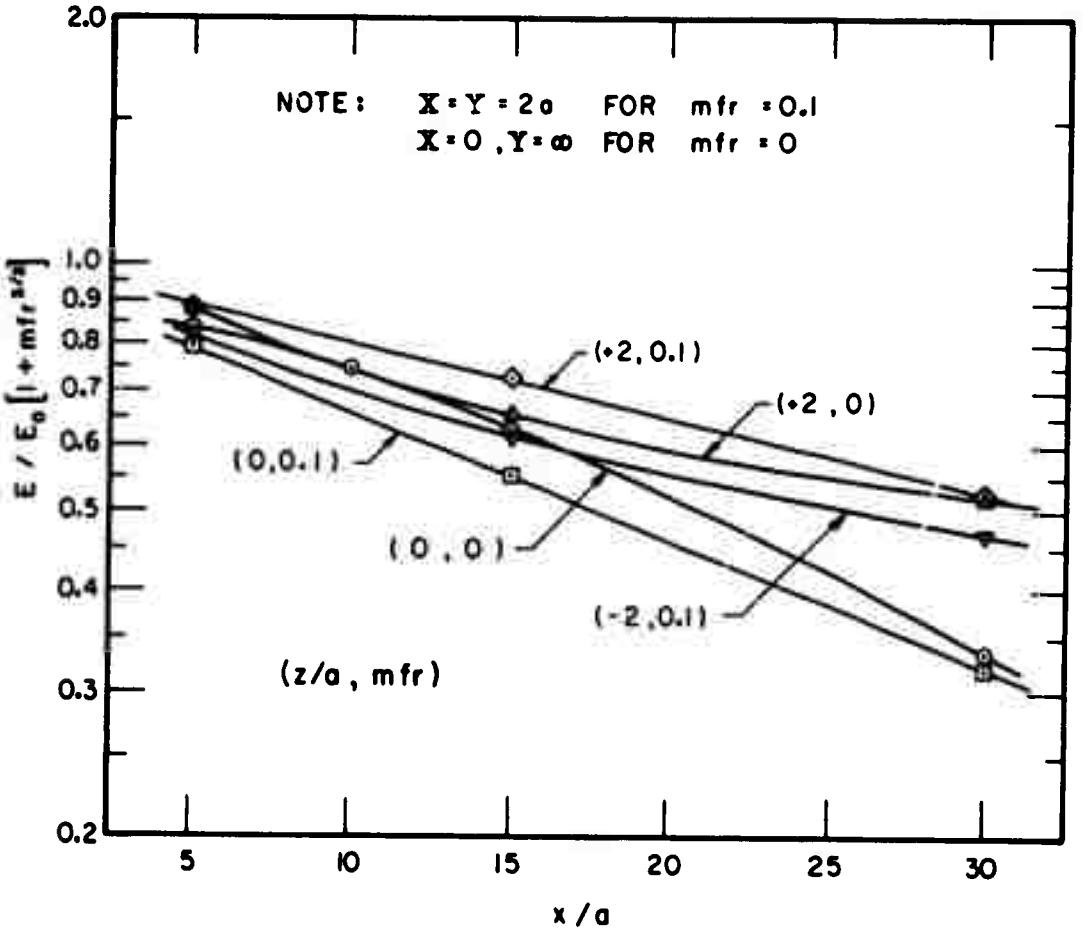

FIG. 53 ENERGY FLUX RATIOS FOR THE RESULTANT AND THE SINGLE BOUNDED JETS

NOZZLE GEOMETRY EFFECT ON THE RESULTANT JET

Results

The data collected to determine the effect of nozzle geometry on the resultant jet is not intended to be exhaustive; its purpose is to establish trends from which the effect may be inferred. Table 8* shows the values of $u(y = 0) / u_0$ for $X/a = 2$, $Y/a = 1, 2, 3$ and $z = 0, \pm 2$. Profiles of $u(y/a) / u_c$ for $z/a = +2$, $x/a = 15$, $X/a = 2$, and $Y/a = 1, 2, 3$ at an mfr = 0 are presented in Figure 55. A dimensional-like plot for y was chosen so as not to mask any effects by non-dimensionalization (e.g. $u(\eta)$). Table 9 gives the three flux ratios, mass, momentum, and energy, as determined from the above velocity profiles; Table 10 presents the static pressures that existed on the standoff pocket walls.

Discussion of Results

In the initial evaluation of the data that were collected to determine the nozzle geometry effect, it was noted that the velocity profiles for $Y/a = 2$ did not fall between the profiles for $Y/a = 1$ and 3. The pattern for 1, 3 and ∞ did, however, follow a consistent pattern. An alternative way to express this unexpected phenomenon is by the mass, momentum and energy flux ratios as shown in Table 9.

---

* Table 8 may be found on page 151.

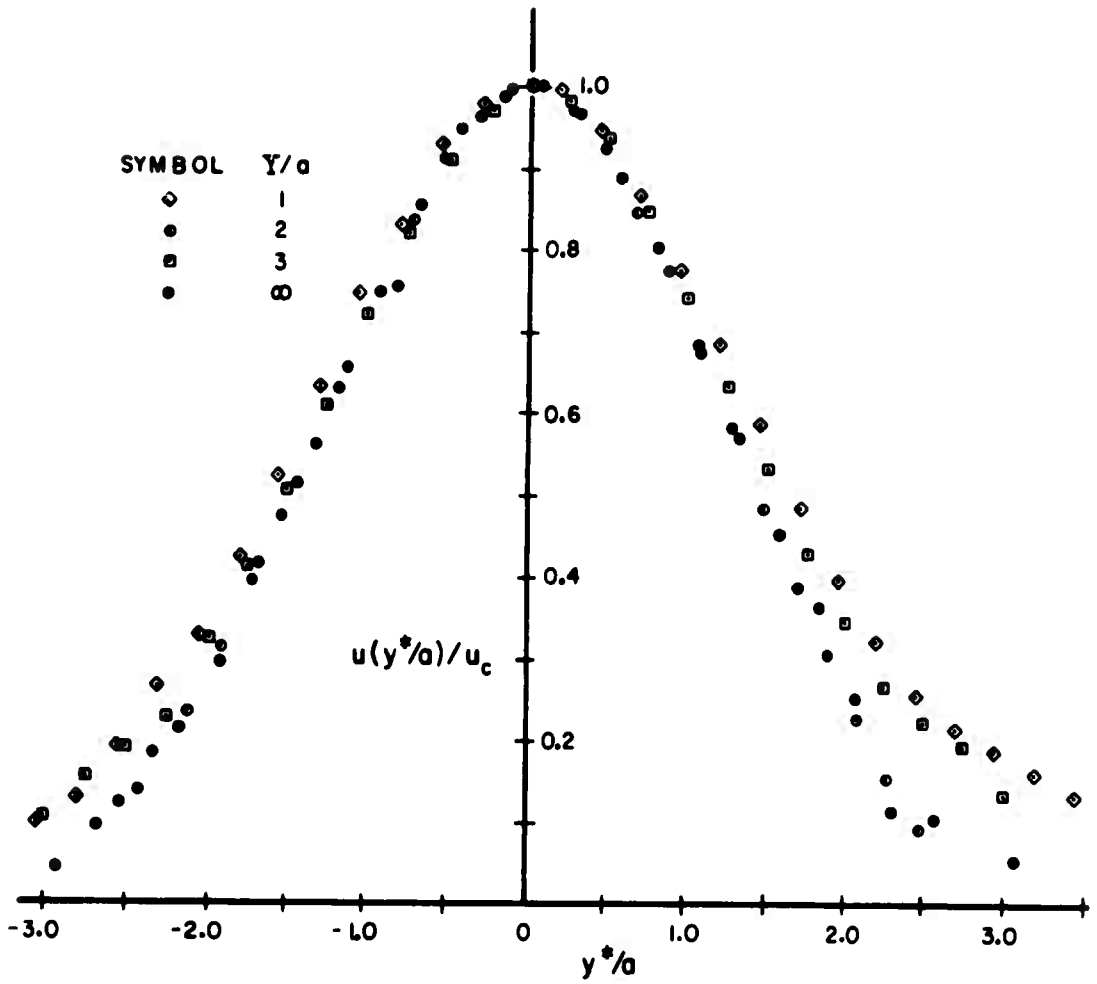

FIG. 55 $u(y^*/a)/u_c$ FOR $z/a = \cdot 2$, $x/a = 15$, AND $X/a = 2$, $Y/a = 1, 2, 3, \infty$ TO SHOW THE EFFECT OF THE NOZZLE GEOMETRY

Table 9

Mass, Momentum, and Energy Flux Ratios

To Show the Effect of the Side Nozzles,

$x/a = 15$, $z/a = +2$, $X/a = 2$

	Y/a			
	1	2	3	∞
M/M_o	2.47	2.05	2.38	2.180
$2bq_c/aq_o$	1.23	1.05	1.22	1.12
E/E_o	0.706	0.601	0.711	0.656

The tabular data come from the velocity profiles and are therefore not independent of them. Consequently, these flux ratios also exhibit an extremum.

A possible flow model could be formulated on the basis of the static pressure data; however, these data showed a consistent trend with Y, viz., a larger Y value leads to a higher pressure, and this made it appear that some combination of effects was causing the unexpected extremum.

Table 10

Values of Static Pressure at he Pocket Walls

For Zero mfr Conditions

	Y/a			
	1	2	3	∞
$\frac{(P-P_{atm})}{\frac{1}{2}\rho u_o^2} \times 10^2$	-2.49	-1.13	-0.69	0

Therefore, it was necessary to develop a flow model which would be compatible with the monotonically decreasing

pressure and which would explain the observations for Y/a = 2. It was reasoned that if an effect were present which altered the vortex stretching action, this could explain the apparent anomoly for Y/a = 2.

Consider the defined region and the power jet flow only. The existence of a low pressure in the pocket implies a standing vortex with a rotation such that the vortex flow is counterclock-w'se in the left pocket and clockwise in the right pocket, see Figure 56. The flow of the standing

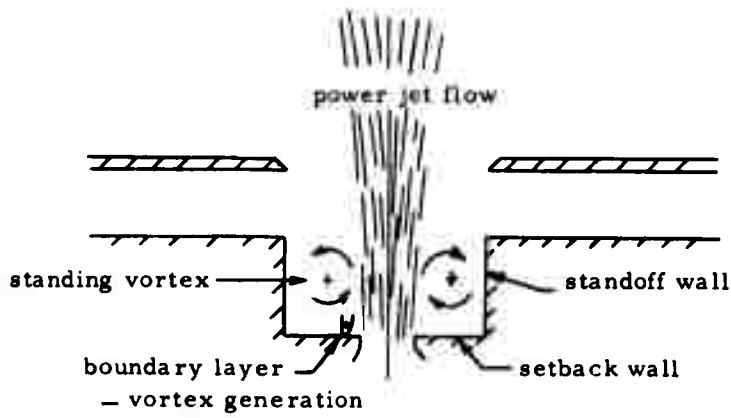

FIGURE 56 Flow model for the nozzle geometry effect

vortex past the forward wall of the power jet nozzle will form a boundary layer on this surface. As a result of this, the entrained flow will contain vorticity (generated in the boundary layer) with its major component in the z direction (-z for the left side pocket and +z for the right pocket). When this vorticity is added to the power jet, the net effect is to reduce the vortex stretching action because the vorticity that is introduced is of the opposite sense from that generated in the

shear layer of the jet. Since this effect tends to retard the development of the three-dimensionality, it is termed a negative effect. An important feature of the phenomenon is that the magnitude of the effect will be dependent on the length of the setback wall (Y) and the strength of the standing vortex (which can be qualitatively inferred from the pocket pressure). The length of the setback wall will determine the development of the boundary layer vortex filaments and the strength of the standing vortex will determine the shear rate near the wall. Therefore, the strength of the entrained vorticity is fixed by a combination of two effects. Consequently, the vorticity that is produced in the boundary layer will be

i) small for very large Y/X values because the standing vortex will be relatively weak,

ii) small for very small Y/X values because the boundary layer will be quite small.

iii) attain a maximum for some Y/X and approach the two extremes asymptotically.

A second feature of the flow model results from the low pocket static pressures. The reduced static pressure in the pockets will cause an early spreading of the jet. However, it will spread more rapidly near the plates because the boundary layer fluid has less x - direction momentum; therefore, this fluid is influenced more by the transverse pressure gradient than the fluid in the central portion (i.e. $\pm z \leq 2.75$). This effect induces an initial velocity profile which resembles a profile resulting from the vortex stretching action; consequently, the proposed

effect is a positive effect. Figure 57 is an arbitrarily drawn graphical representation of the results of these two effects on a typical jet characteristic; M/M_0 is used as the ordinate. The algebraic sum of the two curves can be inferred from the results of Table 9; the solid curve, which is the algebraic sum of the two contributions, was drawn from the tabular data.

Although the above analysis is not quantitative, it offers a flow model and a plausible starting point for further investigations.

Two independent sets of data were collected to establish the effect of the nozzle geometry: the velocity profiles at $x/a = 15$, $z/a = +2$ as discussed above and four groups of u_c/u_0 values. The purpose of the u_c/u_0 data, presented in Table 8, was to establish whether the effect of the nozzle geometry (if any) was of such a nature that it would be apparent in the u_c values.

After careful study of the results shown in the table (for $x/a = 10$ or less), it was concluded that if a meaningful pattern was indicated by the data, it was both very complex and, as a result of too few data, not accessible to direct analysis. However, it was possible to determine that if the effect existed, it was of a reasonably small magnitude since the spread of the u_c/u_0 values for the different geometries is small.

For $x/a = 25$ an interesting pattern is indicated. For the three geometries, $Y/a = 1, 2, 3$, the difference in the u_c/u_0 values is (approximately) 0.04 and 0.02 when the $z/a = +2$ and $z/a = -2$ values are compared with the values

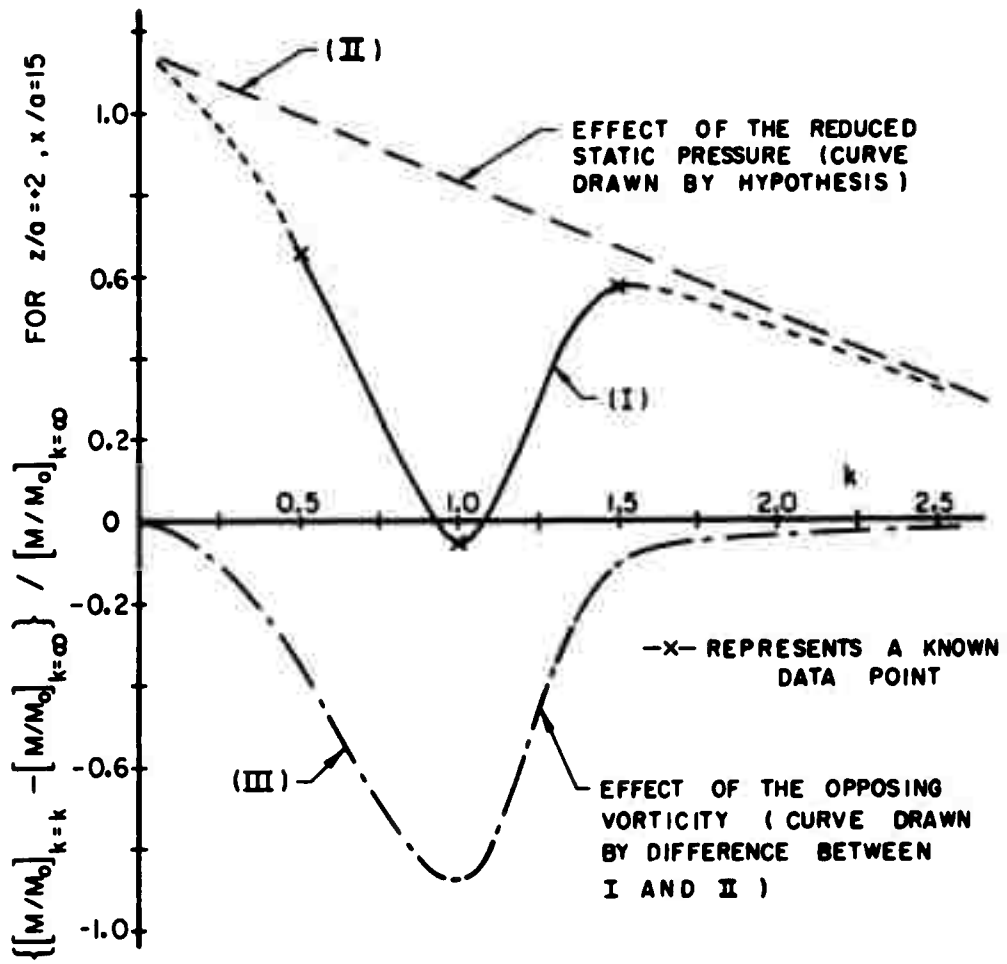

FIG. 57 M/M_0 VERSUS k TO INDICATE THE RELATIVE IMPORTANCE OF THE TWO TERMS IN THE PROPOSED FLOW MODEL FOR THE EFFECT OF THE SIDE NOZZLES

TABLE 8

u_c/u_0 to Show the Effect of the Side Nozzles

X/a	Y/a	x/a = 5	x/a = 10	x/a = 15	x/a = 25	z/a
2	1	0.993	0.864	0.705	0.523	+ 2
2	2	0.99	0.860	0.71	0.541	+ 2
2	3	0.988	0.860	0.72	0.540	+ 2
-	∞	0.995	0.870	0.716	0.552	+ 2
2	1	0.975	0.830	0.678	0.481	0
2	2	0.980	0.810	0.674	0.497	0
2	3	0.983	0.825	0.689	0.502	0
-	∞	0.988	0.840	0.705	0.531	0
2	1	0.971	0.826	0.668	0.50	- 2
2	2	0.995	0.835	0.679	0.518	- 2
2	3	0.987	0.846	0.686	0.519	- 2
-	∞	0.997	0.843	0.686	0.535	- 2

For X/a = 2, z/a	Y/a = 1	Y/a = 2	Y/a = 3	Y/a = ∞	x/a
+ 2-1/2	0.975	0.993	0.982	0.971	5
+ 1	0.976	1.0	0.987	0.985	5
- 1	0.972	0.993	0.986	0.995	5
- 2-1/2	0.975	-	0.984	0.994	5
+ 2-1/2	0.822	0.826	0.804	0.808	10
+ 1	0.843	0.863	0.835	0.850	10
- 1	0.821	0.842	0.840	0.848	10
- 2-1/2	0.804	-	0.796	0.804	10

at z/a = 0. In contrast, for Y = ∞, the values are 0.017 and 0.004 for the same comparison. Another mode of comparison is offered by the ratios

$$\frac{u_c/u_0 \quad z/a = +2}{u_c/u_0 \quad z/a = 0}$$

and similarly for z/a = -2. The value of the ratios for Y = 1, 2, and 3 are virtually equal and the value for Y = ∞ is smaller.

From these observations alone, the conclusions would be that there is no strong effect of the control jet nozzles before x/a = 25 and for this x/a location the nature of the effect is essentially independent of k for k less than or equal to 1.5. Whereas the velocity profiles showed a pronounced extremum for Y/a = 2, the u_c/u_0 values are quite similar. Two conclusions are drawn from these observations; they are, whatever the full effect of the nozzle geometry: i) it has a strong memory characteristic since the same nozzle geometries induced two different types of effects at x/a stations of 15 and 30; ii) it is very complex.

MOMENTUM FLUX RATIO EFFECT ON THE RESULTANT JET

Results

As in the section on the nozzle geometry effect, IX, experiments were conducted to provide trends from which the full effect of the mfr on the resultant jet may be inferred. One geometry and three values of the mfr were investigated. Figures 58 and 59 present the profiles for $u(y^*/a)/u_c$ at $z/a = 0$ and +2 and for the mfr values of 0, 0.1, 0.2. As another mode of comparison, the profiles of $u_*(\xi/a)/u_{c_*}$ and $u_*(\eta_*)/u_{c_*}$ are presented in Figures 60 to 63 for $z/a = 0$ and +2 and for mfr values of 0, 0.1, 0.2. Table II shows the mass, momentum, and energy flux ratios for the resultant jet, for the z/a and mfr parameters as above, and for the x, y, z and ζ, ξ, z co-ordinates respectively.

The two sets of figures ($z/a = 0, +2$), each containing three plots, were considered necessary for a complete presentation of the data for the following reasons:

i) The measured quantities, viz., θ, h_T, and h_s, lead directly to the $u(y^*/a)/u_c$ profiles. Also, since the output ports' configuration can be most easily described in x, y, z co-ordinates, the $u(y^*)$ profiles provide the most meaningful description of the flow into these ports.

ii) The $u_*(\xi/a)/u_{c_*}$ profiles present the velocity distribution in the natural co-ordinates of the flow, viz., ζ, ξ, z. They also offer a meaningful comparison with the $u(y/a)/u_c$

profiles of a single bounded jet as well as the most meaningful form that will indicate profile variations with respect to z.

iii) The profiles of $u_*(\eta_*)$ present the data in such a form that a comparison with the two-dimensional jet is possible. Also, since the Gaussian curve can be plotted on these co-ordinates, the skewness of the profiles is easily seen.

Discussion of Results

A striking feature of the velocity profiles is the regular pattern for $-\xi/a$, viz., a pattern described as "an increasing u_* with increasing mfr for a fixed ξ/a" and the irregular pattern for $+\xi/a$. However, this may be explained by noting that the mass flux is increased for mfr = 0.2 and the rate of infiltration is also increased for this higher mfr with respect to an mfr of 0.1.

In the "Detailed Mean Flow Study" section it was noted that the profiles changed from a skewed left to a skewed right pattern between $x/a = 5$ and 15. From Figures 62 and 63 it is apparent that the profiles are skewed right $(-y^*)$ at $x/a = 15$; furthermore, the skewness is more pronounced for $z/a = +2$ than for $z/a = 0$. This difference is assumed to result from the vortex stretching effects.

With reference to Table 11, the mass flux ratio drops as the mfr increases from 0 to 0.1 for $z/a = 0$; however, the mass flux ratio has the opposite trend for $z/a = +2$. Quantitatively, the ratio

$$\frac{\text{mass flux ratio at a mfr of 0}}{\text{mass flux ratio at a mfr of 0.1}}$$

TABLE 11

Values of the Flux Ratios to Show the Effect of the

mfr (x, y, z and ζ, ξ, z co-ordinates), x/a = 15, k = 1.0

	z/a	mfr		
		0.0	0.1	0.2
$M/M_o(1+[mfr]^{1/2})$	0	2.23	2.02	2.24
$M_*/M_o(1+[mfr]^{1/2})$	0	2.23	2.02	2.24
$M/M_o(1+[mfr]^{1/2})$	+2	2.05	2.34	2.50
$M_*/M_o(1+[mfr]^{1/2})$	+2	2.05	2.34	2.51
$2\,b\,q_c/a\,q_o$	0	1.21	1.26	1.19
$2\,b\,q_c/a\,q_o$	+2	1.05	1.30	1.34
$E/E_o(1+[mfr]^{3/2})$	0	0.726	0.568	0.654
$E_*/E_o(1+[mfr]^{3/2})$	0	0.726	0.570	0.655
$E/E_o(1+[mfr]^{3/2})$	+2	0.601	0.746	0.754
$E_*/E_o(1+[mfr]^{3/2})$	+2	0.601	0.747	0.760

NOTE: The momentum flux ratio for the streamline co-ordinates is not tabulated because there is no reliable way to generate a reference value.

has the values 1.10 and 0.876 for z/a values of 0 and +2 respectively. These values imply the existence of a strong mfr effect on the vortex stretching since increasing the mfr causes a shift of the mass flux toward the walls. The same ratio formed for mfr values of 0.1 and 0.2, has values of 0.90 and 0.935 respectively for z/a = 0 and +2. This is not believed to be a rejection of the conclusion that the mfr level has an effect on the vortex stretching; rather, it is assumed to be indicative of an increase in the infiltration rate with increasing mfr. Two factors support this: i) the mass flux ratio increases with increasing mfr at z/a = +2; ii) the velocity profiles in Figures 62 and 63 show that the profile is more symmetric (i.e. greater infiltration) for z/a = 0 than for z/a = +2.

It is concluded that the mfr does exert a marked effect on the resultant jet; however, the character of this effect is difficult to specify from the available data because there is an interplay between the vortex stretching and the infiltration rate effects.

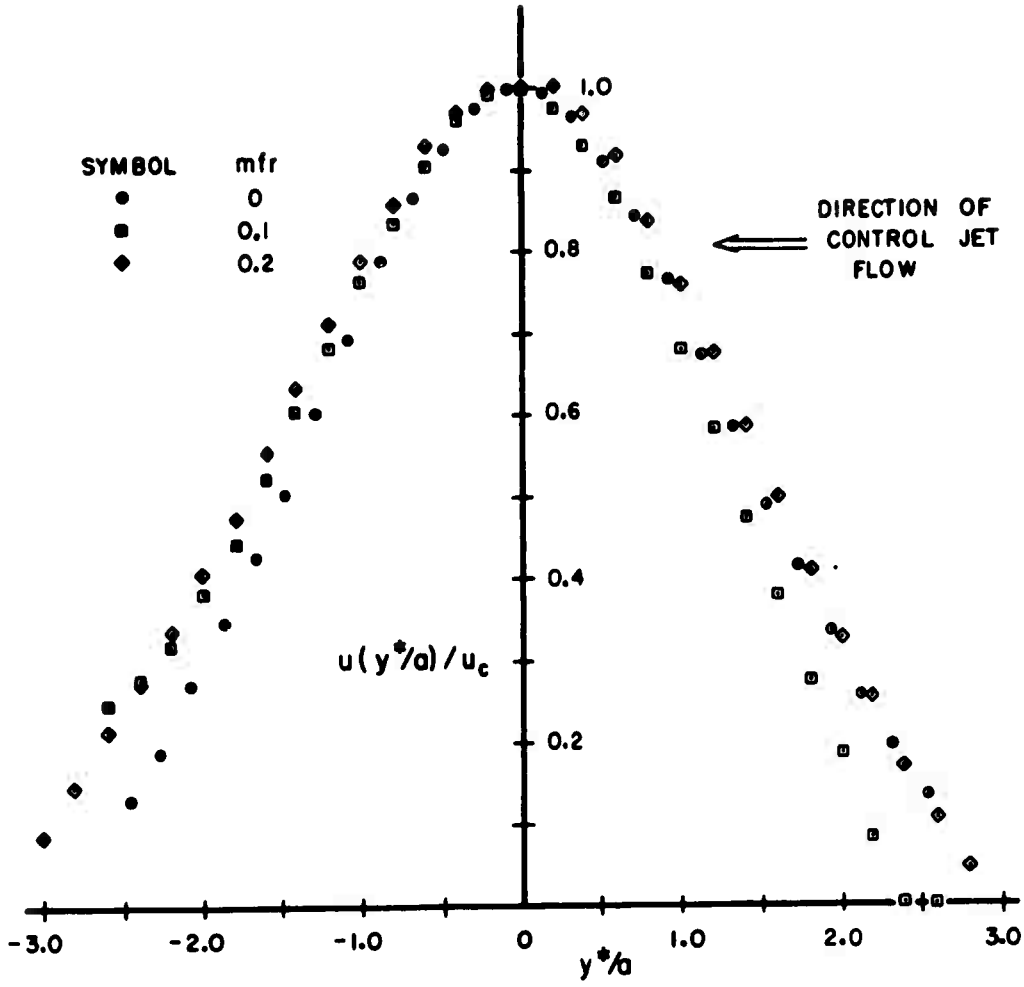

FIG. 58 $u(y^*/a)/u$ FOR $z/a=0$, $x/a=15$, mfr = 0, 0.1, 0.2 TO SHOW THE EFFECT OF THE mfr

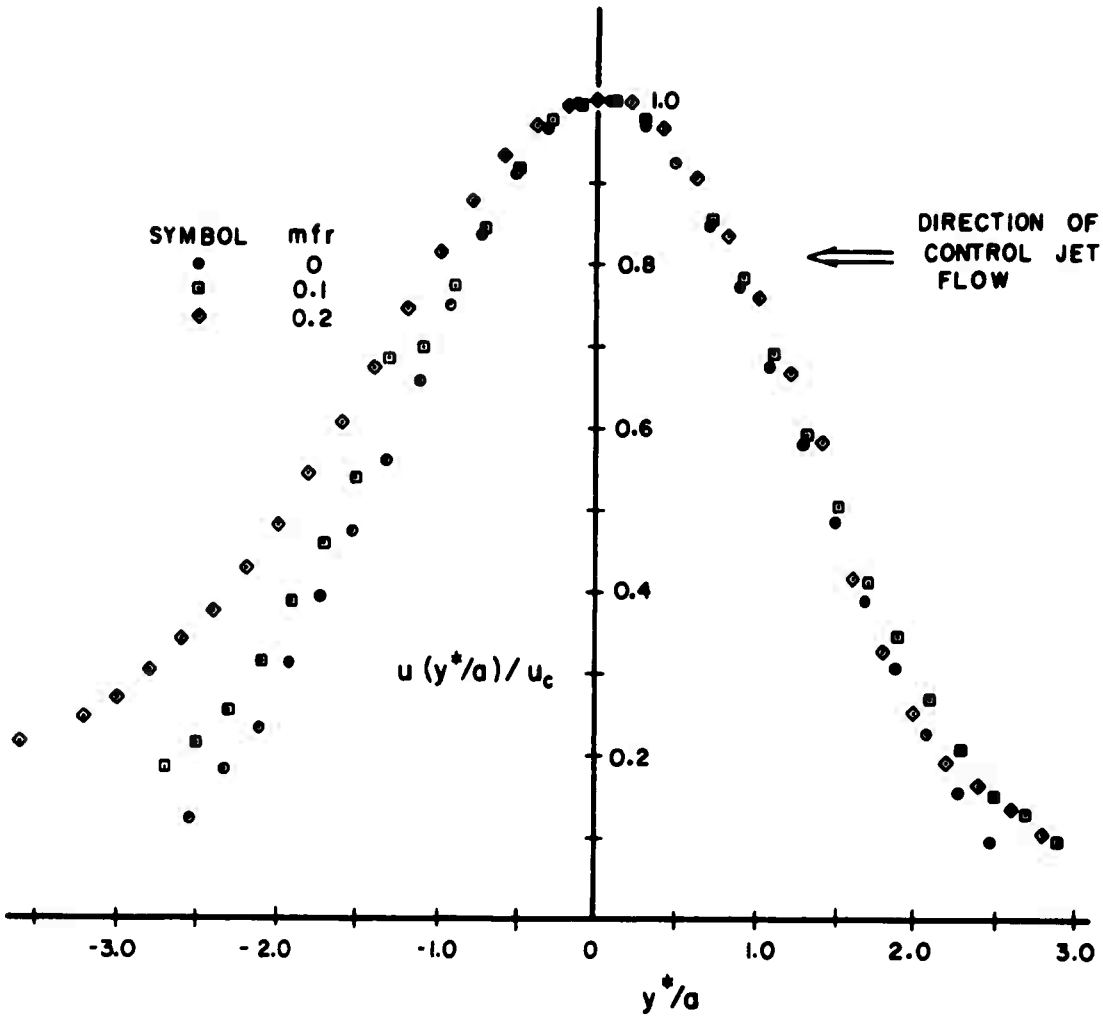

FIG. 59 $u(y^*/a)/u_c$ FOR $z/a = +2$, $x/a = 15$, mfr = 0, 0.1, 0.2 TO SHOW THE EFFECT OF THE mfr

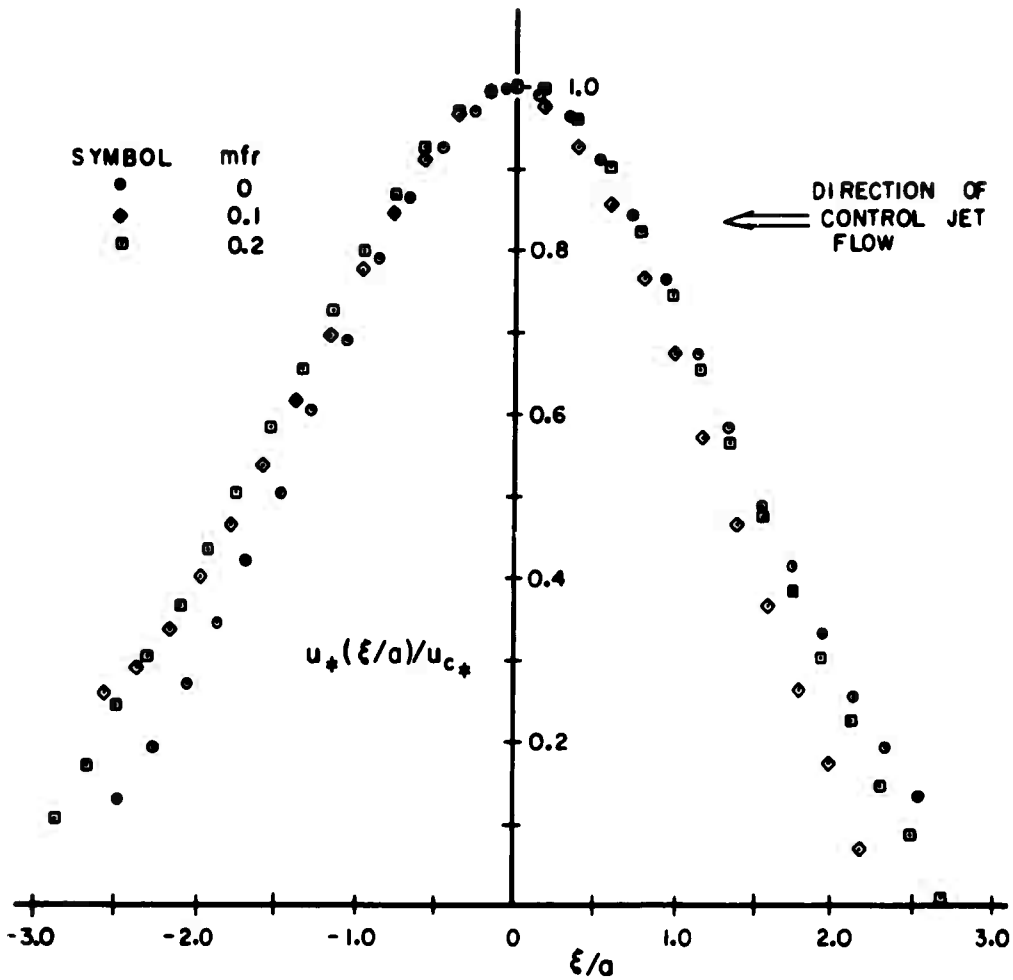

FIG. 60 $u_*(\xi/a)/u_{c_*}$ FOR $z/a=0$, $x/a=15$, mfr = 0, 0.1, 0.2 TO SHOW THE EFFECT OF THE mfr ($X = Y = 2a$)

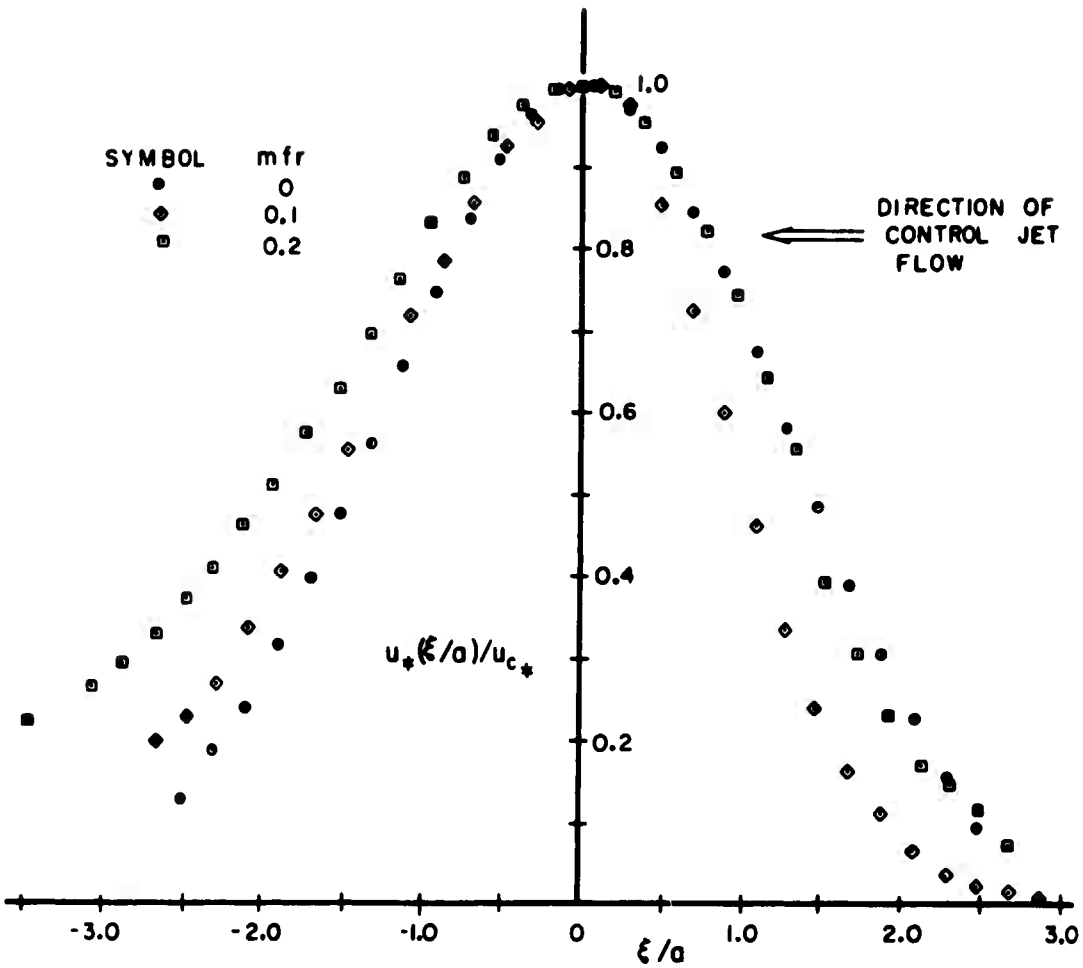

FIG. 61 $u_*(\xi/a)/u_{c_*}$ FOR $z/a = +2$, $x/a = 15$, mfr = 0, 0.1, 0.2 TO SHOW THE EFFECT OF THE mfr

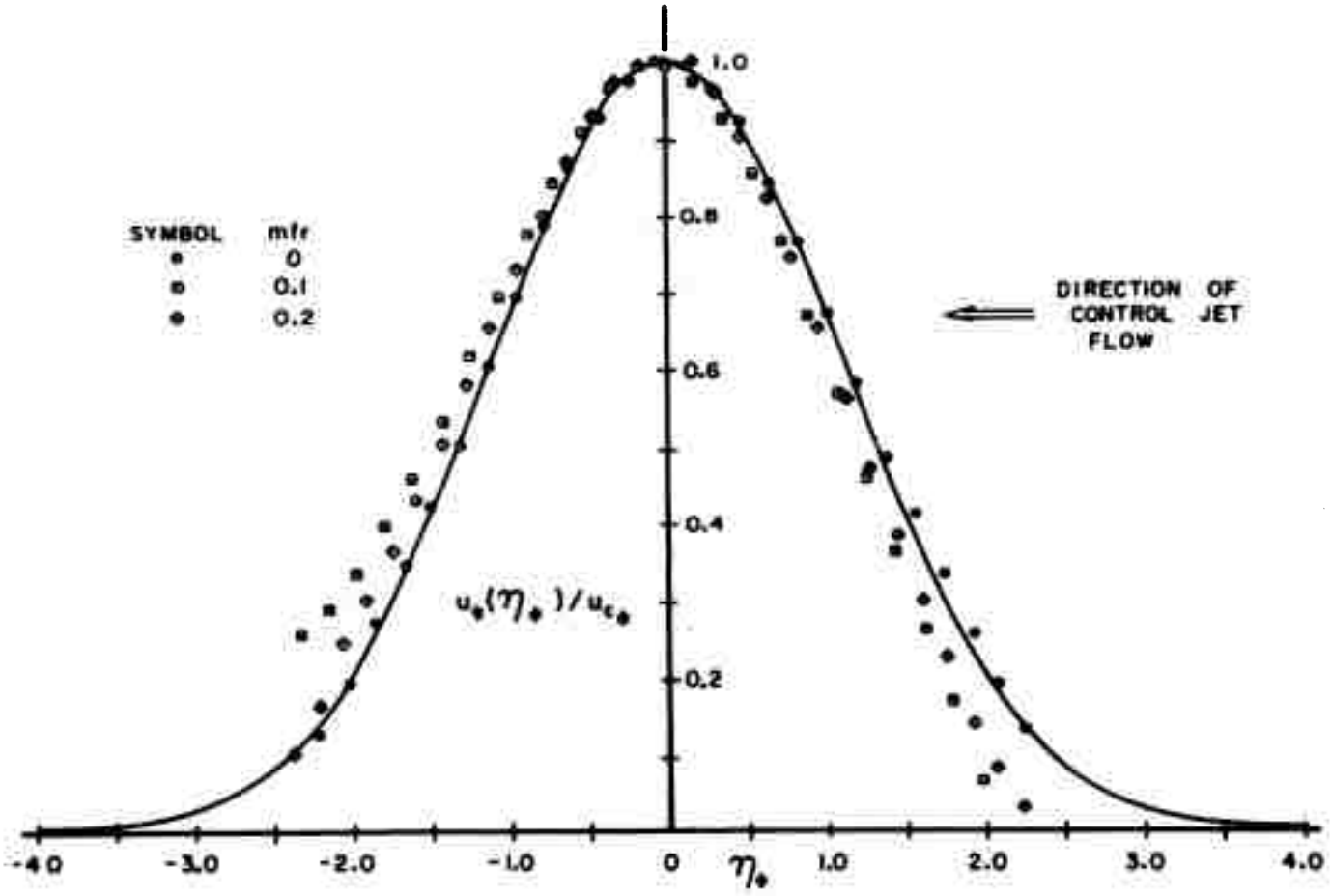

FIG. 62 $u_\phi(\eta_\phi)/u_{c_\phi}$ FOR $z/a = 0$, $x/a = 15$, mfr = 0, 0.1, 0.2 TO SHOW THE EFFECT OF THE mfr ($X = Y = 2a$)

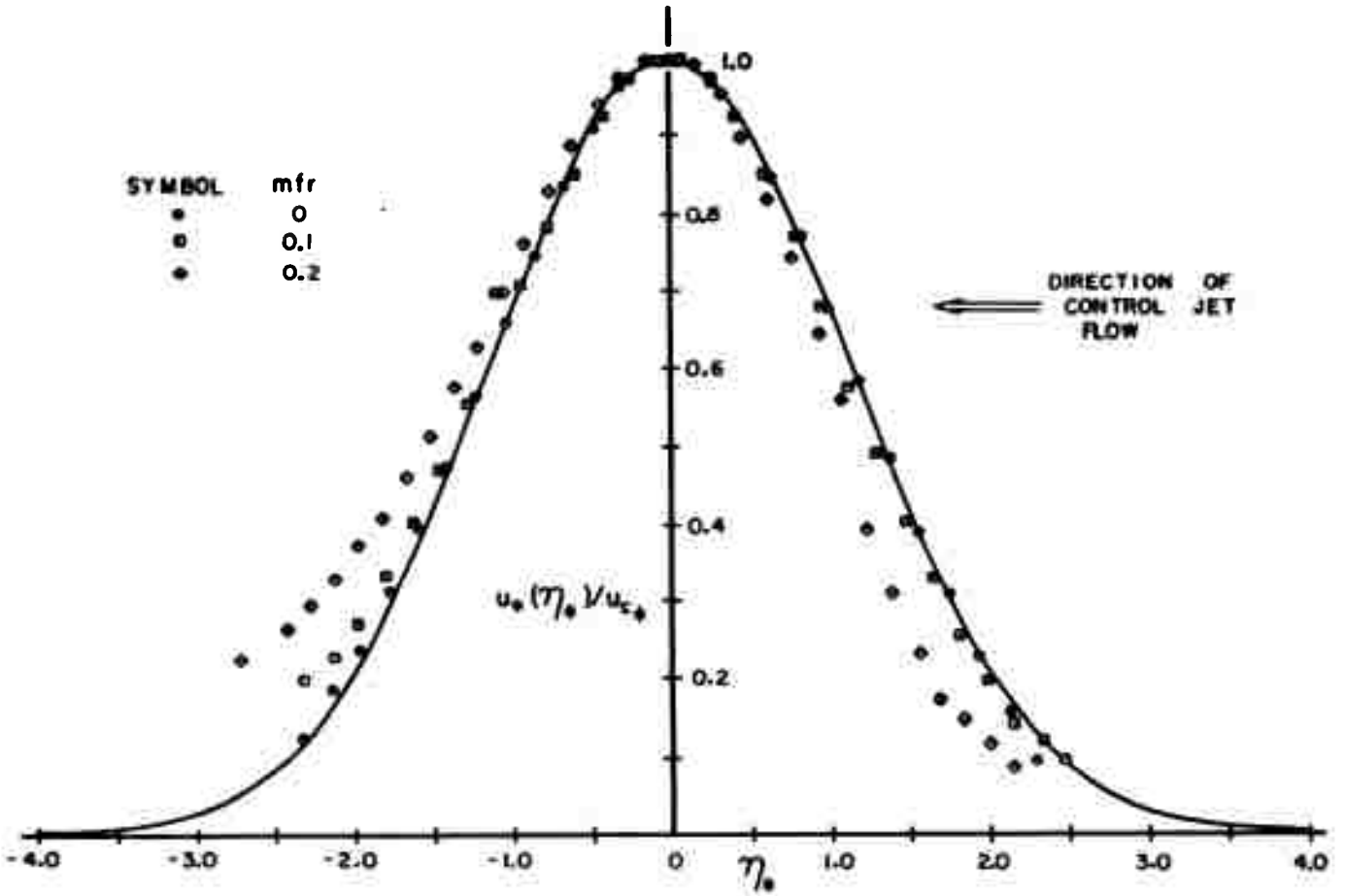

FIG. 63 $u_*(\eta_*)/u_{c_*}$ FOR $z/a = 2$, $x/a = 15$, mfr = 0, 0.1, 0.2 TO SHOW THE EFFECT OF THE mfr

CONCLUSIONS FROM THE STUDY OF INTERSECTING JETS

The following conclusions are supported by the results of the study on intersecting jets for an aspect ratio of six and three nozzle geometries.

1) For the range of setback to standoff wall ratios of 0.5 to 1.5, the smallest ratio provides the conditions for the highest gain, viz., the largest deflection angle and the farthest upstream location of the apparent pivot point.

2) The analytical model proposed provides a satisfactory prediction method for the deflection angle for the geometry of the smallest ratio of setback to standoff wall lengths.

3) The analysis of Manion and Goto (17) provides a satisfactory prediction of the deflection angle for the geometry of the largest ratio of setback to standoff wall lengths. It should be noted that this analysis requires an apriori knowledge of the far side pocket pressure.

4) Detailed mean flow surveys of the resultant jet for one momentum flux ratio and one nozzle geometry indicate that the effects of the vortex stretching are increased following the interaction of the jets as compared with the single bounded jet.

5) The nozzle geometry and the momentum flux ratio have marked and complex effects on the character of the vortex stretching and on the infiltration rate of the control jet into the power jet.

LIST OF REFERENCES

1. Shames, I. H., Mechanics of Fluids, McGraw-Hill, New York, 1962.

2. "Fluid Jet Control Devices", Symposium on Fluid Jet Control Devices - ASME, edited by F. T. Brown, November, 1962.

3. "Proceedings of the Fluid Amplification Symposium", Harry Diamond Laboratories, May 1964.

4. Tollmien, W., "Calculation of Turbulent Expansion Processes", NACA TM 1085, 1956.

5. Görtler, H., "Berechnung von Aufgaben den Freien Turbulenz auf Grund eines neuen Näherungsansatzes", Zeit. angew. Math. u. Mech. 22, 1942, p. 244.

6. Reichardt, H., "Über eine neue Theorie der freien Turbulenz", Zeit. ang. Math. u. Mech. 21, 1941, p. 257. Jour. Roy. Aero. Soc. 47, 1943, p. 167.

7. Hinze, J. P., Turbulence, McGraw-Hill, 1959.

8. Förthmann, E., "Turbulent Jet Expansion", NACA TM 789, 1936.

9. Miller, D. R. and Comings, E. W., "Static Pressure Distribution in the Free Turbulent Jet", Jour. of Fluid Mech., Vol. 3, Part 1, Oct. 1957, pp. 1-16.

10. Townsend, A. A., The Structure of Turbulent Shear Flow, Cambridge Monographs on Mech. and Appl. Math., Cambridge University Press, London, 1956.

11. Van Der Hegge Ziznen, B. G., "Measurements of the Velocity Distributions in a Plane Turbulent Jet of Air", Appl. Sci. Res., Section A, Vol. 7, No. 4, 1958, pp. 256-276.

12. Albertson, M. J., Dai, Y. B., Jensen, R. A., Rouse, H., "Diffusion of Submerged Jets", Proc. ASCE, Dec. 1948, pp. 1571-1596.

13. Van Der Hegge Zijnen, B. G., "Measurements of Turbulence in a Plane Jet of Air by the Diffusion Method and by the Hot-Wire Method", Appl. Sci. Res., Section A, Vol. 7, No. 4, 1958, pp. 293-313.

14. Heskestad, G., "Two Turbulent Shear Flows", The Johns Hopkins University, Department of Mechanics, June 1963.

15. Liepmann, H. W., and Laufer, J., "Investigation of Free Turbulent Mixing", NACA TN 1257, 1947.

16. Olson, R. E., and Miller, D. P., "Aerodynamic Studies of Free and Attached Jets", Fluid Amplification Report 6 for the Harry Diamond Laboratories, Oct. 1963.

17. Manion, F. M. & Goto, J. M., "Jet Interaction in a Defined Region", Harry Diamond Laboratories Report No. R-RCA-6323, 30 August 1963.

18. Goto, J. M., "Interaction of Jets in a Set-back Region", Harry Diamond Laboratories Report No. R-RCA-63-12, 18 April 1963.

19. Reilly, R. J. and Kallevig, J. A., "Flow Visualization and Experimental Studies of a Proportional Fluid Jet Amplifier", Fluid Amplification Symposium, DOFL, Vol. 1, Oct. 1962, p. 125.

20. Reilly, R. J. and Moynihan, "Notes on a Proportional Fluid Jet Amplifier. ASME Fluid Jet Control Devices, Ed. F. T. Brown, Nov. 28, 1962.

21. Pepperone, S. J., Katz, S. and Goto, J. M., "Gain Analysis of the Proportional Fluid Amplifier", Fluid Amplification Report 4, DOFL, Oct. 1962.

22. Olson, R. E., "Investigation of the Aerodynamics of Fluid Amplifiers", Progress Reports 7 and 8 from U.A.C. Res. Lab., Harry Diamond Laboratories Contract Number DA-49-186-AMC-66(x), Jan. 27, and Feb. 28.

23. Fage, "On the Static Pressure in Fully Developed Turbulent Flow", Proc. Roy. Soc., A 155, 1936, pp. 576-596.

24. Laufer, J., "The Structure of Turbulence in Fully Developed Pipe Flow", NACA TR 1174, 1954.

25. Curtet, R., "Sur l' Ecoulement d'un Jet Eutre Parois", Publications Scientifiques et Tecahniques der Ministere de l' Air, No. 359, Paris, 1960. Translation by U. S. Dept. of Commerce, Office of Technical Services, Joint Publications Research Service "On Confined Jet Flow", DO-49-186-003-03535, JPRS: R-2934-D, 4 Jan. 1963.

26. Corrsin, S. and Kissler, A. L., "The Free Stream Boundaries of Turbulent Flows", NACA TN 3133, 1954.

APPENDIX A --

NOZZLE AND CONTRACTION DESIGN

In order to provide for a smooth acceleration of the fluid, a beam deflection curve, pictorially defined in Figure A 1, was employed for all nozzles and contractions used in the present study. A smooth accederation curve is a necessary condition to produce a uniform efflux velocity from the nozzle. An analysis is presented below which establishes the geometric conditions that are necessary for a smooth acceleration.

Consider the one-dimensional, irrotational, and incompressible flow of an inviscid fluid through the nozzle of Figure A 2 whose cross-sectional area (A) is given by the expression

$$A = W - 2g(x)$$

For steady flow, the convective acceleration is $V(dV/dx)$. The continuity of d^2V/dx^2 will guarantee a smooth acceleration of the fluid through the nozzle. After rewriting the continuity equation, $\rho AV =$ constant, in the form

$$\frac{1}{A}\frac{dA}{dx} + \frac{1}{V}\frac{dv}{dx} = 0$$

d^2V/dx^2 can be expressed as

$$\frac{d^2V}{dx^2} = -V/A \frac{d^2A}{dx^2} + \left(\frac{V}{A^2}\right)\left(\frac{dA}{dx}\right)^2$$

Therefore, the requirement that d^2V/dx^2 be continuous can be replaced by the same requirement for d^2A/dx^2.

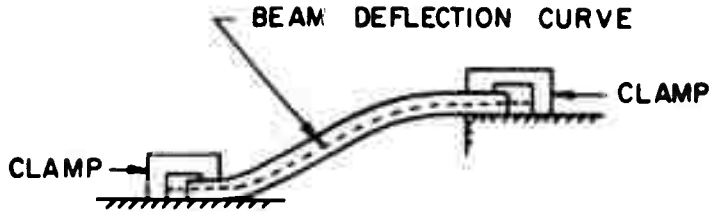

FIG. A1 PICTORIAL DEFINITION OF BEAM DEFLECTION CURVE

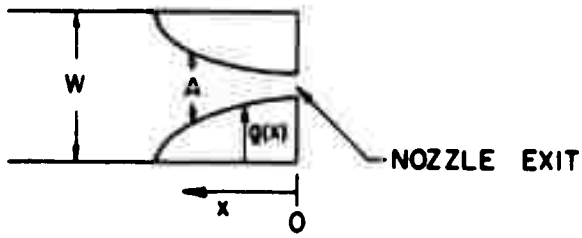

FIG. A2 DEFINITION OF TERMS USED IN APPENDIX A

Since A is proportional to $g(x)$, the continuity of $d^2 V / dx^2$ is also satisfied by the continuity of $d^2 g(x) / dx^2$. But, this condition is guaranteed for the beam deflection curve since the moment, which is related to the term $d^2 g(x) / dx^2$, is continuous.

Because of construction simplifications, a circular arc is commonly used for the curve $g(x)$, i.e. $g(x) = R \sin(\cos^{-1} x/R)$. However, since the radius of curvature, which is related to $d^2 g(x) / dx^2$, is discontinuous at $x = 0$, the fluid (under the restrictions of the analysis) will undergo an instantaneous change in its rate of acceleration. Since this is physically impossible, the fluid will adjust itself in such a manner that the flow streamlines will not follow similar paths over the cross-sectional area, and this adjustment will produce a non-uniform flow at the nozzle exit. The nature of this non-uniformity cannot be predicted by this analysis, since the one-dimensional assumption and a non-uniform profile are incompatible.

The magnitude of this phenomenon is, of course, dependent on the magnitude of R with respect to the nozzle exit width; the non-uniformity becomes less pronounced with increasing values of the ratio $R/(W - 2R)$. A pronounced "dog eared" velocity profile results when this ratio, $R/(W - 2R)$, is too small. It is important to note that the above presentation is quantitatively true only for the assumed inlet flow conditions and constitues no more than a statement of necessary (but not sufficient) conditions. If, for example, a nozzle were designed which satisfied the above requirements but incorporated too small a radius of curvature; then, for a real fluid, the flow pattern could also lead to a "dog eared" profile because of high local accelerations near the walls.

APPENDIX B --

PROBE CALIBRATIONS

Three probes, the forward facing 12 hole static, the tapered total, and the three tube trident, were calibrated for the effects of yaw. Since the same basic calibration technique was employed for the three probes, the general method of testing will be described and then the data and analysis for each probe will be given separately.

The probe to be calibrated was mounted on a vertical support rod attached to the x - y - Θ device. The device was located approximately 2 diameters below the exit of an 8 inch O.D. pipe; the probe tip was on the center line, one diameter from the exit of the pipe. A calibration run consisted of measuring the dynamic head (q) and the probe response as a function of its angular position with respect to the flow.

Static Pressure Probe

Results of the calibration runs for this probe are shown in Figure B 1. In order to develop an empirical formula for Δh_s as a function of Θ, three regions were specified as:

Region I - Θ > 15 degrees, all values of q

Region II - $\Theta \leq$ 15 degrees, $q > 0.4$

Region III - $\Theta \leq$ 15 degrees, $q \leq 0.4$

Since all the Δh_s values of region III were less than 0.02 inches of water, Δh_s was assigned the arbitrary value of 0.

A second order polynominal was assumed for Δh_s,

such that:

$$\Delta h_s = A(q)\,\Theta^2 + B(q)\,\Theta$$

From the three data runs in region II, $A(q) = (0.16q - 0.07)$ and $B = -0.44$.

For I, the relationship between Δh_s and Θ is linear, and therefore can be described as:

$$\Delta h_s = M(q)\,\Theta + N(q)$$

Figure B 2 shows the values of M(q) and N(q) plotted for the values of q tested. The formulas for these functions are:

$$M = [9q - 0.35] \times 10^{-3}$$

$$N = [5q - 0.18] \times 10^{-2}$$

Tapered Total Pressure Probe

Unlike the static pressure probe, the results for this calibration are accurately expressible as a single curve for all q values tested. Figure B 3 shows the experimentally determined points and the assigned calibration curve which follows the equation

$$\frac{\Delta h_T}{q} = \frac{[h_{T_{\Theta=0}} - h_{T_{\Theta=\Theta}}]}{q} = C(\Theta - 6.7) + D(\Theta - 6.7)$$

for $\Theta > 10.7$

and

$$\frac{\Delta h_T}{q} = 0 \quad \text{for} \quad \Theta \leq 10.7$$

The values of C and D were evaluated as 0.4×10^{-3} and -1.55×10^{-3} respectively. This formulation yields a value of Δh_T to within 1 per cent of the measured value for all values of Θ and q investigated.

Trident Probe

The purpose of this calibration was to allow a differential reading of the trident probe to be used as a measure of the yaw angle with respect to the probe axis. Since the differential reading was a function of the dynamic head as well as the angle, the calibration data are presented as plots of Θ vs. $\Delta h_{T_{45}} / q$ with q serving as a parameter. These data, which are presented in Figures B 4 and B 5 are seen to follow straight lines passing through the origin. These straight lines may be represented by the relation

$$\Theta = m(q) \left[\Delta h_{T_{45}} / q \right]$$

Figure B 6 indicates the variation of $m(q)$ with q. Since an empirical formula that could be adapted to a computer program was desired, the following relationship was chosen.

$$m(q) = 31 - 30\, q \quad \text{for} \quad \Theta \leq q \leq 0.1$$

$$m(q) = 28 \quad \text{for} \quad q > 0.1$$

The accuracy of this formulation is dependent upon the magnitude of Θ as indicated by Figures B 4 and B 5. However, the maximum error of the computed angle given by the above formulation will be of the order of 5.5 per cent. Because of the complicated nature of the computation procedure, no general statement can be made as to the effect of this error on the velocity magnitudes except that the errors will not be large enough to become unacceptable (viz. greater than about 5 per cent).

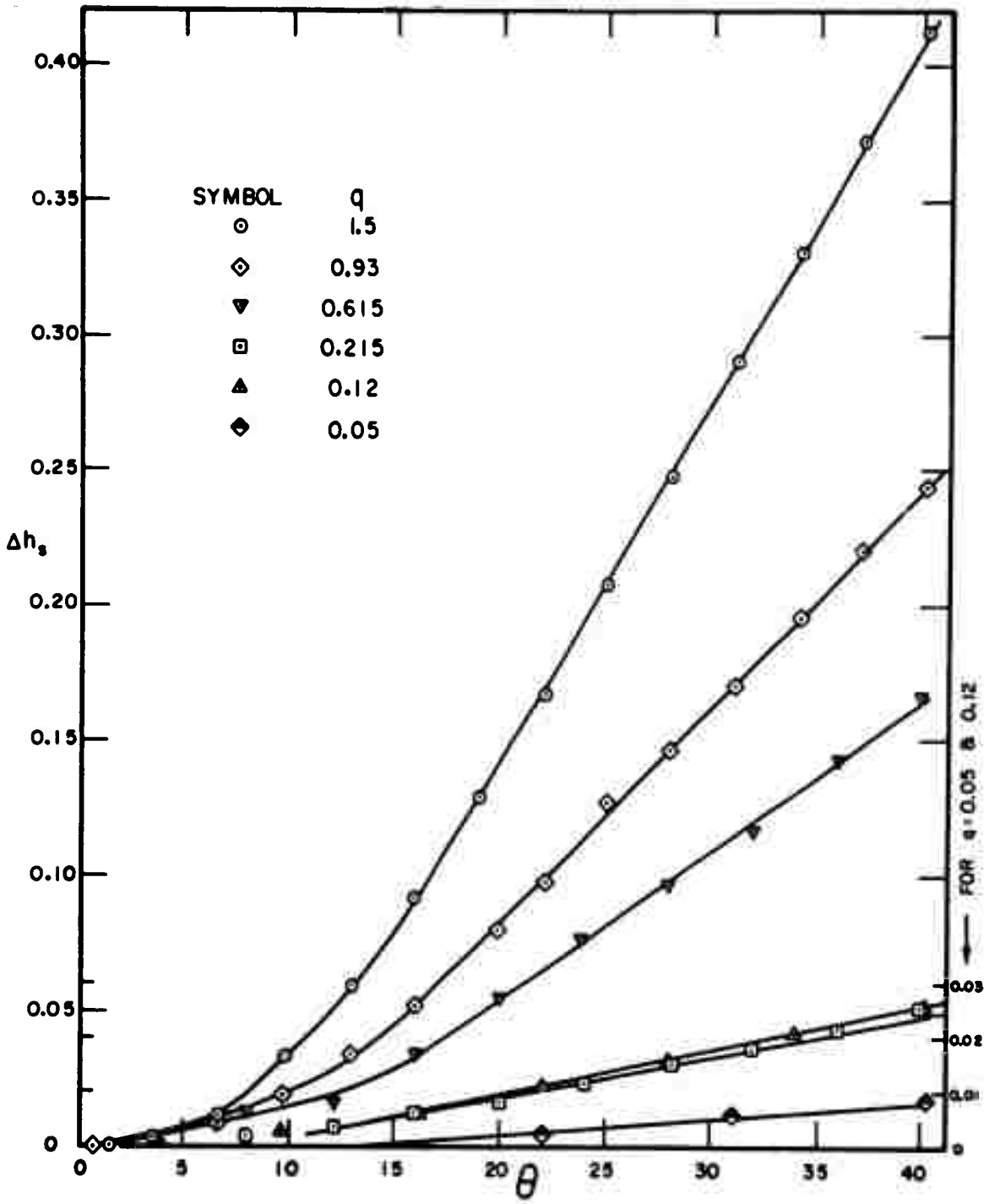

FIG. B I CALIBRATION CURVES FOR THE 12 HOLE STATIC PROBE

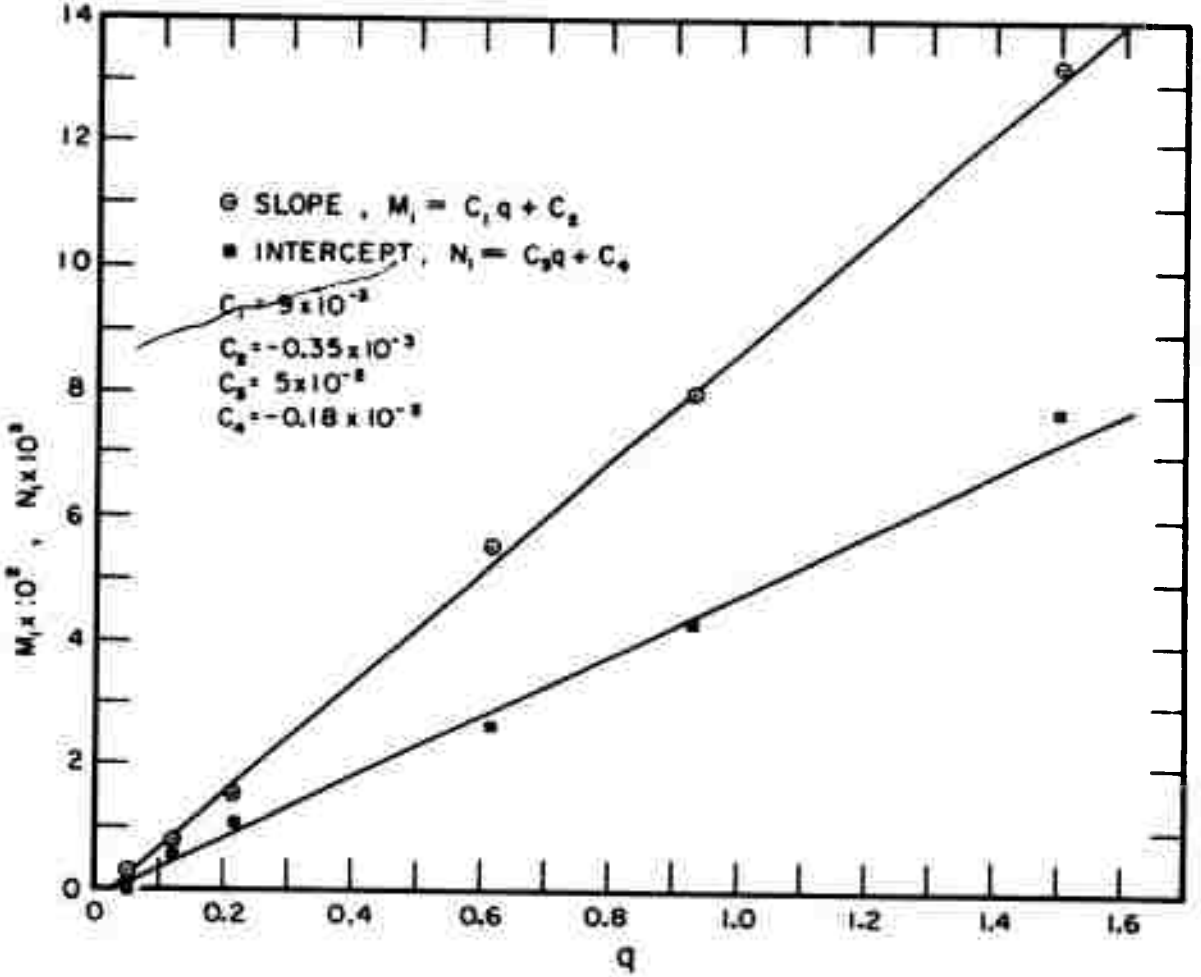

FIG. B2 EVALUATION OF CALIBRATION PARAMETERS , STATIC PROBE

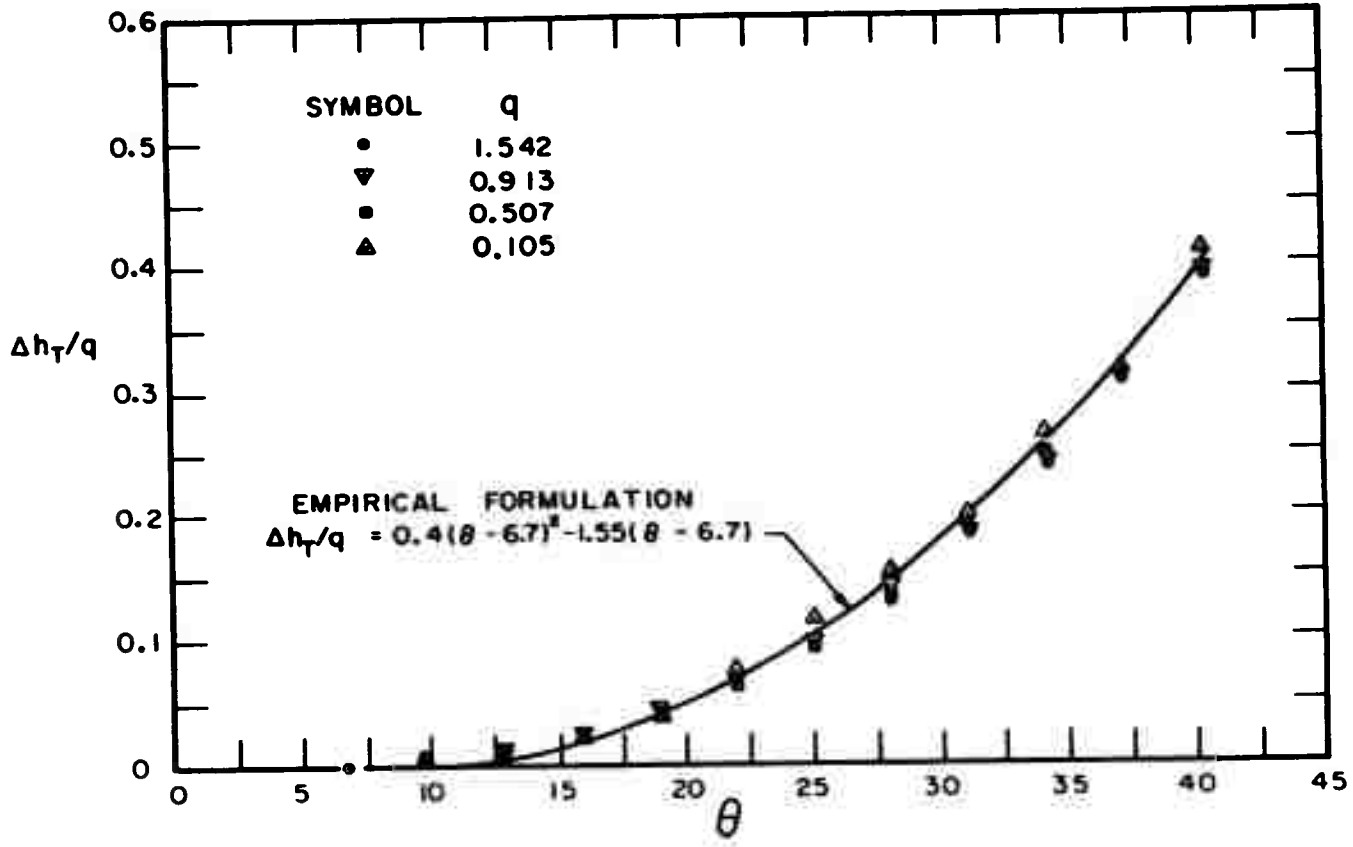

FIG. B3 CALIBRATION CURVE FOR THE TAPERED TOTAL PROBE

BLANK PAGE

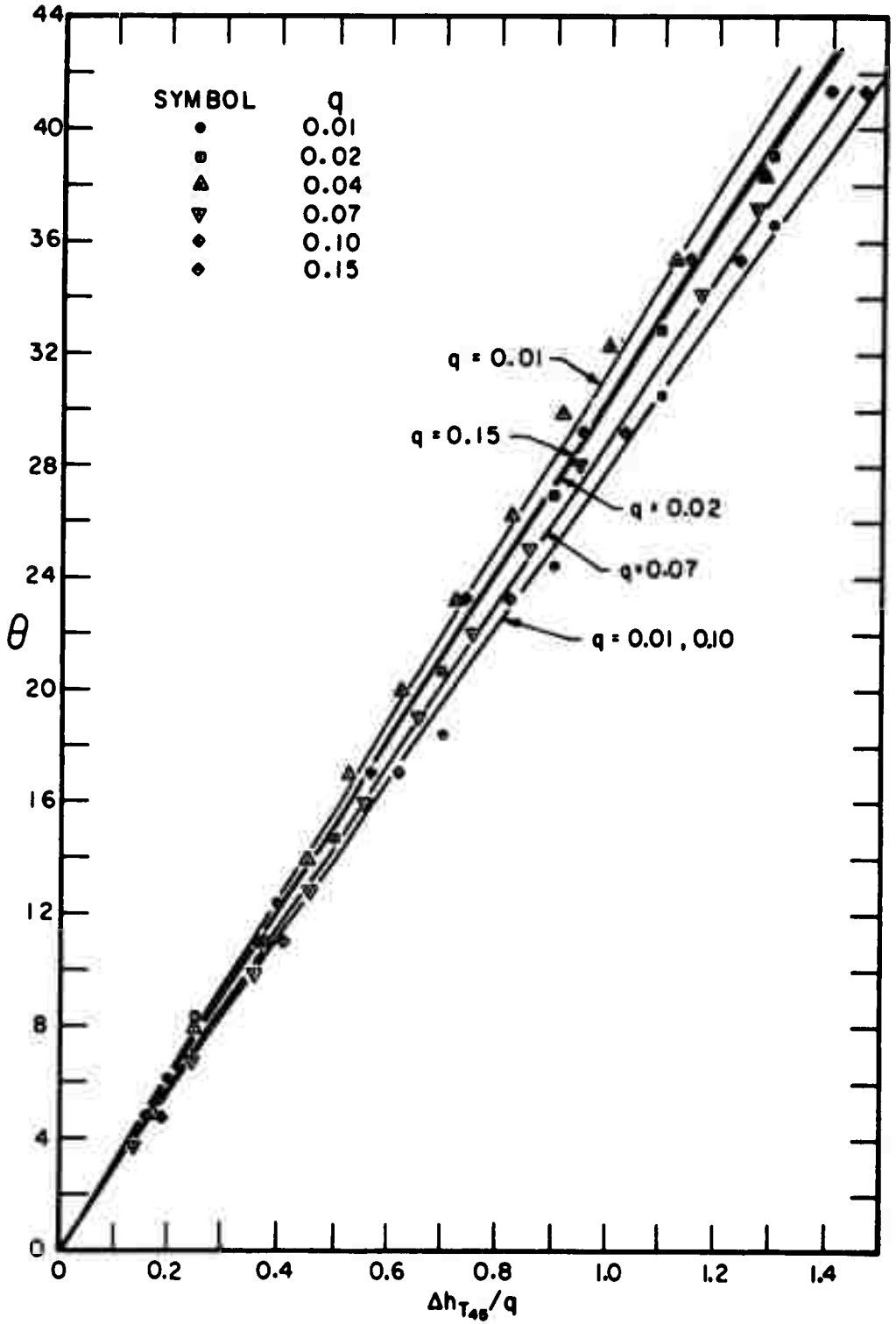

FIG. B4 CALIBRATION CURVE FOR THE TRIDENT PROBE

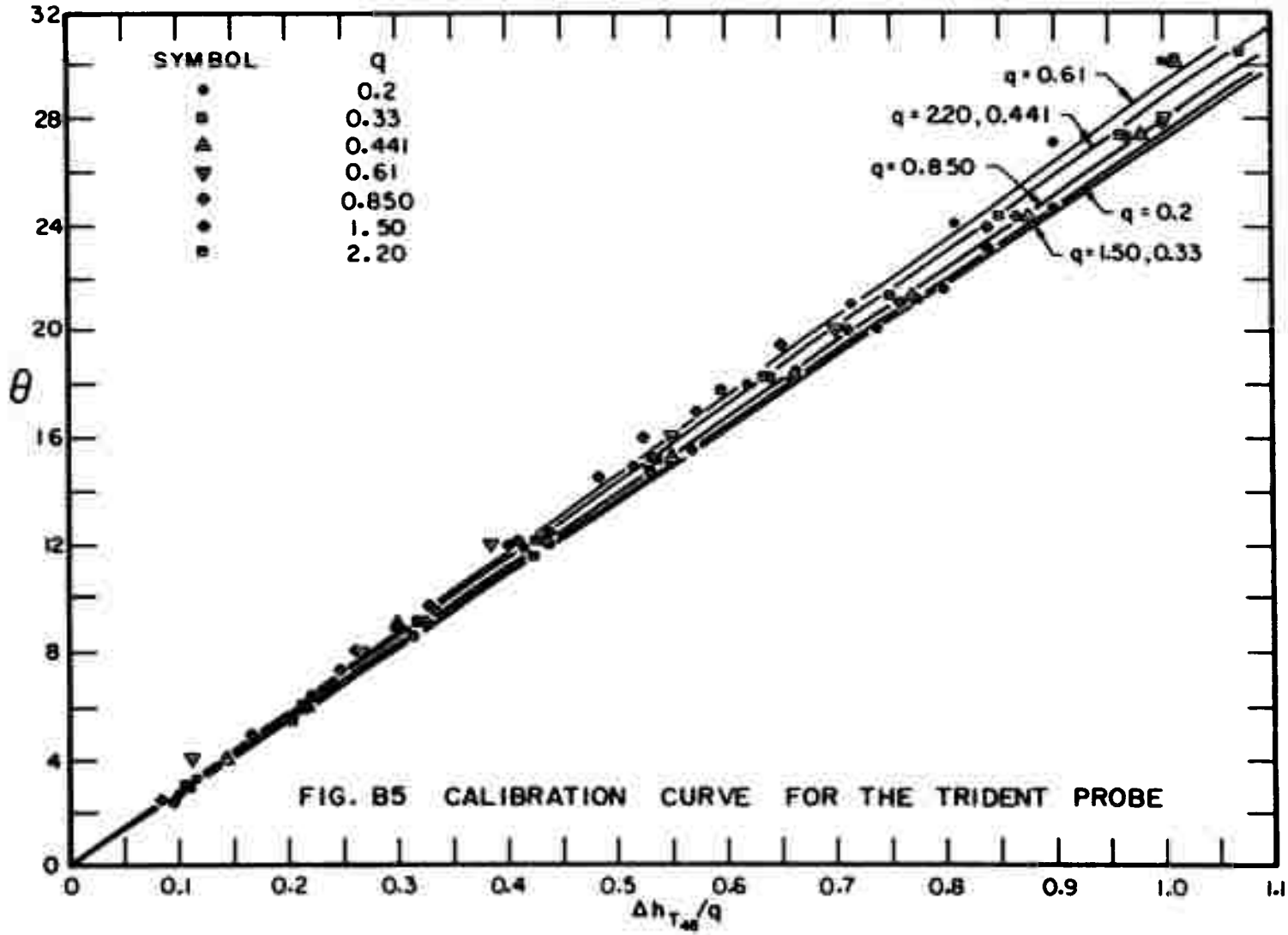

FIG. B5 CALIBRATION CURVE FOR THE TRIDENT PROBE

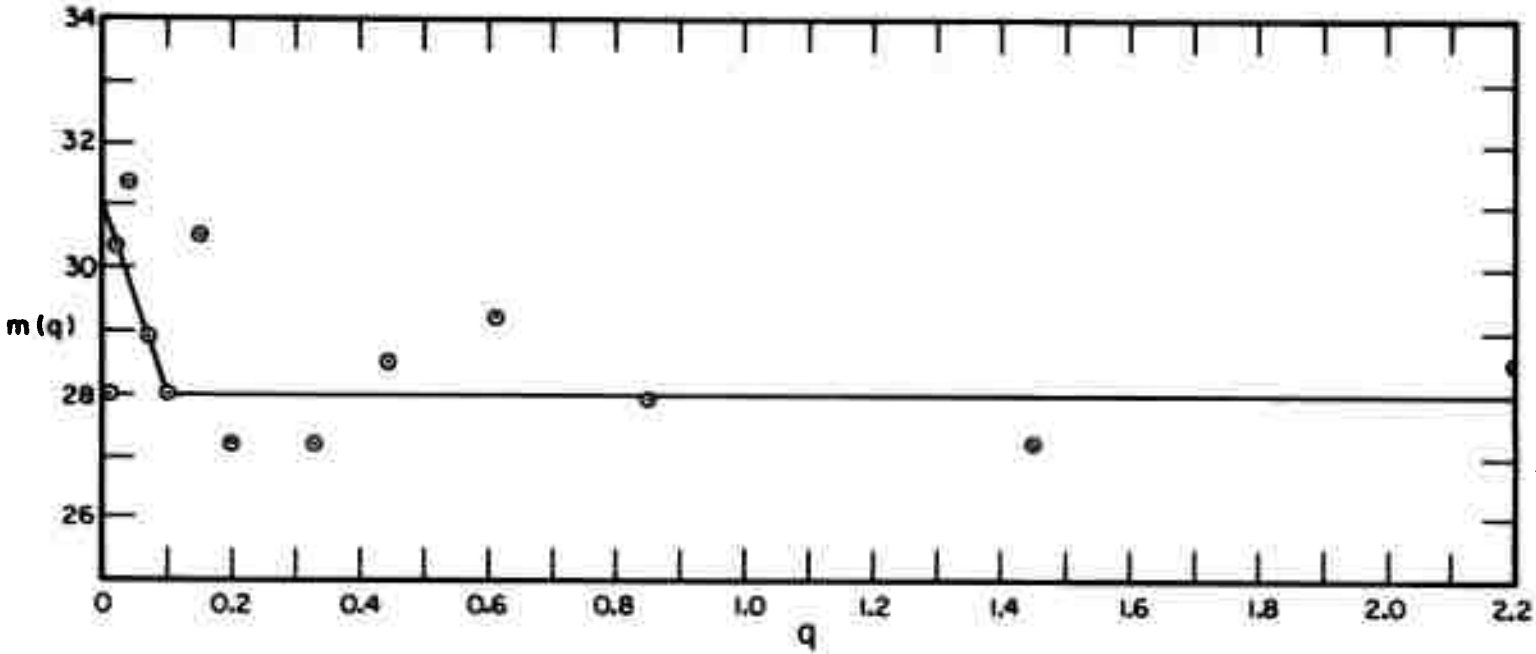

FIG. B6 CALIBRATION PARAMETER FOR THE TRIDENT PROBE

APPENDIX C --

SOLUTION OF EQUATIONS FROM THE JET DEFLECTION ANALYSIS

Eight equations involving eight unknowns were developed in section VII; this appendix presents the reduction of the eight equations to two computation equations. In the presentation below, the steps will be referred to by reference to the equations used; the detailed algebraic steps will not be shown. The equations from the analysis in the body of the text are reproduced here for reference with the exception that equations 2 and 3 have already been used in equation 4 in order to eliminate the variables P_L and P_R.

Equation Number	Equation
4	$\tan \alpha = \dfrac{[q_1/R_1]X' + q_2}{[2q_2/R_2 - q_1/R_1]Y' + q}$
5	$\tan \alpha = \dfrac{q_1 \sin \gamma + q_2 \cos \beta}{q_2 \cos \gamma + q_1 \sin \beta}$
6	$1 + Y'/R_1 = \cos \gamma + (R_2/R_1) \sin \beta$
7	$1 + X'/R_2 = (R_1/R_2) \sin \gamma + \cos \beta$
8	$\tan \alpha = R_1(1-\cos \gamma)/[R_1 \sin \gamma - x_{app}]$
9	$x_{app}/X' = 0.25\, k\, (\overline{Y}/\overline{Y}') + 0.875\,(X/X')$

A non-dimensionalizing procedure will be employed for all factors as given by the relationships:

$q_2/q_1 = mfr$, $\quad Y/X = k$, $\quad x_{app}/X' = \delta$,

$R_1/X' = R'_1$, $\quad R_2/X' = R'_2$

Equations 4 and 9 can be combined to solve for R'_2 in the form of $R'_2 = R'_2(R'_1, \gamma)$.

$$\frac{mfr}{R'_2} = \frac{[1 + R'_1\, mfr][R'_1 \sin\gamma - \delta] - R'^2_1 (1 - \cos\gamma) + k R'_1 (1 - \cos\gamma)}{2 R'^2_1 \quad (1 - \cos\gamma)\, k} \tag{10}$$

Solving equations 6 and 7 for $\sin\beta$ and $\cos\beta$, then squaring and adding the resulting equations, results in another formulation for $R'_2 = R'_2(R'_1, \gamma)$

$$\frac{mfr}{R'_2} = \frac{2 (R'_1 \sin\gamma - 1) \quad mfr}{[R'_1 (1 - \cos\gamma) \; + \; k]^2 \quad + [1 - R'_1 \sin\gamma]^2} \tag{11}$$

Equations 10 and 11 can be equated, eliminating R'_2, and the resulting expression can be reduced to

$$\begin{aligned}
&R'^4_1 \{ 2(1 - \cos\gamma)\, [mfr\, (\sin\gamma) - (1 - \cos\gamma)] \\
&+R'^3_1 \{ 4 \sin\gamma\, (1 - \cos\gamma) - 2\, mfr\, \delta\, (1 - \cos\gamma) \\
&\qquad - 2\, mfr\, (\sin\gamma - k(1 - \cos\gamma)\, \sin\gamma \} \\
&+R'^2_1 \{2\delta [mfr \sin\gamma - k(1 - \cos\gamma)\, mfr - (1 - \cos\gamma) \} \\
&+R'_1 \{ [2\, k\, (1 - \cos\gamma) - 2 \sin\gamma]\, \delta \\
&\qquad + [\sin\gamma - mfr\, \delta + k\, (1 - \cos\gamma)]\, (k^2 + 1) \} \\
&+ (k^2 + 1)\, (-8) = 0
\end{aligned} \tag{12}$$

If equations 6 and 7 are solved for $\sin\beta$ and $\cos\beta$ and if these factors are used in the combined equations 4 and 9, a quadratic expression for R'_2 results.

$$\frac{mfr}{R'_2} = \frac{-B \pm \sqrt{[B^2 - 4AC]}}{2A}$$

where

$$A = 2k(1 - R'_1 \sin\gamma)$$

$$B = \{2k(mfr + \sin\gamma) + (1 - R'_1 \sin\gamma)(1 - 1/R'_1) - [1/R'_1 + mfr][k + R'_1(1 - \cos\gamma)]\}$$

$$C = (mfr + \sin\gamma)(1 - k/R'_1) - \cos\gamma(1/R'_1 + mfr)$$

Equations 11 and 13 can be combined to eliminate R_2, thus yielding a second equation for R'_1 and γ.

$$(mfr)^2 k\, 8(1 - R'_1 \sin\gamma)^3$$
$$+ \{(mfr + \sin\gamma)(1 - k/R'_1) - \cos\gamma(1/R'_1 + mfr)\}$$
$$\{[R'_1(1 - \cos\gamma) + k]^2 + (1 - R'_1 \sin\gamma)^2\}^2$$
$$-2mfr(1 - R'_1 \sin\gamma)\{2k(mfr + \sin\gamma) + (1 - R'_1 \sin\gamma)(1 - 1/R'_1)$$
$$-(1/R'_1 - mfr)[k + R'_1(1 - \cos\gamma)]\}$$
$$\cdot\{[R'_1(1 - \cos\gamma) + k]^2 + [1 - R'_1 \sin\gamma]^2\} = 0 \qquad (14)$$

The computational procedure which was chosen from this point was dictated by the complicated algebraic equations. Using an IBM 7090 for computation, equation 12 was solved for a given value of γ. With the R'_1 from this computation the left side of 14 was evaluated and its value, as well as R'_1, was printed as output. The value of R'_2 and $\tan\alpha$ were then computed from equations 11 and 4 and the resulting value printed as output. Finally, two non-dimensional representations of the pressure were formed as (using equations 2 and 3):

$$Cp_L = \frac{X'P_L}{q_1} = \frac{mfr}{R'_2} \qquad (2a)$$

$$Cp_R = \frac{X'P_R}{q_1} = \frac{mfr}{R'_2} - \frac{1}{R'_1} \qquad (3a)$$

These values were also computed and printed as the final output. This procedure was repeated until all the values of γ ($1 \leq \gamma \leq 42$) were employed, then the entire procedure was

repeated until all of the values of k and the mfr were used (viz., $\kappa = 0.5,\ 1.0,\ 1.5$ and mfr 0.05, 0.10, 0.15, 0.20, 0.25).

Since equation 12 is a fourth order equation, there are four roots; however, only one of these is a physically possible solution. Consequently, the criterion to select the correct value of γ was established as that γ which led to a zero value of equation 14 and positive values of R'_1 and R'_2. Linear interpolations were employed where necessary in the evaluation of the computer print out.

APPENDIX D --

PROGRAM FOR y^* TRAVERSES

The Fortran IV program which was used for the data reduction on an IBM 7090 is presented below.

Method 1 (direct measurement of Θ) and Method 2, as described introduced in the "Detailed Mean Flow Survey" section, VIII, required a different format for the data cards and a change of four Fortran statements. The four changes for Method 2 are listed on the program statement to the right of the regular Method 1 statements. Static pressure and total pressure corrections were made in accordance with the formulas determined in Appendix B; note that these corrections are not iterative. The calculation for the angle from the $\Delta h_{T_{45}}$ data (in Method 2) was applied twice. This calculation actually should be an iterative process, but there was no way to generate a goodness criterion. Repeated application of the computation would lead to an unbounded Θ value; consequently, the arbitrary choice of two repetitions was made. The program was also written such that the maximum (or minimum) angle could be $\pm$ 80 degrees. This was necessary because certain situations arose involving a very small q while $\Delta h_{T_{45}}$ was large enough to yield unrealistically large angles (e.g. a q value of 0.001 inch of water and a $\Delta h_{T_{45}}$ value of 0.004 inch of water would lead to a Θ of 121 degrees).

A complete traverse was taken at $z/a = 0$, at the three stations $x/a = 5$, 15, 30, and for a mfr = 0.1 using Method 1 and Method 2. A comparison of the results from these six traverses gives an indication of the accuracy of Method 2. Figures D-1 to D-3 show the velocity profiles (u/u_c vs y^*) and Figures D-4 to D-6 show the values of Θ^* vs y^*. A plot of u/u_c (from Method 1) is included on the figures to provide a reference for the dimensions of the jet. The agreement shown by the velocity profiles is quite satisfactory. The agreement shown by the two methods for Θ^* is, in general, acceptable except for $x/a = 5$ and y/a less than about -0.75. Since the principal purpose of the data of Method 2 was the establishment of mean velocity profiles, the method was satisfactory.

The variables used in the text of this writing were necessarily changed into Fortran Language variables; the text and the equivalent program variables are:

Program	Text	Program	Text	Program	Text
YS	y^*	HT	h_T	HS	h_s
DIAL	t	DELHT	$h_{T_{45}}$	XOA	x/a
ZOA	z/a	IX	X	IY	Y
FMR	mfr	ZETA	ζ	U0	u_0
TEMP	T	PRESS	B	TC	Θ_c
Q0	q_0	HTC	h_{T_c}	HSC	h_{s_c}
DIAL 0	t_0	CP	C_p	Q	q
VE	V	U	u	V	v

Program	Text	Program	Text	Program	Text
Uouc	u/u_c	UOUCSQ	$(u/u_c)^2$	VOUC	(v/u_c)
US	u_*	T	Θ	XI	ξ
USOUC	(u_*/u_{c_*})	USOUCS	$(u_*/u_{c_*})^2$	YOB	y/b
XIOBS	ξ/b_*	AK	K	EM	m
B	b	E	E	EMOMO	M/M_0
RATIO	$2bq_c/q_0$	EOEO	E/E_0	EMS	m_*
BS	b_*	ES	E_*	DUSDZ	$\partial u_*(x, y)/\partial\zeta$
EMSOMO	M_*/M_0	RATIOS	$2b_*q_c/aq_0$	ESOEO	E_*/E_0

Note TT is used in the computation for Θ

HSP is used in the computation for h_s.

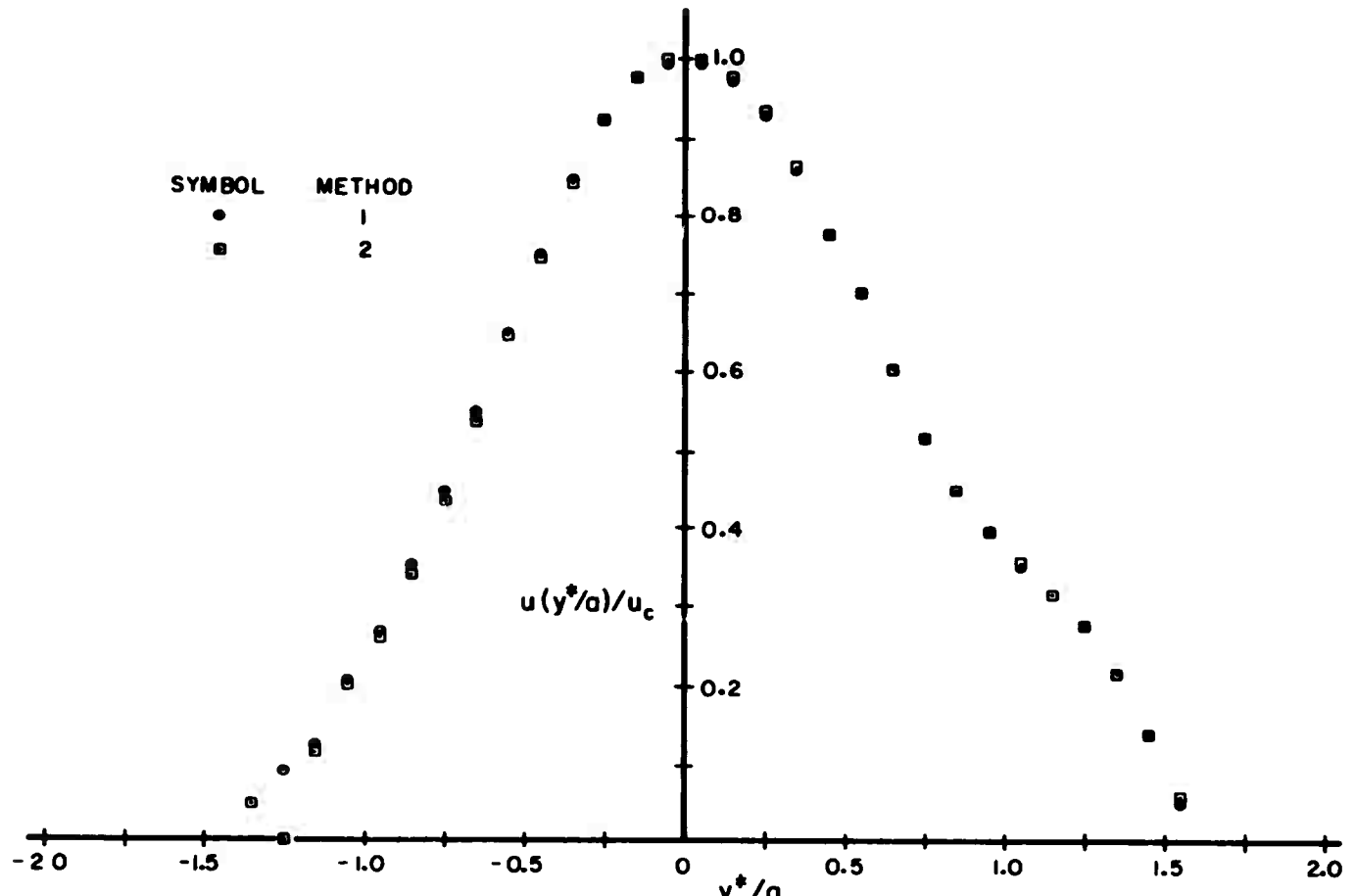

FIG. D1 $u(y^*/a)$ FOR $x/a = 5$, $z/a = 0$ FROM METHOD 1 AND 2 TO SHOW THE EFFECT OF THE MEASUREMENT TECHNIQUE

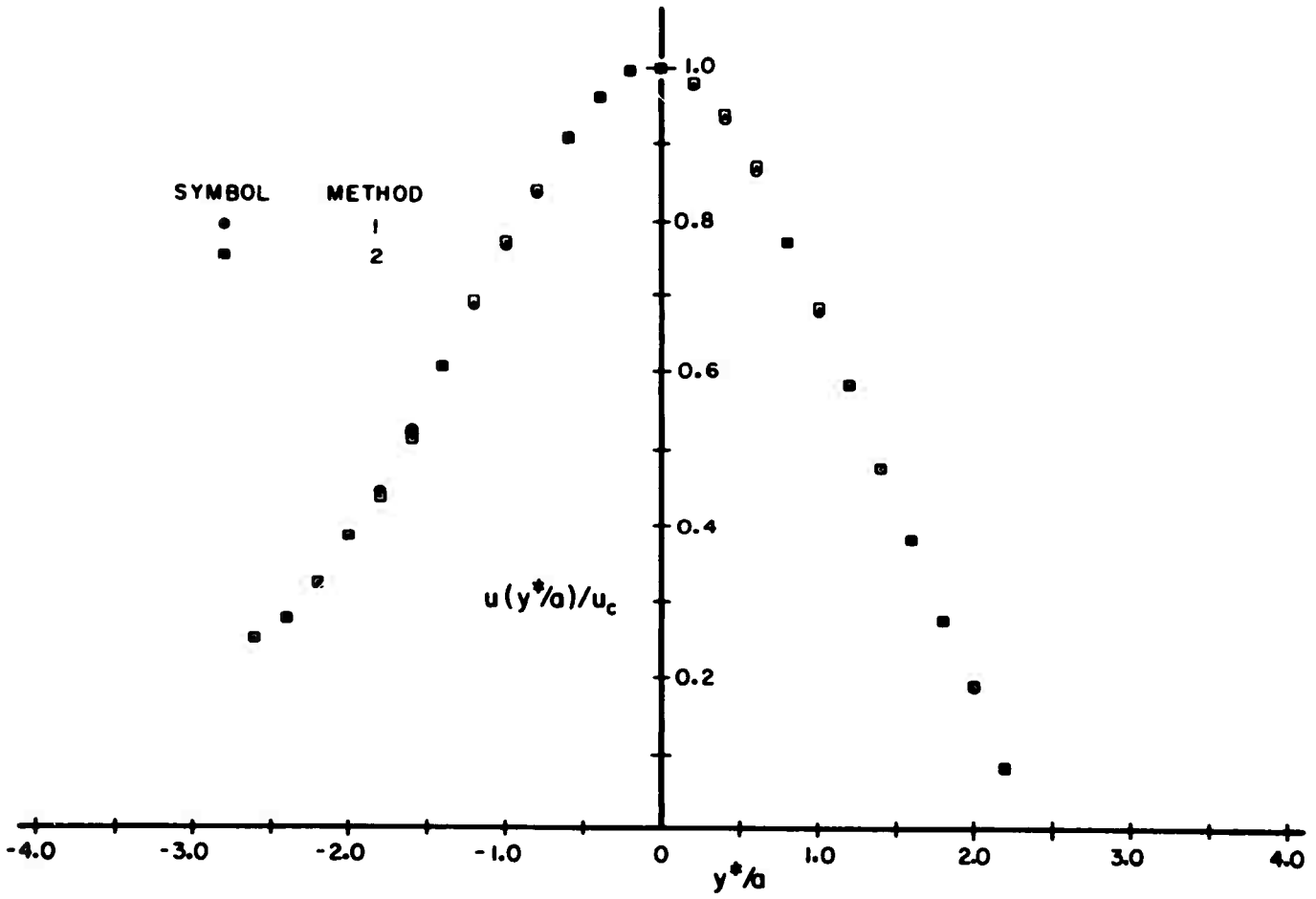

FIG. D2 u(y*/a) FOR x/a=15, z/a=0 FROM METHOD 1 AND 2 TO SHOW THE EFFECT OF THE MEASUREMENT TECHNIQUE

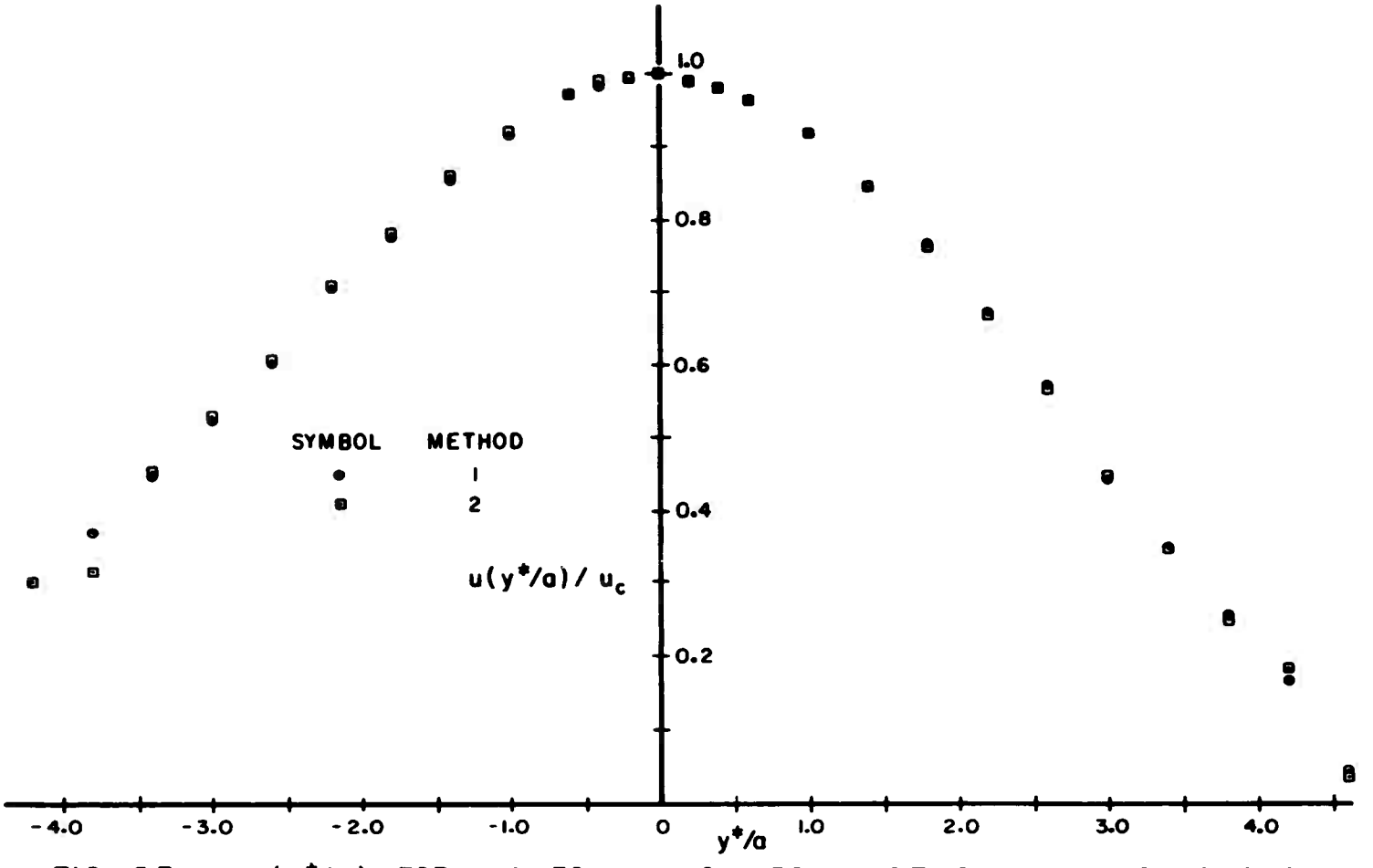

FIG. D3 $u(y^*/a)$ FOR $x/a=30$, $z/a=0$ FROM METHOD 1 AND 2 TO SHOW THE EFFECT OF THE MEASUREMENT TECHNIQUE

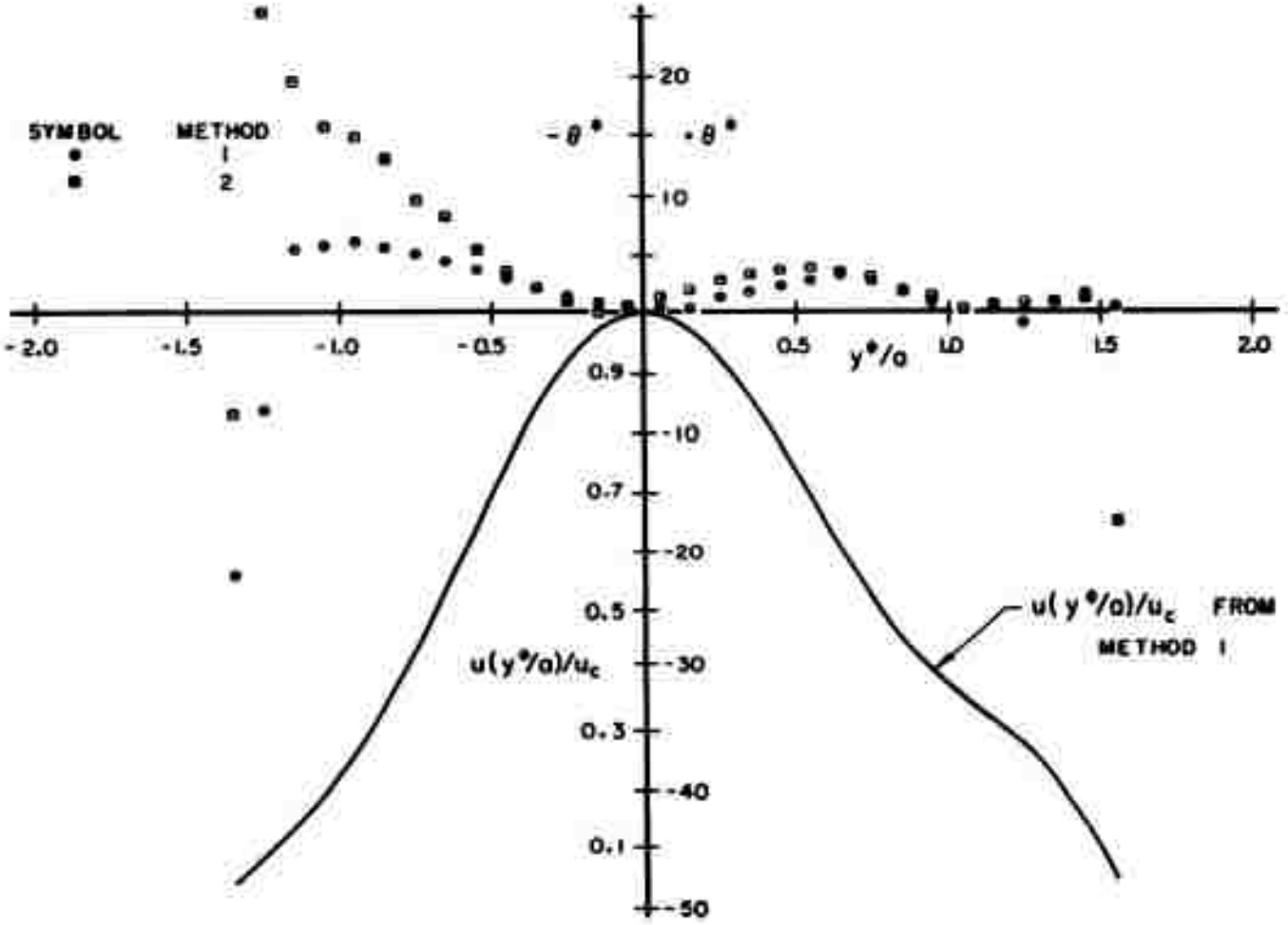

FIG. D-4 θ^* VERSUS y^*/a FOR $x/a=5$, $z/a=0$, METHODS 1 & 2

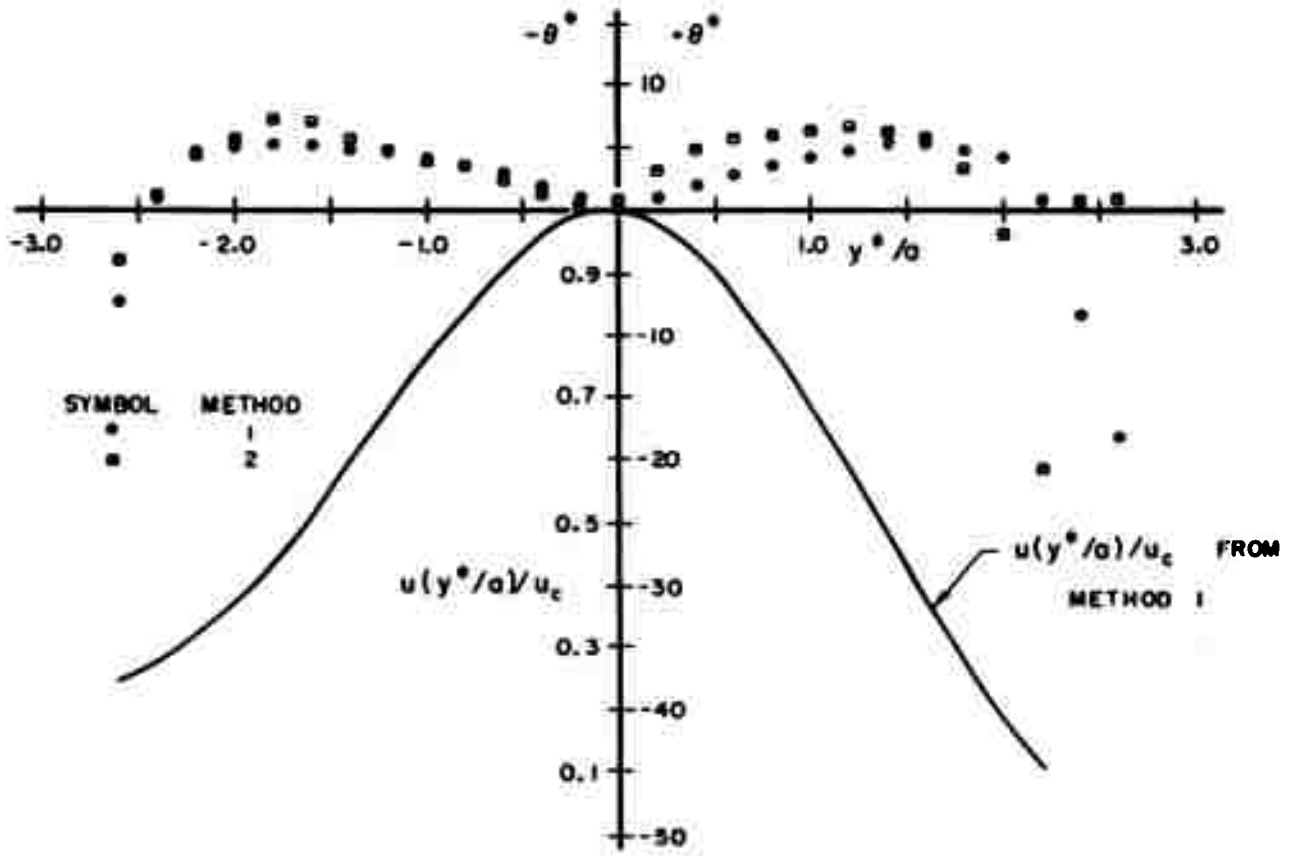

FIG. D5 θ^* VERSUS y^*/a FOR $x/a = 15$, $z/a = 0$, METHODS 1 & 2

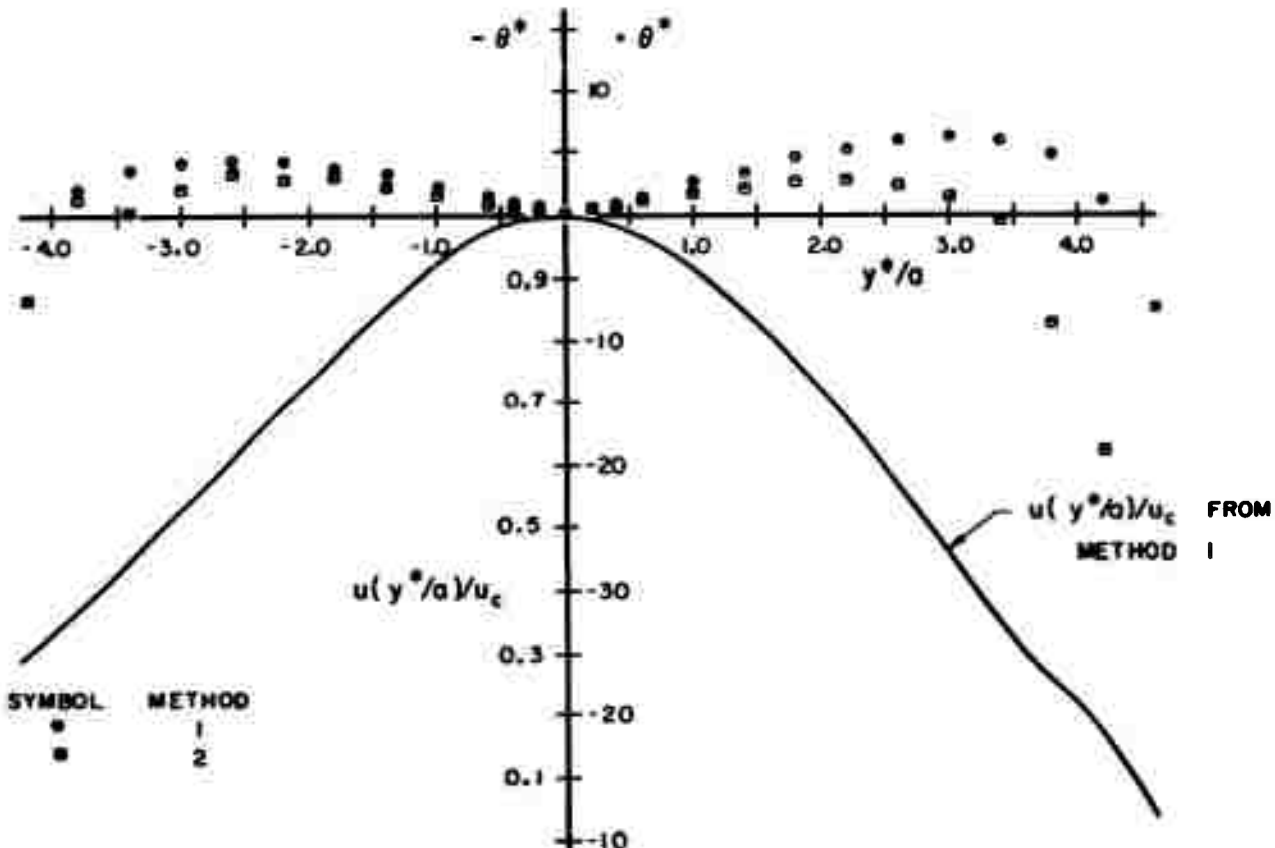

FIG. D6 θ^* VERSUS y^*/a FOR $x/a=30$, $z/a=0$, METHODS 1 & 2

```
      DATA PROCESSING FOR THE PRESENT STUDY  Y STAR TRAVERSES
      DIMENSION TS(50), CP(50), Q(50), VE(50), U(50), V(50), UOUC(50),
     1UCLCSQ(50), VCUC(50), US(50), T(50), Y (50), XI(50), USOUC(50),USO
     2UCS(50),TT(50),YOB(50),XIOBS(50)
1200  READ (5, 200) IXOA, ZOA, IX, IY, FMR, IDAY, INCNTH, IYEAR, NO

 200  FORMAT (I5,F5.2, 2I5,F5.2, 4I5)
      READ (5, 202) N, ZETA, UO, TEMP, PRESS
 202  FORMAT (I12, 4F12.5)
      READ (5, 204) TC, QQ, HTC, HSC, DIALO  READ (5, 204) TC, QQ, HTC, HSC
 204  FORMAT (5F12.5)                        204 FORMAT (4F12.5)
      TC=-TC                2200    READ (5, 206)Y(I),HT, HS, DIAL, DELHT,DIALO
      DO 48 I=1,N            206 FORMAT (6F10.0)
2200    READ (5, 206)Y(I),HT, HS, DIAL, DELHT
 206  FORMAT (5F10.0)
      IF (DIALO) 300, 2, 300
 300  TS(I)=(DIAL-DIALO)/0.164
  15  Q(I)=  HT-HS
 650  AK=15.89*SQRT(TEMP/PRESS)
      QC=HTC-HSC
 651  UC=AK*SQRT(QC)*COS(TC/57.296)
      UCS=AK*SQRT(QC)
  13  IF (ABS(TS(I)+TC)-15.0) 4, 4, 3
   3  HSP=HS+(9.0*Q(I)-0.35)*(ABS(TS(I)+TC)-15.0)*(0.001)
     1  +(5.0*Q(I)  - 0.18)*(0.01)
      IF (HSP-HS) 6,6,301
 301  Q(I)=HT-HSP
      IF (DIALO)  620,800,620
 620  HS=HSP
      GO TO 6
   4  IF (Q(I)-0.4)  6,6,302
 302  HSP=HS+ (0.16*Q(I)-0.07)*  (ABS(TS(I)+TC) **2.0-0.44*ABS(TS(I)+
     1      TC))*(0.001)
      IF (HSP-HS)6, 6, 303
 303  Q(I)=HT-HSP
      IF (DIALO)304, 800, 304
 304  HS=HSP
   6  IF (DIALO) 305, 14, 305
 305  CP(I)=PS/QC
      IF (Q(I))  47,76,76
  76  VE=AK*SQRT(Q(I))
      VE(I) = VE
      U(I)=VE(I)*COS((TS(I)+TC)/57.296)
      V(I)=VE(I) *SIN((TS(I)+TC)/57.296)
      UOLC(I)= U(I)/UC
      UCLCSQ(I)= UCUC(I)*UCUC(I)
      VCLC(I)= V(I)/UC
      US(I)=AK*SQRT(Q(I))*COS(TS(I)/57.256)
      T(I)=TS(I)+TC
      GO TO 48
  47  VE(I)=0.
      U(I)=0.
      V(I)=0.
      UCLC(I)=0.
      UCLCSQ(I)=0.
```

```
      VOLC(I)=0.
      US(I)=0.
   40 CONTINUE
      EM=0.0
      B=0.0
      E=0.0
      DO 24  I=2,N
      DELY=Y(I)-Y(I-1)
      EM=EM+(UOUC(I)+UCUC(I-1))*0.5*DELY
      B=B+(UCUCSQ(I)+UOUCSC(I-1))*0.25*DELY
   24 E= E +((C(I)*U(I) + C(I - 1)*U(I - 1))/(QC*UC))*0.5*DELY
  653 EMCMO=EM*UC/(AK*SQRT(QO))
      RATIC=2.0*B*CC/QO
      EOEO=E*UC*QC /(AK*QC**1.5)
      IF (TC) 306, 1100,  306
  3C6 EMS=0.0
      BS=0.0
      ES=0.0
      XI(1)=Y(1)*CCS(TC/57.296)
      DUSDZ=(UCS*0.05678*(ABS(Y(1)/B))**2.0/B-1.14*UC/ZETA**1.5)*
     1  EXP(-0.3927*((ABS(Y(1)/B))**2.0))
      US(1)=US(1)+DUSDZ*Y(1)*SIN(TC/57.296)
      USCUC(1)=US(1)/UCS
      USCUCS(1)=USCUC(1)**2.0
      DO 36 J=2,N
      XI(J)=Y(J)*CCS(TC/57.296)
      DUSDZ=(UCS*0.05678*(ABS(Y(J)/B))**2.0/B-1.14*UO/ZETA**1.5)*
     1  EXP(-0.3927*((ABS(Y(J)/B))**2.0))
      US(J)=US(J)+DUSDZ*Y(J)*SIN(TC/57.296)
      USCUC(J)=US(J)/UCS
      USCUCS(J)=USCUC(J)**2.0
      DELXI=XI(J)-XI(J-1)
      EMS=EMS+0.5*(USCUC(J)+USCUC(J-1))*DELXI
      BS=BS+0.25*(USCUCS(J)+USCUCS(J-1))*DELXI
   36 ES=ES+(USCUC(J)**3.0/COS(TS(J)/57.296)**2.0
     1+USCUC(J-1)**3.0/COS(TS(J-1)/57.296)**2.0)*0.5*DELXI
      EMSOMO=EMS*UCS/(AK*SQRT(QO))
      RATIOS=2.0*BS*CC/QO
      ESCEO=ES*UCS*CC/(AK*CO**1.5)
      GO TO  1100
    2 Q(I)=HT-HS
      IF  (Q(I))  47,610, 610
  610 IF(Q(I)-0.1) 307, 307, 308
  3C7 T(I)=(31.0-3C.0*C(I))*(-DELHT/Q(I))
      GO TO 309
  3C8 T(I)=2E.0*(-DELHT/Q(I))
  309 CONTINUE
      IF (ABS(T(I))-80.0) 185,185,180
  18C IF  (T(I))  181,181,182
  181 HT=HT+C(I)* (0.4*86.7**2.0-1.55*86.7) *C.0C1
      Q(I)=HT-HS
      TS(I)=-80.0-TC
      GO TO 13
  182 HT=HT+C(I)* (0.4*86.7**2.0-1.55*86.7) *0.0C1
      Q(I)=HT-HS
      TS(I)=80.0-TC
```

```
      GO TO 13
  185 IF (ABS(T(I))-10.7)  12, 12, 310
  310 HT=HT+C(I)* (0.4*(ABS(T(I))-6.7)**2.0-1.55* (ABS(T(I))-6.7))*
     1    (0.001)
   12 Q(I)=HT-HS
      TS(I) = T(I) - TC
      GO TO 13
   14 Q(I)=HT-HS
  800 IF(Q(I)-0.1)  311, 311, 312
  311 TT(I) = (31.0 - 30.0*Q(I))*(-DELHT/Q(I))
      GO TO 3131
  312 TT(I) = 28.0*(-DELHT/Q(I))
 3131 IF  (ABS(TT(I))-80.0)  313,313,190
  190 IF(TT(I))  191,191,192
  191 HT=HT+C(I)* (0.4*86.7**2.0-1.55*86.7) *0.001
      TS(I)=-80.0-TC
      DIALO=1.0
      GO TO 15
  192 HT=HT+C(I)* (0.4*86.7**2.0-1.55*86.7) *0.001
      TS(I)=+80.0-TC
      DIALO=1.0
      GO TO 15
  313 IF (ABS(TT(I))-10.7)315,315,314
  314 HT=HT+C(I)*(0.4*(ABS(TT(I))-6.7)**2.0-1.55*(ABS(TT(I))-6.7))*
     1    (0.001)
  315 CONTINUE
  316 TS(I) = TT(I) - TC
      DIALO = 1.0
      GO TO 15
 1201 FORMAT  (F12.5)
 1100 WRITE(6,201)  IXCA,ZCA    IX,IY,FMR,IDAY,IMONTH,IYEAR,NO
  201 FORMAT(1H1,15,F6.2,215,F6.2,415                          ///)
  654 WRITE (6, 100)
  100  FORMAT(1HO,8X,2HYS,10X,2HTS,10X,1HT,10X,1HQ,10X,2HCP,10X,1HV,10X,
     2  4HLOLC, 10X,  4HVELC///)
      DO 104 I = 1, N
      YOB(I)=Y(I)/P
      XICBS(I)=XI(I)/BS
  104 WRITE(6,101)Y(I),TS(I),T(I),C(I),CP(T),VE(I),UOUC(I),VOUC(I)
  101 FORMAT(6X,F9.3,3X,F9.2,3X,F9.2,1PE10.2,1X,1PE10.2,  1PE10.2,4X,
     21PE10.2,4X,1PE10.2)
  656 WRITE(6,102)
  102  FORMAT(1H1,8X,6HUOLCSQ,9X,2HXI,10X,2HUS,9X,5HUSOLC,9X,6HUSOLCS,9X,
     2  3HY/B,9X,5HXIOBS///)
  657 WRITE(6,103) (UOUCSC(I),XI(I),US(I),USOUC(I),USOUCS(I),YOB(I),
     2  XICBS(I),I=1,N))
  103  FORMAT(7X,1PE10.2,0PF9.3,4X, 1PE9.2,4X,1PE9.2,4X,1PE9.2,5X,
     2  1P1E9.2,3X,1PE9.2)
  650 WRITE (6, 106) UC, EM, M, E, EMOMO, RATIO, ECEC
  106 FORMAT (/// 6H  UC =, 1PE9.2, 7H,  EM =, E9.2, 6H,  B =, E9.2,
     1  6H,  E=,E9.2,
     2      10H,   EMOM =, E9.2, 1 H,  RATIO =, E9.2, 9H,  EOLO =,
     3      E9.2  )
      WRITE (6, 108) UCS, EMS, BS, ES, EMSOMC, RATIOS, ESUEO
  108 FORMAT (///6H UCS =, 1PE9.2, 7H, EMS =, E9.2, 6H, BS =, E9.2,
     1  5H, ES=,E9.2,
```

```
2      10H, EMSOMO =, E9.2, 10H, RATIOS =, E9.2, 9H, ESOEO =,
3      E9.2)
 GO TO 1200
 END
```

APPENDIX E --

y^* TRAVERSE RESULTS

This appendix presents the computer results from the 37 data runs that comprised the y^* traverses. The other traverse data (u(z)) is implicitly presented in Figures 9 and 10.

The presentation of the y^* traverses involves reproductions of the original results sheets. They are presented in the following order:

i) "Single Bounded Jet"

ii) "Detailed Mean Flow Survey" x/a = 5, 15, 30

iii) "Nozzle Geometry Effect on the Resultant Jet"

iv) "mfr Effect on the Resultant Jet"

v) Comparison of Method 1 and 2.

For each data set in which the mfr = 0, the complete results are presented on one page; for mfr not equal to zero the second page of the set presents the results for the natural co-ordinates (ζ, ξ, z).

Each set of data is specified by 9 numbers. These are: x/a, z/a, X, Y, mfr, day, month year, program path number. The 9 numbers are listed at the beginning of each set of results.

An interesting fact, that is not shown in these results, is the existance of negative gage total pressure readings for the extremities of the jet. Since these measurements were made with the total pressure probe facing the flow (x - y -Θ traverse device) the negative gage pressure is not a result of yaw induced errors.

5 0. 0 0 0. 20 4 64 1

YS	TS	T	Q	CP	V	UOUC	VOUC	Y/B
-1.450	29.02	29.02	-0.	-6.94E-03	-0.	-0.	-0.	-2.72E 00
-1.350	10.12	10.12	8.00E-03	-8.79E-03	6.07E 00	5.99E-02	1.07E-02	-2.53E 00
-1.250	-2.56	-2.56	3.20E-02	-1.11E-02	1.21E 01	1.22E-01	-5.44E-03	-2.34E 00
-1.150	-4.82	-4.82	5.90E-02	-1.34E-02	1.65E 01	1.65E-01	-1.39E-02	-2.15E 00
-1.050	-6.16	-6.16	1.21E-01	-1.67E-02	2.36E 01	2.35E-01	-2.54E-02	-1.97E 00
-0.950	-6.16	-6.16	2.10E-01	-2.08E-02	3.11E 01	3.10E-01	-3.34E-02	-1.78E 00
-0.850	-6.10	-6.10	3.35E-01	-2.31E-02	3.93E 01	3.91E-01	-4.18E-02	-1.59E 00
-0.750	-5.24	-5.24	4.90E-01	-2.54E-02	4.75E 01	4.74E-01	-4.35E-02	-1.40E 00
-0.650	-4.02	-4.02	6.93E-01	-2.70E-02	5.65E 01	5.65E-01	-3.98E-02	-1.22E 00
-0.550	-3.41	-3.41	9.40E-01	-2.78E-02	6.58E 01	6.58E-01	-3.93E-02	-1.03E 00
-0.450	-2.80	-2.80	1.22E 00	-2.78E-02	7.50E 01	7.51E-01	-3.68E-02	-8.43E-01
-0.350	-2.07	-2.07	1.54E 00	-2.42E-02	8.42E 01	8.43E-01	-3.05E-02	-6.55E-01
-0.250	-1.46	-1.46	1.83E 00	-1.84E-02	9.17E 01	9.19E-01	-2.35E-02	-4.68E-01
-0.150	-0.85	-0.85	2.05E 00	-1.43E-02	9.71E 01	9.73E-01	-1.45E-02	-2.81E-01
-0.050	-0.24	-0.24	2.16E 00	-1.20E-02	9.97E 01	9.99E-01	-4.25E-03	-9.36E-02
0.050	0.24	0.24	2.16E 00	-1.20E-02	9.98E 01	10.00E-01	4.26E-03	9.36E-02
0.150	0.98	0.98	2.03E 00	-1.38E-02	9.68E 01	9.70E-01	1.65E-02	2.81E-01
0.250	1.71	1.71	1.83E 00	-1.83E-02	9.19E 01	9.20E-01	2.74E-02	4.68E-01
0.300	2.68	2.68	1.42E 00	-2.27E-02	8.10E 01	8.11E-01	3.80E-02	5.62E-01
0.450	3.17	3.17	1.25E 00	-2.72E-02	7.58E 01	7.59E-01	4.20E-02	8.43E-01
0.550	3.90	3.90	9.75E-01	-2.31E-02	6.70E 01	6.70E-01	4.57E-02	1.03E 00
0.650	4.76	4.76	7.02E-01	-2.41E-02	5.69E 01	5.68E-01	4.73E-02	1.22E 00
0.750	5.37	5.37	5.03E-01	-2.30E-02	4.81E 01	4.80E-01	4.51E-02	1.40E 00
0.850	6.34	6.34	3.24E-01	-2.04E-02	3.86E 01	3.85E-01	4.28E-02	1.59E 00
0.950	7.07	7.07	2.03E-01	-1.76E-02	3.06E 01	3.04E-01	3.77E-02	1.78E 00
1.050	6.95	6.95	1.17E-01	-1.48E-02	2.32E 01	2.31E-01	2.82E-02	1.97E 00
1.150	6.95	6.95	5.60E-02	-1.20E-02	1.61E 01	1.60E-01	1.95E-02	2.15E 00
1.250	4.63	4.63	2.10E-02	-9.72E-03	9.84E 00	9.83E-02	7.96E-03	2.34E 00
1.350	-2.07	-2.07	7.00E-03	-7.87E-03	5.68E 00	5.69E-02	-2.06E-03	2.53E 00

UC = 9.98E 01, EM = 1.48E 00, S = 5.34E-01, E=, 8.69E-01,

EMOM = 1.46E 00, RATIC = 1.04E 00, EOEO = 8.34E-01

5 2.00 0 0 0. 2 7 64 1

YS	TS	T	Q	CP	V	UOUC	VOUC	Y/B
-1.340	27.13	27.13	8.00E-03	-8.90E-03	5.77E 00	5.45E-02	2.79E-02	-2.38E 00
-1.140	6.71	6.71	5.20E-02	-2.44E-02	1.57E 01	1.55E-01	1.82E-02	-2.02E 00
-0.940	-3.23	-3.23	1.60E-01	-2.20E-02	2.76E 01	2.73E-01	-1.54E-02	-1.67E 00
-0.740	-4.70	-4.70	4.76E-01	-2.76E-02	4.75E 01	4.71E-01	-3.87E-02	-1.31E 00
-0.640	-4.45	-4.45	7.24E-01	-2.77E-02	5.86E 01	5.81E-01	-4.52E-02	-1.13E 00
-0.540	-4.45	-4.45	1.06E 00	-2.73E-02	7.09E 01	7.02E-01	-5.47E-02	-9.57E-01
-0.440	-3.35	-3.35	1.38E 00	-2.55E-02	8.11E 01	8.04E-01	-4.71E-02	-7.80E-01
-0.340	-2.50	-2.50	1.74E 00	-2.01E-02	9.10E 01	9.03E-01	-3.94E-02	-6.03E-01
-0.240	-1.52	-1.52	2.01E 00	-1.43E-02	9.77E 01	9.70E-01	-2.58E-02	-4.25E-01
-0.040	-0.30	-0.30	2.11E 00	-7.03E-03	1.00E 02	9.96E-01	-5.30E-03	-7.09E-02
0.160	1.04	1.04	2.10E 00	-8.83E-03	9.98E 01	9.92E-01	1.79E-02	2.84E-01
0.260	2.01	2.01	1.89E 00	-1.28E-02	9.47E 01	9.40E-01	3.30E-02	4.61E-01
0.360	2.62	2.62	1.64E 00	-1.78E-02	8.82E 01	8.75E-01	4.01E-02	6.38E-01
0.460	3.60	3.60	1.28E 00	-2.22E-02	7.79E 01	7.72E-01	4.85E-02	8.15E-01
0.560	4.21	4.21	1.01E 00	-2.51E-02	6.92E 01	6.86E-01	5.04E-02	9.93E-01
0.660	5.06	5.06	7.05E-01	-2.58E-02	5.79E 01	5.73E-01	5.07E-02	1.17E 00
0.760	5.55	5.55	4.80E-01	-2.52E-02	4.77E 01	4.72E-01	4.58E-02	1.35E 00
0.960	5.91	5.91	1.84E-01	-2.06E-02	2.96E 01	2.92E-01	3.03E-02	1.70E 00
1.160	3.96	3.96	4.10E-02	-1.45E-02	1.40E 01	1.38E-01	9.58E-03	2.06E 00
1.360	-24.70	-24.70	7.00E-03	-8.90E-03	5.77E 00	5.20E-02	-2.39E-02	2.41E 00

UC = 1.01E 02, EP = 1.50E 00, B = 5.64E-01, E=, 9.51E-01,

EPOM = 1.47E 00, RATIO = 1.08E 00, EOEO = 8.96E-01

10 0. 0 0 0. 20 5 64 1

YS	TS	T	Q	CP	V	UOUC	VOUC	Y/B
-2.050	21.95	21.95	7.00E-03	-1.41E-02	-0.	6.22E-02	2.51E-02	-2.61E 00
-1.800	3.41	3.41	3.20E-02	-1.93E-02	1.22E 01	1.43E-01	8.54E-03	-2.29E 00
-1.550	-3.17	-3.17	5.80E-02	-2.76E-02	2.13E 01	2.50E-01	-1.39E-02	-1.97E 00
-1.450	-3.29	-3.29	1.48E-01	-3.72E-02	2.61E 01	3.28E-01	-1.77E-02	-1.84E 00
-1.300	-3.54	-3.54	2.29E-01	-3.98E-02	3.25E 01	3.83E-01	-2.36E-02	-1.65E 00
-1.150	-3.54	-3.54	3.50E-01	-4.17E-02	4.01E 01	4.73E-01	-2.92E-02	-1.46E 00
-1.050	-3.29	-3.29	4.26E-01	-4.24E-02	4.43E 01	5.22E-01	-3.00E-02	-1.34E 00
-0.950	-2.99	-2.99	5.22E-01	-4.29E-02	4.91E 01	5.78E-01	-3.02E-02	-1.21E 00
-0.800	-2.80	-2.80	6.78E-01	-4.35E-02	5.59E 01	6.59E-01	-3.23E-02	-1.02E 00
-0.650	-2.38	-2.38	8.79E-01	-4.41E-02	6.31E 01	7.50E-01	-3.12E-02	-8.27E-01
-0.550	-2.01	-2.01	1.03E 00	-4.35E-02	6.85E 01	8.12E-01	-2.85E-02	-7.00E-01
-0.450	-1.52	-1.52	1.15E 00	-4.16E-02	7.29E 01	8.59E-01	-2.29E-02	-5.72E-01
-0.250	-0.49	-0.49	1.41E 00	-4.04E-02	8.06E 01	9.51E-01	-8.09E-03	-3.18E-01
-0.050	0.61	0.61	1.55E 00	-4.04E-02	8.47E 01	9.98E-01	1.06E-02	-6.36E-02
0.150	1.83	1.83	1.50E 00	-4.02E-02	8.31E 01	9.80E-01	3.13E-02	1.91E-01
0.350	3.05	3.05	1.30E 00	-4.10E-02	7.74E 01	9.12E-01	4.86E-02	4.45E-01
0.450	3.48	3.48	1.16E 00	-4.09E-02	7.33E 01	8.63E-01	5.24E-02	5.72E-01
0.550	3.90	3.90	1.02E 00	-4.09E-02	6.87E 01	8.09E-01	5.52E-02	7.00E-01
0.700	4.57	4.57	8.27E-01	-3.97E-02	6.10E 01	7.26E-01	5.81E-02	8.90E-01
0.850	5.24	5.24	6.27E-01	-3.99E-02	5.30E 01	6.32E-01	5.80E-02	1.08E 00
0.950	5.67	5.67	5.19E-01	-3.89E-02	4.89E 01	5.74E-01	5.70E-02	1.21E 00
1.050	6.22	6.22	4.20E-01	-3.85E-02	4.42E 01	5.16E-01	5.62E-02	1.34E 00
1.200	6.71	6.71	2.91E-01	-2.95E-02	3.67E 01	4.29E-01	5.05E-02	1.53E 00
1.350	7.01	7.01	1.88E-01	-2.76E-02	2.95E 01	3.45E-01	4.24E-02	1.72E 00
1.450	7.07	7.07	1.35E-01	-2.57E-02	2.50E 01	2.92E-01	3.62E-02	1.84E 00
1.550	7.07	7.07	9.80E-02	-2.44E-02	2.13E 01	2.49E-01	3.09E-02	1.97E 00
1.700	6.34	6.34	4.80E-02	-1.67E-02	1.49E 01	1.74E-01	1.94E-02	2.16E 00
1.850	3.29	3.29	1.20E-02	-1.09E-02	7.44E 00	8.76E-02	5.04E-03	2.35E 00
1.950	-0.61	-0.61	5.00E-03	-9.63E-03	4.80E 00	5.66E-02	-6.03E-04	2.48E 00

UC = 6.48E 01, EP = 2.20E 00, C = 7.86E-01, E=, 1.26E 00,

EPOM = 1.85E 00, RATIO = 1.10E 00, EDEC = 7.44E-01

15 0. 0 0 0. 20 4 64 1

YS	TS	T	Q	CP	V	UOUC	VCUC	Y/B
-2.550	15.91	15.91	1.10E-02	-2.76E-02	4.8CE 00	9.51E-02	2.71E-02	-2.41E 00
-2.300	2.26	3.41	-3.00E-02	-3.56E-02	0.	C.	C.	-2.17E 00
-2.050	-2.38	-2.38	7.50E-02	-4.44E-02	1.86E 01	2.58E-01	-1.07E-02	-1.93E 00
-1.800	-3.72	-3.72	1.39E-01	-5.24E-02	2.53E 01	3.51E-01	-2.26E-02	-1.70E 00
-1.550	-4.09	-4.09	2.34E-01	-6.13E-02	3.29E 01	4.55E-01	-3.25E-02	-1.46E 00
-1.300	-3.90	-3.90	3.49E-01	-6.58E-02	4.01E 01	5.56E-01	-3.79E-02	-1.23E 00
-1.050	-3.66	-3.66	5.14E-01	-7.01E-02	4.87E 01	6.75E-01	-4.24E-02	-9.51E-01
-0.800	-3.72	-3.72	6.93E-01	-7.33E-02	5.65E 01	7.83E-01	-5.09E-02	-7.55E-01
-0.550	-2.38	-2.38	8.84E-01	-7.44E-02	6.39E 01	8.86E-01	-3.68E-02	-5.19E-01
-0.300	-0.73	-0.73	1.04E 00	-7.55E-02	6.93E 01	9.61E-01	-1.23E-02	-2.83E-01
-0.050	-0.30	-0.30	1.12E 00	-7.56E-02	7.21E 01	10.00E-01	-5.32E-03	-4.72E-02
0.200	2.38	2.38	1.09E 00	-7.51E-02	7.09E 01	9.83E-01	4.08E-02	1.89E-01
0.450	3.35	3.35	9.73E-01	-7.39E-02	6.78E 01	9.28E-01	5.44E-02	4.25E-01
0.700	4.57	4.57	7.91E-01	-7.19E-02	6.04E 01	8.36E-01	6.69E-02	6.61E-01
0.950	5.55	5.55	6.14E-01	-7.04E-02	5.32E 01	7.35E-01	7.14E-02	8.96E-01
1.200	6.52	6.52	4.31E-01	-6.76E-02	4.46E 01	6.15E-01	7.03E-02	1.13E 00
1.450	7.26	7.26	2.87E-01	-6.40E-02	3.64E 01	5.01E-01	6.38E-02	1.37E 00
1.700	7.68	7.68	1.73E-01	-5.42E-02	2.83E 01	3.89E-01	5.24E-02	1.60E 00
1.950	7.68	7.68	9.50E-02	-4.44E-02	2.09E 01	2.88E-01	3.88E-02	1.84E 00
2.200	6.77	6.77	4.10E-02	-3.64E-02	1.38E 01	1.90E-01	2.25E-02	2.08E 00
2.450	2.50	2.50	2.00E-02	-2.93E-02	9.61E 00	1.33E-01	5.82E-03	2.31E 00
2.700	-23.11	-23.11	7.00E-03	-2.22E-02	5.68E 00	7.26E-02	-3.10E-02	2.55E 00
2.950	-44.45	-44.45	5.00E-03	-1.69E-02	4.8CE 00	4.76E-02	-4.67E-02	2.78E 00

UC = 7.21E 01, EP = 2.92E 00, E = 1.06E 00, E=, 1.73E 00,

EMOM = 2.08E 00, RATIO = 1.07E 00, EOEO = 6.23E-01

15 2.00 0 0 0. 2 7 64 1

YS	TS	T	Q	CP	V	UOUC	VOUC	Y/B
-2.925	29.88	29.88	3.00E-03	-2.03E-02	4.87E 00	4.46E-02	2.56E-02	-2.66E 00
-2.675	17.99	17.99	1.10E-02	-2.47E-02	7.23E 00	9.37E-02	3.04E-02	-2.44E 00
-2.425	4.51	4.51	2.20E-02	-3.00E-02	1.02E 01	1.39E-01	1.10E-02	-2.21E 00
-2.175	-1.52	-1.52	5.20E-02	-3.71E-02	1.57E 01	2.14E-01	-5.70E-03	-1.98E 00
-1.925	-3.84	-3.84	1.00E-01	-4.41E-02	2.18E 01	2.96E-01	-1.99E-02	-1.75E 00
-1.675	-5.06	-5.06	1.97E-01	-5.30E-02	3.06E 01	4.15E-01	-3.68E-02	-1.53E 00
-1.425	-4.88	-4.88	3.03E-01	-6.00E-02	3.79E 01	5.15E-01	-4.40E-02	-1.30E 00
-1.175	-4.57	-4.57	4.53E-01	-6.44E-02	4.64E 01	6.30E-01	-5.04E-02	-1.07E 00
-0.925	-4.15	-4.15	6.49E-01	-6.49E-02	5.55E 01	7.55E-01	-5.47E-02	-8.42E-01
-0.675	-3.29	-3.29	8.33E-01	-6.48E-02	6.29E 01	8.56E-01	-4.93E-02	-6.15E-01
-0.425	-2.68	-2.68	1.02E 00	-6.39E-02	6.97E 01	9.49E-01	-4.45E-02	-3.87E-01
-0.175	-0.98	-0.98	1.11E 00	-6.44E-02	7.26E 01	9.90E-01	-1.69E-02	-1.59E-01
0.075	0.37	0.37	1.13E 00	-6.44E-02	7.34E 01	10.00E-01	6.39E-03	6.83E-02
0.325	1.71	1.71	1.06E 00	-6.42E-02	7.10E 01	9.68E-01	2.89E-02	2.96E-01
0.575	2.93	2.93	8.97E-01	-6.40E-02	6.53E 01	8.89E-01	4.54E-02	5.24E-01
0.825	3.66	3.66	7.32E-01	-6.39E-02	5.90E 01	8.02E-01	5.13E-02	7.51E-01
1.075	4.51	4.51	5.29E-01	-6.42E-02	5.01E 01	6.81E-01	5.37E-02	9.79E-01
1.325	5.12	5.12	3.73E-01	-6.09E-02	4.21E 01	5.71E-01	5.12E-02	1.21E 00
1.575	4.63	4.63	2.37E-01	-5.65E-02	3.35E 01	4.56E-01	3.70E-02	1.43E 00
1.825	4.02	4.02	1.52E-01	-5.03E-02	2.69E 01	3.65E-01	2.57E-02	1.66E 00
2.075	2.13	2.13	7.50E-02	-4.41E-02	1.89E 01	2.57E-01	9.58E-03	1.89E 00
2.325	-3.54	-3.54	1.50E-02	-1.32E-02	8.44E 00	1.15E-01	-7.10E-03	2.12E 00
2.575	-12.80	-12.80	1.40E-02	-2.65E-02	8.15E 00	1.08E-01	-2.46E-02	2.34E 00
3.075	-34.15	-34.15	5.00E-03	-1.77E-02	4.87E 00	5.50E-02	-3.73E-02	2.80E 00

UC = 7.34E 01, EM = 3.05E 00, L = 1.10E 00, E=, 1.80E 00,

EMOM = 2.18E 00, RATIO = 1.12E 00, EOEO = 6.56E-01

30 0. 0 0 0. 1 7 64 1

YS	TS	T	Q	CP	V	UOUC	VOUC	Y/B
-4.450	19.15	19.15	5.00E-03	-5.81E-02	6.85E 00	9.62E-02	3.34E-02	-2.21E 00
-4.200	8.78	8.78	1.00E-02	-6.22E-02	6.85E 00	1.42E-01	2.20E-02	-2.08E 00
-3.950	2.20	2.20	1.50E-02	-6.64E-02	6.39E 00	1.76E-01	6.74E-03	-1.96E 00
-3.700	-0.37	-0.37	2.70E-02	-7.26E-02	1.13E 01	2.37E-01	-1.51E-03	-1.83E 00
-3.450	-1.71	-1.71	3.80E-02	-7.68E-02	1.33E 01	2.81E-01	-8.37E-03	-1.71E 00
-3.200	-2.56	-2.56	7.20E-02	-8.71E-02	1.84E 01	3.86E-01	-1.73E-02	-1.59E 00
-2.950	-3.41	-3.41	8.60E-02	-9.54E-02	2.01E 01	4.22E-01	-2.52E-02	-1.46E 00
-2.700	-3.78	-3.78	1.23E-01	-9.96E-02	2.40E 01	5.04E-01	-3.33E-02	-1.34E 00
-2.450	-4.15	-4.15	1.40E-01	-1.04E-01	2.56E 01	5.38E-01	-3.90E-02	-1.22E 00
-2.200	-4.27	-4.27	1.92E-01	-1.08E-01	3.00E 01	6.29E-01	-4.70E-02	-1.09E 00
-1.950	-3.90	-3.90	2.44E-01	-1.12E-01	3.38E 01	7.10E-01	-4.84E-02	-9.67E-01
-1.700	-3.66	-3.66	2.86E-01	-1.16E-01	3.66E 01	7.69E-01	-4.92E-02	-8.43E-01
-1.450	-3.41	-3.41	3.33E-01	-1.20E-01	3.95E 01	8.30E-01	-4.95E-02	-7.19E-01
-1.200	-3.17	-3.17	3.59E-01	-1.22E-01	4.10E 01	8.62E-01	-4.77E-02	-5.95E-01
-0.950	-2.32	-2.32	4.02E-01	-1.22E-01	4.34E 01	9.13E-01	-3.69E-02	-4.71E-01
-0.700	-1.83	-1.83	4.38E-01	-1.24E-01	4.53E 01	9.53E-01	-3.04E-02	-3.47E-01
-0.450	-1.46	-1.46	4.66E-01	-1.27E-01	4.67E 01	9.83E-01	-2.51E-02	-2.23E-01
-0.200	-0.73	-0.73	4.82E-01	-1.29E-01	4.75E 01	10.00E-01	-1.28E-02	-9.92E-02
0.050	0.37	0.37	4.82E-01	-1.29E-01	4.75E 01	10.00E-01	6.39E-03	2.48E-02
0.300	0.85	0.85	4.72E-01	-1.29E-01	4.70E 01	9.89E-01	1.47E-02	1.49E-01
0.550	1.65	1.65	4.51E-01	-1.27E-01	4.60E 01	9.67E-01	2.78E-02	2.73E-01
0.800	2.32	2.32	4.20E-01	-1.24E-01	4.44E 01	9.33E-01	3.77E-02	3.97E-01
1.050	2.99	2.99	3.87E-01	-1.22E-01	4.26E 01	8.95E-01	4.67E-02	5.21E-01
1.300	3.54	3.54	3.51E-01	-1.20E-01	4.06E 01	8.52E-01	5.26E-02	6.45E-01
1.550	4.76	4.76	3.06E-01	-1.16E-01	3.79E 01	7.96E-01	6.61E-02	7.69E-01
1.800	5.61	5.61	2.69E-01	-1.16E-01	3.55E 01	7.43E-01	7.30E-02	8.93E-01
2.050	5.85	5.85	2.24E-01	-1.12E-01	3.24E 01	6.78E-01	6.95E-02	1.02E 00
2.300	5.98	5.98	1.91E-01	-1.10E-01	2.95E 01	6.26E-01	6.55E-02	1.14E 00
2.550	5.73	5.73	1.45E-01	-1.04E-01	2.61E 01	5.46E-01	5.48E-02	1.26E 00
2.800	5.55	5.55	1.22E-01	-9.75E-02	2.39E 01	5.01E-01	4.86E-02	1.39E 00
3.050	5.12	5.12	9.00E-02	-9.34E-02	2.05E 01	4.30E-01	3.80E-02	1.51E 00
3.300	4.76	4.76	6.80E-02	-8.92E-02	1.79E 01	3.74E-01	3.11E-02	1.64E 00
3.550	4.62	4.62	5.60E-02	-8.30E-02	1.53E 01	3.21E-01	2.26E-02	1.76E 00
3.800	3.66	3.66	3.20E-02	-7.26E-02	1.32E 01	2.57E-01	1.64E-02	1.88E 00
4.050	0.12	0.12	2.10E-02	-6.64E-02	9.92E 00	2.09E-01	4.44E-04	2.01E 00
4.300	-2.07	-2.07	10.00E-03	-5.60E-02	6.85E 00	1.44E-01	-5.21E-03	2.13E 00

UC = 4.75E 01, EP = 5.39E 00, C = 2.02E 00, E= 3.33E 00,

EMOM = 2.51E 00, RATIO = 8.76E-01, EOEO = 3.37E-01

30 2.00 0 0 0. 1 7 64 1

YS	TS	T	Q	CP	V	UOUC	VOUC	Y/B
-5.650	-10.37	-10.37	2.30E-02	-3.07E-02	1.69E 01	2.00E-01	-3.67E-02	-2.25E 00
-5.150	-9.76	-9.76	3.50E-02	-4.15E-02	1.29E 01	2.48E-01	-4.26E-02	-2.05E 00
-4.650	-9.88	-9.88	5.10E-02	-4.87E-02	1.56E 01	2.99E-01	-5.21E-02	-1.85E 00
-4.150	-9.63	-9.63	8.00E-02	-6.32E-02	1.95E 01	3.75E-01	-6.36E-02	-1.65E 00
-3.650	-9.63	-9.63	1.12E-01	-6.68E-02	2.31E 01	4.43E-01	-7.52E-02	-1.45E 00
-3.150	-8.90	-8.90	1.58E-01	-7.76E-02	2.74E 01	5.28E-01	-8.26E-02	-1.25E 00
-2.650	-7.68	-7.68	2.25E-01	-9.03E-02	3.27E 01	6.32E-01	-8.52E-02	-1.05E 00
-2.150	-6.71	-6.71	3.12E-01	-1.03E-01	3.85E 01	7.45E-01	-8.77E-02	-8.56E-01
-1.650	-5.24	-5.24	3.86E-01	-1.01E-01	4.28E 01	8.31E-01	-7.63E-02	-6.57E-01
-1.150	-3.78	-3.78	4.59E-01	-9.74E-02	4.67E 01	9.08E-01	-6.00E-02	-4.58E-01
-0.650	-2.20	-2.20	5.28E-01	-9.56E-02	5.01E 01	9.75E-01	-3.74E-02	-2.59E-01
-0.150	-0.73	-0.73	5.53E-01	-9.57E-02	5.12E 01	9.99E-01	-1.28E-02	-5.97E-02
0.350	1.10	1.10	5.49E-01	-9.74E-02	5.11E 01	9.95E-01	1.91E-02	1.39E-01
0.850	2.62	2.62	5.05E-01	-9.92E-02	4.90E 01	9.54E-01	4.37E-02	3.38E-01
1.350	4.15	4.15	4.38E-01	-1.05E-01	4.56E 01	8.87E-01	6.43E-02	5.37E-01
1.850	5.37	5.37	3.58E-01	-1.05E-01	4.12E 01	8.00E-01	7.52E-02	7.36E-01
2.350	6.59	6.59	2.85E-01	-9.93E-02	3.68E 01	7.13E-01	8.23E-02	9.35E-01
2.850	7.93	7.93	2.09E-01	-9.75E-02	3.15E 01	6.08E-01	8.47E-02	1.13E 00
3.350	8.41	8.41	1.55E-01	-9.03E-02	2.71E 01	5.23E-01	7.74E-02	1.33E 00
3.850	8.78	8.78	1.02E-01	-7.22E-02	2.20E 01	4.24E-01	6.55E-02	1.53E 00
4.350	8.78	8.78	7.60E-02	-6.86E-02	1.90E 01	3.66E-01	5.65E-02	1.73E 00
4.850	9.45	9.45	6.00E-02	-6.32E-02	1.69E 01	3.25E-01	5.40E-02	1.93E 00

UC = 5.13E 01, EM = 6.76E 00, B = 2.51E 00, E= 4.12E 00,

EMOM = 3.38E 00, RATIC = 1.25E 00, EOEO = 5.14E-01

5 -2.50 2 2 0.10 10 6 64 2

YS	TS	T	Q	CP	V	UOUC	VOUC
-1.400	68.09	59.59	1.58E-02	-1.00E-02	2.36E 01	4.34E-02	7.40E-02
-1.250	37.38	28.88	1.23E-02	-1.14E-02	7.59E 00	6.65E-02	3.67E-02
-1.100	-12.60	-21.10	2.29E-02	-1.55E-02	1.03E 01	9.64E-02	-3.72E-02
-0.950	-16.19	-24.69	7.66E-02	-1.73E-02	1.89E 01	1.72E-01	-7.90E-02
-0.800	-3.08	-11.58	1.82E-01	-2.56E-02	2.91E 01	2.85E-01	-5.85E-02
-0.650	-3.98	-12.48	6.31E-01	-2.75E-02	5.42E 01	5.30E-01	-1.17E-01
-0.500	-1.02	-9.52	1.18E 00	-2.81E-02	7.41E 01	7.31E-01	-1.23E-01
-0.350	-1.04	-9.54	1.60E 00	-2.45E-02	8.63E 01	8.52E-01	-1.43E-01
-0.200	0.08	-8.42	2.01E 00	-2.37E-02	9.69E 01	9.59E-01	-1.42E-01
-0.050	1.46	-7.04	2.19E 00	-2.41E-02	1.01E 02	1.00E 00	-1.24E-01
0.100	1.94	-6.56	1.94E 00	-2.01E-02	9.52E 01	9.46E-01	-1.09E-01
0.250	3.23	-5.27	1.94E 00	-2.55E-02	9.51E 01	9.47E-01	-8.74E-02
0.400	2.57	-5.93	1.42E 00	-2.60E-02	8.13E 01	8.09E-01	-8.40E-02
0.550	1.60	-6.90	9.74E-01	-2.47E-02	6.74E 01	6.69E-01	-8.10E-02
0.700	-3.75	-12.25	6.31E-01	-2.12E-02	5.42E 01	5.30E-01	-1.15E-01
0.850	-1.16	-9.66	4.06E-01	-1.64E-02	4.35E 01	4.29E-01	-7.30E-02
1.000	-2.98	-11.48	2.81E-01	-1.23E-02	3.62E 01	3.55E-01	-7.21E-02
1.150	-3.72	-12.22	1.95E-01	-9.59E-03	3.02E 01	2.95E-01	-6.39E-02
1.300	-3.87	-12.37	1.25E-01	-9.13E-03	2.41E 01	2.36E-01	-5.17E-02
1.450	-3.22	-11.72	6.23E-02	-8.22E-03	1.70E 01	1.67E-01	-3.46E-02
1.600	6.72	-1.78	1.57E-01	-7.31E-02	2.71E 01	2.71E-01	-8.43E-03
1.750	7.32	-1.18	1.19E-01	-5.94E-02	2.36E 01	2.36E-01	-4.84E-03

UC = 9.99E 01, EM = 1.57E 00, B = 5.51E-01, E=, 8.89E-01,

EMOM = 1.52E 00, RATIO = 1.05E 00, EOEO = 8.22E-01

UOUCSQ	XI	US	USOUC	USOUCS	Y/B	XI OBS
1.89E-03	-1.385	4.13E 00	4.09E-02	1.67E-03	-2.54E 00	-2.55E 00
4.42E-03	-1.235	7.09E 00	7.02E-02	4.92E-03	-2.27E 00	-2.28E 00
9.30E-03	-1.088	1.11E 01	1.10E-01	1.22E-02	-2.00E 00	-2.01E 00
2.95E-02	-0.940	1.91E 01	1.89E-01	3.56E-02	-1.72E 00	-1.73E 00
8.14E-02	-0.791	2.97E 01	2.94E-01	8.62E-02	-1.45E 00	-1.46E 00
2.81E-01	-0.643	5.43E 01	5.38E-01	2.89E-01	-1.18E 00	-1.19E 00
5.34E-01	-0.495	7.4.E 01	7.32E-01	5.36E-01	-9.07E-01	-9.12E-01
7.26E-01	-0.346	8.61E 01	8.52E-01	7.25E-01	-6.35E-01	-6.39E-01
9.19E-01	-0.198	9.66E 01	9.56E-01	9.14E-01	-3.63E-01	-3.65E-01
1.01E 00	-0.049	1.01E 02	9.98E- 1	9.96E-01	-9.07E-02	-9.12E-02
8.95E-01	0.099	9.53E 01	9.43E-01	8.89E-01	1.81E-01	1.82E-01
8.97E-01	0.247	9.52E 01	9.42E-01	8.88E-01	4.54E-01	4.56E-01
6.54E-01	0.396	8.14E 01	8.06E-01	6.49E-01	7.26E-01	7.30E-01
4.48E-01	0.544	6.74E 01	6.67E-01	4.44E-01	9.98E-01	1.00E 00
2.81E-01	0.692	5.36E 01	5.32E-01	2.83E-01	1.27E 00	1.28E 00
1.84E-01	0.841	4.28E 01	4.23E-01	1.79E-01	1.54E 00	1.55E 00
1.26E-01	0.989	3.52E 01	3.48E-01	1.21E-01	1.81E 00	1.82E 00
8.71E-02	1.137	2.96E 01	2.87E-01	8.26E-02	2.09E 00	2.10E 00
5.57E-02	1.286	2.31E 01	2.28E-01	5.21E-02	2.36E 00	2.37E 00
2.79E-02	1.434	1.61E 01	1.60E-01	2.55E-02	2.63E 00	2.65E 00
7.32E-02	1.582	2.62E 01	2.59E-01	6.72E-02	2.90E 00	2.92E 00
5.55E-02	1.731	2.29E 01	2.27E-01	5.13E-02	3.18E 00	3.19E 00

UCS = 1.01E 02, EMS = 1.55E 00, BS = 5.42E-01, ES= 8.75E-01,

EMSOMO = 1.52E 00, RATIOS = 1.04E 00, ESOEO = 8.19E-01

5 -2.00 2 2 0.10 10 6 63 2

YS	TS	T	Q	CP	V	UOUC	VOUC
-1.850	-31.38	-39.88	5.38E-03	-4.98E-03	5.60E 00	3.83E-02	-3.20E-02
-1.700	8.50	0.	-0.	-5.44E-03	-0.	-0.	-0.
-1.550	-21.15	-29.65	6.11E-03	-7.25E-03	5.36E 00	4.62E-02	-2.63E-02
-1.400	-17.88	-26.38	1.31E-02	-9.06E-03	7.84E 00	6.97E-02	-3.46E-02
-1.250	-12.99	-21.49	3.71E-02	-1.27E-02	1.32E 01	1.22E-01	-4.80E-02
-1.100	-26.01	-34.51	6.71E-02	-1.25E-02	1.78E 01	1.45E-01	-9.99E-02
-0.950	-15.00	-23.50	1.15E-01	-1.58E-02	2.33E 01	2.12E-01	-9.21E-02
-0.800	-2.38	-10.88	2.83E-01	-2.58E-02	3.65E 01	3.56E-01	-6.84E-02
-0.650	1.11	-7.39	6.07E-01	-3.02E-02	5.34E 01	5.26E-01	-6.81E-02
-0.500	2.41	-6.09	1.01E 00	-3.21E-02	6.89E 01	6.80E-01	-7.26E-02
-0.350	3.32	-5.18	1.62E 00	-3.23E-02	8.73E 01	8.63E-01	-7.83E-02
-0.200	3.03	-5.47	2.05E 00	-2.94E-02	9.81E 01	9.69E-01	-9.28E-02
-0.050	1.18	-7.32	2.20E 00	-2.30E-02	1.02E 02	1.00E 00	-1.29E-01
0.100	-0.22	-8.72	2.14E 00	-1.87E-02	1.00E 02	9.83E-01	-1.51E-01
0.250	0.93	-7.57	1.87E 00	-2.20E-02	9.37E 01	9.22E-01	-1.23E-01
0.400	0.03	-8.47	1.45E 00	-2.26E-02	8.27E 01	8.12E-01	-1.21E-01
0.550	-1.81	-10.31	1.03E 00	-2.23E-02	6.97E 01	6.80E-01	-1.24E-01
0.700	-3.70	-12.20	6.91E-01	-2.09E-02	5.70E 01	5.53E-01	-1.20E-01
0.850	-3.87	-12.37	4.54E-01	-1.70E-02	4.62E 01	4.48E-01	-9.83E-02
1.000	-0.47	-8.97	3.12E-01	-1.22E-02	3.83E 01	3.76E-01	-5.93E-02
1.150	4.75	-3.75	2.24E-01	-1.09E-02	3.25E 01	3.21E-01	-2.11E-02
1.300	8.50	0.	1.30E-01	-9.06E-03	2.47E 01	2.45E-01	0.
1.450	13.74	5.24	5.60E-02	-9.52E-03	1.62E 01	1.60E-01	1.47E-02
1.600	27.82	19.32	1.65E-02	-7.25E-03	8.81E 00	8.25E-02	2.89E-02
1.750	34.27	25.77	6.67E-03	-4.53E-03	5.60E 00	5.01E-02	2.42E-02

UC = 1.01E 02, EM = 1.59E 00, B = 5.57E-01, E=, 9.01E-01,

EMOM = 1.55E 00, RATIO = 1.07E 00, EOE? = 8.43E-01

UOUCSQ	XI	US	USOUC	USOUCS	Y/B	XIOBS
1.47E-03	-1.830	4.67E 00	4.58E-02	2.10E-03	-3.32E 00	-3.34E 00
0.	-1.681	5.58E-01	5.48E-03	3.00E-05	-3.05E 00	-3.07E 00
2.14E-03	-1.533	5.76E 00	5.66E-02	3.20E-03	-2.78E 00	-2.80E 00
4.86E-03	-1.385	8.41E 00	8.26E-02	6.82E-03	-2.51E 00	-2.53E 00
1.49E-02	-1.236	1.39E 01	1.37E-01	1.87E-02	-2.24E 00	-2.26E 00
2.11E-02	-1.088	1.70E 01	1.67E-01	2.79E-02	-1.98E 00	-1.99E 00
4.49E-02	-0.940	2.34E 01	2.29E-01	5.26E-02	-1.71E 00	-1.72E 00
1.27E-01	-0.791	3.70E 01	3.64E-01	1.32E-01	-1.44E 00	-1.44E 00
2.76E-01	-0.643	5.36E 01	5.26E-01	2.77E-01	-1.17E 00	-1.17E 00
4.63E-01	-0.495	6.88E 01	6.75E-01	4.56E-01	-8.98E-01	-9.03E-01
7.45E-01	-0.346	8.69E 01	8.53E-01	7.27E-01	-6.28E-01	-6.32E-01
9.40E-01	-0.198	9.77E 01	9.59E-01	9.20E-01	-3.59E-01	-3.61E-01
1.00E 00	-0.049	1.02E 02	9.98E-01	9.95E-01	-8.98E-02	-9.03E-02
9.67E-01	0.099	1.00E 02	9.85E-01	9.71E-01	1.80E-01	1.81E-01
8.50E-01	0.247	9.40E 01	9.22E-01	8.51E-01	4.49E-01	4.51E-01
6.59E-01	0.396	8.30E 01	8.14E-01	6.63E-01	7.18E-01	7.22E-01
4.63E-01	0.544	6.97E 01	6.84E-01	4.68E-01	9.88E-01	9.93E-01
3.06E-01	0.692	5.65E 01	5.55E-01	3.08E-01	1.26E 00	1.26E 00
2.01E-01	0.841	4.54E 01	4.46E-01	1.99E-01	1.53E 00	1.53E 00
1.41E-01	0.989	3.73E 01	3.67E-01	1.34E-01	1.80E 00	1.81E 00
1.03E-01	1.137	3.13E 01	3.07E-01	9.42E-02	2.07E 00	2.08E 00
6.02E-02	1.286	2.34E 01	2.30E-01	5.28E-02	2.33E 00	2.35E 00
2.57E-02	1.434	1.49E 01	1.46E-01	2.13E-02	2.60E 00	2.62E 00
6.81E-03	1.582	7.10E 00	6.96E-02	4.85E-03	2.87E 00	2.89E 00
2.51E-03	1.731	4.14E 00	4.06E-02	1.65E-03	3.14E 00	3.16E 00

UCS = 1.02E 02, EMS = 1.58E 00, BS = 5.48E-01, ES= 8.87E-01,

EMSOMO = 1.55E 00, RATIOS = 1.06E 00, ESOED = 8.40E-01

5 -1.00 2 2 0.10 10 6 64 2

YS	TS	T	Q	CP	V	UDUC	VDUC
			Not Good		Not Good	Not Good	Not Good
-1.850	48.38	39.88	5.38E-03	-3.61E-03	1.18E 01	3.82E-02	3.19E-02
-1.700	26.79	18.29	1.73E-02	-7.22E-03	8.97E 00	8.47E-02	2.80E-02
-1.550	13.54	5.14	5.70E-02	-8.57E-03	1.63E 01	1.62E-01	1.45E-02
-1.400	9.5	1.06	1.32E-01	-8.12E-03	2.48E 01	2.47E-01	4.57E-03
-1.250	6.60	-1.90	2.21E-01	-8.12E-03	3.21E 01	3.19E-01	-1.06E-02
-1.100	-5.73	-14.23	3.28E-01	-1.04E-02	3.91E 01	3.77E-01	-9.56E-02
-0.950	0.39	-8.11	4.49E-01	-1.53E-02	4.57E 01	4.51E-01	-6.42E-02
-0.800	-0.84	-9.34	6.90E-01	-2.01E-02	5.67E 01	5.57E-01	-9.15E-02
-0.650	-1.36	-9.86	9.94E-01	-2.19E-02	6.81E 01	6.67E-01	-1.16E-01
-0.500	-0.97	-9.47	1.40E 00	-2.15E-02	8.09E 01	7.94E-01	-1.32E-01
-0.350	-0.54	-9.14	1.79E 00	-1.97E-02	9.14E 01	8.98E-01	-1.44E-01
-0.200	0.12	-8.38	2.09E 00	-1.95E-02	9.87E 01	9.71E-01	-1.43E-01
-0.050	0.99	-7.51	2.18E 00	-2.12E-02	1.01E 02	9.95E-01	-1.31E-01
0.050	2.81	-5.69	2.66E 00	-2.75E-01	1.11E 02	1.10E 00	-1.10E-01
0.100	1.40	-7.10	2.01E 00	-2.44E-02	9.69E 01	9.56E-01	-1.19E-01
0.250	1.75	-6.75	1.60E 00	-2.71E-02	8.63E 01	8.53E-01	-1.01E-01
0.400	1.32	-7.18	1.07E 00	-2.98E-02	7.07E 01	6.98E-01	-8.79E-02
0.550	0.85	-7.65	6.59E-01	-3.12E-02	5.54E 01	5.46E-01	-7.34E-02
0.700	-2.42	-10.92	3.33E-01	-2.62E-02	3.94E 01	3.85E-01	-7.43E-02
0.850	-11.06	-19.56	1.49E-01	-1.62E-02	2.63E 01	2.47E-01	-8.77E-02
1.000	-7.22	-15.72	1.45E-01	-1.24E-02	2.60E 01	2.49E-01	-7.00E-02
1.150	-44.89	-53.39	4.89E-02	-9.11E-03	1.51E 01	8.96E-02	-1.21E-01
1.300	-71.50	-80.00	3.00E-02	-9.03E-03	1.18E 01	2.04E-02	-1.16E-01

5 0. 2 2 0.10 25 4 64 1

YS	TS	T	Q	CP	V	UOUC	VOUC
-1.350	22.20	13.70	4.00E-03	-1.02E-02	4.80E 00	4.23E-02	1.03E-02
-1.250	8.17	-0.33	1.70E-02	-1.25E-02	8.85E 00	8.98E-02	-5.16E-04
-1.15.	-5.61	-14.11	3.40E-02	-1.58E-02	1.25E 01	1.23E-01	-3.10E-02
-1.05.	-5.9[illegible]	-14.48	9.30E-02	-2.00E-02	2.07E 01	2.03E-01	-5.25E-02
-0.95.	-6.22	-14.72	1.60E-01	-2.41E-02	2.71E 01	2.67E-01	-7.00E-02
-0.850	-6.85	-14.35	2.76E-01	-2.83E-02	3.57E 01	3.51E-01	-8.97E-02
-0.750	-6.12	-13.62	4.40E-01	-3.25E-02	4.50E 01	4.44E-01	-1.08E-01
-0.65.	-4.57	-13.07	6.64E-01	-3.20E-02	5.53E 01	5.47E-01	-1.27E-01
-0.55.	-3.[illegible]	-12.16	9.22E-01	-3.10E-02	6.52E 01	6.47E-01	-1.39E-01
-0.45.	-2.[illegible]	-11.43	1.23E 00	-3.01E-02	7.53E 01	7.49E-01	-1.51E-01
-0.350	-0.19	-10.63	1.56E 00	-2.70E-02	8.47E 01	8.45E-01	-1.59E-01
-0.250	-1.46	-9.96	1.84E 00	-2.52E-02	9.22E 01	9.21E-01	-1.62E-01
-0.150	-0.73	-9.23	2.05E 00	-2.40E-02	9.71E 01	9.73E-01	-1.58E-01
-0.050	-0.16	-8.68	2.15E 00	-2.33E-02	9.95E 01	9.98E-01	-1.52E-01
0.050	0.24	-8.26	2.13E 00	-2.43E-02	9.91E 01	9.96E-01	-1.44E-01
0.15.	0.24	-8.26	2.03E 00	-2.43E-02	9.68E 01	9.72E-01	-1.41E-01
0.25.	1.22	-7.28	1.84E 00	-2.64E-02	9.20E 01	9.25E-01	-1.18E-01
0.35.	1.71	-6.79	1.58E 00	-2.65E-02	8.54E 01	8.60E-01	-1.02E-01
0.45.	2.38	-6.12	1.26E 00	-2.66E-02	7.63E 01	7.70E-01	-8.25E-02
0.55.	2.66	-5.82	1.04E 00	-2.41E-02	6.93E 01	7.00E-01	-7.13E-02
0.650	3.05	-5.45	7.72E-01	-2.16E-02	5.96E 01	6.02E-01	-5.75E-02
0.750	2.66	-5.82	5.73E-01	-1.78E-02	5.14E 01	5.19E-01	-5.29E-02
0.850	1.95	-6.55	4.32E-01	-1.49E-02	4.46E 01	4.50E-01	-5.16E-02
0.950	0.73	-7.77	3.37E-01	-1.25E-02	3.94E 01	3.96E-01	-5.41E-02
1.050	-5.30	-13.80	2.74E-01	-1.11E-02	3.55E 01	3.50E-01	-8.60E-02
1.250	-0.73	-9.23	1.62E-01	-1.11E-02	2.73E 01	2.74E-01	-4.45E-02
1.450	1.71	-6.79	4.20E-02	-1.02E-02	1.39E 01	1.40E-01	-1.67E-02
1.550	0.49	-8.01	5.00E-03	-8.36E-03	4.80E 00	4.82E-02	-6.79E-03

UC = 9.[illegible] C1, EM = 1.57E 00, B = 5.61E-01, E=, 9.09E-01,

EMOM = 1.50E 00, RATIO = 1.05E 00, EOEO = 8.20E-01

UOUCSQ	XI	US	USOUC	USOUCS	Y/B	XIOBS
1.79E-03	-1.335	4.96E 00	4.98E-02	2.48E-03	-2.41E 00	-2.41E 00
6.07E-03	-1.236	9.81E 00	9.85E-02	9.69E-03	-2.23E 00	-2.23E 00
1.52E-02	-1.137	1.35E 01	1.36E-01	1.84E-02	-2.05E 00	-2.05E 00
4.14E-02	-1.038	2.16E 01	2.17E-01	4.69E-02	-1.87E 00	-1.87E 00
7.10E-02	-0.940	2.76E 01	2.80E-01	7.81E-02	-1.69E 00	-1.69E 00
1.23E-01	-0.841	3.61E 01	3.63E-01	1.32E-01	-1.52E 00	-1.52E 00
1.97E-01	-0.742	4.53E 01	4.54E-01	2.07E-01	-1.34E 00	-1.34E 00
2.99E-01	-0.643	5.53E 01	5.55E-01	3.08E-01	-1.16E 00	-1.16E 00
4.18E-01	-0.544	6.50E 01	6.53E-01	4.26E-01	-9.81E-01	-9.81E-01
5.61E-01	-0.445	7.50E 01	7.53E-01	5.67E-01	-8.03E-01	-8.03E-01
7.14E-01	-0.346	8.44E 01	8.47E-01	7.18E-01	-6.24E-01	-6.24E-01
8.49E-01	-0.247	9.19E 01	9.22E-01	8.50E-01	-4.46E-01	-4.46E-01
9.47E-01	-0.148	9.69E 01	9.73E-01	9.47E-01	-2.68E-01	-2.68E-01
9.96E-01	-0.049	9.94E 01	9.98E-01	9.96E-01	-8.92E-02	-8.92E-02
9.91E-01	0.049	9.92E 01	9.96E-01	9.91E-01	8.92E-02	8.92E-02
9.45E-01	0.148	9.70E 01	9.73E-01	9.47E-01	2.68E-01	2.68E-01
8.58E-01	0.247	9.22E 01	9.26E-01	8.58E-01	4.46E-01	4.46E-01
7.40E-01	0.346	8.56E 01	8.59E-01	7.39E-01	6.24E-01	6.24E-01
5.92E-01	0.445	7.64E 01	7.67E-01	5.88E-01	8.03E-01	8.03E-01
4.89E-01	0.544	6.92E 01	6.95E-01	4.83E-01	9.81E-01	9.81E-01
3.63E-01	0.643	5.93E 01	5.96E-01	3.55E-01	1.16E 00	1.16E 00
2.69E-01	0.742	5.09E 01	5.11E-01	2.61E-01	1.34E 00	1.34E 00
2.02E-01	0.841	4.39E 01	4.41E-01	1.94E-01	1.52E 00	1.52E 00
1.57E-01	0.940	3.85E 01	3.87E-01	1.50E-01	1.69E 00	1.69E 00
1.23E-01	1.038	3.44E 01	3.45E-01	1.19E-01	1.87E 00	1.87E 00
7.49E-02	1.236	2.63E 01	2.64E-01	6.95E-02	2.23E 00	2.23E 00
1.97E-02	1.434	1.30E 01	1.31E-01	1.71E-02	2.59E 00	2.59E 00
2.33E-03	1.533	4.04E 00	4.05E-02	1.64E-03	2.76E 00	2.76E 00

UCS = 9.96E 01, EMS = 1.55E 00, BS = 5.55E-01, ES= 8.99E-01,

EMSOMO = 1.50E 00, RATIOS = 1.04E 00, ESOEO = 8.20E-01

5 1.00 2 2 0.10 9 6 64 2

YS	TS	T	Q	CP	V	UOUC	VOUC
-1.425	-71.50	-80.00	-6.00E-03	-9.98E-03	3.79E 00	0.	0.
-1.275	8.50	0.	5.00E-03	-1.02E-02	4.89E 00	4.86E-02	0.
-1.125	-19.10	-27.60	4.24E-02	-1.48E-02	1.42E 01	1.25E-01	-6.55E-02
-0.975	-9.50	-18.00	2.16E-01	-1.34E-02	3.21E 01	3.03E-01	-9.86E-02
-0.825	-15.53	-24.03	3.13E-01	-7.14E-03	3.87E 01	3.51E-01	-1.56E-01
-0.675	-7.56	-16.06	5.75E-01	-1.75E-02	5.25E 01	5.01E-01	-1.44E-01
-0.525	-4.05	-12.55	1.05E 00	-2.94E-02	7.10E 01	6.86E-01	-1.53E-01
-0.375	-3.74	-12.24	1.51E 00	-2.70E-02	8.51E 01	8.26E-01	-1.79E-01
-0.225	-1.81	-10.31	1.94E 00	-2.50E-02	9.64E 01	9.42E-01	-1.71E-01
-0.075	-0.39	-8.89	2.16E 00	-2.45E-02	1.02E 02	9.97E-01	-1.56E-01
0.075	0.43	-8.07	2.13E 00	-2.45E-02	1.01E 02	9.93E-01	-1.41E-01
0.225	0.93	-7.57	1.94E 00	-2.58E-02	9.64E 01	9.49E-01	-1.26E-01
0.375	1.29	-7.21	1.53E 00	-2.69E-02	8.57E 01	8.44E-01	-1.07E-01
0.525	4.65	-3.85	1.13E 00	-2.89E-02	7.35E 01	7.28E-01	-4.90E-02
0.675	1.96	-6.54	7.92E-01	-2.39E-02	6.16E 01	6.07E-01	-6.97E-02
0.825	1.54	-6.96	5.43E-01	-2.00E-02	5.10E 01	5.03E-01	-6.13E-02
0.975	0.95	-7.55	3.71E-01	-1.43E-02	4.21E 01	4.15E-01	-5.50E-02
1.125	3.33	-5.17	2.71E-01	-1.20E-02	3.60E 01	3.56E-01	-3.22E-02
1.275	1.46	-7.04	1.79E-01	-1.11E-02	2.93E 01	2.88E-01	-3.56E-02
1.425	0.34	-8.16	8.70E-02	-1.11E-02	2.04E 01	2.01E-01	-2.88E-02
1.575	-8.42	-16.92	2.75E-02	-1.02E-02	1.15E 01	1.09E-01	-3.31E-02
1.725	-8.12	-16.62	9.46E-03	-6.46E-03	6.73E 00	6.40E-02	-1.91E-02

UC = 1.01E 02, EM = 1.63E 00, B = 5.78E-01, E=, 9.40E-01,

EMOM = 1.57E 00, RATIO = 1.09E 00, EOEO = 8.55E-01

UOUCSQ	XI	US	USOUC	USOUCS	Y/B	XIOBS
0.	-1.409	9.70E-01	9.59E-03	9.19E-05	-2.46E 00	-2.46E 00
2.36E-03	-1.261	5.91E 00	5.80E-02	3.36E-03	-2.20E 00	-2.20E 00
1.57E-02	-1.113	1.45E 01	1.42E-01	2.03E-02	-1.95E 00	-1.94E 00
9.20E-02	-0.964	3.25E 01	3.19E-01	1.02E-01	-1.69E 00	-1.68E 00
1.23E-01	-0.816	3.78E 01	3.71E-01	1.38E-01	-1.43E 00	-1.42E 00
2.51E-01	-0.668	5.22E 01	5.12E-01	2.63E-01	-1.17E 00	-1.17E 00
4.74E-01	-0.519	7.07E 01	6.94E-01	4.82E-01	-9.08E-01	-9.07E-01
6.82E-01	-0.371	8.47E 01	8.31E-01	6.91E-01	-6.48E-01	-6.48E-01
8.87E-01	-0.223	9.61E 01	9.44E-01	8.91E-01	-3.89E-01	-3.89E-01
9.94E-01	-0.074	1.02E 02	9.97E-01	9.94E-01	-1.30E-01	-1.30E-01
9.87E-01	0.074	1.01E 02	9.93E-01	9.87E-01	1.30E-01	1.30E-01
9.05E-01	0.223	9.67E 01	9.49E-01	9.01E-01	3.89E-01	3.89E-01
7.12E-01	0.371	8.59E 01	8.44E-01	7.12E-01	6.48E-01	6.48E-01
5.30E-01	0.519	7.33E 01	7.20E-01	5.19E-01	9.08E-01	9.07E-01
3.69E-01	0.668	6.13E 01	6.02E-01	3.63E-01	1.17E 00	1.17E 00
2.53E-01	0.816	5.04E 01	4.95E-01	2.45E-01	1.43E 00	1.42E 00
1.72E-01	0.964	4.13E 01	4.05E-01	1.64E-01	1.69E 00	1.68E 00
1.27E-01	1.113	3.49E 01	3.43E-01	1.18E-01	1.95E 00	1.94E 00
8.32E-02	1.261	2.82E 01	2.77E-01	7.67E-02	2.20E 00	2.20E 00
4.02E-02	1.409	1.94E 01	1.91E-01	3.64E-02	2.46E 00	2.46E 00
1.19E-02	1.558	1.08E 01	1.03E-01	1.07E-02	2.72E 00	2.72E 00
4.15E-03	1.706	6.05E 00	5.95E-02	3.54E-03	2.98E 00	2.98E 00
1.42E-03	1.854	3.32E 00	3.27E-02	1.07E-03	3.24E 00	3.24E 00

UCS = 1.02E 02, EMS = 1.61E 00, BS = 5.73E-01, ES= 9.30E-01,

EMSOMO = 1.57E 00, RATIOS = 1.08E 00, ESOEO = 8.55E-01

5 2.00 2 2 0.10 22 6 64 1

YS	TS	T	Q	CP	V	UOUC	VOUC
-1.250	20.18	11.68	3.00E-03	-1.12E-02	6.87E 00	3.63E-02	7.50E-03
-1.100	5.79	-2.71	2.60E-02	-1.39E-02	1.11E 01	1.09E-01	-5.15E-03
-0.950	-2.87	-11.37	1.16E-01	-1.64E-02	2.34E 01	2.26E-01	-4.54E-02
-0.800	-3.96	-12.46	3.32E-01	-2.33E-02	3.96E 01	3.81E-01	-8.41E-02
-0.650	-3.96	-12.46	6.73E-01	-2.61E-02	5.64E 01	5.42E-01	-1.20E-01
-0.500	-3.35	-11.85	1.18E 00	-2.72E-02	7.45E 01	7.18E-01	-1.51E-01
-0.350	-2.36	-10.86	1.72E 00	-2.47E-02	9.01E 01	8.71E-01	-1.67E-01
-0.200	-1.46	-9.96	2.11E 00	-2.56E-02	9.99E 01	9.68E-01	-1.70E-01
-0.050	-0.55	-9.05	2.23E 00	-2.53E-02	1.03E 02	9.97E-01	-1.59E-01
0.100	0.55	-7.95	2.19E 00	-2.51E-02	1.02E 02	9.91E-01	-1.38E-01
0.250	1.89	-6.61	2.06E 00	-2.79E-02	9.87E 01	9.65E-01	-1.12E-01
0.400	2.74	-5.76	1.64E 00	-2.91E-02	8.79E 01	8.61E-01	-8.68E-02
0.550	3.35	-5.15	1.18E 00	-2.87E-02	7.46E 01	7.32E-01	-6.59E-02
0.700	3.60	-4.90	8.10E-01	-2.67E-02	6.18E 01	6.05E-01	-5.20E-02
0.850	2.74	-5.76	5.07E-01	-2.31E-02	4.89E 01	4.79E-01	-4.83E-02
1.000	0.90	-7.52	3.51E-01	-1.84E-02	4.07E 01	3.97E-01	-5.25E-02
1.150	-0.43	-8.93	2.44E-01	-1.39E-02	3.39E 01	3.30E-01	-5.19E-02
1.300	-0.18	-8.68	1.46E-01	-1.16E-02	2.63E 01	2.56E-01	-3.90E-02
1.450	0.06	-8.44	6.10E-02	-1.07E-02	1.70E 01	1.65E-01	-2.45E-02
1.600	-2.38	-10.98	2.00E-02	-9.85E-03	9.72E 00	9.39E-02	-1.81E-02
1.750	-21.28	-29.78	1.00E-02	-7.61E-03	6.87E 00	5.87E-02	-3.36E-02

UC = 1.02E 02, EM = 1.59E 00, B = 5.78E-01, E=, 9.52E-01,

EMOM = 1.56E 00, RATIO = 1.13E 00, EOED = 9.08E-01

UOUCSC	XI	US	USOUC	USOUCS	Y/B	XIOBS
1.32E-03	-1.236	4.62E 00	4.49E-02	2.02E-03	-2.16E 00	-2.17E 00
1.19E-02	-1.088	1.20E 01	1.17E-01	1.38E-02	-1.90E 00	-1.91E 00
5.10E-02	-0.940	2.42E 01	2.36E-01	5.55E-02	-1.64E 00	-1.65E 00
1.45E-01	-0.791	4.00E 01	3.89E-01	1.52E-01	-1.38E 00	-1.39E 00
2.94E-01	-0.643	5.64E 01	5.49E-01	3.01E-01	-1.12E 00	-1.13E 00
5.15E-01	-0.396	7.41E 01	7.22E-01	5.21E-01	-6.92E-01	-6.94E-01
7.59E-01	-0.346	8.98E 01	8.74E-01	7.64E-01	-6.05E-01	-6.07E-01
9.38E-01	-0.198	9.96E 01	9.70E-01	9.40E-01	-3.46E-01	-3.47E-01
9.94E-01	-0.049	1.02E 02	9.98E-01	9.95E-01	-8.65E-02	-8.67E-02
9.83E-01	0.099	1.02E 02	9.91E-01	9.83E-01	1.73E-01	1.73E-01
9.31E-01	0.247	9.89E 01	9.63E-01	9.28E-01	4.32E-01	4.34E-01
7.41E-01	0.396	8.80E 01	8.57E-01	7.35E-01	6.92E-01	6.94E-01
5.35E-01	0.544	7.46E 01	7.26E-01	5.27E-01	9.51E-01	9.54E-01
3.68E-01	0.692	6.15E 01	5.98E-01	3.58E-01	1.21E 00	1.21E 00
2.30E-01	0.841	4.82E 01	4.70E-01	2.21E-01	1.47E 00	1.47E 00
1.58E-01	0.989	3.98E 01	3.88E-01	1.50E-01	1.73E 00	1.73E 00
1.09E-01	1.137	3.29E 01	3.20E-01	1.02E-01	1.99E 00	2.00E 00
6.53E-02	1.286	2.52E 01	2.45E-01	6.01E-02	2.25E 00	2.26E 00
2.73E-02	1.434	1.60E 01	1.56E-01	2.43E-02	2.51E 00	2.52E 00
8.83E-03	1.582	8.93E 00	8.69E-02	7.56E-03	2.77E 00	2.78E 00
3.45E-03	1.731	5.82E 00	5.67E-02	3.21E-03	3.03E 00	3.04E 00

UCS = 1.03E 02, EMS = 1.57E 00, BS = 5.70E-01, ES= 9.40E-01,

EMSOMC = 1.55E 00, RATIOS = 1.11E 00, ESOEO = 9.06E-01

5 2.50 2 2 0.10 8 6 64 2

YS	TS	T	Q	CP	V	UOUC	VOUC
-1.300	-71.50	-80.00	3.00E-02	-9.98E-03	5.6.E 00	2.05E-02	-1.16E-01
-1.150	-71.50	-80.00	9.37E-02	2.98E-02	2.10E 01	3.62E-02	-2.05E-01
-1.000	-71.50	-80.00	2.96E-01	1.85E-01	3.73E 01	6.44E-02	-3.65E-01
-0.850	-48.26	-56.76	5.10E-01	1.35E-01	4.90E 01	2.66E-01	-4.07E-01
-0.700	-26.73	-35.23	6.38E-01	5.32E-02	5.48E 01	4.44E-01	-3.14E-01
-0.550	-12.86	-21.36	9.54E-01	1.59E-02	6.70E 01	6.19E-01	-2.42E-01
-0.400	-3.75	-12.25	1.47E 00	-2.61E-02	8.31E 01	8.06E-01	-1.75E-01
-0.250	0.98	-7.52	1.95E 00	-2.95E-02	9.59E 01	9.44E-01	-1.25E-01
-0.100	4.23	-4.27	2.26E 00	-2.91E-02	1.03E 02	1.02E 00	-7.62E-02
0.050	6.16	-2.34	2.21E 00	-2.94E-02	1.02E 02	1.01E 00	-4.14E-02
0.200	7.28	-1.22	2.06E 00	-3.07E-02	9.85E 01	9.78E-01	-2.09E-02
0.350	7.96	-0.54	1.72E 00	-3.08E-02	8.99E 01	8.92E-01	-8.38E-03
0.500	8.50	0.	1.30E 00	-2.90E-02	7.83E 01	7.78E-01	0.
0.650	8.97	0.47	9.02E-01	-2.58E-02	6.51E 01	6.47E-01	5.26E-03
0.800	9.22	0.72	5.81E-01	-2.09E-02	5.23E 01	5.19E-01	6.55E-03
0.950	9.64	1.14	3.68E-01	-1.50E-02	4.16E 01	4.13E-01	8.23E-03
1.100	9.59	1.09	2.58E-01	-1.13E-02	3.48E 01	3.46E-01	6.55E-03
1.250	10.19	1.69	1.66E-01	-9.52E-03	2.79E 01	2.77E-01	8.17E-03
1.450	10.34	1.84	7.80E-02	-9.07E-03	1.92E 01	1.90E-01	6.10E-03
1.550	14.81	6.31	2.40E-02	-8.16E-03	1.06E 01	1.05E-01	1.16E-02
1.700	34.27	25.77	6.67E-03	-5.90E-03	5.60E 00	5.01E-02	2.42E-02

UCS = 1.02E 02, EMS = 1.55E 00, BS = 5.66E-01, ES= 9.61E-01,

EMSOMO = 1.52E 00, RATIOS = 1.09E 00, ESOEO = 9.08E-01

UOUCSQ	XI	US	USOUC	USOUCS	Y/B	XIOBS
4.19E-04	-1.286	4.83E 00	4.74E-02	2.25E-03	-2.24E 00	-2.27E 00
1.31E-03	-1.137	7.71E 00	7.57E-02	5.73E-03	-1.98E 00	-2.01E 00
4.14E-03	-0.989	1.27E 01	1.25E-01	1.56E-02	-1.72E 00	-1.75E 00
7.10E-02	-0.841	3.32E 01	3.26E-01	1.06E-01	-1.46E 00	-1.49E 00
1.97E-01	-0.692	4.92E 01	4.83E-01	2.33E-01	-1.21E 00	-1.22E 00
3.84E-01	-0.544	6.52E 01	6.40E-01	4.10E-01	-9.48E-01	-9.61E-01
6.50E-01	-0.396	8.26E 01	8.11E-01	6.58E-01	-6.89E-01	-6.99E-01
8.91E-01	-0.247	9.56E 01	9.39E-01	8.81E-01	-4.31E-01	-4.37E-01
1.04E 00	-0.099	1.03E 02	1.01E 00	1.02E 00	-1.72E-01	-1.75E-01
1.02E 00	0.049	1.01E 02	9.96E-01	9.92E-01	8.62E-02	8.74E-02
9.56E-01	0.198	9.8.E 01	9.62E-01	9.25E-01	3.45E-01	3.50E-01
7.96E-01	0.346	8.93E 01	8.77E-01	7.69E-01	6.03E-01	6.12E-01
6.05E-01	0.495	7.76E 01	7.62E-01	5.81E-01	8.62E-01	8.74E-01
4.18E-01	0.643	6.42E 01	6.31E-01	3.98E-01	1.12E 00	1.14E 00
2.69E-01	0.791	5.11E 01	5.02E-01	2.52E-01	1.38E 00	1.40E 00
1.71E-01	0.940	4.02E 01	3.95E-01	1.56E-01	1.64E 00	1.66E 00
1.20E-01	1.088	3.33E 01	3.27E-01	1.07E-01	1.90E 00	1.92E 00
7.69E-02	1.236	2.64E 01	2.60E-01	6.74E-02	2.15E 00	2.19E 00
3.61E-02	1.434	1.79E 01	1.76E-01	3.08E-02	2.50E 00	2.53E 00
1.10E-02	1.533	9.43E 00	9.26E-02	8.57E-03	2.67E 00	2.71E 00
2.51E-03	1.681	3.96E 00	3.91E-02	1.53E-03	2.93E 00	2.97E 00

UC = 1.01E 02, EM = 1.56E 00, B = 5.80E-01, E=, 9.78E-01,

EMOM = 1.52E 00, RATIO = 1.12E 00, EOEO = 9.14E-01

15 -2.50 2 2 0.10 11 6 64 2

YS	TS	T	Q	CP	V	UOUC	VOUC
-3.850	-17.00	-25.50	2.64E-02	-1.64E-02	4.11E 00	1.46E-01	-6.95E-02
-3.600	-12.98	-21.48	3.35E-02	-2.22E-02	1.25E 01	1.69E-01	-6.66E-02
-3.350	-12.29	-20.79	4.15E-02	-2.56E-02	1.39E 01	1.89E-01	-7.18E-02
-3.100	-12.07	-20.57	4.92E-02	-2.96E-02	1.51E 01	2.06E-01	-7.74E-02
-2.850	-11.72	-20.22	6.07E-02	-3.42E-02	1.68E 01	2.29E-01	-8.45E-02
-2.600	-9.81	-18.31	8.07E-02	-4.07E-02	1.94E 01	2.68E-01	-8.86E-02
-2.350	-8.74	-17.24	1.12E-01	-4.47E-02	2.29E 01	3.18E-01	-9.86E-02
-2.100	-8.94	-17.44	1.60E-01	-4.77E-02	2.73E 01	3.79E-01	-1.19E-01
-1.850	-8.39	-16.89	2.28E-01	-5.23E-02	3.26E 01	4.54E-01	-1.38E-01
-1.600	-7.55	-16.15	3.12E-01	-5.52E-02	3.82E 01	5.33E-01	-1.54E-01
-1.350	-5.93	-14.43	4.47E-01	-7.78E-02	4.56E 01	6.43E-01	-1.65E-01
-1.100	-4.90	-13.40	5.79E-01	-7.71E-02	5.19E 01	7.35E-01	-1.75E-01
-0.850	-4.07	-12.57	7.05E-01	-7.75E-02	5.73E 01	8.14E-01	-1.81E-01
-0.600	-2.84	-11.34	8.53E-01	-7.87E-02	6.31E 01	8.99E-01	-1.80E-01
-0.350	-1.61	-10.11	9.63E-01	-7.49E-02	6.70E 01	9.59E-01	-1.71E-01
-0.100	-0.27	-8.77	1.03E 00	-7.23E-02	6.93E 01	9.96E-01	-1.54E-01
0.150	0.99	-7.51	1.02E 00	-7.23E-02	6.91E 01	9.97E-01	-1.31E-01
0.400	2.37	-6.13	9.71E-01	-6.85E-02	6.73E 01	9.73E-01	-1.04E-01
0.650	3.58	-4.92	8.54E-01	-6.61E-02	6.31E 01	9.14E-01	-7.87E-02
0.900	4.93	-3.57	7.26E-01	-6.41E-02	5.82E 01	8.45E-01	-5.26E-02
1.150	6.05	-2.45	5.72E-01	-5.97E-02	5.16E 01	7.50E-01	-3.21E-02
1.400	7.23	-1.27	4.42E-01	-5.69E-02	4.54E 01	6.60E-01	-1.46E-02
1.650	8.28	-0.22	3.20E-01	-5.30E-02	3.86E 01	5.62E-01	-2.14E-03
1.900	8.61	0.31	2.26E-01	-4.92E-02	3.25E 01	4.72E-01	2.55E-03
2.150	9.38	0.88	1.59E-01	-4.53E-02	2.72E 01	3.96E-01	6.08E-03
2.400	9.78	1.28	1.09E-01	-3.76E-02	2.25E 01	3.28E-01	7.35E-03
2.650	9.36	0.86	8.30E-02	-3.18E-02	1.97E 01	2.85E-01	4.29E-03

UC = 6.88E 01, EM = 3.93E 00, E = 1.35E 00, E=, 2.16E 00,

EMOM = 2.62E 00, RATIO = 1.22E 00, EOEO = 6.50E-01

UOUCSQ	XI	US	USOUC	USOUCS	Y/B	XIOBS
2.12E-02	-3.808	1.11E 01	1.60E-01	2.56E-02	-2.85E 00	-2.85E 00
2.86E-02	-3.560	1.28E 01	1.84E-01	3.39E-02	-2.66E 00	-2.67E 00
3.57E-02	-3.313	1.43E 01	2.06E-01	4.23E-02	-2.48E 00	-2.48E 00
4.25E-02	-3.066	1.56E 01	2.24E-01	5.03E-02	-2.29E 00	-2.30E 00
5.27E-02	-2.819	1.73E 01	2.49E-01	6.18E-02	-2.11E 00	-2.11E 00
7.17E-02	-2.571	1.99E 01	2.87E-01	8.21E-02	-1.92E 00	-1.93E 00
1.01E-01	-2.324	2.34E 01	3.36E-01	1.13E-01	-1.74E 00	-1.74E 00
1.44E-01	-2.077	2.76E 01	3.97E-01	1.58E-01	-1.55E 00	-1.56E 00
2.06E-01	-1.830	3.27E 01	4.71E-01	2.22E-01	-1.37E 00	-1.37E 00
2.84E-01	-1.582	3.81E 01	5.48E-01	3.01E-01	-1.18E 00	-1.19E 00
4.13E-01	-1.335	4.55E 01	6.55E-01	4.29E-01	-9.99E-01	-1.00E 00
5.40E-01	-1.088	5.16E 01	7.44E-01	5.54E-01	-8.14E-01	-8.15E-01
6.62E-01	-0.841	5.71E 01	8.21E-01	6.74E-01	-6.29E-01	-6.30E-01
8.08E-01	-0.593	6.29E 01	9.04E-01	8.18E-01	-4.44E-01	-4.45E-01
9.20E-01	-0.346	6.69E 01	9.62E-01	9.25E-01	-2.59E-01	-2.59E-01
9.92E-01	-0.099	6.93E 01	9.96E-01	9.92E-01	-7.40E-02	-7.41E-02
9.93E-01	0.148	6.92E 01	9.95E-01	9.89E-01	1.11E-01	1.11E-01
9.46E-01	0.395	6.73E 01	9.68E-01	9.37E-01	2.96E-01	2.96E-01
8.35E-01	0.643	6.31E 01	9.07E-01	8.23E-01	4.81E-01	4.82E-01
7.13E-01	0.890	5.8cE 01	8.35E-01	6.97E-01	6.66E-01	6.67E-01
5.63E-01	1.137	5.13E 01	7.38E-01	5.45E-01	8.51E-01	8.52E-01
4.36E-01	1.385	4.49E 01	6.45E-01	4.16E-01	1.04E 00	1.04E 00
3.15E-01	1.632	3.79E 01	5.45E-01	2.97E-01	1.22E 00	1.22E 00
2.23E-01	1.879	3.16E 01	4.54E-01	2.06E-01	1.41E 00	1.41E 00
1.57E-01	2.125	2.62E 01	3.77E-01	1.42E-01	1.59E 00	1.59E 00
1.07E-01	2.374	2.15E 01	3.09E-01	9.52E-02	1.78E 00	1.78E 00
8.18E-02	2.621	1.86E 01	2.67E-01	7.15E-02	1.96E 00	1.96E 00
5.62E-02	2.868	1.53E 01	2.20E-01	4.85E-02	2.15E 00	2.15E 00

UCS = 6.95E 01, EMS = 3.89E 00, BS = 1.33E 00, ES= 2.13E 00,

EMSOMO = 2.62E 00, RATIOS = 1.21E 00, ESOEO = 6.49E-01

15 -2.00 2 2 0.10 11 6 64 2

YS	TS	T	Q	CP	V	UOUC	VOUC
-3.350	38.02	29.52	1.52E-02	-2.13E-02	8.68E 00	1.02E-01	5.79E-02
-3.000	34.70	26.20	1.64E-02	-2.49E-02	8.73E 00	1.09E-01	5.38E-02
-2.850	25.85	17.35	1.81E-02	-2.93E-02	9.17E 00	1.22E-01	3.82E-02
-2.600	-0.59	-9.09	3.30E-02	-3.82E-02	1.24E 01	1.71E-01	-2.74E-02
-2.350	-1.90	-10.40	6.30E-02	-4.89E-02	1.71E 01	2.35E-01	-4.32E-02
-2.100	-4.27	-12.77	1.10E-01	-5.69E-02	2.26E 01	3.09E-01	-7.00E-02
-1.850	-5.58	-14.08	1.81E-01	-6.40E-02	2.90E 01	3.93E-01	-9.86E-02
-1.600	-5.60	-14.10	2.81E-01	-7.11E-02	3.62E 01	4.90E-01	-1.23E-01
-1.350	-5.39	-13.89	4.07E-01	-7.91E-02	4.35E 01	5.90E-01	-1.46E-01
-1.100	-4.41	-12.91	5.67E-01	-8.05E-02	5.14E 01	7.00E-01	-1.60E-01
-0.850	-3.23	-11.73	7.48E-01	-8.47E-02	5.90E 01	8.07E-01	-1.68E-01
-0.600	-2.66	-11.16	8.98E-01	-8.54E-02	6.46E 01	8.86E-01	-1.75E-01
-0.350	-1.37	-9.87	1.04E 00	-8.25E-02	6.97E 01	9.59E-01	-1.67E-01
-0.100	-1.50	-10.00	1.12E 00	-7.95E-02	7.22E 01	9.93E-01	-1.75E-01
0.150	1.32	-7.18	1.11E 00	-8.15E-02	7.19E 01	9.97E-01	-1.26E-01
0.400	2.13	-6.37	10.00E-01	-7.52E-02	6.82E 01	9.47E-01	-1.06E-01
0.650	2.87	-5.63	8.46E-01	-7.65E-02	6.28E 01	8.73E-01	-8.60E-02
0.900	3.72	-4.78	6.59E-01	-7.05E-02	5.54E 01	7.71E-01	-6.45E-02
1.150	4.33	-4.17	4.70E-01	-6.66E-02	4.68E 01	6.52E-01	-4.75E-02
1.400	4.34	-4.16	3.20E-01	-6.22E-02	3.86E 01	5.38E-01	-3.91E-02
1.650	4.08	-4.42	2.06E-01	-5.87E-02	3.10E 01	4.31E-01	-3.33E-02
1.900	1.75	-6.75	1.14E-01	-5.16E-02	2.30E 01	3.20E-01	-3.79E-02
2.150	-3.22	-11.72	6.23E-02	-4.36E-02	1.70E 01	2.33E-01	-4.83E-02
2.400	-10.74	-19.24	4.03E-02	-3.53E-02	1.37E 01	1.81E-01	-6.31E-02
2.650	-20.40	-28.90	3.04E-02	-2.84E-02	1.19E 01	1.45E-01	-8.03E-02
2.900	-20.26	-28.76	2.45E-02	-2.22E-02	1.07E 01	1.31E-01	-7.18E-02
3.150	-18.08	-26.58	1.62E-02	-1.78E-02	8.68E 00	1.09E-01	-5.43E-02

UC = 7.16E 01, EM = 3.27E 00, B = 1.15E 00, E=, 1.86E 00,

EMOM = 2.27E 00, RATIO = 1.13E 00, EOEO = 6.32E-01

LOUCSQ	XI	US	USOUC	USOUCS	Y/B	XIOBS
1.05E-02	-3.313	7.12E 00	9.84E-02	9.69E-03	-2.92E 00	-2.92E 00
1.20E-02	-2.967	7.85E 00	1.09E-01	1.18E-02	-2.62E 00	-2.61E 00
1.50E-02	-2.819	9.0 E 00	1.24E-01	1.55E-02	-2.49E 00	-2.48E 00
2.92E-02	-2.571	1.32E 01	1.83E-01	3.34E-02	-2.27E 00	-2.26E 00
5.54E-02	-2.324	1.8 E 01	2.49E-01	6.18E-02	-2.05E 00	-2.05E 00
9.52E-02	-2.077	2.34E 01	3.24E-01	1.05E-01	-1.83E 00	-1.83E 00
1.55E-01	-1.830	2.96E 01	4.09E-01	1.67E-01	-1.61E 00	-1.61E 00
2.40E-01	-1.582	3.65E 01	5.05E-01	2.55E-01	-1.40E 00	-1.39E 00
3.48E-01	-1.335	4.37E 01	6.04E-01	3.64E-01	-1.18E 00	-1.18E 00
4.90E-01	-1.088	5.14E 01	7.10E-01	5.04E-01	-9.60E-01	-9.57E-01
6.51E-01	-0.841	5.89E 01	8.14E-01	6.63E-01	-7.42E-01	-7.40E-01
7.85E-01	-0.593	6.45E 01	8.91E-01	7.94E-01	-5.24E-01	-5.22E-01
9.20E-01	-0.346	6.96E 01	9.61E-01	9.24E-01	-3.05E-01	-3.05E-01
9.87E-01	-0.099	7.21E 01	9.97E-01	9.94E-01	-8.73E-02	-8.70E-02
9.95E-01	0.148	7.2 E 01	9.94E-01	9.89E-01	1.31E-01	1.31E-01
8.97E-01	0.395	6.82E 01	9.43E-01	8.89E-01	3.49E-01	3.48E-01
7.61E-01	0.643	6.27E 01	8.67E-01	7.52E-01	5.67E-01	5.66E-01
5.95E-01	0.890	5.52E 01	7.63E-01	5.83E-01	7.85E-01	7.83E-01
4.25E-01	1.137	4.64E 01	6.42E-01	4.12E-01	1.00E 00	1.00E 00
2.89E-01	1.385	3.81E 01	5.26E-01	2.77E-01	1.22E 00	1.22E 00
1.86E-01	1.632	3.03E 01	4.19E-01	1.75E-01	1.44E 00	1.44E 00
1.02E-01	1.879	2.23E 01	3.08E-01	9.47E-02	1.66E 00	1.65E 00
5.43E-02	2.126	1.61E 01	2.23E-01	4.98E-02	1.88E 00	1.87E 00
3.27E-02	2.374	1.20E 01	1.74E-01	3.02E-02	2.09E 00	2.09E 00
2.12E-02	2.621	1.03E 01	1.43E-01	2.03E-02	2.31E 00	2.31E 00
1.71E-02	2.868	9.29E 00	1.28E-01	1.65E-02	2.53E 00	2.52E 00
1.18E-02	3.115	7.69E 00	1.06E-01	1.12E-02	2.75E 00	2.74E 00

UCS = 7.24E 01, EMS = 3.24E 00, BS = 1.14E 00, ES= 1.84E 00,

EMSOMO = 2.27E 00, RATIOS = 1.12E 00, ESOED = 6.33E-01

15 -1.00 2 2 0.10 11 6 64 2

YS	TS	T	Q	CP	V	UOUC	VOUC
-3.100	35.12	26.62	1.30E-02	-2.40E-02	8.24E 00	9.72E-02	4.87E-02
-2.850	37.38	28.88	1.23E-02	-2.67E-02	7.58E 00	9.28E-02	5.12E-02
-2.600	11.88	3.38	1.80E-02	-3.38E-02	9.15E 00	1.28E-01	7.55E-03
-2.350	-2.95	-11.45	4.41E-02	-4.45E-02	1.43E 01	1.96E-01	-3.98E-02
-2.100	-7.49	-15.99	8.52E-02	-5.07E-02	1.99E 01	2.58E-01	-7.67E-02
-1.850	-6.22	-14.72	1.54E-01	-6.23E-02	2.68E 01	3.62E-01	-9.52E-02
-1.600	-6.15	-14.65	2.52E-01	-7.12E-02	3.42E 01	4.63E-01	-1.21E-01
-1.350	-5.08	-13.58	3.84E-01	-7.92E-02	4.23E 01	5.75E-01	-1.39E-01
-1.100	-3.78	-12.28	5.43E-01	-8.41E-02	5.03E 01	6.85E-01	-1.49E-01
-0.850	-2.85	-11.35	7.16E-01	-8.57E-02	5.77E 01	7.91E-01	-1.59E-01
-0.600	-2.00	-10.50	8.93E-01	-8.91E-02	6.45E 01	8.86E-01	-1.64E-01
-0.350	-1.08	-9.58	1.04E 00	-8.84E-02	6.97E 01	9.61E-01	-1.62E-01
-0.100	-0.25	-8.75	1.12E 00	-8.89E-02	7.22E 01	9.98E-01	-1.54E-01
0.150	0.51	-7.69	1.11E 00	-8.54E-02	7.19E 01	9.96E-01	-1.34E-01
0.400	1.95	-6.55	1.01E 00	-8.74E-02	6.87E 01	9.54E-01	-1.09E-01
0.650	2.74	-5.76	8.50E-01	-8.45E-02	6.29E 01	8.75E-01	-6.83E-02
0.900	3.66	-4.84	6.76E-01	-8.11E-02	5.61E 01	7.81E-01	-6.62E-02
1.150	4.13	-4.37	4.81E-01	-7.20E-02	4.73E 01	6.59E-01	-5.04E-02
1.400	5.50	-3.00	4.20E-01	-6.67E-02	4.42E 01	6.17E-01	-3.23E-02
1.650	4.78	-3.72	2.03E-01	-5.60E-02	3.07E 01	4.29E-01	-2.79E-02
1.900	3.12	-5.38	1.04E-01	-4.80E-02	2.21E 01	3.06E-01	-2.89E-02
2.150	-1.32	-9.82	5.10E-02	-4.00E-02	1.54E 01	2.12E-01	-3.67E-02
2.400	-9.03	-17.53	2.66E-02	-3.11E-02	1.11E 01	1.48E-01	-4.69E-02
2.650	-21.03	-29.53	1.40E-02	-2.22E-02	8.24E 00	1.00E-01	-5.68E-02

UC = 7.15E 01, EM = 3.13E 00, B = 1.13E 00, E=, 1.85E 00,

EMOM = 2.17E 00, RATIO = 1.11E 00, EOEO = 6.31E-01

LOUCSQ	XI	US	USOUC	USOUCS	Y/B	XI OBS
9.44E-03	-3.066	6.97E 00	9.64E-02	9.29E-03	-2.74E 00	-2.74E 00
8.61E-03	-2.819	6.76E 00	9.35E-02	8.74E-03	-2.52E 00	-2.51E 00
1.63E-02	-2.571	9.79E 00	1.35E-01	1.83E-02	-2.29E 00	-2.29E 00
3.86E-02	-2.324	1.52E 01	2.10E-01	4.41E-02	-2.07E 00	-2.07E 00
7.16E-02	-2.077	2.06E 01	2.85E-01	8.11E-02	-1.85E 00	-1.85E 00
1.31E-01	-1.830	2.74E 01	3.78E-01	1.43E-01	-1.63E 00	-1.63E 00
2.14E-01	-1.582	3.46E 01	4.78E-01	2.29E-01	-1.41E 00	-1.41E 00
3.30E-01	-1.335	4.25E 01	5.88E-01	3.45E-01	-1.19E 00	-1.19E 00
4.71E-01	-1.088	5.03E 01	6.96E-01	4.84E-01	-9.71E-01	-9.71E-01
6.26E-01	-0.841	5.77E 01	7.97E-01	6.36E-01	-7.50E-01	-7.50E-01
7.85E-01	-0.593	6.44E 01	8.90E-01	7.92E-01	-5.30E-01	-5.29E-01
9.23E-01	-0.346	6.96E 01	9.62E-01	9.26E-01	-3.09E-01	-3.09E-01
9.95E-01	-0.099	7.22E 01	9.98E-01	9.96E-01	-8.83E-02	-8.82E-02
9.92E-01	0.148	7.19E 01	9.95E-01	9.89E-01	1.32E-01	1.32E-01
9.10E-01	0.395	6.87E 01	9.50E-01	9.03E-01	3.53E-01	3.53E-01
7.65E-01	0.643	6.29E 01	8.69E-01	7.56E-01	5.74E-01	5.74E-01
6.11E-01	0.890	5.59E 01	7.74E-01	5.98E-01	7.94E-01	7.94E-01
4.35E-01	1.137	4.7.E 01	6.50E-01	4.22E-01	1.01E 00	1.01E 00
3.81E-01	1.385	4.36E 01	6.03E-01	3.63E-01	1.24E 00	1.24E 00
1.84E-01	1.632	3.0.E 01	4.15E-01	1.72E-01	1.46E 00	1.46E 00
9.38E-02	1.879	2.12E 01	2.93E-01	8.59E-02	1.68E 00	1.68E 00
4.50E-02	2.126	1.45E 01	2.01E-01	4.04E-02	1.90E 00	1.90E 00
2.20E-02	2.374	1.01E 01	1.40E-01	1.96E-02	2.12E 00	2.12E 00
1.01E-02	2.621	6.88E 00	9.51E-02	9.04E-03	2.34E 00	2.34E 00

UCS = 7.23E 01, EMS = 3.10E 00, BS = 1.12E 00, ES= 1.83E 00,

EMSOMC = 2.17E 00, RATIOS = 1.10E 00, ESOEO = 6.31E-01

15 0. 2 2 0.10 24 4 64 1

YS	TS	T	Q	CP	V	UOUC	VCUC
-2.600	7.32	-1.18	6.40E-02	-7.54E-02	5.73E 00	2.48E-01	-5.13E-03
-2.400	-0.98	-9.48	8.20E-02	-8.48E-02	1.96E 01	2.77E-01	-4.63E-02
-2.200	-4.63	-13.13	1.12E-01	-9.52E-02	2.29E 01	3.20E-01	-7.46E-02
-2.000	-5.00	-13.50	1.61E-01	-9.99E-02	2.75E 01	3.83E-01	-9.19E-02
-1.800	-5.18	-13.68	2.18E-01	-1.04E-01	3.20E 01	4.45E-01	-1.08E-01
-1.600	-5.18	-13.68	3.00E-01	-1.07E-01	3.75E 01	5.22E-01	-1.27E-01
-1.400	-4.88	-13.38	3.99E-01	-1.07E-01	4.33E 01	6.03E-01	-1.43E-01
-1.200	-4.63	-13.13	5.11E-01	-1.05E-01	4.90E 01	6.83E-01	-1.59E-01
-1.000	-4.02	-12.52	6.38E-01	-9.99E-02	5.47E 01	7.65E-01	-1.70E-01
-0.800	-3.41	-11.91	7.60E-01	-9.41E-02	5.97E 01	8.37E-01	-1.77E-01
-0.600	-2.93	-11.43	8.82E-01	-8.66E-02	6.44E 01	9.04E-01	-1.83E-01
-0.400	-1.83	-10.33	9.90E-01	-8.18E-02	6.82E 01	9.61E-01	-1.75E-01
-0.200	-0.80	-9.35	1.05E 00	-7.70E-02	7.03E 01	9.94E-01	-1.64E-01
0.	0.	-8.50	1.06E 00	-7.27E-02	7.05E 01	9.98E-01	-1.49E-01
0.200	0.98	-7.52	1.00E 00	-6.85E-02	6.86E 01	9.75E-01	-1.29E-01
0.400	1.89	-6.61	9.09E-01	-6.45E-02	6.53E 01	9.30E-01	-1.08E-01
0.600	2.68	-5.82	7.80E-01	-5.68E-02	6.05E 01	8.63E-01	-8.79E-02
0.800	3.35	-5.15	6.24E-01	-5.12E-02	5.41E 01	7.72E-01	-6.96E-02
1.000	4.02	-4.48	4.83E-01	-4.51E-02	4.76E 01	6.80E-01	-5.32E-02
1.200	4.63	-3.87	3.52E-01	-3.68E-02	4.07E 01	5.81E-01	-3.93E-02
1.400	5.12	-3.38	2.36E-01	-2.92E-02	3.33E 01	4.76E-01	-2.81E-02
1.600	5.12	-3.38	1.50E-01	-2.36E-02	2.65E 01	3.80E-01	-2.24E-02
1.800	4.76	-3.74	8.00E-02	-1.85E-02	1.94E 01	2.77E-01	-1.81E-02
2.000	4.15	-4.35	3.60E-02	-1.51E-02	1.30E 01	1.86E-01	-1.41E-02
2.200	0.61	-7.89	7.00E-03	-1.13E-02	5.73E 00	8.13E-02	-1.13E-02

UC = 6.58E 01, EM = 3.00E 00, E = 1.11E 00, E= 1.82E 00,

EMCM = 2.02E 00, RATIO = 1.03E 00, EOEO = 5.68E-01

LCUCSC	XI	US	USCUC	USOLCS	Y/B	XIOBS
6.16E-02	-2.571	1.80E 01	2.55E-01	6.50E-02	-2.34E 00	-2.33E 00
7.69E-02	-2.374	2.03E 01	2.90E-01	8.41E-02	-2.16E 00	-2.15E 00
1.02E-01	-2.176	2.37E 01	3.36E-01	1.13E-01	-1.98E 00	-1.97E 00
1.47E-01	-1.978	2.82E 01	4.00E-01	1.60E-01	-1.80E 00	-1.79E 00
1.98E-01	-1.780	3.26E 01	4.62E-01	2.13E-01	-1.62E 00	-1.61E 00
2.73E-01	-1.582	3.80E 01	5.38E-01	2.89E-01	-1.44E 00	-1.43E 00
3.64E-01	-1.385	4.36E 01	6.17E-01	3.81E-01	-1.26E 00	-1.25E 00
4.67E-01	-1.187	4.91E 01	6.95E-01	4.84E-01	-1.08E 00	-1.07E 00
5.86E-01	-0.989	5.47E 01	7.75E-01	6.01E-01	-9.00E-01	-8.95E-01
7.01E-01	-0.791	5.96E 01	8.45E-01	7.14E-01	-7.20E-01	-7.16E-01
8.16E-01	-0.593	6.42E 01	9.10E-01	8.27E-01	-5.40E-01	-5.37E-01
9.23E-01	-0.396	6.81E 01	9.64E-01	9.30E-01	-3.60E-01	-3.58E-01
9.88E-01	-0.198	7.03E 01	9.96E-01	9.91E-01	-1.80E-01	-1.79E-01
9.96E-01	0.	7.05E 01	9.98E-01	9.96E-01	0.	0.
9.50E-01	0.198	6.87E 01	9.73E-01	9.47E-01	1.80E-01	1.79E-01
8.64E-01	0.396	6.54E 01	9.26E-01	8.58E-01	3.60E-01	3.58E-01
7.44E-01	0.593	6.05E 01	8.58E-01	7.35E-01	5.40E-01	5.37E-01
5.97E-01	0.791	5.41E 01	7.66E-01	5.86E-01	7.20E-01	7.16E-01
4.62E-01	0.989	4.74E 01	6.71E-01	4.51E-01	9.00E-01	8.95E-01
3.38E-01	1.187	4.03E 01	5.70E-01	3.25E-01	1.08E 00	1.07E 00
2.27E-01	1.385	3.27E 01	4.64E-01	2.15E-01	1.26E 00	1.25E 00
1.44E-01	1.582	2.59E 01	3.66E-01	1.34E-01	1.44E 00	1.43E 00
7.68E-02	1.780	1.86E 01	2.63E-01	6.54E-02	1.62E 00	1.61E 00
2.45E-02	1.978	1.22E 01	1.72E-01	2.57E-02	1.80E 00	1.79E 00
6.62E-03	2.176	4.88E 00	6.91E-02	4.78E-03	1.98E 00	1.97E 00

LCS = 7.06E 01, EMS = 2.97E 00, BS = 1.10E 00, ES= 1.81E 00,
EMSCMO = 2.02E 00, RATICS = 1.02E 00, ESOEO = 5.70E-01

15 1.00 2 2 0.10 17 6 64 2

YS	TS	T	Q	CP	V	UOUC	VOUC
-3.900	8.50	0.	-0.	-2.13E-02	9.49E 00	-0.	-0.
-3.600	36.76	28.26	1.87E-02	-2.75E-02	9.31E 00	1.15E-01	6.16E-02
-3.300	32.21	23.71	2.10E-02	-3.55E-02	9.86E 00	1.26E-01	5.55E-02
-3.000	19.27	10.77	2.80E-02	-4.88E-02	1.14E 01	1.57E-01	2.98E-02
-2.700	10.12	1.62	3.70E-02	-5.77E-02	1.31E 01	1.83E-01	5.17E-03
-2.500	0.93	-7.57	5.80E-02	-7.28E-02	1.64E 01	2.27E-01	-3.02E-02
-2.200	-5.28	-13.78	9.68E-02	-8.43E-02	2.12E 01	2.88E-01	-7.06E-02
-1.900	-10.18	-18.68	1.62E-01	-8.49E-02	2.74E 01	3.64E-01	-1.23E-01
-1.600	-13.53	-19.03	2.66E-01	-8.29E-02	3.51E 01	4.64E-01	-1.60E-01
-1.300	-9.02	-17.52	4.04E-01	-7.66E-02	4.33E 01	5.77E-01	-1.82E-01
-1.000	-6.23	-14.73	6.20E-01	-9.64E-02	5.36E 01	7.25E-01	-1.91E-01
-0.700	-4.27	-12.77	8.26E-01	-8.69E-02	6.19E 01	8.44E-01	-1.91E-01
-0.400	-2.42	-10.92	1.00E 00	-7.94E-02	6.81E 01	9.35E-01	-1.80E-01
-0.100	-0.36	-8.86	1.12E 00	-7.25E-02	7.21E 01	9.97E-01	-1.55E-01
0.200	1.51	-6.99	1.10E 00	-6.84E-02	7.15E 01	9.92E-01	-1.22E-01
0.500	2.58	-5.82	9.62E-01	-5.98E-02	6.68E 01	9.30E-01	-9.47E-02
0.800	4.10	-4.40	7.44E-01	-5.25E-02	5.88E 01	8.19E-01	-6.31E-02
1.100	4.63	-3.87	5.07E-01	-4.16E-02	4.85E 01	6.77E-01	-4.57E-02
1.400	4.69	-3.81	2.94E-01	-3.19E-02	3.69E 01	5.15E-01	-3.43E-02
1.700	3.64	-4.86	1.44E-01	-2.31E-02	2.58E 01	3.60E-01	-3.06E-02
2.000	-1.75	-10.25	4.90E-02	-1.69E-02	1.51E 01	2.07E-01	-3.75E-02
2.300	-18.05	-26.55	1.94E-02	-1.06E-02	9.49E 00	1.19E-01	-5.93E-02

UC = 7.15E 01, EM = 3.17E 00, B = 1.11E 00, E=, 1.82E 00,

EMOM = 2.20E 00, RATIO = 1.10E 00, EOEO = 6.21E-01

UOUCSQ	XI	US	USOUC	USOUCS	Y/B	XIOBS
0.	-3.857	2.02E-01	2.80E-03	7.83E-06	-3.50E 00	-3.48E 00
1.31E-02	-3.550	7.78E 00	1.08E-01	1.16E-02	-3.23E 00	-3.21E 00
1.59E-02	-3.264	8.82E 00	1.22E-01	1.49E-02	-2.96E 00	-2.94E 00
2.45E-02	-2.967	1.14E 01	1.58E-01	2.49E-02	-2.69E 00	-2.68E 00
3.35E-02	-2.670	1.37E 01	1.89E-01	3.58E-02	-2.42E 00	-2.41E 00
5.17E-02	-2.473	1.73E 01	2.39E-01	5.69E-02	-2.24E 00	-2.23E 00
8.28E-02	-2.176	2.21E 01	3.04E-01	9.24E-02	-1.98E 00	-1.96E 00
1.32E-01	-1.879	2.78E 01	3.84E-01	1.48E-01	-1.71E 00	-1.70E 00
2.16E-01	-1.582	3.51E 01	4.86E-01	2.36E-01	-1.44E 00	-1.43E 00
3.33E-01	-1.285	4.31E 01	5.96E-01	3.55E-01	-1.17E 00	-1.16E 00
5.26E-01	-0.989	5.34E 01	7.39E-01	5.46E-01	-8.98E-01	-8.92E-01
7.13E-01	-0.692	6.17E 01	8.53E-01	7.28E-01	-6.28E-01	-6.25E-01
8.75E-01	-0.396	6.81E 01	9.40E-01	8.84E-01	-3.59E-01	-3.57E-01
9.93E-01	-0.099	7.21E 01	9.97E-01	9.95E-01	-8.98E-02	-8.92E-02
9.85E-01	0.198	7.15E 01	9.89E-01	9.79E-01	1.80E-01	1.78E-01
8.64E-01	0.495	6.68E 01	9.24E-01	8.54E-01	4.49E-01	4.46E-01
6.71E-01	0.791	5.86E 01	8.11E-01	6.57E-01	7.18E-01	7.14E-01
4.58E-01	1.088	4.81E 01	6.66E-01	4.43E-01	9.88E-01	9.82E-01
2.66E-01	1.385	3.64E 01	5.03E-01	2.53E-01	1.26E 00	1.25E 00
1.30E-01	1.681	2.51E 01	3.47E-01	1.21E-01	1.53E 00	1.52E 00
4.30E-02	1.978	1.42E 01	1.97E-01	3.88E-02	1.80E 00	1.78E 00
1.41E-02	2.275	8.14E 00	1.13E-01	1.27E-02	2.06E 00	2.05E 00

UCS = 7.23E 01, EMS = 3.14E 00, BS = 1.11E 00, ES= 1.80E 00,

EMSOMG = 2.20E 00, RATIOS = 1.09E 00, ESOEO = 6.23E-01

15 2.00 2 2 0.10 1 6 64 1

YS	TS	T	Q	CP	V	UOUC	VOUC
-2.700	4.27	-4.23	4.20E-02	-4.12E-02	8.32E 00	1.86E-01	-1.37E-02
-2.500	0.37	-9.13	5.70E-02	-4.60E-02	1.62E 01	2.15E-01	-3.07E-02
-2.300	-2.20	-10.70	8.20E-02	-5.17E-02	1.95E 01	2.56E-01	-4.83E-02
-2.100	-3.54	-12.04	1.28E-01	-5.90E-02	2.43E 01	3.18E-01	-6.78E-02
-1.900	-4.51	-13.01	1.93E-01	-6.70E-02	2.99E 01	3.89E-01	-8.99E-02
-1.700	-5.06	-13.56	2.71E-01	-7.35E-02	3.54E 01	4.60E-01	-1.11E-01
-1.500	-5.18	-13.68	3.74E-01	-8.00E-02	4.16E 01	5.40E-01	-1.31E-01
-1.300	-4.88	-13.38	5.95E-01	-8.12E-02	5.25E 01	6.82E-01	-1.62E-01
-1.100	-4.39	-12.89	6.21E-01	-8.58E-02	5.36E 01	6.98E-01	-1.60E-01
-0.900	-4.02	-12.52	7.66E-01	-8.55E-02	5.95E 01	7.75E-01	-1.72E-01
-0.700	-3.41	-11.91	9.06E-01	-8.52E-02	6.47E 01	8.45E-01	-1.79E-01
-0.500	-2.56	-11.06	1.06E 00	-8.48E-02	7.01E 01	9.20E-01	-1.80E-01
-0.300	-1.59	-10.09	1.18E 00	-8.34E-02	7.39E 01	9.73E-01	-1.73E-01
-0.100	-0.61	-9.11	1.23E 00	-8.15E-02	7.54E 01	9.95E-01	-1.60E-01
0.100	0.61	-7.89	1.24E 00	-8.03E-02	7.56E 01	1.00E 00	-1.39E-01
0.300	1.71	-6.79	1.18E 00	-7.74E-02	7.38E 01	9.80E-01	-1.17E-01
0.500	2.68	-5.82	1.06E 00	-7.34E-02	6.98E 01	9.29E-01	-9.46E-02
0.700	3.54	-4.96	8.96E-01	-6.97E-02	6.43E 01	8.57E-01	-7.44E-02
0.900	4.39	-4.11	7.47E-01	-6.64E-02	5.88E 01	7.84E-01	-5.63E-02
1.100	5.00	-3.50	5.79E-01	-6.36E-02	5.17E 01	6.90E-01	-4.22E-02
1.300	5.37	-3.13	4.24E-01	-5.98E-02	4.43E 01	5.91E-01	-3.24E-02
1.500	5.49	-3.01	3.08E-01	-5.49E-02	3.77E 01	5.04E-01	-2.65E-02
1.700	5.24	-3.26	2.12E-01	-5.01E-02	3.13E 01	4.18E-01	-2.38E-02
1.900	4.88	-3.62	1.45E-01	-4.44E-02	2.59E 01	3.45E-01	-2.19E-02
2.100	3.05	-5.45	8.90E-02	-3.96E-02	2.03E 01	2.70E-01	-2.58E-02
2.300	0.	-8.50	5.30E-02	-3.47E-02	1.56E 01	2.07E-01	-3.09E-02
2.500	-6.71	-15.21	3.00E-02	-2.99E-02	1.18E 01	1.52E-01	-4.13E-02
2.700	-12.80	-21.30	2.30E-02	-2.50E-02	1.03E 01	1.28E-01	-5.01E-02
2.900	-18.90	-27.40	1.50E-02	-2.02E-02	8.32E 00	9.88E-02	-5.12E-02

UC = 7.48E 01, EV = 3.21E 00, U = 1.16E 00, E=, 1.90E 00,

EMOM = 2.34E 00, RATIO = 1.26E 00, EOEO = 7.46E-01

UOUCSQ	XI	US	USOUC	USOUCS	Y/B	XIOBS
3.45E-02	-2.670	1.48E 01	1.95E-01	3.81E-02	-2.32E 00	-2.32E 00
4.61E-02	-2.473	1.71E 01	2.27E-01	5.14E-02	-2.15E 00	-2.14E 00
6.54E-02	-2.275	2.04E 01	2.69E-01	7.25E-02	-1.97E 00	-1.97E 00
1.01E-01	-2.077	2.51E 01	3.33E-01	1.11E-01	-1.80E 00	-1.80E 00
1.51E-01	-1.879	3.06E 01	4.04E-01	1.63E-01	-1.63E 00	-1.63E 00
2.11E-01	-1.681	3.59E 01	4.75E-01	2.25E-01	-1.46E 00	-1.46E 00
2.92E-01	-1.484	4.13E 01	5.54E-01	3.07E-01	-1.29E 00	-1.29E 00
4.65E-01	-1.286	5.26E 01	6.95E-01	4.83E-01	-1.12E 00	-1.11E 00
4.87E-01	-1.088	5.36E 01	7.08E-01	5.02E-01	-9.44E-01	-9.43E-01
6.03E-01	-0.890	5.94E 01	7.85E-01	6.16E-01	-7.73E-01	-7.72E-01
7.16E-01	-0.692	6.45E 01	8.53E-01	7.28E-01	-6.01E-01	-6.00E-01
8.47E-01	-0.495	7.00E 01	9.25E-01	8.57E-01	-4.29E-01	-4.29E-01
9.47E-01	-0.297	7.38E 01	9.76E-01	9.53E-01	-2.58E-01	-2.57E-01
9.91E-01	-0.099	7.54E 01	9.97E-01	9.93E-01	-8.59E-02	-8.58E-02
1.00E 00	0.099	7.56E 01	1.00E 00	1.00E 00	8.59E-02	8.58E-02
9.60E-01	0.297	7.38E 01	9.76E-01	9.53E-01	2.58E-01	2.57E-01
8.63E-01	0.495	6.98E 01	9.24E-01	8.53E-01	4.29E-01	4.29E-01
7.35E-01	0.692	6.43E 01	8.50E-01	7.22E-01	6.01E-01	6.00E-01
6.14E-01	0.890	5.85E 01	7.74E-01	5.99E-01	7.73E-01	7.72E-01
4.76E-01	1.088	5.13E 01	6.79E-01	4.61E-01	9.44E-01	9.43E-01
3.49E-01	1.286	4.37E 01	5.78E-01	3.35E-01	1.12E 00	1.11E 00
2.54E-01	1.484	3.71E 01	4.90E-01	2.40E-01	1.29E 00	1.29E 00
1.75E-01	1.681	3.08E 01	4.08E-01	1.63E-01	1.46E 00	1.46E 00
1.19E-01	1.879	2.50E 01	3.31E-01	1.09E-01	1.63E 00	1.63E 00
7.25E-02	2.077	1.94E 01	2.56E-01	6.56E-02	1.80E 00	1.80E 00
4.28E-02	2.275	1.47E 01	1.95E-01	3.79E-02	1.97E 00	1.97E 00
2.31E-02	2.473	1.08E 01	1.42E-01	2.03E-02	2.15E 00	2.14E 00
1.65E-02	2.671	9.18E 00	1.21E-01	1.47E-02	2.32E 00	2.32E 00
9.76E-03	2.868	7.09E 00	9.37E-02	8.78E-03	2.49E 00	2.49E 00

UCS = 7.56E 01, ECS = 3.18E 00, BS = 1.15E 00, ES= 1.88E 00,

EMSOMC = 2.34E 00, RATIOS = 1.25E 00, ESOEO = 7.47E-01

15 2.50 2 2 0.10 18 6 64 2

YS	TS	T	Q	CP	V	UOUC	VOUC
-4.300	-13.56	-22.06	3.28E-02	-2.51E-02	-0.	1.61E-01	-6.52E-02
-4.000	-11.81	-20.31	4.60E-02	-3.24E-02	1.46E 01	1.93E-01	-7.13E-02
-3.700	-10.58	-19.08	5.98E-02	-3.85E-02	1.67E 01	2.21E-01	-7.66E-02
-3.400	-11.12	-19.62	7.29E-02	-4.44E-02	1.84E 01	2.44E-01	-8.69E-02
-3.100	-8.30	-16.80	9.44E-02	-5.47E-02	2.10E 01	2.82E-01	-8.51E-02
-2.800	-10.31	-18.81	1.15E-01	-6.27E-02	2.32E 01	3.08E-01	-1.05E-01
-2.500	-12.29	-20.79	1.48E-01	-6.50E-02	2.63E 01	3.45E-01	-1.31E-01
-2.200	-12.52	-21.02	2.06E-01	-6.77E-02	3.10E 01	4.06E-01	-1.56E-01
-1.900	-11.37	-19.87	2.89E-01	-6.37E-02	3.67E 01	4.84E-01	-1.75E-01
-1.600	-9.69	-18.19	4.03E-01	-5.99E-02	4.33E 01	5.78E-01	-1.90E-01
-1.300	-8.31	-16.81	5.38E-01	-5.24E-02	5.01E 01	6.73E-01	-2.03E-01
-1.000	-5.72	-14.22	7.31E-01	-7.23E-02	5.83E 01	7.94E-01	-2.01E-01
-0.700	-4.09	-12.59	8.94E-01	-6.33E-02	6.45E 01	8.84E-01	-1.97E-01
-0.400	-2.23	-10.73	1.03E 00	-5.77E-02	6.93E 01	9.56E-01	-1.81E-01
-0.100	-0.38	-8.88	1.11E 00	-5.46E-02	7.19E 01	9.98E-01	-1.56E-01
0.200	1.44	-7.06	1.09E 00	-5.39E-02	7.12E 01	9.93E-01	-1.23E-01
0.500	3.08	-5.42	1.01E 00	-5.16E-02	6.85E 01	9.57E-01	-9.08E-02
0.800	4.74	-3.76	8.37E-01	-4.69E-02	6.24E 01	8.75E-01	-5.75E-02
1.100	5.49	-3.01	5.82E-01	-4.20E-02	5.20E 01	7.30E-01	-3.83E-02
1.400	6.18	-2.32	3.93E-01	-3.41E-02	4.28E 01	6.00E-01	-2.43E-02
1.700	2.90	-5.60	2.50E-01	-2.69E-02	3.41E 01	4.77E-01	-4.67E-02
2.000	8.50	0.	1.51E-01	-1.89E-02	2.65E 01	3.72E-01	0.
2.300	5.20	-3.30	8.60E-02	-1.44E-02	2.00E 01	2.80E-01	-1.62E-02
2.600	1.28	-7.22	5.10E-02	-9.87E-03	1.54E 01	2.15E-01	-2.72E-02
2.900	-5.34	-13.84	2.75E-02	-6.28E-03	1.13E 01	1.54E-01	-3.80E-02
3.200	-15.45	-23.95	1.74E-02	-4.49E-03	9.00E 00	1.15E-01	-5.13E-02
3.500	-18.12	-26.62	1.30E-02	-3.59E-03	7.78E 00	9.76E-02	-4.89E-02

UC = 7.12E 01, EM = 3.99E 00, B = 1.36E 00, E=, 2.18E 00,

EMOM = 2.75E 00, RATIO = 1.32E 00, EOEO = 7.32E-01

UOUCSQ	XI	US	USOUC	USOUCS	Y/B	XIOBS
2.59E-02	-4.253	1.24E 01	1.72E-01	2.95E-02	-3.17E 00	-3.14E 00
3.71E-02	-3.956	1.40E 01	2.05E-01	4.22E-02	-2.95E 00	-2.92E 00
4.90E-02	-3.659	1.57E 01	2.36E-01	5.57E-02	-2.72E 00	-2.70E 00
5.94E-02	-3.363	1.88E 01	2.61E-01	6.82E-02	-2.50E 00	-2.48E 00
7.94E-02	-3.066	2.16E 01	2.99E-01	8.96E-02	-2.28E 00	-2.26E 00
9.49E-02	-2.769	2.37E 01	3.28E-01	1.08E-01	-2.06E 00	-2.04E 00
1.19E-01	-2.473	2.65E 01	3.68E-01	1.35E-01	-1.84E 00	-1.82E 00
1.65E-01	-2.176	3.09E 01	4.29E-01	1.84E-01	-1.62E 00	-1.60E 00
2.34E-01	-1.879	3.65E 01	5.06E-01	2.56E-01	-1.40E 00	-1.39E 00
3.34E-01	-1.582	4.3 E 01	5.97E-01	3.56E-01	-1.18E 00	-1.17E 00
4.53E-01	-1.286	4.96E 01	6.89E-01	4.75E-01	-9.57E-01	-9.48E-01
6.31E-01	-0.989	5.8 E 01	8.06E-01	6.49E-01	-7.36E-01	-7.29E-01
7.81E-01	-0.692	6.42E 01	8.92E-01	7.96E-01	-5.15E-01	-5.10E-01
9.13E-01	-0.396	6.91E 01	9.60E-01	9.21E-01	-2.95E-01	-2.92E-01
9.95E-01	-0.099	7.19E 01	9.98E-01	9.96E-01	-7.36E-02	-7.29E-02
9.85E-01	0.198	7.13E 01	9.90E-01	9.79E-01	1.47E-01	1.46E-01
9.16E-01	0.495	6.60E 01	9.51E-01	9.05E-01	3.68E-01	3.65E-01
7.65E-01	0.791	6.25E 01	8.65E-01	7.49E-01	5.89E-01	5.83E-01
5.32E-01	1.088	5.15E 01	7.19E-01	5.17E-01	8.10E-01	8.02E-01
3.60E-01	1.385	4.25E 01	5.88E-01	3.46E-01	1.03E 00	1.02E 00
2.27E-01	1.681	3.37E 01	4.68E-01	2.19E-01	1.25E 00	1.24E 00
1.39E-01	1.978	2.56E 01	3.56E-01	1.27E-01	1.47E 00	1.46E 00
7.87E-02	2.275	1.92E 01	2.66E-01	7.10E-02	1.69E 00	1.68E 00
4.61E-02	2.571	1.46E 01	2.02E-01	4.10E-02	1.91E 00	1.90E 00
2.38E-02	2.868	1.04E 01	1.45E-01	2.10E-02	2.14E 00	2.11E 00
1.33E-02	3.165	7.86E 00	1.09E-01	1.20E-02	2.36E 00	2.33E 00
9.53E-03	3.462	6.7 E 00	9.31E-02	8.66E-03	2.58E 00	2.55E 00

UCS = 7.20E 01, EMS = 3.98E 00, BS = 1.36E 00, ES= 2.17E 00,

EMSOMO = 2.78E 00, RATIOS = 1.32E 00, ESOEO = 7.35E-01

3C -2.50 2 2 0.10 11 6 64 2

YS	TS	T	Q	CP	V	UOUC	VOUC
-5.750	-26.58	-35.08	9.13E-02	-4.27E-02	1.36E 01	3.48E-01	-2.44E-01
-5.250	-25.44	-33.94	9.90E-02	-4.22E-02	2.15E 01	3.67E-01	-2.47E-01
-4.750	-22.15	-30.65	1.15E-01	-4.81E-02	2.32E 01	4.10E-01	-2.43E-01
-4.250	-19.05	-27.55	1.37E-01	-5.38E-02	2.52E 01	4.61E-01	-2.40E-01
-3.750	-15.75	-24.25	1.68E-01	-5.21E-02	2.80E 01	5.26E-01	-2.37E-01
-3.250	-12.08	-20.58	2.13E-01	-6.08E-02	3.15E 01	6.08E-01	-2.28E-01
-2.750	-9.70	-18.20	2.61E-01	-6.55E-02	3.49E 01	6.82E-01	-2.24E-01
-2.250	-6.23	-14.73	3.37E-01	-1.03E-01	3.96E 01	7.90E-01	-2.38E-01
-1.750	-4.57	-13.07	4.04E-01	-1.04E-01	4.34E 01	8.71E-01	-2.32E-01
-1.250	-2.97	-11.47	4.52E-01	-9.81E-02	4.59E 01	9.27E-01	-1.86E-01
-1.000	-2.10	-10.60	4.75E-01	-9.54E-02	4.71E 01	9.53E-01	-1.78E-01
-0.750	-1.37	-9.87	4.89E-01	-9.52E-02	4.78E 01	9.69E-01	-1.69E-01
-0.500	-0.37	-8.87	5.13E-01	-9.30E-02	4.89E 01	9.95E-01	-1.55E-01
-0.250	0.24	-8.26	5.17E-01	-9.12E-02	4.91E 01	1.00E 00	-1.45E-01
0.	0.64	-7.86	5.16E-01	-8.95E-02	4.91E 01	1.00E 00	-1.38E-01
0.250	1.09	-7.41	5.10E-01	-8.78E-02	4.88E 01	9.96E-01	-1.29E-01
0.500	-1.30	-9.80	5.00E-01	-8.72E-02	4.83E 01	9.80E-01	-1.69E-01
0.750	3.45	-5.05	4.85E-01	-8.67E-02	4.75E 01	9.75E-01	-8.62E-02
1.250	5.10	-3.40	4.32E-01	-8.51E-02	4.49E 01	9.23E-01	-5.49E-02
1.750	6.79	-1.71	3.69E-01	-8.51E-02	4.15E 01	8.54E-01	-2.55E-02
2.250	8.27	-0.23	2.99E-01	-8.32E-02	3.73E 01	7.69E-01	-3.14E-03
2.750	10.78	2.28	2.46E-01	-8.32E-02	3.39E 01	6.97E-01	2.77E-02
3.250	13.26	4.76	1.91E-01	-7.54E-02	2.98E 01	6.12E-01	5.10E-02
3.750	16.12	7.62	1.47E-01	-7.16E-02	2.62E 01	5.34E-01	7.15E-02
4.250	18.50	10.00	1.12E-01	-6.19E-02	2.29E 01	4.63E-01	6.17E-02
4.750	22.63	14.13	8.18E-02	-5.80E-02	1.95E 01	3.90E-01	9.81E-02
5.250	24.77	16.27	6.39E-02	-4.68E-02	1.73E 01	3.41E-01	9.96E-02
5.750	28.14	19.64	3.96E-02	-4.02E-02	1.36E 01	2.64E-01	9.41E-02

UC = 4.86E 01, EM = 7.74E 00, B = 2.91E 00, E=, 4.84E 00,

EMOM = 3.64E 00, RATIO = 1.32E 00, EOEO = 5.13E-01

UOUCSQ	XI	US	USOUC	USOUCS	Y/B	XIOBS
1.21E-01	-5.687	1.9[illegible]E 01	3.87E-01	1.50E-01	-1.97E 00	-1.97E 00
1.35E-01	-5.192	1.99E 01	4.06E-01	1.65E-01	-1.80E 00	-1.80E 00
1.68E-01	-4.698	2.19E 01	4.46E-01	1.99E-01	-1.63E 00	-1.63E 00
2.12E-01	-4.203	2.42E 01	4.93E-01	2.43E-01	-1.46E 00	-1.46E 00
2.77E-01	-3.709	2.72E 01	5.54E-01	3.07E-01	-1.29E 00	-1.29E 00
3.69E-01	-3.214	3.1[illegible]E 01	6.31E-01	3.98E-01	-1.11E 00	-1.12E 00
4.65E-01	-2.720	3.44E 01	7.01E-01	4.91E-01	-9.43E-01	-9.44E-01
6.24E-01	-2.225	3.94E 01	8.02E-01	6.43E-01	-7.72E-01	-7.72E-01
7.58E-01	-1.731	4.32E 01	8.80E-01	7.74E-01	-6.00E-01	-6.00E-01
8.59E-01	-1.236	4.56E 01	9.32E-01	8.69E-01	-4.29E-01	-4.29E-01
9.08E-01	-0.989	4.7[illegible]E 01	9.57E-01	9.15E-01	-3.43E-01	-3.43E-01
9.39E-01	-0.742	4.77E 01	9.71E-01	9.43E-01	-2.57E-01	-2.57E-01
9.90E-01	-0.495	4.89E 01	9.95E-01	9.90E-01	-1.72E-01	-1.72E-01
1.00E 00	-0.247	4.91E 01	10.00E-01	9.99E-01	-8.58E-02	-8.58E-02
1.00E 00	0.	4.91E 01	9.99E-01	9.98E-01	0.	0.
9.93E-01	0.247	4.88E 01	9.94E-01	9.88E-01	8.58E-02	8.58E-02
9.60E-01	0.495	4.83E 01	9.84E-01	9.69E-01	1.72E-01	1.72E-01
9.51E-01	0.742	4.75E 01	9.68E-01	9.37E-01	2.57E-01	2.57E-01
8.51E-01	1.236	4.48E 01	9.12E-01	8.32E-01	4.29E-01	4.29E-01
7.29E-01	1.731	4.13E 01	8.41E-01	7.07E-01	6.00E-01	6.00E-01
5.91E-01	2.225	3.70E 01	7.53E-01	5.67E-01	7.72E-01	7.72E-01
4.86E-01	2.720	3.32E 01	6.77E-01	4.58E-01	9.43E-01	9.44E-01
3.75E-01	3.214	2.89E 01	5.89E-01	3.47E-01	1.11E 00	1.12E 00
2.86E-01	3.709	2.49E 01	5.07E-01	2.57E-01	1.29E 00	1.29E 00
2.15E-01	4.203	2.13E 01	4.34E-01	1.88E-01	1.46E 00	1.46E 00
1.52E-01	4.698	1.76E 01	3.58E-01	1.28E-01	1.63E 00	1.63E 00
1.16E-01	5.192	1.52E 01	3.09E-01	9.53E-02	1.80E 00	1.80E 00
6.95E-02	5.687	1.14E 01	2.33E-01	5.42E-02	1.97E 00	1.97E 00

UCS = 4.91E 01, EMS = 7.65E 00, BS = 2.88E 00, ES= 4.79E 00,

EMSOMO = 3.64E 00, RATIOS = 1.30E 00, ESOEO = 5.14E-01

30 -2.00 2 2 0.10 11 6 64 2

YS	TS	T	Q	CP	V	UOUC	VOUC
-5.500	-16.68	-25.18	5.41E-02	-7.04E-02	1.54E 01	2.92E-01	-1.37E-01
-5.000	-18.50	-27.00	6.90E-02	-7.20E-02	1.79E 01	3.25E-01	-1.66E-01
-4.500	-17.68	-26.18	8.51E-02	-7.10E-02	1.99E 01	3.64E-01	-1.79E-01
-4.000	-17.07	-25.57	1.11E-01	-7.10E-02	2.27E 01	4.17E-01	-1.99E-01
-3.500	-13.09	-21.59	1.57E-01	-7.98E-02	2.71E 01	5.12E-01	-2.03E-01
-3.000	-11.03	-19.53	2.04E-01	-8.75E-02	3.08E 01	5.91E-01	-2.10E-01
-2.500	-9.29	-17.79	2.66E-01	-8.57E-02	3.52E 01	6.82E-01	-2.19E-01
-2.000	-5.98	-14.48	3.45E-01	-1.21E-01	4.01E 01	7.89E-01	-2.04E-01
-1.500	-4.23	-12.73	4.11E-01	-1.23E-01	4.38E 01	8.69E-01	-1.96E-01
-1.000	-2.78	-11.28	4.60E-01	-1.20E-01	4.63E 01	9.24E-01	-1.84E-01
-0.750	-1.55	-10.05	4.93E-01	-1.19E-01	4.79E 01	9.60E-01	-1.70E-01
-0.500	-0.69	-9.19	5.18E-01	-1.19E-01	4.91E 01	9.87E-01	-1.60E-01
-0.250	0.20	-8.30	5.26E-01	-1.17E-01	4.95E 01	9.97E-01	-1.45E-01
0.	0.97	-7.53	5.28E-01	-1.14E-01	4.96E 01	1.00E 00	-1.32E-01
0.250	1.68	-6.82	5.25E-01	-1.14E-01	4.95E 01	10.00E-01	-1.20E-01
0.500	2.33	-6.17	5.13E-01	-1.14E-01	4.89E 01	9.89E-01	-1.07E-01
0.750	3.13	-5.37	4.96E-01	-1.15E-01	4.81E 01	9.74E-01	-9.14E-02
1.000	3.71	-4.79	4.68E-01	-1.13E-01	4.67E 01	9.47E-01	-7.93E-02
1.500	5.09	-3.41	4.10E-01	-1.13E-01	4.37E 01	8.88E-01	-5.30E-02
2.000	6.37	-2.13	3.29E-01	-1.11E-01	3.92E 01	7.96E-01	-2.96E-02
2.500	7.64	-0.86	2.61E-01	-1.09E-01	3.49E 01	7.09E-01	-1.06E-02
3.000	8.50	0.	1.96E-01	-1.08E-01	3.02E 01	6.15E-01	0.
3.500	9.67	1.17	1.43E-01	-1.02E-01	2.58E 01	5.25E-01	1.08E-02
4.000	10.44	1.94	1.01E-01	-8.68E-02	2.17E 01	4.41E-01	1.49E-02
4.500	10.87	2.37	7.30E-02	-7.55E-02	1.84E 01	3.75E-01	1.55E-02
5.500	9.44	0.94	3.20E-02	-5.28E-02	1.22E 01	2.48E-01	4.07E-03
5.000	11.39	2.89	5.10E-02	-6.60E-02	1.54E 01	3.13E-01	1.58E-02

UC = 4.92E 01, EP = 7.03E 00, B = 2.65E 00, E= 4.37E 00,

EMOM = 3.34E 00, RATIO = 1.23E 00, EOEO = 4.81E-01

UOUCSQ	XI	US	USOUC	USOUCS	Y/B	XI OBS
8.55E-02	-5.440	1.58E 01	3.18E-01	1.01E-01	-2.08E 00	-2.07E 00
1.06E-01	-4.945	1.76E 01	3.54E-01	1.25E-01	-1.89E 00	-1.88E 00
1.32E-01	-4.451	1.95E 01	3.92E-01	1.54E-01	-1.70E 00	-1.69E 00
1.74E-01	-3.956	2.21E 01	4.45E-01	1.98E-01	-1.51E 00	-1.51E 00
2.62E-01	-3.462	2.67E 01	5.37E-01	2.88E-01	-1.32E 00	-1.32E 00
3.49E-01	-2.967	3.04E 01	6.12E-01	3.75E-01	-1.13E 00	-1.13E 00
4.65E-01	-2.473	3.46E 01	7.01E-01	4.91E-01	-9.44E-01	-9.41E-01
6.23E-01	-1.978	3.98E 01	8.01E-01	6.42E-01	-7.55E-01	-7.53E-01
7.55E-01	-1.484	4.36E 01	8.77E-01	7.69E-01	-5.66E-01	-5.65E-01
8.53E-01	-0.989	4.62E 01	9.29E-01	8.62E-01	-3.78E-01	-3.77E-01
9.22E-01	-0.742	4.79E 01	9.63E-01	9.27E-01	-2.83E-01	-2.82E-01
9.74E-01	-0.495	4.91E 01	9.88E-01	9.75E-01	-1.89E-01	-1.88E-01
9.94E-01	-0.247	4.95E 01	9.96E-01	9.92E-01	-9.44E-02	-9.41E-02
1.00E 00	0.	4.96E 01	9.98E-01	9.96E-01	0.	0.
9.99E-01	0.247	4.95E 01	9.96E-01	9.91E-01	9.44E-02	9.41E-02
9.77E-01	0.495	4.89E 01	9.84E-01	9.67E-01	1.89E-01	1.88E-01
9.48E-01	0.742	4.81E 01	9.67E-01	9.35E-01	2.83E-01	2.82E-01
8.96E-01	0.989	4.67E 01	9.39E-01	8.82E-01	3.78E-01	3.77E-01
7.88E-01	1.484	4.36E 01	8.78E-01	7.70E-01	5.66E-01	5.65E-01
6.34E-01	1.978	3.89E 01	7.84E-01	6.14E-01	7.55E-01	7.53E-01
5.03E-01	2.473	3.45E 01	6.94E-01	4.82E-01	9.44E-01	9.41E-01
3.78E-01	2.967	2.97E 01	5.98E-01	3.58E-01	1.13E 00	1.13E 00
2.76E-01	3.462	2.52E 01	5.06E-01	2.56E-01	1.32E 00	1.32E 00
1.95E-01	3.956	2.09E 01	4.21E-01	1.77E-01	1.51E 00	1.51E 00
1.41E-01	4.451	1.76E 01	3.54E-01	1.26E-01	1.70E 00	1.69E 00
6.17E-02	5.440	1.15E 01	2.31E-01	5.32E-02	2.08E 00	2.07E 00
9.81E-02	4.945	1.46E 01	2.93E-01	8.57E-02	1.89E 00	1.88E 00

UCS = 4.97E 01, EMS = 6.97E 00, BS = 2.63E 00, ES= 4.33E 00,

EMSOMO = 3.36E 00, RATIOS = 1.22E 00, ESOEO = 4.82E-01

30 -1.00 2 2 0.10 12 6 64 2

YS	TS	T		CP	V	UOUC	VOUC
-5.500	35.80	27.30	2.03E-02	-5.81E-02	1.03E 01	1.84E-01	9.52E-02
-5.000	22.79	14.29	2.15E-02	-7.05E-02	1.09E 01	2.07E-01	5.27E-02
-4.500	4.34	-4.16	3.60E-02	-8.30E-02	1.30E 01	2.76E-01	-2.00E-02
-4.000	-3.78	-12.28	5.74E-02	-9.34E-02	1.64E 01	3.41E-01	-7.42E-02
-3.500	-3.95	-12.45	1.04E-01	-1.10E-01	2.20E 01	4.58E-01	-1.01E-01
-3.000	-3.87	-12.37	1.52E-01	-1.20E-01	2.66E 01	5.55E-01	-1.22E-01
-2.500	-3.99	-12.49	2.14E-01	-1.29E-01	3.16E 01	6.58E-01	-1.46E-01
-2.000	-3.63	-12.13	2.78E-01	-1.37E-01	3.60E 01	7.51E-01	-1.61E-01
-1.500	-1.69	-10.19	3.71E-01	-1.47E-01	4.16E 01	8.73E-01	-1.57E-01
-1.000	-0.90	-9.40	4.32E-01	-1.49E-01	4.49E 01	9.44E-01	-1.56E-01
-0.500	-0.14	-8.64	4.77E-01	-1.48E-01	4.71E 01	9.94E-01	-1.51E-01
0.	0.36	-8.14	4.82E-01	-1.48E-01	4.74E 01	1.00E 00	-1.43E-01
0.500	1.39	-7.11	4.65E-01	-1.49E-01	4.66E 01	9.85E-01	-1.23E-01
1.000	2.28	-6.22	4.05E-01	-1.45E-01	4.35E 01	9.21E-01	-1.00E-01
1.500	3.47	-5.03	3.34E-01	-1.41E-01	3.95E 01	8.38E-01	-7.38E-02
2.000	3.24	-5.26	2.50E-01	-1.35E-01	3.41E 01	7.25E-01	-6.68E-02
2.500	2.83	-5.67	1.63E-01	-1.27E-01	2.76E 01	5.85E-01	-5.81E-02
3.000	2.28	-6.22	1.17E-01	-1.18E-01	2.34E 01	4.95E-01	-5.40E-02
3.500	-1.26	-9.76	7.10E-02	-1.06E-01	1.82E 01	3.82E-01	-6.58E-02
4.000	-4.88	-13.38	4.47E-02	-9.13E-02	1.44E 01	2.99E-01	-7.12E-02
4.500	-17.70	-26.20	2.60E-02	-7.68E-02	1.10E 01	2.11E-01	-1.04E-01
5.000	-19.24	-27.74	2.26E-02	-6.43E-02	1.03E 01	1.94E-01	-1.02E-01

UC = 4.69E 01, EM = 6.34E 00, B = 2.34E 00, E=, 3.84E 00,

EMOM = 2.88E 00, RATIO = 9.83E-01, EOEG = 3.66E-01

UOUCSQ	XI	US	USOUC	USOUCS	Y/B	XIOBS
3.40E-02	-5.445	8.42E 00	1.78E-01	3.15E-02	-2.35E 00	-2.35E 00
4.28E-02	-4.945	9.79E 00	2.07E-01	4.27E-02	-2.14E 00	-2.14E 00
7.60E-02	-4.451	1.35E 01	2.84E-01	8.08E-02	-1.93E 00	-1.92E 00
1.16E-01	-3.956	1.68E 01	3.55E-01	1.26E-01	-1.71E 00	-1.71E 00
2.10E-01	-3.462	2.24E 01	4.72E-01	2.23E-01	-1.50E 00	-1.50E 00
3.08E-01	-2.967	2.69E 01	5.67E-01	3.21E-01	-1.28E 00	-1.28E 00
4.33E-01	-2.473	3.17E 01	6.68E-01	4.46E-01	-1.07E 00	-1.07E 00
5.63E-01	-1.978	3.60E 01	7.59E-01	5.75E-01	-8.56E-01	-8.56E-01
7.62E-01	-1.484	4.15E 01	8.76E-01	7.68E-01	-6.42E-01	-6.42E-01
8.92E-01	-0.989	4.40E 01	9.45E-01	8.93E-01	-4.28E-01	-4.28E-01
9.88E-01	-0.495	4.71E 01	9.93E-01	9.87E-01	-2.14E-01	-2.14E-01
1.00E 00	0.	4.74E 01	10.00E-01	9.99E-01	0.	0.
9.71E-01	0.495	4.68E 01	9.83E-01	9.66E-01	2.14E-01	2.14E-01
8.49E-01	0.989	4.35E 01	9.17E-01	8.41E-01	4.28E-01	4.28E-01
7.03E-01	1.484	3.94E 01	8.32E-01	6.92E-01	6.42E-01	6.42E-01
5.26E-01	1.978	3.48E 01	7.18E-01	5.16E-01	8.56E-01	8.56E-01
3.42E-01	2.473	2.74E 01	5.78E-01	3.34E-01	1.07E 00	1.07E 00
2.45E-01	2.967	2.31E 01	4.86E-01	2.36E-01	1.28E 00	1.28E 00
1.46E-01	3.462	1.78E 01	3.75E-01	1.41E-01	1.50E 00	1.50E 00
8.97E-02	3.956	1.39E 01	2.93E-01	8.57E-02	1.71E 00	1.71E 00
4.43E-02	4.451	9.92E 00	2.09E-01	4.38E-02	1.93E 00	1.92E 00
3.75E-02	4.945	9.12E 00	1.92E-01	3.70E-02	2.14E 00	2.14E 00

UCS = 4.74E 01, EMS = 6.28E 00, BS = 2.31E 00, ES= 3.80E 00,

EMSOMG = 2.88E 00, RATIOS = 9.73E-01, ESOEO = 3.67E-01

30 0.0 2 2 0.10 25 4 64 1

YS	TS	T	Q	CP	V	UOUC	VOUC
-3.800	-2.20	-10.70	6.60E-02	-1.19E-01	2.16E 00	3.72E-01	-7.03E-02
-3.400	-3.66	-12.16	9.60E-02	-1.30E-01	2.12E 01	4.47E-01	-9.62E-02
-3.000	-4.27	-12.77	1.31E-01	-1.40E-01	2.48E 01	5.21E-01	-1.18E-01
-2.600	-4.39	-12.89	1.76E-01	-1.51E-01	2.87E 01	6.03E-01	-1.38E-01
-2.200	-4.27	-12.77	2.39E-01	-1.57E-01	3.34E 01	7.03E-01	-1.59E-01
-1.800	-3.78	-12.28	2.91E-01	-1.62E-01	3.69E 01	7.77E-01	-1.69E-01
-1.400	-3.29	-11.79	3.52E-01	-1.64E-01	4.06E 01	8.57E-01	-1.79E-01
-1.000	-2.32	-10.82	4.01E-01	-1.64E-01	4.33E 01	9.17E-01	-1.75E-01
-0.600	-1.59	-10.09	4.47E-01	-1.61E-01	4.57E 01	9.71E-01	-1.73E-01
-0.400	-1.10	-9.60	4.60E-01	-1.59E-01	4.64E 01	9.86E-01	-1.67E-01
-0.200	-0.61	-9.11	4.66E-01	-1.57E-01	4.67E 01	9.94E-01	-1.59E-01
0.	0.	-8.50	4.70E-01	-1.55E-01	4.69E 01	10.00E-01	-1.49E-01
0.200	0.61	-7.89	4.62E-01	-1.53E-01	4.65E 01	9.93E-01	-1.38E-01
0.400	0.98	-7.52	4.50E-01	-1.49E-01	4.59E 01	9.81E-01	-1.30E-01
0.600	1.59	-6.91	4.34E-01	-1.47E-01	4.51E 01	9.65E-01	-1.17E-01
1.000	2.68	-5.82	3.91E-01	-1.40E-01	4.28E 01	9.17E-01	-9.35E-02
1.400	3.41	-5.09	3.32E-01	-1.32E-01	3.94E 01	8.46E-01	-7.53E-02
1.800	4.51	-3.99	2.72E-01	-1.21E-01	3.57E 01	7.67E-01	-5.35E-02
2.200	5.24	-3.26	2.08E-01	-1.13E-01	3.12E 01	6.72E-01	-3.82E-02
2.600	5.85	-2.65	1.50E-01	-1.00E-01	2.65E 01	5.71E-01	-2.64E-02
3.000	6.10	-2.40	9.10E-02	-8.72E-02	2.06E 01	4.45E-01	-1.86E-02
3.400	5.85	-2.65	5.70E-02	-7.45E-02	1.63E 01	3.52E-01	-1.63E-02
3.800	4.88	-3.62	3.00E-02	-6.38E-02	1.18E 01	2.55E-01	-1.61E-02
4.200	1.22	-7.28	1.30E-02	-5.32E-02	7.80E 00	1.67E-01	-2.13E-02
4.600	-7.32	-15.82	1.00E-03	-4.47E-02	2.16E 00	4.49E-02	-1.27E-02

UC = 4.64E 01, EM = 5.58E 00, B = 2.15E 00, E=, 3.59E 00,

EMOM = 2.50E 00, RATIO = 8.84E-01, EOEO = 3.30E-01

UOUCSQ	XI	US	USOUC	USOUCS	Y/B	XIOBS
1.39E-01	-3.758	1.81E 01	3.86E-01	1.49E-01	-1.76E 00	-1.76E 00
2.00E-01	-3.363	2.16E 01	4.61E-01	2.12E-01	-1.58E 00	-1.58E 00
2.71E-01	-2.967	2.50E 01	5.34E-01	2.85E-01	-1.39E 00	-1.39E 00
3.64E-01	-2.571	2.89E 01	6.15E-01	3.79E-01	-1.21E 00	-1.21E 00
4.94E-01	-2.176	3.35E 01	7.14E-01	5.10E-01	-1.02E 00	-1.02E 00
6.04E-01	-1.780	3.69E 01	7.86E-01	6.18E-01	-8.35E-01	-8.36E-01
7.34E-01	-1.385	4.05E 01	8.63E-01	7.46E-01	-6.50E-01	-6.50E-01
8.42E-01	-0.989	4.32E 01	9.22E-01	8.50E-01	-4.64E-01	-4.64E-01
9.42E-01	-0.593	4.57E 01	9.74E-01	9.48E-01	-2.78E-01	-2.79E-01
9.72E-01	-0.396	4.63E 01	9.88E-01	9.76E-01	-1.86E-01	-1.86E-01
9.87E-01	-0.198	4.67E 01	9.95E-01	9.90E-01	-9.28E-02	-9.29E-02
9.99E-01	0.	4.69E 01	10.00E-01	9.99E-01	0.	0.
9.86E-01	0.198	4.65E 01	9.92E-01	9.83E-01	9.28E-02	9.29E-02
9.62E-01	0.396	4.59E 01	9.79E-01	9.58E-01	1.86E-01	1.86E-01
9.30E-01	0.593	4.51E 01	9.62E-01	9.25E-01	2.78E-01	2.79E-01
8.42E-01	0.989	4.28E 01	9.12E-01	8.32E-01	4.64E-01	4.64E-01
7.16E-01	1.385	3.94E 01	8.40E-01	7.05E-01	6.50E-01	6.50E-01
5.89E-01	1.780	3.55E 01	7.58E-01	5.74E-01	8.35E-01	8.36E-01
4.51E-01	2.176	3.09E 01	6.60E-01	4.35E-01	1.02E 00	1.02E 00
3.26E-01	2.571	2.61E 01	5.57E-01	3.10E-01	1.21E 00	1.21E 00
1.98E-01	2.967	2.02E 01	4.30E-01	1.85E-01	1.39E 00	1.39E 00
1.24E-01	3.363	1.58E 01	3.37E-01	1.13E-01	1.58E 00	1.58E 00
6.50E-02	3.758	1.13E 01	2.41E-01	5.79E-02	1.76E 00	1.76E 00
2.78E-02	4.154	7.24E 00	1.54E-01	2.38E-02	1.95E 00	1.95E 00
2.01E-03	4.549	1.58E 00	3.37E-02	1.14E-03	2.13E 00	2.14E 00

UCS = 4.69E 01, EMS = 5.51E 00, BS = 2.13E 00, ES= 3.55E 00,

EMSOMO = 2.49E 00, RATIOS = 8.74E-01, ESOEO = 3.30E-01

30 1.00 2 2 0.10 17 6 64 2

YS	TS	T	Q	CP	V	UOUC	VOUC
-5.000	-4.46	-4.04	3.70E-02	-8.65E-02	9.63E 00	2.69E-01	-1.90E-02
-4.500	-8.33	-11.53	5.12E-02	-9.81E-02	1.54E 01	3.11E-01	-6.34E-02
-4.000	-8.32	-16.52	7.48E-02	-1.08E-01	1.87E 01	3.68E-01	-1.09E-01
-3.500	-9.17	-17.57	1.11E-01	-1.08E-01	2.27E 01	4.44E-01	-1.42E-01
-3.000	-8.72	-17.20	1.56E-01	-1.15E-01	2.71E 01	5.33E-01	-1.65E-01
-2.500	-7.36	-15.56	2.19E-01	-1.18E-01	3.19E 01	6.31E-01	-1.76E-01
-2.000	-4.87	-13.17	3.08E-01	-1.46E-01	3.79E 01	7.58E-01	-1.77E-01
-1.500	-3.35	-11.85	3.79E-01	-1.48E-01	4.20E 01	8.45E-01	-1.77E-01
-1.000	-1.54	-10.04	4.55E-01	-1.44E-01	4.60E 01	9.31E-01	-1.65E-01
-0.500	0.39	-8.41	4.99E-01	-1.43E-01	4.82E 01	9.80E-01	-1.45E-01
0.	1.49	-7.01	5.19E-01	-1.43E-01	4.92E 01	1.00E 00	-1.23E-01
0.500	2.59	-5.91	4.98E-01	-1.38E-01	4.81E 01	9.84E-01	-1.02E-01
1.000	3.39	-5.11	4.38E-01	-1.31E-01	4.52E 01	9.24E-01	-8.27E-02
1.500	3.90	-4.80	3.65E-01	-1.19E-01	4.12E 01	8.44E-01	-6.80E-02
2.000	4.02	-4.48	2.75E-01	-1.12E-01	3.58E 01	7.33E-01	-5.74E-02
2.500	3.12	-5.38	1.77E-01	-1.00E-01	2.87E 01	5.87E-01	-5.53E-02
3.000	1.95	-6.55	1.24E-01	-8.46E-02	2.40E 01	4.91E-01	-5.63E-02
3.500	-1.72	-10.22	6.80E-02	-7.31E-02	1.78E 01	3.65E-01	-6.49E-02
4.000	-14.40	-22.90	3.13E-02	-5.77E-02	1.21E 01	2.28E-01	-9.65E-02
4.500	-19.94	-28.44	2.71E-02	-5.19E-02	1.12E 01	2.03E-01	-1.10E-01
5.000	-26.98	-35.48	1.99E-02	-4.04E-02	9.63E 00	1.61E-01	-1.15E-01

UC = 4.87E 01, EM = 6.19E 00, B = 2.29E 00, E=, 3.76E 00,

EMOM = 2.92E 00, RATIO = 1.04E 00, EOEO = 4.03E-01

LOUCSC	XI	US	USOUC	USOUCS	Y/B	XIOBS
7.24E-02	-4.945	1.37E 01	2.78E-01	7.71E-02	-2.18E 00	-2.17E 00
5.66E-02	-4.451	1.60E 01	3.25E-01	1.06E-01	-1.96E 00	-1.96E 00
1.35E-01	-3.956	1.90E 01	3.86E-01	1.49E-01	-1.75E 00	-1.74E 00
1.97E-01	-3.462	2.28E 01	4.64E-01	2.16E-01	-1.53E 00	-1.52E 00
2.84E-01	-2.967	2.71E 01	5.51E-01	3.04E-01	-1.31E 00	-1.30E 00
3.99E-01	-2.473	3.18E 01	6.47E-01	4.19E-01	-1.09E 00	-1.09E 00
5.74E-01	-1.978	3.78E 01	7.68E-01	5.90E-01	-8.73E-01	-8.70E-01
7.14E-01	-1.484	4.19E 01	8.52E-01	7.25E-01	-6.55E-01	-6.52E-01
8.67E-01	-0.989	4.59E 01	9.33E-01	8.71E-01	-4.37E-01	-4.35E-01
9.61E-01	-0.495	4.82E 01	9.79E-01	9.58E-01	-2.18E-01	-2.17E-01
1.01E 00	0.	4.92E 01	9.99E-01	9.98E-01	0.	0.
9.68E-01	0.495	4.81E 01	9.78E-01	9.57E-01	2.18E-01	2.17E-01
8.54E-01	0.989	4.51E 01	9.17E-01	8.42E-01	4.37E-01	4.35E-01
7.13E-01	1.484	4.12E 01	8.37E-01	7.00E-01	6.55E-01	6.52E-01
5.37E-01	1.978	3.56E 01	7.24E-01	5.25E-01	8.73E-01	8.70E-01
3.45E-01	2.473	2.85E 01	5.79E-01	3.35E-01	1.09E 00	1.09E 00
2.41E-01	2.967	2.37E 01	4.82E-01	2.32E-01	1.31E 00	1.30E 00
1.29E-01	3.462	1.73E 01	3.52E-01	1.24E-01	1.53E 00	1.52E 00
5.21E-02	3.956	1.11E 01	2.27E-01	5.13E-02	1.75E 00	1.74E 00
4.12E-02	4.451	9.97E 00	2.03E-01	4.11E-02	1.96E 00	1.96E 00
2.60E-02	4.945	8.06E 00	1.63E-01	2.65E-02	2.18E 00	2.17E 00

UCS = 4.92E 01, EMS = 6.14E 00, BS = 2.27E 00, ES= 9.73E 00,

EMSOMO = 2.93E 00, RATIOS = 1.03E 00, ESOEO = 4.03E-01

30 2.00 2 2 0.10 26 4 64 1

YS	TS	T	Q	CP	V	UOUC	VOUC
-4.900	-19.33	-27.83	1.10E-01	-9.51E-02	1.12E 01	3.90E-01	-2.06E-01
-4.500	-15.98	-24.48	1.27E-01	-9.90E-02	2.44E 01	4.32E-01	-1.97E-01
-4.100	-13.54	-22.04	1.59E-01	-9.80E-02	2.73E 01	4.93E-01	-2.00E-01
-3.700	-12.62	-21.12	1.94E-01	-9.32E-02	3.01E 01	5.47E-01	-2.11E-01
-3.300	-10.79	-19.29	2.24E-01	-9.35E-02	3.23E 01	5.95E-01	-2.08E-01
-2.900	-9.57	-18.07	2.71E-01	-8.90E-02	3.56E 01	6.60E-01	-2.15E-01
-2.500	-8.23	-16.73	3.29E-01	-8.42E-02	3.92E 01	7.31E-01	-2.20E-01
-2.100	-7.01	-15.51	3.82E-01	-8.16E-02	4.22E 01	7.93E-01	-2.20E-01
-1.700	-5.67	-14.17	4.63E-01	-1.10E-01	4.65E 01	8.79E-01	-2.22E-01
-1.300	-4.33	-12.83	5.11E-01	-1.06E-01	4.89E 01	9.29E-01	-2.11E-01
-0.900	-2.99	-11.49	5.48E-01	-1.05E-01	5.06E 01	9.66E-01	-1.96E-01
-0.700	-2.26	-10.76	5.61E-01	-1.06E-01	5.12E 01	9.80E-01	-1.86E-01
-0.500	-1.65	-10.15	5.71E-01	-1.06E-01	5.16E 01	9.91E-01	-1.77E-01
-0.300	-1.04	-9.54	5.71E-01	-1.06E-01	5.16E 01	9.93E-01	-1.67E-01
-0.100	-0.43	-8.93	5.76E-01	-1.06E-01	5.19E 01	9.99E-01	-1.57E-01
0.	0.	-8.50	5.76E-01	-1.07E-01	5.19E 01	1.00E 00	-1.50E-01
0.100	0.43	-8.07	5.77E-01	-1.07E-01	5.19E 01	1.00E 00	-1.42E-01
0.300	1.04	-7.46	5.64E-01	-1.06E-01	5.13E 01	9.92E-01	-1.30E-01
0.700	2.26	-6.24	5.23E-01	-9.98E-02	4.94E 01	9.57E-01	-1.05E-01
1.100	3.72	-4.78	4.73E-01	-9.18E-02	4.70E 01	9.13E-01	-7.63E-02
1.500	4.82	-3.68	4.01E-01	-8.85E-02	4.33E 01	8.42E-01	-5.42E-02
1.900	5.91	-2.59	3.36E-01	-7.99E-02	3.96E 01	7.71E-01	-3.48E-02
2.300	6.52	-1.98	2.73E-01	-7.12E-02	3.57E 01	6.96E-01	-2.40E-02
2.700	7.87	-0.63	2.11E-01	-6.25E-02	3.14E 01	6.12E-01	-6.77E-03
3.100	7.99	-0.51	1.42E-01	-5.56E-02	2.58E 01	5.02E-01	-4.49E-03
3.500	7.99	-0.51	1.07E-01	-4.69E-02	2.24E 01	4.36E-01	-3.90E-03
3.900	7.99	-0.51	7.70E-02	-3.82E-02	1.90E 01	3.70E-01	-3.30E-03
4.300	7.99	-0.51	5.90E-02	-3.30E-02	1.66E 01	3.24E-01	-2.89E-03
4.700	7.99	-0.51	4.60E-02	-2.78E-02	1.47E 01	2.86E-01	-2.55E-03
5.100	6.77	-1.73	3.30E-02	-2.26E-02	1.24E 01	2.42E-01	-7.31E-03
5.400	5.06	-3.44	2.70E-02	-2.26E-02	1.12E 01	2.19E-01	-1.31E-02

UC = 5.13E 01, EM = 6.88E 00, B = 2.61E 00, E=, 4.35E 00,

EMOM = 3.41E 00, RATIO = 1.31E 00, EDEO = 5.43E-01

UOUCSQ	XI	US	USOUC	USOUCS	Y/B	XIOBS
1.52E-01	-4.846	2.20E 01	4.23E-01	1.79E-01	-1.88E 00	-1.86E 00
1.87E-01	-4.451	2.40E 01	4.62E-01	2.13E-01	-1.73E 00	-1.71E 00
2.43E-01	-4.055	2.70E 01	5.21E-01	2.71E-01	-1.57E 00	-1.56E 00
2.99E-01	-3.659	2.97E 01	5.73E-01	3.28E-01	-1.42E 00	-1.41E 00
3.54E-01	-3.264	3.20E 01	6.18E-01	3.82E-01	-1.27E 00	-1.26E 00
4.35E-01	-2.868	3.53E 01	6.80E-01	4.62E-01	-1.11E 00	-1.10E 00
5.35E-01	-2.473	3.88E 01	7.49E-01	5.61E-01	-9.58E-01	-9.51E-01
6.30E-01	-2.077	4.19E 01	8.08E-01	6.53E-01	-8.05E-01	-7.99E-01
7.73E-01	-1.681	4.62E 01	8.91E-01	7.94E-01	-6.52E-01	-6.47E-01
8.62E-01	-1.286	4.86E 01	9.38E-01	8.79E-01	-4.98E-01	-4.95E-01
9.34E-01	-0.890	5.04E 01	9.72E-01	9.45E-01	-3.45E-01	-3.42E-01
9.61E-01	-0.692	5.11E 01	9.85E-01	9.70E-01	-2.68E-01	-2.66E-01
9.82E-01	-0.495	5.16E 01	9.94E-01	9.88E-01	-1.92E-01	-1.90E-01
9.86E-01	-0.297	5.16E 01	9.95E-01	9.90E-01	-1.15E-01	-1.14E-01
9.98E-01	-0.099	5.19E 01	1.00E 00	1.00E 00	-3.83E-02	-3.80E-02
1.00E 00	0.	5.19E 01	1.00E 00	1.00E 00	0.	0.
1.00E 00	0.099	5.19E 01	1.00E 00	1.00E 00	3.83E-02	3.80E-02
9.84E-01	0.297	5.19E 01	9.90E-01	9.80E-01	1.15E-01	1.14E-01
9.16E-01	0.692	4.94E 01	9.53E-01	9.08E-01	2.68E-01	2.66E-01
8.33E-01	1.088	4.70E 01	9.06E-01	8.20E-01	4.22E-01	4.18E-01
7.09E-01	1.484	4.32E 01	8.33E-01	6.94E-01	5.75E-01	5.71E-01
5.95E-01	1.879	3.94E 01	7.60E-01	5.78E-01	7.28E-01	7.23E-01
4.84E-01	2.275	3.54E 01	6.83E-01	4.67E-01	8.82E-01	8.75E-01
3.74E-01	2.671	3.10E 01	5.97E-01	3.57E-01	1.04E 00	1.03E 00
2.52E-01	3.066	2.53E 01	4.87E-01	2.38E-01	1.19E 00	1.18E 00
1.90E-01	3.462	2.18E 01	4.21E-01	1.77E-01	1.34E 00	1.33E 00
1.37E-01	3.857	1.84E 01	3.54E-01	1.25E-01	1.50E 00	1.48E 00
1.05E-01	4.253	1.59E 01	3.07E-01	9.44E-02	1.65E 00	1.64E 00
8.16E-02	4.648	1.39E 01	2.69E-01	7.23E-02	1.80E 00	1.79E 00
5.85E-02	5.044	1.17E 01	2.26E-01	5.11E-02	1.96E 00	1.94E 00
4.77E-02	5.341	1.06E 01	2.04E-01	4.16E-02	2.07E 00	2.05E 00

UCS = 5.19E 01, EMS = 6.83E 00, BS = 2.60E 00, ES= 4.33E 00,

EMSOMO = 3.42E 00, RATIOS = 1.31E 00, ESOEO = 5.46E-01

30 2.50 2 2 0.10 17 6 64 2

YS	TS	T	Q	CP	V	UOUC	VOUC
-7.250	12.43	3.93	3.80E-02	-5.61E-02	-0.	2.60E-01	1.79E-02
-6.750	-0.27	-8.77	4.40E-02	-6.32E-02	1.43E 01	2.78E-01	-4.28E-02
-6.250	-9.39	-17.89	5.51E-02	-6.76E-02	1.60E 01	2.99E-01	-9.65E-02
-5.750	-12.61	-21.11	7.23E-02	-6.83E-02	1.83E 01	3.36E-01	-1.30E-01
-5.250	-11.27	-19.77	9.67E-02	-7.53E-02	2.12E 01	3.92E-01	-1.41E-01
-4.750	-11.48	-19.98	1.21E-01	-7.77E-02	2.37E 01	4.37E-01	-1.59E-01
-4.250	-9.73	-18.23	1.54E-01	-8.06E-02	2.68E 01	4.99E-01	-1.64E-01
-3.750	-8.65	-17.15	1.83E-01	-8.26E-02	2.92E 01	5.48E-01	-1.69E-01
-3.250	-7.82	-16.32	2.36E-01	-8.05E-02	3.31E 01	6.24E-01	-1.83E-01
-2.750	-10.10	-18.60	2.90E-01	-6.54E-02	3.67E 01	6.83E-01	-2.30E-01
-2.250	-7.49	-15.99	3.55E-01	-6.67E-02	4.07E 01	7.67E-01	-2.20E-01
-1.750	-5.06	-13.56	4.42E-01	-9.62E-02	4.54E 01	8.66E-01	-2.09E-01
-1.250	-3.56	-12.06	4.95E-01	-9.07E-02	4.80E 01	9.21E-01	-1.97E-01
-0.750	-2.11	-10.61	5.41E-01	-8.98E-02	5.02E 01	9.68E-01	-1.81E-01
-0.250	-0.71	-9.21	5.70E-01	-8.82E-02	5.15E 01	9.98E-01	-1.62E-01
0.250	0.84	-7.66	5.67E-01	-8.22E-02	5.14E 01	9.99E-01	-1.34E-01
0.750	-0.66	-9.16	5.35E-01	-7.85E-02	4.99E 01	9.67E-01	-1.56E-01
1.250	3.77	-4.73	4.74E-01	-7.70E-02	4.70E 01	9.19E-01	-7.60E-02
1.750	5.21	-3.29	4.04E-01	-7.37E-02	4.34E 01	8.50E-01	-4.89E-02
2.250	7.01	-1.49	3.28E-01	-6.67E-02	3.91E 01	7.67E-01	-2.00E-02
2.750	9.05	0.55	2.55E-01	-6.14E-02	3.45E 01	6.76E-01	6.48E-03
3.250	9.92	1.42	1.97E-01	-5.61E-02	3.03E 01	5.94E-01	1.47E-02
3.750	13.26	4.76	1.47E-01	-4.74E-02	2.62E 01	5.12E-01	4.26E-02
4.250	17.75	9.25	1.06E-01	-3.68E-02	2.22E 01	4.30E-01	7.01E-02
4.750	21.80	13.30	8.12E-02	-2.98E-02	1.94E 01	3.71E-01	8.78E-02
5.250	25.36	16.86	6.62E-02	-2.26E-02	1.75E 01	3.30E-01	9.99E-02
5.750	28.36	19.86	5.06E-02	-2.39E-02	1.53E 01	2.83E-01	1.02E-01
6.250	31.09	22.59	3.57E-02	-2.28E-02	1.29E 01	2.34E-01	9.73E-02

UC = 5.09E 01, EM = 8.34E 00, B = 2.98E 00, E=, 4.80E 00,

EMOM = 4.12E 00, RATIO = 1.48E 00, EOEO = 5.90E-01

UOUCSQ	XI	US	USOUC	USOUCS	Y/B	XIOBS
6.78E-02	-7.170	1.35E 01	2.62E-01	6.89E-02	-2.43E 00	-2.43E 00
7.71E-02	-6.676	1.49E 01	2.89E-01	8.35E-02	-2.27E 00	-2.26E 00
8.94E-02	-6.181	1.64E 01	3.18E-01	1.01E-01	-2.10E 00	-2.10E 00
1.13E-01	-5.687	1.85E 01	3.59E-01	1.29E-01	-1.93E 00	-1.93E 00
1.54E-01	-5.192	2.13E 01	4.14E-01	1.72E-01	-1.76E 00	-1.76E 00
1.91E-01	-4.698	2.37E 01	4.59E-01	2.11E-01	-1.60E 00	-1.59E 00
2.49E-01	-4.203	2.68E 01	5.19E-01	2.70E-01	-1.43E 00	-1.43E 00
3.00E-01	-3.709	2.91E 01	5.66E-01	3.20E-01	-1.26E 00	-1.26E 00
3.89E-01	-3.214	3.29E 01	6.39E-01	4.09E-01	-1.09E 00	-1.09E 00
4.67E-01	-2.720	3.62E 01	7.02E-01	4.93E-01	-9.23E-01	-9.22E-01
5.89E-01	-2.225	4.03E 01	7.82E-01	6.11E-01	-7.56E-01	-7.55E-01
7.50E-01	-1.731	4.51E 01	8.76E-01	7.67E-01	-5.88E-01	-5.87E-01
8.49E-01	-1.235	4.78E 01	9.28E-01	8.61E-01	-4.20E-01	-4.19E-01
9.38E-01	-0.742	5.01E 01	9.72E-01	9.45E-01	-2.52E-01	-2.52E-01
9.97E-01	-0.247	5.15E 01	10.00E-01	9.99E-01	-8.40E-02	-8.38E-02
9.99E-01	0.247	5.14E 01	9.98E-01	9.95E-01	8.40E-02	8.38E-02
9.35E-01	0.742	5.01E 01	9.70E-01	9.41E-01	2.52E-01	2.52E-01
8.44E-01	1.236	4.78E 01	9.12E-01	8.31E-01	4.20E-01	4.19E-01
7.22E-01	1.731	4.33E 01	8.40E-01	7.06E-01	5.88E-01	5.87E-01
5.88E-01	2.225	3.88E 01	7.54E-01	5.68E-01	7.56E-01	7.55E-01
4.57E-01	2.720	3.40E 01	6.60E-01	4.36E-01	9.23E-01	9.22E-01
3.53E-01	3.214	2.97E 01	5.77E-01	3.32E-01	1.09E 00	1.09E 00
2.62E-01	3.709	2.52E 01	4.90E-01	2.40E-01	1.26E 00	1.26E 00
1.85E-01	4.203	2.08E 01	4.04E-01	1.63E-01	1.43E 00	1.43E 00
1.38E-01	4.698	1.76E 01	3.42E-01	1.17E-01	1.60E 00	1.59E 00
1.09E-01	5.192	1.53E 01	2.98E-01	8.86E-02	1.76E 00	1.76E 00
8.02E-02	5.687	1.29E 01	2.51E-01	6.30E-02	1.93E 00	1.93E 00
5.46E-02	6.181	1.05E 01	2.03E-01	4.12E-02	2.10E 00	2.10E 00

UCS = 5.15E 01, EMS = 8.23E 00, BS = 2.95E 00, ES= 4.76E 00,

EMSOMO = 4.11E 00, RATIOS = 1.47E 00, ESOEO = 5.91E-01

15 2.00 2 1 0.0 28 6 64 1

YS	TS	T	Q	CP	V	UOUC	VOUC	Y/B
-3.050	19.51	19.51	1.30E-02	-2.45E-02	1.13E 01	1.00E-01	3.56E-02	-2.46E 00
-2.800	10.37	10.37	2.00E-02	-3.06E-02	9.74E 00	1.30E-01	2.38E-02	-2.26E 00
-2.550	3.05	3.05	4.30E-02	-3.76E-02	1.43E 01	1.94E-01	1.03E-02	-2.06E 00
-2.300	-3.05	-3.05	8.00E-02	-4.63E-02	1.95E 01	2.64E-01	-1.41E-02	-1.86E 00
-2.050	-5.61	-5.61	1.25E-01	-5.41E-02	2.43E 01	3.29E-01	-3.23E-02	-1.66E 00
-1.800	-6.10	-6.10	2.07E-01	-6.29E-02	3.13E 01	4.23E-01	-4.52E-02	-1.45E 00
-1.550	-6.10	-6.10	3.15E-01	-6.99E-02	3.86E 01	5.22E-01	-5.57E-02	-1.26E 00
-1.300	-6.10	-6.10	4.63E-01	-7.67E-02	4.66E 01	6.33E-01	-6.35E-02	-1.05E 00
-1.050	-4.88	-4.88	6.41E-01	-7.48E-02	5.51E 01	7.46E-01	-6.05E-02	-8.48E-01
-0.800	-3.78	-3.78	7.96E-01	-8.41E-02	6.14E 01	8.32E-01	-5.50E-02	-6.46E-01
-0.550	-2.80	-2.80	9.87E-01	-8.51E-02	6.84E 01	9.28E-01	-4.54E-02	-4.44E-01
-0.300	-1.46	-1.46	1.10E 00	-8.63E-02	7.22E 01	9.79E-01	-2.50E-02	-2.42E-01
-0.050	0.	0.	1.14E 00	-8.73E-02	7.37E 01	1.00E 00	0.	-4.04E-02
0.200	1.34	1.34	1.14E 00	-8.63E-02	7.36E 01	9.99E-01	2.34E-02	1.62E-01
0.450	2.80	2.80	1.03E 00	-8.50E-02	7.00E 01	9.48E-01	4.65E-02	3.63E-01
0.700	4.02	4.02	8.66E-01	-8.39E-02	6.41E 01	8.68E-01	6.10E-02	5.65E-01
0.950	5.24	5.24	6.91E-01	-7.95E-02	5.72E 01	7.74E-01	7.10E-02	7.67E-01
1.200	5.61	5.61	5.42E-01	-7.56E-02	5.07E 01	6.84E-01	6.72E-02	9.69E-01
1.450	6.10	6.10	4.00E-01	-6.99E-02	4.36E 01	5.88E-01	6.28E-02	1.17E 00
1.700	6.10	6.10	2.74E-01	-6.46E-02	3.60E 01	4.86E-01	5.20E-02	1.37E 00
1.950	5.49	5.49	1.83E-01	-5.50E-02	2.95E 01	3.98E-01	3.82E-02	1.58E 00
2.200	3.41	3.41	1.20E-01	-4.80E-02	2.39E 01	3.23E-01	1.93E-02	1.78E 00
2.450	0.	0.	7.60E-02	-3.84E-02	1.90E 01	2.58E-01	0.	1.98E 00
2.700	-7.32	-7.32	5.50E-02	-3.23E-02	1.61E 01	2.17E-01	-2.79E-02	2.18E 00
2.950	-14.63	-14.63	4.30E-02	-2.62E-02	1.43E 01	1.88E-01	-4.90E-02	2.38E 00
3.200	-21.95	-21.95	3.40E-02	-2.18E-02	1.27E 01	1.60E-01	-6.44E-02	2.58E 00
3.450	-29.27	-29.27	2.70E-02	-1.75E-02	1.13E 01	1.34E-01	-7.51E-02	2.79E 00

UC = 7.37E 01, EM = 3.50E 00, B = 1.24E 00, E=, 2.01E 00,

EMOM = 2.47E 00, RATIO = 1.23E 00, E[illegible]0 = 7.06E-01

15 2.00 2 3 0.0 30 6 64 1

YS	TS	T	Q	CP	V	UOUC	VOUC	Y/B
-3.000	20.12	20.12	1.50E-02	-2.11E-02	1.08E 01	1.06E-01	3.87E-02	-2.59E 00-
-2.750	12.80	12.80	3.10E-02	-3.13E-02	1.21E 01	1.58E-01	3.59E-02	-2.38E 00-
-2.500	2.44	2.44	4.40E-02	-3.29E-02	1.44E 01	1.93E-01	8.20E-03	-2.16E 00-
-2.250	-3.05	-3.05	6.20E-02	-3.97E-02	1.71E 01	2.29E-01	-1.22E-02	-1.95E 00-
-2.000	-5.98	-5.98	1.26E-01	-4.73E-02	2.43E 01	3.24E-01	-3.40E-02	-1.73E 00-
-1.750	-6.71	-6.71	2.07E-01	-5.66E-02	3.12E 01	4.15E-01	-4.88E-02	-1.51E 00-
-1.500	-7.01	-7.01	3.10E-01	-6.33E-02	3.81E 01	5.08E-01	-6.25E-02	-1.30E 00-
-1.250	-6.46	-6.46	4.45E-01	-6.75E-02	4.57E 01	6.09E-01	-6.90E-02	-1.08E 00-
-1.000	-5.85	-5.85	6.22E-01	-6.93E-02	5.40E 01	7.21E-01	-7.39E-02	-8.65E-01-
-0.750	-5.00	-5.00	8.03E-01	-6.98E-02	6.14E 01	8.20E-01	-7.18E-02	-6.48E-01-
-0.500	-3.90	-3.90	9.94E-01	-6.99E-02	6.83E 01	9.14E-01	-6.24E-02	-4.32E-01-
-0.250	-2.68	-2.68	1.12E 00	-7.04E-02	7.26E 01	9.73E-01	-4.56E-02	-2.16E-01
0.	-1.22	-1.22	1.18E 00	-7.09E-02	7.45E 01	10.00E-01	-2.13E-02	0.
0.250	0.	0.	1.14E 00	-6.93E-02	7.32E 01	9.82E-01	0.	2.16E-01
0.500	1.59	1.59	1.02E 00	-6.91E-02	6.92E 01	9.29E-01	2.57E-02	4.32E-01
0.750	2.68	2.68	8.52E-01	-6.89E-02	6.32E 01	8.47E-01	3.97E-02	6.48E-01
1.000	3.41	3.41	6.52E-01	-6.90E-02	5.53E 01	7.41E-01	4.42E-02	8.65E-01
1.250	4.15	4.15	4.80E-01	-6.75E-02	4.74E 01	6.35E-01	4.60E-02	1.08E 00
1.500	4.39	4.39	3.36E-01	-6.42E-02	3.97E 01	5.31E-01	4.08E-02	1.30E 00
1.750	4.02	4.02	2.20E-01	-5.91E-02	3.21E 01	4.30E-01	3.03E-02	1.51E 00
2.000	3.05	3.05	1.41E-01	-5.15E-02	2.57E 01	3.45E-01	1.84E-02	1.73E 00
2.250	1.22	1.22	8.50E-02	-4.48E-02	2.00E 01	2.68E-01	5.70E-03	1.95E 00
2.500	-3.66	-3.66	5.90E-02	-3.72E-02	1.66E 01	2.23E-01	-1.42E-02	2.16E 00
2.750	-9.76	-9.76	4.70E-02	-3.13E-02	1.48E 01	1.96E-01	-3.38E-02	2.38E 00
3.000	-17.68	-17.68	2.50E-02	-2.53E-02	1.08E 01	1.38E-01	-4.41E-02	2.59E 00

UC = 7.45E 01, EM = 3.28E 00, E = 1.16E 00, E=, 1.86E 00,

EMOM = 2.38E 00, RATIO = 1.22E 00, EQEO = 3.11E-01

15 0.0 2 2 0.0 3 6 64 1

YS	TS	T	Q	CP	V	UOUC	VOUC	Y/B
-2.475	3.90	3.90	2.00E-02	-3.25E-02	1.01E 01	1.30E-01	8.90E-03	-2.22E 00
-2.275	-0.37	-0.37	4.40E-02	-3.76E-02	1.43E 01	1.94E-01	-1.24E-03	-2.04E 00
-2.075	-3.41	-3.41	8.60E-02	-4.79E-02	1.99E 01	2.71E-01	-1.62E-02	-1.86E 00
-1.875	-4.39	-4.39	1.39E-01	-5.47E-02	2.54E 01	3.44E-01	-2.64E-02	-1.68E 00
-1.675	-4.88	-4.88	2.12E-01	-6.16E-02	3.13E 01	4.24E-01	-3.62E-02	-1.50E 00
-1.475	-5.00	-5.00	3.01E-01	-6.93E-02	3.73E 01	5.05E-01	-4.42E-02	-1.32E 00
-1.275	-5.00	-5.00	4.27E-01	-7.44E-02	4.44E 01	6.02E-01	-5.27E-02	-1.14E 00
-1.075	-4.39	-4.39	5.63E-01	-7.93E-02	5.10E 01	6.92E-01	-5.31E-02	-9.64E-01
-0.875	-3.78	-3.78	7.30E-01	-8.42E-02	5.81E 01	7.89E-01	-5.21E-02	-7.85E-01
-0.675	-3.05	-3.05	8.73E-01	-8.42E-02	6.35E 01	8.63E-01	-4.60E-02	-6.05E-01
-0.475	-2.32	-2.32	1.00E 00	-8.44E-02	6.81E 01	9.26E-01	-3.75E-02	-4.26E-01
-0.275	-1.22	-1.22	1.11E 00	-8.46E-02	7.17E 01	9.75E-01	-2.08E-02	-2.47E-01
-0.075	-0.37	-0.37	1.16E 00	-8.47E-02	7.34E 01	9.98E-01	-6.37E-03	-6.73E-02
0.125	0.73	0.73	1.15E 00	-8.47E-02	7.30E 01	9.93E-01	1.27E-02	1.12E-01
0.325	1.95	1.95	1.08E 00	-8.36E-02	7.08E 01	9.62E-01	3.28E-02	2.91E-01
0.525	2.93	2.93	9.72E-01	-8.33E-02	6.71E 01	9.11E-01	4.66E-02	4.71E-01
0.725	3.66	3.66	8.31E-01	-8.23E-02	6.20E 01	8.42E-01	5.38E-02	6.50E-01
0.925	4.51	4.51	6.84E-01	-8.06E-02	5.62E 01	7.63E-01	6.02E-02	8.29E-01
1.125	5.00	5.00	5.37E-01	-7.84E-02	4.98E 01	6.75E-01	5.91E-02	1.01E 00
1.325	5.37	5.37	4.01E-01	-7.36E-02	4.31E 01	5.83E-01	5.48E-02	1.19E 00
1.525	5.24	5.24	2.83E-01	-6.67E-02	3.62E 01	4.90E-01	4.50E-02	1.37E 00
1.725	5.12	5.12	2.04E-01	-5.90E-02	3.07E 01	4.16E-01	3.73E-02	1.55E 00
1.925	4.51	4.51	1.32E-01	-5.30E-02	2.47E 01	3.35E-01	2.64E-02	1.73E 00
2.125	2.68	2.68	7.80E-02	-4.53E-02	1.90E 01	2.58E-01	1.21E-02	1.91E 00
2.325	0.85	0.85	4.50E-02	-3.85E-02	1.44E 01	1.96E-01	2.92E-03	2.08E 00
2.525	-4.63	-4.63	2.20E-02	-3.17E-02	1.01E 01	1.37E-01	-1.11E-02	2.26E 00

UC = 7.35E 01, EM = 3.03E 00, E = 1.12E 00, E= 1.82E 00,

EMOM = 2.23E 00, RATIO = 1.21E 00, EOEO = 7.26E-01

15 2.00 2 2 0.0 3 6 64 1

YS	TS	Y	Q	CP	V	UOUC	VOUC	Y/B
-2.525	6.34	6.34	1.10E-02	-3.90E-02	7.75E 00	1.02E-01	1.13E-02	-2.34E 00
-2.325	0.24	0.24	3.00E-02	-4.75E-02	1.18E 01	1.69E-01	7.19E-04	-2.15E 00
-2.125	-3.41	-3.41	5.40E-02	-5.42E-02	1.56E 01	2.26E-01	-1.35E-02	-1.97E 00
-1.925	-4.63	-4.63	9.90E-02	-6.08E-02	2.14E 01	3.06E-01	-2.48E-02	-1.78E 00
-1.725	-5.24	-5.24	1.60E-01	-6.84E-02	2.72E 01	3.88E-01	-3.56E-02	-1.60E 00
-1.525	-5.12	-5.12	2.38E-01	-7.41E-02	3.32E 01	4.74E-01	-4.25E-02	-1.41E 00
-1.325	-4.82	-4.82	3.32E-01	-7.79E-02	3.92E 01	5.60E-01	-4.72E-02	-1.23E 00
-1.125	-4.27	-4.27	4.57E-01	-8.27E-02	4.60E 01	6.57E-01	-4.91E-02	-1.04E 00
-0.925	-3.66	-3.66	5.92E-01	-8.24E-02	5.23E 01	7.48E-01	-4.79E-02	-8.57E-01
-0.725	-3.11	-3.11	7.42E-01	-8.23E-02	5.86E 01	8.38E-01	-4.55E-02	-6.72E-01
-0.525	-2.26	-2.26	8.72E-01	-8.24E-02	6.35E 01	9.10E-01	-3.58E-02	-4.86E-01
-0.325	-1.46	-1.46	9.77E-01	-8.26E-02	6.72E 01	9.63E-01	-2.46E-02	-3.01E-01
-0.125	-0.49	-0.49	1.05E 00	-8.27E-02	6.96E 01	9.98E-01	-8.49E-03	-1.16E-01
0.075	0.24	0.24	1.05E 00	-8.27E-02	6.97E 01	10.00E-01	4.26E-03	6.95E-02
0.275	1.22	1.22	9.95E-01	-8.07E-02	6.78E 01	9.72E-01	2.07E-02	2.55E-01
0.475	2.20	2.20	8.95E-01	-8.05E-02	6.43E 01	9.22E-01	3.53E-02	4.40E-01
0.675	3.17	3.17	7.55E-01	-8.04E-02	5.91E 01	8.46E-01	4.68E-02	6.25E-01
0.875	3.90	3.90	6.30E-01	-8.04E-02	5.40E 01	7.72E-01	5.26E-02	8.10E-01
1.075	4.51	4.51	4.85E-01	-8.07E-02	4.73E 01	6.77E-01	5.34E-02	9.96E-01
1.275	5.12	5.12	3.61E-01	-7.70E-02	4.09E 01	5.83E-01	5.23E-02	1.18E 00
1.475	5.85	5.85	2.52E-01	-7.32E-02	3.41E 01	4.87E-01	4.99E-02	1.37E 00
1.675	5.61	5.61	1.65E-01	-6.65E-02	2.76E 01	3.94E-01	3.87E-02	1.55E 00
1.875	5.61	5.61	1.04E-01	-6.08E-02	2.19E 01	3.13E-01	3.07E-02	1.74E 00
2.075	4.76	4.76	5.70E-02	-5.42E-02	1.62E 01	2.32E-01	1.93E-02	1.92E 00
2.275	2.56	2.56	3.00E-02	-4.75E-02	1.18E 01	1.69E-01	7.55E-03	2.11E 00
2.475	-7.07	-7.07	1.30E-02	-4.09E-02	7.75E 00	1.10E-01	-1.37E-02	2.29E 00

UC = 6.97E 01, EM = 2.94E 00, B = 1.08E 00, E=, 1.77E 00,

EMOM = 2.05E 00, RATIO = 1.05E 00, EOEO = 6.01E-01

15 0. 2 2 0.20 1 6 64 1

YS	TS	T	Q	CP	V	UDUC	VDUC
-3.000	6.52	-9.68	8.00E-03	-3.92E-02	4.30E 00	8.77E-02	-1.49E-02
-2.800	1.04	-15.16	2.30E-02	-4.38E-02	1.03E 01	1.46E-01	-3.94E-02
-2.600	-4.09	-20.29	5.42E-02	-5.30E-02	1.58E 01	2.17E-01	-8.02E-02
-2.400	-4.70	-20.90	8.64E-02	-6.05E-02	2.03E 01	2.73E-01	-1.04E-01
-2.200	-5.18	-21.38	1.32E-01	-6.53E-02	2.47E 01	3.36E-01	-1.32E-01
-2.000	-5.30	-21.50	1.90E-01	-6.87E-02	2.97E 01	4.04E-01	-1.59E-01
-1.800	-4.94	-21.14	2.64E-01	-7.32E-02	3.49E 01	4.77E-01	-1.84E-01
-1.600	-4.57	-20.77	3.59E-01	-7.70E-02	4.07E 01	5.57E-01	-2.11E-01
-1.400	-4.21	-20.41	4.63E-01	-7.78E-02	4.63E 01	6.34E-01	-2.36E-01
-1.200	-3.72	-19.92	5.79E-01	-7.81E-02	5.17E 01	7.11E-01	-2.58E-01
-1.000	-3.35	-19.55	7.05E-01	-7.76E-02	5.71E 01	7.87E-01	-2.79E-01
-0.800	-2.50	-18.70	8.32E-01	-8.37E-02	6.20E 01	8.59E-01	-2.91E-01
-0.600	-2.01	-18.21	9.55E-01	-7.78E-02	6.64E 01	9.23E-01	-3.04E-01
-0.400	-1.16	-17.36	1.04E 00	-7.92E-02	6.94E 01	9.69E-01	-3.03E-01
-0.200	-0.43	-16.63	1.10E 00	-8.27E-02	7.12E 01	9.98E-01	-2.98E-01
-0.	0.43	-15.77	1.10E 00	-8.89E-02	7.14E 01	1.01E 00	-2.84E-01
0.200	1.28	-14.92	1.09E 00	-1.19E-01	7.10E 01	1.00E 00	-2.68E-01
0.400	1.89	-14.31	1.01E 00	-1.14E-01	6.82E 01	9.67E-01	-2.47E-01
0.600	2.62	-13.58	8.94E-01	-1.10E-01	6.43E 01	9.14E-01	-2.21E-01
0.800	3.35	-12.85	7.45E-01	-1.05E-01	5.87E 01	8.37E-01	-1.91E-01
1.000	3.78	-12.42	6.11E-01	-9.64E-02	5.31E 01	7.59E-01	-1.67E-01
1.200	4.33	-11.87	4.79E-01	-9.21E-02	4.70E 01	6.73E-01	-1.42E-01
1.400	4.82	-11.38	3.62E-01	-8.11E-02	4.09E 01	5.86E-01	-1.18E-01
1.600	5.06	-11.14	2.62E-01	-7.20E-02	3.48E 01	4.99E-01	-9.83E-02
1.800	4.94	-11.26	1.76E-01	-6.29E-02	2.85E 01	4.09E-01	-8.15E-02
2.000	4.45	-11.75	1.13E-01	-5.29E-02	2.28E 01	3.27E-01	-6.81E-02
2.200	3.78	-12.42	6.90E-02	-4.47E-02	1.79E 01	2.55E-01	-5.62E-02
2.400	-0.79	-16.99	3.10E-02	-3.01E-02	1.20E 01	1.67E-01	-5.12E-02
2.600	-8.72	-24.92	1.40E-02	-2.37E-02	8.04E 00	1.07E-01	-4.96E-02
2.800	-27.01	-43.21	4.00E-03	-1.82E-02	4.30E 00	4.58E-02	-4.31E-02

UC = 6.84E 01, EM = 3.37E 00, σ = 1.25E 00, E= 2.07E 00,

EMOM = 2.24E 00, RATIO = 1.19E 00, EOEO = 6.54E-01

UOUCSQ	XI	US	USOUC	USOUCS	Y/B	XIOBS
7.68E-03	-2.881	7.51E 00	1.05E-01	1.11E-02	-2.40E 00	-2.39E 00
2.12E-02	-2.689	1.19E 01	1.67E-01	2.78E-02	-2.24E 00	-2.23E 00
4.71E-02	-2.497	1.74E 01	2.44E-01	5.97E-02	-2.08E 00	-2.07E 00
7.45E-02	-2.305	2.15E 01	3.02E-01	9.12E-02	-1.92E 00	-1.91E 00
1.13E-01	-2.113	2.61E 01	3.66E-01	1.34E-01	-1.76E 00	-1.75E 00
1.63E-01	-1.921	3.06E 01	4.33E-01	1.88E-01	-1.60E 00	-1.60E 00
2.27E-01	-1.729	3.59E 01	5.04E-01	2.54E-01	-1.44E 00	-1.44E 00
3.11E-01	-1.536	4.14E 01	5.82E-01	3.39E-01	-1.28E 00	-1.28E 00
4.02E-01	-1.344	4.67E 01	6.56E-01	4.30E-01	-1.12E 00	-1.12E 00
5.06E-01	-1.152	5.19E 01	7.29E-01	5.31E-01	-9.60E-01	-9.57E-01
6.19E-01	-0.960	5.7 E 01	8.01E-01	6.42E-01	-8.00E-01	-7.98E-01
7.38E-01	-0.768	6.18E 01	8.69E-01	7.54E-01	-6.40E-01	-6.38E-01
8.52E-01	-0.575	6.62E 01	9.30E-01	8.65E-01	-4.80E-01	-4.79E-01
9.38E-01	-0.384	6.92E 01	9.72E-01	9.45E-01	-3.20E-01	-3.19E-01
9.96E-01	-0.192	7.11E 01	9.99E-01	9.98E-01	-1.60E-01	-1.60E-01
1.01E 00	-0.	7.14E 01	1.00E 00	1.01E 00	-0.	-0.
1.01E 00	0.192	7.11E 01	9.99E-01	9.98E-01	1.60E-01	1.60E-01
9.36E-01	0.384	6.84E 01	9.60E-01	9.22E-01	3.20E-01	3.19E-01
8.35E-01	0.576	6.43E 01	9.04E-01	8.17E-01	4.80E-01	4.79E-01
7.00E-01	0.768	5.87E 01	8.24E-01	6.79E-01	6.40E-01	6.38E-01
5.76E-01	0.960	5.29E 01	7.44E-01	5.53E-01	8.00E-01	7.98E-01
4.54E-01	1.152	4.66E 01	6.55E-01	4.29E-01	9.60E-01	9.57E-01
3.44E-01	1.344	4.02E 01	5.65E-01	3.19E-01	1.12E 00	1.12E 00
2.49E-01	1.536	3.38E 01	4.75E-01	2.26E-01	1.28E 00	1.28E 00
1.67E-01	1.729	2.73E 01	3.84E-01	1.47E-01	1.44E 00	1.44E 00
1.07E-01	1.921	2.15E 01	3.01E-01	9.09E-02	1.60E 00	1.60E 00
6.51E-02	2.113	1.63E 01	2.29E-01	5.26E-02	1.76E 00	1.75E 00
2.80E-02	2.305	1.04E 01	1.46E-01	2.12E-02	1.92E 00	1.91E 00
1.14E-02	2.497	6.34E 00	8.90E- 2	7.92E-03	2.08E 00	2.07E 00
2.10E-03	2.689	2.20E 00	3.18E-02	1.01E-03	2.24E 00	2.23E 00

UCS = 7.12E 01, EMS = 3.25E 00, BS = 1.20E 00, ES= 1.99E 00,

EMSOMO = 2.24E 00, RATIOS = 1.15E 00, ESOEO = 6.55E-01

15 2.00 2 2 0.20 2 6 64 1

YS	TS	T	Q	CP	V	UOUC	VOUC
-3.600	3.78	-12.42	5.20E-02	-4.92E-02	8.03E 00	2.14E-01	-4.70E-02
-3.200	2.26	-13.94	7.00E-02	-6.11E-02	1.80E 01	2.46E-01	-6.11E-02
-3.000	-0.85	-17.05	8.64E-02	-6.65E-02	1.99E 01	2.69E-01	-8.27E-02
-2.800	-2.93	-19.13	1.11E-01	-7.29E-02	2.26E 01	3.02E-01	-1.05E-01
-2.600	-3.90	-20.10	1.44E-01	-7.95E-02	2.57E 01	3.41E-01	-1.25E-01
-2.400	-4.88	-21.08	1.79E-01	-8.53E-02	2.87E 01	3.78E-01	-1.46E-01
-2.200	-5.49	-21.69	2.32E-01	-8.90E-02	3.27E 01	4.29E-01	-1.71E-01
-2.000	-5.73	-21.93	2.93E-01	-9.13E-02	3.67E 01	4.81E-01	-1.94E-01
-1.800	-5.61	-21.81	3.75E-01	-9.14E-02	4.15E 01	5.45E-01	-2.18E-01
-1.600	-5.37	-21.57	4.56E-01	-8.97E-02	4.58E 01	6.02E-01	-2.38E-01
-1.400	-5.00	-21.20	5.66E-01	-8.60E-02	5.11E 01	6.73E-01	-2.61E-01
-1.200	-4.70	-20.90	6.84E-01	-7.70E-02	5.61E 01	7.41E-01	-2.83E-01
-1.000	-4.02	-20.22	8.17E-01	-7.14E-02	6.14E 01	8.14E-01	-3.00E-01
-0.800	-3.11	-19.31	9.34E-01	-6.67E-02	6.56E 01	8.75E-01	-3.06E-01
-0.600	-2.32	-18.52	1.05E 00	-5.68E-02	6.95E 01	9.32E-01	-3.12E-01
-0.400	-1.46	-17.66	1.13E 00	-5.16E-02	7.21E 01	9.70E-01	-3.09E-01
-0.200	-0.49	-16.69	1.17E 00	-4.91E-02	7.34E 01	9.94E-01	-2.98E-01
-0.	0.49	-15.71	1.17E 00	-4.66E-02	7.36E 01	1.00E 00	-2.82E-01
0.200	1.34	-14.86	1.16E 00	-7.34E-02	7.31E 01	9.97E-01	-2.64E-01
0.400	2.32	-13.88	1.07E 00	-7.17E-02	7.02E 01	9.63E-01	-2.38E-01
0.600	3.29	-12.91	9.41E-01	-6.84E-02	6.58E 01	9.07E-01	-2.08E-01
0.800	4.15	-12.05	7.94E-01	-6.69E-02	6.05E 01	8.36E-01	-1.78E-01
1.000	4.88	-11.32	6.54E-01	-6.25E-02	5.49E 01	7.60E-01	-1.52E-01
1.200	5.37	-10.83	4.97E-01	-5.68E-02	4.78E 01	6.64E-01	-1.27E-01
1.400	5.73	-10.47	3.79E-01	-5.00E-02	4.18E 01	5.81E-01	-1.07E-01
1.600	5.85	-10.35	1.92E-01	-4.41E-02	2.97E 01	4.13E-01	-7.55E-02
1.800	4.39	-11.81	1.21E-01	-3.90E-02	2.36E 01	3.27E-01	-6.83E-02
2.000	3.41	-12.79	7.30E-02	-3.22E-02	1.88E 01	2.53E-01	-5.73E-02
2.200	0.12	-16.08	4.26E-02	-2.77E-02	1.40E 01	1.90E-01	-5.48E-02
2.400	-2.01	-18.21	3.20E-02	-2.37E-02	1.21E 01	1.63E-01	-5.36E-02
2.600	-4.76	-20.96	2.35E-02	-1.95E-02	1.03E 01	1.36E-01	-5.20E-02
2.800	-9.63	-25.83	1.40E-02	-1.53E-02	8.03E 00	1.02E-01	-4.94E-02

UC = 7.08E 01, EP = 3.63E 00, b = 1.31E 00, E=, 2.14E 00,

EMOM = 2.50E 00, RATIO = 1.34E 00, EOEC = 7.54E-01

UOUCSQ	XI	US	USOUC	USOUCS	Y/B	XIOBS
4.56E-02	-3.457	1.60E 01	2.25E-01	5.07E-02	-2.75E 00	-2.72E 00
6.06E-02	-3.073	1.94E 01	2.63E-01	6.94E-02	-2.44E 00	-2.42E 00
7.26E-02	-2.881	2.15E 01	2.92E-01	8.54E-02	-2.29E 00	-2.27E 00
9.11E-02	-2.689	2.42E 01	3.29E-01	1.08E-01	-2.14E 00	-2.12E 00
1.17E-01	-2.497	2.71E 01	3.71E-01	1.38E-01	-1.99E 00	-1.97E 00
1.43E-01	-2.305	3.02E 01	4.09E-01	1.68E-01	-1.83E 00	-1.81E 00
1.84E-01	-2.113	3.4 E 01	4.61E-01	2.13E-01	-1.68E 00	-1.66E 00
2.32E-01	-1.921	3.78E 01	5.13E-01	2.63E-01	-1.53E 00	-1.51E 00
2.97E-01	-1.729	4.24E 01	5.75E-01	3.30E-01	-1.38E 00	-1.36E 00
3.63E-01	-1.536	4.68E 01	6.29E- 1	3.96E-01	-1.22E 00	-1.21E 00
4.53E-01	-1.344	5.18E 01	6.97E-01	4.85E-01	-1.07E 00	-1.06E 00
5.49E-01	-1.152	5.6 E 01	7.62E-01	5.80E-01	-9.17E-01	-9.07E-01
6.62E-01	-0.960	6.12E 01	8.31E-01	6.90E-01	-7.64E-01	-7.56E-01
7.65E-01	-0.766	6.54E 01	8.87E- 1	7.87E-01	-6.11E-01	-6.05E-01
8.68E-01	-0.576	6.93E 01	9.40E-01	8.84E-01	-4.58E-01	-4.54E-01
9.42E-01	-0.384	7.19E 01	9.76E-01	9.52E-01	-3.06E-01	-3.02E-01
9.88E-01	-0.192	7.35E 01	9.95E-01	9.90E-01	-1.53E-01	-1.51E-01
1.00E 00	-0.	7.36E 01	9.98E-01	9.96E-01	-0.	-0.
9.94E-01	0.192	7.31E 01	9.91E-01	9.83E-01	1.53E-01	1.51E-01
9.27E-01	0.384	7.05E 01	9.54E- 1	9.10E-01	3.06E-01	3.02E-01
8.22E-01	0.576	6.59E 01	8.94E-01	8.00E-01	4.58E-01	4.54E-01
6.98E-01	0.768	6.04E 01	8.20E- 1	6.73E-01	6.11E-01	6.05E-01
5.78E-01	0.960	5.47E 01	7.42E-01	5.50E-01	7.64E-01	7.56E-01
4.41E-01	1.152	4.74E 01	6.44E-01	4.14E-01	9.17E-01	9.07E-01
3.37E-01	1.344	4.11E 01	5.58E-01	3.11E-01	1.07E 00	1.06E 00
1.71E-01	1.536	2.84E 01	3.92E- 1	1.53E-01	1.22E 00	1.21E 00
1.07E-01	1.729	2.26E 01	3.06E-01	9.35E-02	1.38E 00	1.36E 00
6.39E-02	1.921	1.71E 01	2.31E-01	5.35E-02	1.53E 00	1.51E 00
3.62E-02	2.113	1.26E 01	1.70E-01	2.90E-02	1.68E 00	1.66E 00
2.66E-02	2.305	1.05E 01	1.43E- 1	2.05E-02	1.83E 00	1.81E 00
1.84E-02	2.497	8.6 E 00	1.17E-01	1.36E-02	1.99E 00	1.97E 00
1.04E-02	2.689	6.26E 00	8.50E-02	7.22E-03	2.14E 00	2.12E 00

UCS = 7.37E 01, EMS = 3.51E 00, BS = 1.27E 00, ES= 2.07E 00,

EMSOMC = 2.51E 00, RATIOS = 1.30E 00, ESOEO = 7.60E-01

5 0. 2 2 0.10 21 6 64 2

YS	TS	T	Q	CP	V	UDUC	VDUC
-1.350	8.50	0.	4.00E-03	-1.02E-02	5.54E 00	4.36E-02	0.
-1.250	-25.44	-33.94	-7.30E-02	-4.22E-02	0.	0.	0.
-1.150	-19.57	-28.07	4.79E-02	-1.49E-02	1.49E 01	1.33E-01	-7.16E-02
-1.050	-15.66	-24.16	1.01E-01	-1.55E-02	2.16E 01	2.00E-01	-8.97E-02
-0.950	-14.78	-23.28	1.67E-01	-1.56E-02	2.78E 01	2.59E-01	-1.11E-01
-0.850	-13.09	-21.59	2.80E-01	-1.45E-02	3.59E 01	3.39E-01	-1.34E-01
-0.750	-9.70	-18.20	4.34E-01	-1.67E-02	4.47E 01	4.31E-01	-1.42E-01
-0.650	-7.30	-15.80	6.55E-01	-1.74E-02	5.49E 01	5.37E-01	-1.52E-01
-0.550	-5.40	-13.90	9.35E-01	-2.91E-02	6.56E 01	6.47E-01	-1.60E-01
-0.450	-3.66	-12.16	1.24E 00	-2.90E-02	7.54E 01	7.49E-01	-1.61E-01
-0.350	-2.19	-10.69	1.56E 00	-2.69E-02	8.47E 01	8.45E-01	-1.60E-01
-0.250	-0.90	-9.40	1.85E 00	-2.63E-02	9.22E 01	9.24E-01	-1.53E-01
-0.150	0.04	-8.46	2.05E 00	-2.57E-02	9.72E 01	9.76E-01	-1.45E-01
-0.050	0.56	-7.94	2.15E 00	-2.48E-02	9.96E 01	1.00E 00	-1.40E-01
0.050	1.29	-7.21	2.14E 00	-2.63E-02	9.92E 01	9.99E-01	-1.26E-01
0.150	1.98	-6.52	2.04E 00	-2.73E-02	9.69E 01	9.77E-01	-1.12E-01
0.250	2.72	-5.78	1.84E 00	-2.83E-02	9.21E 01	9.30E-01	-9.41E-02
0.350	3.20	-5.30	1.59E 00	-2.80E-02	8.55E 01	8.64E-01	-8.01E-02
0.450	3.52	-4.98	1.28E 00	-2.74E-02	7.63E 01	7.72E-01	-6.73E-02
0.550	3.80	-4.70	1.04E 00	-2.46E-02	6.93E 01	7.01E-01	-5.76E-02
0.650	3.60	-4.90	7.72E-01	-2.17E-02	5.96E 01	6.03E-01	-5.17E-02
0.750	3.13	-5.37	5.73E-01	-1.78E-02	5.14E 01	5.19E-01	-4.88E-02
0.850	2.34	-6.16	4.32E-01	-1.49E-02	4.46E 01	4.50E-01	-4.86E-02
0.950	1.44	-7.06	3.37E-01	-1.25E-02	3.94E 01	3.97E-01	-4.92E-02
1.050	0.32	-8.18	2.74E-01	-1.11E-02	3.55E 01	3.57E-01	-5.13E-02
1.150	0.65	-7.85	2.14E-01	-1.11E-02	3.14E 01	3.16E-01	-4.35E-02
1.250	0.72	-7.78	1.62E-01	-1.11E-02	2.73E 01	2.75E-01	-3.75E-02
1.350	0.92	-7.58	9.30E-02	-1.07E-02	2.07E 01	2.08E-01	-2.77E-02
1.450	1.42	-7.08	4.20E-02	-1.02E-02	1.39E 01	1.40E-01	-1.74E-02
1.550	-17.27	-25.77	6.67E-03	-8.36E-03	5.54E 00	5.07E-02	-2.45E-02

UC = 9.85E 01, EM = 1.56E 00, B = 5.61E-01, E= 9.12E-01,

EMOM = 1.50E 00, RATIO = 1.06E 00, EDE = 8.23E-01

UOUCSQ	XI	US	USOUC	USOUCS	Y/B	XIOBS
1.90E-03	-1.335	5.24E 00	5.26E-02	2.76E-03	-2.41E 00	-2.41E 00
0.	-1.236	1.05E 00	1.05E-02	1.11E-04	-2.23E 00	-2.23E 00
1.77E-02	-1.137	1.51E 01	1.51E-01	2.28E-02	-2.05E 00	-2.05E 00
4.00E-02	-1.038	2.10E 01	2.19E-01	4.78E-02	-1.87E 00	-1.87E 00
6.70E-02	-0.940	2.77E 01	2.78E-01	7.73E-02	-1.69E 00	-1.70E 00
1.15E-01	-0.841	3.56E 01	3.58E-01	1.28E-01	-1.51E 00	-1.52E 00
1.86E-01	-0.742	4.45E 01	4.47E-01	2.00E-01	-1.34E 00	-1.34E 00
2.85E-01	-0.643	5.47E 01	5.49E-01	3.01E-01	-1.16E 00	-1.16E 00
4.15E-01	-0.544	6.55E 01	6.56E-01	4.30E-01	-9.80E-01	-9.82E-01
5.85E-01	-0.445	7.51E 01	7.54E-01	5.68E-01	-8.02E-01	-8.04E-01
7.74E-01	-0.346	8.44E 01	8.47E-01	7.18E-01	-6.24E-01	-6.25E-01
8.86E-01	-0.247	9.24E 01	9.23E-01	8.52E-01	-4.45E-01	-4.46E-01
9.58E-01	-0.148	9.71E 01	9.74E-01	9.49E-01	-2.67E-01	-2.68E-01
1.00E 00	-0.049	9.95E 01	9.99E-01	9.97E-01	-8.91E-02	-8.93E-02
9.96E-01	0.049	9.91E 01	9.96E-01	9.93E-01	8.91E-02	8.93E-02
9.85E-01	0.148	9.71E 01	9.74E-01	9.49E-01	2.67E-01	2.68E-01
9.65E-01	0.247	9.28E 01	9.26E-01	8.58E-01	4.45E-01	4.46E-01
7.46E-01	0.346	8.58E 01	8.59E-01	7.38E-01	6.24E-01	6.25E-01
5.95E-01	0.445	7.64E 01	7.67E-01	5.88E-01	8.02E-01	8.04E-01
4.92E-01	0.544	6.92E 01	6.95E-01	4.83E-01	9.80E-01	9.82E-01
3.64E-01	0.643	5.93E 01	5.96E-01	3.55E-01	1.16E 00	1.16E 00
2.70E-01	0.742	5.09E 01	5.11E-01	2.61E-01	1.34E 00	1.34E 00
2.03E-01	0.841	4.39E 01	4.41E-01	1.94E-01	1.51E 00	1.52E 00
1.58E-01	0.940	3.85E 01	3.87E-01	1.50E-01	1.69E 00	1.70E 00
1.27E-01	1.038	3.45E 01	3.47E-01	1.20E-01	1.87E 00	1.87E 00
9.97E-02	1.137	3.03E 01	3.05E-01	9.28E-02	2.05E 00	2.05E 00
7.55E-02	1.236	2.62E 01	2.64E-01	6.95E-02	2.23E 00	2.23E 00
4.34E-02	1.335	1.97E 01	1.98E-01	3.91E-02	2.41E 00	2.41E 00
1.96E-02	1.434	1.30E 01	1.31E-01	1.71E-02	2.58E 00	2.59E 00
2.57E-03	1.533	4.53E 00	4.55E-02	2.07E-03	2.76E 00	2.77E 00

UCS = 9.96E 01, EMS = 1.54E 00, BS = 5.54E-01, ES= 9.00E-01,

EMSOMO = 1.50E 00, RATIOS = 1.04E 00, ESOEO = 8.21E-01

15 0. 2 2 0.10 21 6 64 2

YS	TS	T	Q	CP	V	UOUC	VOUC
-2.600	3.96	-4.54	6.40E-02	-7.52E-02	8.46E 00	2.47E-01	-1.96E-02
-2.400	-1.07	-9.57	8.20E-02	-8.46E-02	1.96E 01	2.77E-01	-4.67E-02
-2.200	-4.54	-13.04	1.13E-01	-9.49E-02	2.31E 01	3.22E-01	-7.45E-02
-2.000	-5.68	-14.18	1.65E-01	-9.96E-02	2.78E 01	3.86E-01	-9.75E-02
-1.800	-7.37	-15.87	2.15E-01	-9.31E-02	3.18E 01	4.37E-01	-1.24E-01
-1.600	-7.14	-15.64	2.95E-01	-9.19E-02	3.72E 01	5.12E-01	-1.43E-01
-1.400	-5.72	-14.22	4.08E-01	-1.07E-01	4.38E 01	6.07E-01	-1.54E-01
-1.200	-4.70	-13.20	5.18E-01	-1.04E-01	4.93E 01	6.87E-01	-1.61E-01
-1.000	-4.06	-12.56	6.44E-01	-9.95E-02	5.50E 01	7.68E-01	-1.71E-01
-0.800	-3.44	-11.94	7.64E-01	-9.37E-02	5.99E 01	8.38E-01	-1.77E-01
-0.600	-2.44	-10.94	8.84E-01	-8.71E-02	6.44E 01	9.05E-01	-1.75E-01
-0.400	-1.18	-9.68	9.91E-01	-8.27E-02	6.82E 01	9.62E-01	-1.64E-01
-0.200	-0.33	-8.83	1.05E 00	-7.76E-02	7.04E 01	9.95E-01	-1.54E-01
0.	0.70	-7.80	1.06E 00	-7.35E-02	7.05E 01	9.99E-01	-1.37E-01
0.200	3.14	-5.36	1.01E 00	-7.10E-02	6.87E 01	9.79E-01	-9.18E-02
0.400	4.81	-3.69	9.11E-01	-6.68E-02	6.54E 01	9.34E-01	-6.02E-02
0.600	5.63	-2.87	7.82E-01	-5.79E-02	6.06E 01	8.66E-01	-4.33E-02
0.800	5.92	-2.58	6.25E-01	-5.15E-02	5.42E 01	7.74E-01	-3.48E-02
1.000	6.33	-2.17	4.83E-01	-4.51E-02	4.76E 01	6.81E-01	-2.58E-02
1.200	6.51	-1.99	3.52E-01	-3.67E-02	4.07E 01	5.81E-01	-2.02E-02
1.400	6.13	-2.37	2.36E-01	-2.91E-02	3.33E 01	4.76E-01	-1.97E-02
1.600	5.70	-2.80	1.50E-01	-2.35E-02	2.65E 01	3.79E-01	-1.85E-02
1.800	3.14	-5.36	8.00E-02	-1.88E-02	1.94E 01	2.76E-01	-2.59E-02
2.000	-1.89	-10.39	3.60E-02	-1.50E-02	1.30E 01	1.83E-01	-3.35E-02
2.200	-20.92	-29.42	1.52E-02	-1.13E-02	8.46E 00	1.05E-01	-5.94E-02

UC = 6.99E 01, EM = 3.01E 00, B = 1.11E 00, E= 1.82E 00,

EMOM = 2.03E 00, RATIO = 1.04E 00, EOED = 5.71E-01

LOUCSQ	XI	US	USOUC	USOUCS	Y/B	XIOBS
6.11E-02	-2.571	1.81E 01	2.56E-01	6.56E-02	-2.33E 00	-2.33E 00
7.66E-02	-2.374	2.05E 01	2.90E-01	8.39E-02	-2.15E 00	-2.15E 00
1.03E-01	-2.176	2.39E 01	3.38E-01	1.14E-01	-1.97E 00	-1.97E 00
1.49E-01	-1.978	2.85E 01	4.03E-01	1.62E-01	-1.79E 00	-1.79E 00
1.91E-01	-1.780	3.22E 01	4.56E-01	2.08E-01	-1.61E 00	-1.61E 00
2.63E-01	-1.582	3.75E 01	5.30E-01	2.81E-01	-1.44E 00	-1.44E 00
3.68E-01	-1.385	4.40E 01	6.22E-01	3.87E-01	-1.26E 00	-1.26E 00
4.72E-01	-1.187	4.94E 01	6.99E-01	4.88E-01	-1.08E 00	-1.08E 00
5.89E-01	-0.989	5.50E 01	7.77E-01	6.04E-01	-8.97E-01	-8.97E-01
7.03E-01	-0.791	5.98E 01	8.46E-01	7.15E-01	-7.18E-01	-7.18E-01
8.16E-01	-0.593	6.43E 01	9.10E-01	8.27E-01	-5.38E-01	-5.38E-01
9.25E-01	-0.396	6.81E 01	9.64E-01	9.29E-01	-3.59E-01	-3.59E-01
9.89E-01	-0.198	7.03E 01	9.95E-01	9.90E-01	-1.79E-01	-1.79E-01
9.98E-01	0.	7.05E 01	9.97E-01	9.94E-01	0.	0.
9.58E-01	0.198	6.87E 01	9.71E-01	9.44E-01	1.79E-01	1.79E-01
8.72E-01	0.396	6.53E 01	9.23E-01	8.52E-01	3.59E-01	3.59E-01
7.49E-01	0.593	6.04E 01	8.54E-01	7.29E-01	5.38E-01	5.38E-01
5.99E-01	0.791	5.39E 01	7.62E-01	5.81E-01	7.18E-01	7.18E-01
4.63E-01	0.989	4.72E 01	6.68E-01	4.46E-01	8.97E-01	8.97E-01
3.38E-01	1.187	4.01E 01	5.68E-01	3.22E-01	1.08E 00	1.08E 00
2.26E-01	1.385	3.27E 01	4.62E-01	2.14E-01	1.26E 00	1.26E 00
1.44E-01	1.582	2.58E 01	3.65E-01	1.34E-01	1.44E 00	1.44E 00
7.62E-02	1.780	1.86E 01	2.64E-01	6.95E-02	1.61E 00	1.61E 00
3.35E-02	1.978	1.22E 01	1.72E-01	2.97E-02	1.79E 00	1.79E 00
1.11E-02	2.176	7.05E 00	9.97E-02	9.93E-03	1.97E 00	1.97E 00

UCS = 7.07E 01, EMS = 2.98E 00, BS = 1.10E 00, ES= 1.81E 00,

EMSOMO = 2.03E 00, RATIOS = 1.02E 00, ESOEO = 5.72E-01

30 0. 2 2 0.10 20 6 64 2

YS	TS	T	Q	CP	V	UOUC	VOUC
-4.200	6.68	-1.82	4.10E-02	-1.09E-01	8.38E 00	2.98E-01	-9.46E-03
-3.800	-1.16	-9.66	4.60E-02	-1.19E-01	1.47E 01	3.12E-01	-5.31E-02
-3.400	-0.29	-8.79	9.60E-02	-1.30E-01	2.12E 01	4.52E-01	-6.98E-02
-3.000	-2.19	-10.69	1.31E-01	-1.40E-01	2.48E 01	5.25E-01	-9.90E-02
-2.600	-3.40	-11.90	1.77E-01	-1.51E-01	2.88E 01	6.07E-01	-1.28E-01
-2.200	-2.90	-11.40	2.40E-01	-1.57E-01	3.35E 01	7.08E-01	-1.43E-01
-1.800	-3.02	-11.52	2.92E-01	-1.62E-01	3.70E 01	7.81E-01	-1.59E-01
-1.400	-2.24	-10.74	3.52E-01	-1.64E-01	4.06E 01	8.60E-01	-1.63E-01
-1.000	-1.62	-10.12	4.01E-01	-1.64E-01	4.33E 01	9.19E-01	-1.64E-01
-0.600	-0.74	-9.24	4.47E-01	-1.61E-01	4.57E 01	9.73E-01	-1.58E-01
-0.400	-0.64	-9.14	4.60E-01	-1.59E-01	4.64E 01	9.87E-01	-1.59E-01
-0.200	-0.37	-8.87	4.66E-01	-1.57E-01	4.67E 01	9.94E-01	-1.55E-01
0.	0.15	-8.35	4.70E-01	-1.55E-01	4.69E 01	1.00E 00	-1.47E-01
0.200	0.47	-8.03	4.62E-01	-1.53E-01	4.65E 01	9.92E-01	-1.40E-01
0.400	0.88	-7.62	4.50E-01	-1.49E-01	4.59E 01	9.80E-01	-1.31E-01
0.600	1.08	-7.42	4.34E-01	-1.47E-01	4.51E 01	9.63E-01	-1.25E-01
1.000	1.70	-6.80	3.91E-01	-1.40E-01	4.28E 01	9.16E-01	-1.09E-01
1.400	2.17	-6.33	3.32E-01	-1.32E-01	3.94E 01	8.45E-01	-9.36E-02
1.800	2.58	-5.92	2.72E-01	-1.21E-01	3.57E 01	7.65E-01	-7.93E-02
2.200	2.78	-5.72	2.08E-01	-1.13E-01	3.12E 01	6.69E-01	-6.71E-02
2.600	2.43	-6.07	1.50E-01	-1.00E-01	2.65E 01	5.68E-01	-6.04E-02
3.000	1.59	-6.91	9.20E-02	-8.94E-02	2.07E 01	4.44E-01	-5.38E-02
3.400	-0.49	-8.99	5.70E-02	-7.45E-02	1.63E 01	3.48E-01	-5.50E-02
3.800	-8.53	-17.03	3.17E-02	-6.38E-02	1.22E 01	2.51E-01	-7.69E-02
4.200	-18.92	-27.42	1.90E-02	-5.32E-02	9.43E 00	1.81E-01	-9.37E-02
4.600	-71.50	-80.00	1.50E-02	-4.47E-02	8.38E 00	3.14E-02	-1.78E-01

UC = 4.64E 01, EM = 5.70E 00, B = 2.17E 00, E= 3.60E 00,

EMOM = 2.55E 00, RATIO = 8.92E-01, EOEO = 3.31E-01

LOUCSQ	XI	US	USOUC	USOUCS	Y/B	XIOBS
8.91E-02	-4.154	1.43E 01	3.05E-01	9.32E-02	-1.93E 00	-1.93E 00
9.72E-02	-3.758	1.52E 01	3.24E-01	1.05E-01	-1.75E 00	-1.75E 00
2.04E-01	-3.363	2.16E 01	4.61E-01	2.13E-01	-1.56E 00	-1.56E 00
2.75E-01	-2.967	2.51E 01	5.35E-01	2.86E-01	-1.38E 00	-1.38E 00
3.69E-01	-2.571	2.90E 01	6.18E-01	3.81E-01	-1.20E 00	-1.19E 00
5.01E-01	-2.176	3.36E 01	7.16E-01	5.13E-01	-1.01E 00	-1.01E 00
6.10E-01	-1.780	3.70E 01	7.88E-01	6.21E-01	-8.28E-01	-8.27E-01
7.39E-01	-1.385	4.05E 01	8.64E-01	7.47E-01	-6.44E-01	-6.43E-01
8.45E-01	-0.989	4.32E 01	9.22E-01	8.50E-01	-4.60E-01	-4.59E-01
9.47E-01	-0.593	4.57E 01	9.74E-01	9.49E-01	-2.76E-01	-2.76E-01
9.75E-01	-0.396	4.63E 01	9.88E-01	9.76E-01	-1.84E-01	-1.84E-01
9.89E-01	-0.198	4.67E 01	9.95E-01	9.90E-01	-9.20E-02	-9.19E-02
1.00E 00	0.	4.69E 01	10.00E-01	9.99E-01	0.	0.
9.85E-01	0.198	4.65E 01	9.92E-01	9.83E-01	9.20E-02	9.19E-02
9.61E-01	0.396	4.59E 01	9.79E-01	9.59E-01	1.84E-01	1.84E-01
9.28E-01	0.593	4.51E 01	9.62E-01	9.25E-01	2.76E-01	2.76E-01
8.39E-01	0.989	4.28E 01	9.13E-01	8.33E-01	4.60E-01	4.59E-01
7.13E-01	1.385	3.94E 01	8.40E-01	7.06E-01	6.44E-01	6.43E-01
5.85E-01	1.780	3.56E 01	7.59E-01	5.76E-01	8.28E-01	8.27E-01
4.48E-01	2.176	3.16E 01	6.62E-01	4.38E-01	1.01E 00	1.01E 00
3.23E-01	2.571	2.66E 01	5.59E-01	3.13E-01	1.20E 00	1.19E 00
1.97E-01	2.967	2.04E 01	4.35E-01	1.89E-01	1.38E 00	1.38E 00
1.21E-01	3.363	1.59E 01	3.39E-01	1.15E-01	1.56E 00	1.56E 00
6.31E-02	3.758	1.15E 01	2.46E-01	6.05E-02	1.75E 00	1.75E 00
3.26E-02	4.154	8.36E 00	1.78E-01	3.18E-02	1.93E 00	1.93E 00
9.84E-04	4.549	2.09E 00	4.46E-02	1.99E-03	2.12E 00	2.11E 00

UCS = 4.69E 01, EMS = 5.64E 00, BS = 2.15E 00, ES= 3.57E 00,

EMSOMO = 2.56E 00, RATIOS = 8.84E-01, ESOEO = 3.32E-01

BLANK PAGE